

# Statistical inference for radial generalised Pareto distributions and return sets in geometric extremes

Ioannis Papastathopoulos <sup>\*1</sup>, Lambert De Monte <sup>†1</sup>, Ryan Campbell <sup>‡2</sup>, and Håvard Rue <sup>§3</sup>

<sup>1</sup>School of Mathematics and Maxwell Institute for Mathematical Sciences, University of Edinburgh, Edinburgh, EH9 3FD, Scotland

<sup>2</sup>School of Mathematical Sciences, Lancaster University, Lancaster, LA1 4YF, England

<sup>3</sup>Statistics Program, King Abdullah University of Science and Technology, Thuwal 23955-6900, Saudi Arabia

## Abstract

We use a functional analogue of the quantile function for probability measures on  $\mathbb{R}^d$  to characterize a novel limit Poisson point process for radially recentred and rescaled random vectors under a radial-directional decomposition. This limit process yields new multivariate distributions, including *radial generalised Pareto distributions*, exhibiting stability for extrapolation to extremal sets along any direction. We show that the normalising functions leading to the limit Poisson point process correspond to a novel class of sets visited with fixed probability, with geometric properties determined by the conditional distribution of the radius given the direction and the Radon-Nikodym derivative of the directional probability distribution relative to reference spherical measures. This leads to return sets, defined by the complement of these probability sets and expressed by their return period. We identify an important member, the *isotropic return set*, where all directions of exceedances outside the set are equally likely. Building on the limit Poisson point process likelihood, we develop parsimonious statistical models leveraging links between limit distribution parameters, with novel diagnostics for assessing convergence to the limiting distribution. These models enable Bayesian inference for return sets with arbitrarily large return periods and probabilities of unobserved extreme events, incorporating directional information from observations outside probability sets. The framework supports efficient computations in dimensions  $d = 2$  and  $d = 3$ . We demonstrate the utility of the methods through simulations and case studies involving hydrological and oceanographic data, showcasing potential for robust and interpretable analysis of multivariate extremes.

---

\*i.papastathopoulos@ed.ac.uk

†l.demonte@ed.ac.uk

‡r.campbell3@lancaster.ac.uk

§haavard.rue@kaust.ed.sa

*Keywords:* Bayesian inference, isotropic return set, limit set, Poisson process, quantile set, radial generalised Pareto, return set, starshaped set

## 1 Introduction

The multivariate nature of extreme events casts a shadow of potentially devastating consequences upon ecosystems, infrastructures, as well as financial, economic, and insurance sectors. Knowledge of the frequency and magnitude of extreme events is crucial in enhancing planning strategies and adaptation efforts. The statistical properties of univariate extremes are well-established (Balkema & de Haan 1974, Pickands 1975, Davison & Smith 1990), but statistical inference for multivariate random processes is much more intricate: one must analyse how random processes interact with and influence each other. A common way to describe the extremal dependence structure of a real-valued random vector  $\mathbf{X} = (X_1, \dots, X_d)$  is through the coefficient of tail dependence

$$\chi_q(A) = \mathbb{P} \left[ \bigcap_{j \in A} \{F_j(X_j) > q\} \right] / (1 - q), \quad q \in (0, 1), \quad A \subseteq \{1, \dots, d\}, |A| > 1, \quad (1)$$

where  $F_j$  is the cumulative distribution function of  $X_j$ . When  $\lim_{q \rightarrow 1} \chi_q(A) = 0$ , the variables in  $A$  are unlikely to grow large together and we say that they exhibit asymptotic independence. Conversely, when  $\lim_{q \rightarrow 1} \chi_q(A) > 0$ , the variables in  $A$  are likely to grow large together and the variables in  $A$  exhibit asymptotic dependence. The different dependence structures that can be present within subgroups of the marginal variables of  $\mathbf{X}$  can make inference for rare events challenging and extrapolation inaccurate.

Classical approaches to multivariate extreme events often rely on the framework of multivariate regular variation (MRV) (de Haan & Resnick 1977), which posits that the point processes of exceedances of a random vector over a high threshold, when suitably renormalised, converge in distribution to a non-degenerate non-homogenous Poisson point process (de Haan 1984). This provides a framework for understanding the joint behaviour of extreme observations and leads to meaningful limit distributions that can be used for statistical inference of multivariate extremes. In practice, MRV is applied in a way that does not adequately describe relationships among asymptotically independent random variables (Nolde & Wadsworth 2022). This is due to the type of the renormalisation that is employed: given a random sample of  $n$   $d$ -dimensional observations, all components are normalised by the same amount. This leads to considering the dependence structure only in a single direction in  $\mathbb{R}^d$  (see Figure 1 and Section 2.2).

Another drawback of MRV is the limited set of directions in the multivariate space in which one can extrapolate the model. Under MRV, the probability of lying in an extremal set is estimated by shifting the extremal set and performing empirical probability estimation on the translated set. When the translated set does not contain observations from the initial dataset, the estimate the probability of interest is inevitably 0. To correct the joint rate of tail decay in the case of weaker extremal dependence, the notion of hidden regular variation (HRV) was introduced (Ledford & Tawn 1996, 1997, Maulik & Resnick 2004). However, HRV also suffers from the drawback that it

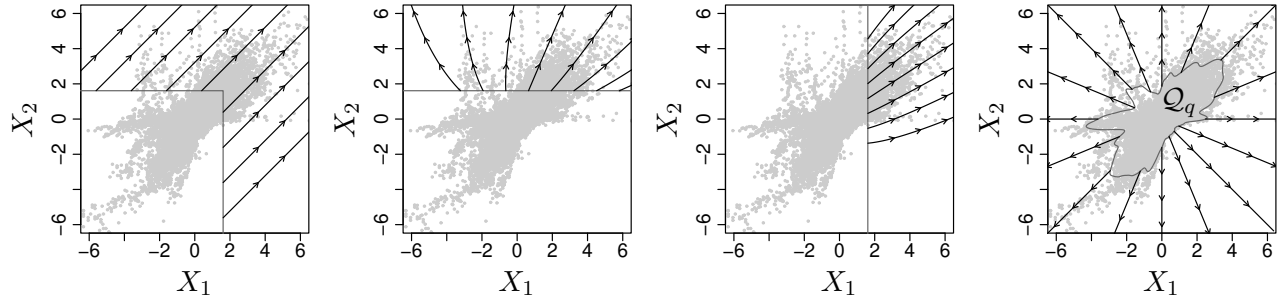


Figure 1: Directions along which MEVT frameworks allow extrapolation to tail regions of a bivariate Thames tributary river flow dataset transformed so that each marginal distribution is standard Laplace: (a) MRV, (b) and (c) conditional extremes given  $X_2$  and  $X_1$  are large, respectively, and (d) geometric extremes, with  $\mathcal{Q}_q$  illustrating the posterior mean of the quantile set ( $q = 0.95$ ). The support of the distribution of exceedances is inscribed by the region containing the arrows.

does not allow extrapolation along directions where not all variables are simultaneously large. To extrapolate to a wider range of extremal regions with a wider array of dependence structures, the frameworks of conditional extremes (Heffernan & Tawn 2004) and angular dependence (Wadsworth & Tawn 2013) have been introduced, but statistical methodology based on these frameworks suffers from drawbacks. Despite its wide applicability and widespread adoption, the conditional extremal inference method of Heffernan & Tawn (2004) is based on composite likelihood methods and on gluing separate models post-fit, making statistical inference and computations unwieldy. While the angular dependence method of Wadsworth & Tawn (2013) permits extrapolation in regions where variables are not simultaneously extreme, it is only useful for joint survival regions. Recently, a characterisation of extremal dependence through the limiting geometry of observations from  $\mathbf{X}$  has become of interest. The *limit set*, whose boundary arises as the limiting hull of appropriately scaled sample clouds, provides insight into the extremal dependence structure of  $\mathbf{X}$ . The *gauge function*, whose unit level set is in one-to-one correspondence with the boundary of the limit set, has been shown to connect several known coefficients describing extremal dependence of known copulas (Nolde 2014, Nolde & Wadsworth 2022). Wadsworth & Campbell (2024) proposed a framework for performing statistical inference for multivariate extremes using this geometric approach. Using a radial-directional decomposition, this framework treats the gauge function as a rate parameter of a left-truncated gamma model for the distribution of radii conditioned on angles on the unit simplex. Inference for the gauge function and its associated limit set is based on parametric models derived from known copulas in  $d$ -dimensions and standard exponential margins, and a maximum likelihood approach is implemented within the rate parameter of the truncated Gamma distribution. The result is a new statistical inference method in estimating extremal probabilities with great flexibility relative to state-of-the-art methods in multivariate extremes. Also in exponential margins and in a bivariate setting, Simpson & Tawn (2024a) estimate the gauge function via the generalised Pareto (GP) distribution (Pickands 1975) for the conditional distribution of the excess radii given angles on the simplex, and showing improvements in the estimation of extremal

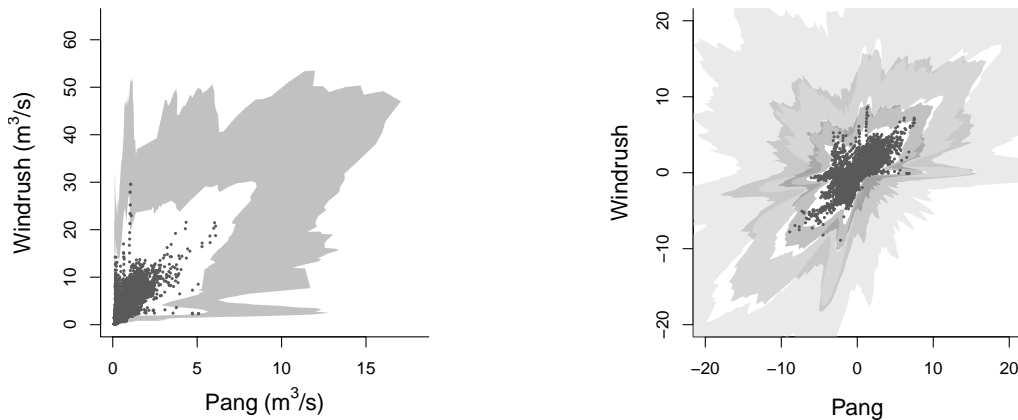


Figure 2: Simultaneous prediction intervals for the boundary of river flow return level-sets of the Thames tributaries. *Left*: original margins, return period of  $T = 10^3$  days. *Right*: standard Laplace margins, return periods from dark to light grey,  $T = 10^3$ ,  $10^5$ , and  $T = 10^9$  days.

dependence coefficients derived from the estimated gauge (Nolde & Wadsworth 2022).

In this paper, we develop a framework that leverages the structure of weak limits in suitably radially renormalized multivariate exceedances in  $\mathbb{R}^d$ . Multivariate exceedances are observations that lie within a *return set*, defined as the complement of a *probability set*. Among the infinite class of probability sets that are visited with a prespecified probability, we identify two key types: quantile sets and isotropic probability sets. These sets are characterized by the distribution of directions associated with extreme events. Specifically, the quantile set is defined via the conditional quantile of the radius, ensuring that the directional distribution of exceedances matches the directional distribution of all events. In contrast, the isotropic probability set is defined such that the directional distribution of exceedances is uniform. The quantile set derives its name from its role as a  $d$ -dimensional generalisation of quantiles, addressing challenges in multivariate extreme value theory that arise from the absence of natural ordering in  $\mathbb{R}^d$  (Barnett 1976). This concept parallels the quantile regions introduced by Hallin et al. (2021), but our definition is specifically designed for extrapolation beyond the observed data. Likewise, the isotropic return set derives its name from its key property, which balances exceedances across all directions.

By specifying an appropriate sequence of quantile sets, we show under mild conditions that the framework of MRV be suitably extended to the cone  $\mathbb{R}^d \setminus \{\mathbf{0}\}$ . We further show that similar extensions are also available for light-tailed and bounded multivariate distributions. A key property of our framework is that it is applicable to any  $d \geq 1$ . In the multivariate setting ( $d > 1$ ), our framework enables the modelling of the entire joint tail, accommodating scenarios where subsets of components are extreme. This approach can capture behaviours across the entire spectrum of multivariate space and reveal hidden dependencies, thereby bridging the gap between theory and practice. Using radially recentered and rescaled exceedances over high quantile sets, we characterise non-trivial limit distributions on  $\mathbb{R}^d$ , termed *radially-stable generalised Pareto distributions*. The radial stability properties of these families of distributions permit extrapolation beyond the range of observed data along any direction (see Figure 1) and lead to the notion of *return sets*, a geometric  $d$ -dimensional extension of the uni-dimensional (upper-tail) return level (Coles 2001). This yields

an interpretable way to communicate the risk associated with extreme multivariate events allowing decision-makers, policymakers, and the general public to understand the likelihood of experiencing impact from *joint extreme events*.

Throughout our work, inference is done in a Bayesian manner, allowing us to obtain inferences for any functional of the joint tail distribution. Our methods account for multiple sources of uncertainty in the estimation, including that of uncertainty in the estimation of the marginal tails as well as the multivariate threshold, which is typically not accounted for in previous statistical methods for multivariate extremes. We use prediction intervals for functionals of interest, allowing us for example to quantify uncertainty via simultaneous prediction bands when the functional of interest consists of the boundary of a distribution-dependent set. The flexibility and accuracy of our modelling approach is illustrated in Figure 2, where the posterior return level sets are shown on a bivariate dataset of river flow measurements ( $m^3/s$ ) displaying a complicated dependence structure. Simultaneous prediction intervals for posterior estimates of the lower-boundary of the return level sets for various return periods are shown with growing uncertainty as the return period increases, which is expected. Our definition of the return level sets are linked with the findings in [Hallin et al. \(2021\)](#), which is based on optimal transportation theory. However, we are able to use our model to obtain these same curves far beyond the domain of our data with uncertainty estimated coherently through the posterior distribution. We note the similarities with [Hallin et al. \(2021\)](#) by estimation of return level curves on a series of bivariate Gaussian mixture distributions, presented in Supplementary Material 8.

The paper is organised as follows. In Section 2, we initiate our findings through classical univariate extreme value theory and multivariate regular variation, and introduces the main results, which include the weak convergence of radially recentred and rescaled exceedances to a Poisson point process. Our findings lead to a novel class of limit multivariate distributions that are presented in Section 2.7 and to novel return level-sets presented in Section 2.4. Section 3 details methodology for statistical inference of extremes using hierarchical Bayesian models with latent Gaussian random effects on Euclidean spheres. Finally, Section 4 illustrates the merits of our approach on a 3-dimensional data set of extreme sea levels in Newlyn, England. Publicly available code can be accessed via our R package `geometricExtremes` at GitHub to use the methodology discussed herein.

## 2 Theory

### 2.1 Notation and background

*Notation linked with measures:* Let  $\mu$  be a measure on a topological space  $\mathbb{E}$  and let  $h : \mathbb{E} \rightarrow \mathbb{R}$  be a measurable function. The support of a measure  $\mu$  is denoted by  $\text{supp}(\mu)$  and is the smallest closed subset of  $\mathbb{E}$  such that  $\mu(\mathbb{E} \setminus \text{supp}(\mu)) = 0$ . The integral of  $h$  with respect to  $\mu$  is denoted by  $\mu(h) = \int_{\mathbb{E}} h d\mu$ . The Dirac measure centred at  $x \in \mathbb{E}$ , denoted by  $\delta_x$ , is defined by  $\delta_x(h) = h(x)$ . A measure  $\nu$  is said to be absolutely continuous with respect to another measure  $\mu$ , denoted as  $\nu \ll \mu$ , if for every measurable set  $A$ ,  $\mu(A) = 0$  implies  $\nu(A) = 0$ . We write  $M_+(\mathbb{E})$  for the space

of nonnegative Radon measures on Borel subsets of  $\mathbb{E}$ ,  $M_1(\mathbb{E})$  for the space of Radon probability measures on Borel subsets of  $\mathbb{E}$  and  $M_p(\mathbb{E})$  for the space of all locally finite point measures on  $\mathbb{E}$ . Given a standard probability space  $(\Omega, \mathcal{F}, \mathbb{P})$ , we let a random point measure  $P$  on  $\mathbb{E}$  be a measurable map  $P : \Omega \rightarrow M_p(\mathbb{E})$ , such that  $P = \sum_{i=1}^N \delta_{X_i}$  where  $N : \Omega \rightarrow \mathbb{N} \cup \{\infty\}$  is a discrete random variable, representing the number of atoms of the point measure and given  $\{N = n\}$ ,  $X_i : \Omega \rightarrow \mathbb{E}$ ,  $i = 1, \dots, n$ , are random variables representing the location of the atoms. For notational simplicity, when subscripts become cumbersome, we also write  $\delta[x]$  to denote the Dirac measure  $\delta_x$ . The indicator random variable  $\mathbb{1}_A : \Omega \rightarrow \mathbb{R}$  is defined for  $A \in \mathcal{F}$  by  $\mathbb{1}_A(\omega) = 1$  if  $\omega \in A$  and  $\mathbb{1}_A(\omega) = 0$  otherwise. For a probability measure  $\mu$  defined on a subset  $\mathcal{E}$  of a topological space  $\mathbb{E}$ , then  $\mu(B) = \mu(B \cap \mathcal{E})$  for all  $B \in \mathcal{B}(\mathbb{E})$ , that is, the measure is always interpreted as its extension to the entire ambient space  $\mathbb{E}$ .

*Notation linked with vague convergence:* For a sequence of measures  $\mu_n$  and  $\mu$  on a nice space  $\mathbb{E}$ , we say that  $\mu_n$  converges vaguely to  $\mu$  in  $M_+(\mathbb{E})$ , denoted by  $\mu_n \xrightarrow{v} \mu$ , if  $\mu_n(B) \rightarrow \mu(B)$  for all relatively compact sets  $B \subset \mathbb{E}$  for which the boundary of  $B$  has  $\mu$  measure zero, that is,  $\mu(\partial B) = 0$ . An equivalent definition which is based on probing the behaviour of measures by integrating them along compactly supported continuous test functions is given in Appendix 1.1. Additionally, we write  $\mathbb{E}_\xi = \{x \in \mathbb{R} : 1 + \xi x > 0\}$  for  $\xi \in \mathbb{R}$ , and  $\overline{\mathbb{E}}_\xi$  denotes  $\mathbb{E}_\xi \cup \sup \mathbb{E}_\xi$ , where  $\sup \mathbb{E}_\xi := \sup\{x \in \mathbb{R} : x \in \mathbb{E}_\xi\}$ , that is, the right closure of the interval  $\mathbb{E}_\xi$ .

*Notation linked with weak convergence of a random point measure to a Poisson point process:* A sequence of random point measures  $P_n$  converges weakly in  $M_p(\mathbb{E})$  to a Poisson point process  $P$  with intensity measure  $\mu(dx)$  if the sequence of Laplace functionals of suitable test functions converges to the Laplace functional of the Poisson point process, *i.e.*, if for any  $h \in C_K^+(\mathbb{E})$ ,

$$\lim_{n \rightarrow \infty} \mathbb{E}[\exp\{-P_n(h)\}] = \exp\left\{-\int_{\mathbb{E}} [1 - \exp\{-h(x)\}] \mu(dx)\right\},$$

where  $C_K^+(\mathbb{E})$  denotes the space of continuous functions with compact support on  $\mathbb{E}$ .

*Notation linked with distributions and measure transportation* A random element  $Z : \Omega \rightarrow \mathbb{E}$  follows a distribution  $\mathbb{P}_Z$  and write  $Z \sim \mathbb{P}_Z$  whenever  $\mathbb{P}_Z(A) = \mathbb{P}(Z \in A)$ . Push-forward of measures, cyclically monotonic, When  $\mathbb{E} = \mathbb{R}^d$  with  $d \geq 1$ , then we let  $F_Z(\mathbf{x}) = \mathbb{P}_Z((-\infty, x_1] \times \dots \times (-\infty, x_d])$ ,  $\mathbf{x} = (x_1, \dots, x_d) \in \mathbb{R}^d$ , denote the corresponding cumulative distribution function of  $Z$ . For a nondecreasing function  $F : \mathbb{R} \rightarrow \mathbb{R}$ , the left-continuous inverse is defined by  $F^{-1}(y) = \inf\{x : F(x) \geq y\}$ . Two cumulative distribution functions  $G_1, G_2 : \mathbb{R}^d \rightarrow [0, 1]$  are said to be of the same type if there exist constants  $\mathbf{a} > 0$  and  $\mathbf{b}$  such that  $G_1(\mathbf{a}\mathbf{x} + \mathbf{b}) = G_2(\mathbf{x})$  for all  $\mathbf{x} \in \mathbb{R}^d$ , with vector algebra interpreted as elementwise.

*Notation linked with starshaped sets:* A set  $\mathcal{B} \subset \mathbb{R}^d$  is called starshaped at  $\mathbf{x} \in \mathcal{B}$  if every point  $\mathbf{y} \in \mathcal{B}$  is visible from  $\mathbf{x}$  in the sense that the closed line segment  $\{(1-t)\mathbf{x} + t\mathbf{y} : t \in [0, 1]\} \subset \mathcal{B}$ . If  $\mathcal{B}$  is starshaped at  $\mathbf{0}$  and compact in  $\mathbb{R}^d$ , then we call  $\mathcal{B}$  a star-body. The collection of all star-bodies is denoted by  $\star$ . A star-body  $\mathcal{B}$  is in one-to-one correspondence with its radial function  $r_{\mathcal{B}} : \mathbb{S}^{d-1} \rightarrow [0, \infty)$  given by  $r_{\mathcal{B}}(\mathbf{w}) = \sup\{\lambda > 0 : \lambda\mathbf{w} \in \mathcal{B}\}$ . Star-bodies are endowed with well-defined algebraic operations through their radial functions. For instance, for  $\mathcal{A}, \mathcal{B} \in \star$ ,  $\mathcal{A} + \mathcal{B}$

and  $\mathcal{A} \cdot \mathcal{B}$  are interpreted as the star-bodies with radial functions  $r_{\mathcal{A}+\mathcal{B}} = r_{\mathcal{A}} + r_{\mathcal{B}}$  and  $r_{\mathcal{A}\cdot\mathcal{B}} = r_{\mathcal{A}} \cdot r_{\mathcal{B}}$ . Additional information about starshaped sets and radial functions can be found in Supplementary Materials 1.3 and 1.4.

## 2.2 Univariate extremes

A complete characterisation of all possible non-trivial limit laws of extremes of a univariate random variable  $X$  with probability distribution  $F_X$  relies on regular variation and its extensions, postulating location and scale constants  $a_n > 0$  and  $b_n$ , and  $\alpha_n > 0$  and  $\beta_n \in \mathbb{R}$ , for  $n = 1, 2, \dots$ , alongside shape parameters  $\xi_{\{+1\}}, \xi_{\{-1\}} \in \mathbb{R}$  and non-degenerate limit measures  $\nu_{\{+1\}}$  and  $\nu_{\{-1\}}$ , such that

$$n\mathbb{P}[\{X - b_n\}/a_n \in \cdot] \xrightarrow{v} \nu_{\{+1\}}(\cdot) \quad \text{and} \quad n\mathbb{P}[\{(-X) - \beta_n\}/\alpha_n \in \cdot] \xrightarrow{v} \nu_{\{-1\}}(\cdot) \quad (2)$$

as  $n \rightarrow \infty$ , in  $M_+(\overline{\mathbb{E}}_{\xi_{\{+1\}}})$  and  $M_+(\overline{\mathbb{E}}_{\xi_{\{-1\}}})$ , respectively. Standard references include [Resnick \(1987\)](#) and [de Haan & Ferreira \(2006\)](#). The location and scale renormalisations in (2) imply that the *exponent functions* of the limit measures, defined by

$$\Lambda_{\{+1\}}(z) := \nu_{\{+1\}}(z, \sup \mathbb{E}_{\xi_{\{+1\}}}] \quad \text{and} \quad \Lambda_{\{-1\}}(z) := \nu_{\{-1\}}(z, \sup \mathbb{E}_{\xi_{\{-1\}}}],$$

satisfy the functional equations

$$n \Lambda_{\{+1\}}(a_n + b_n z) = \Lambda_{\{+1\}}(z) \quad \text{and} \quad n \Lambda_{\{-1\}}(\alpha_n + \beta_n z) = \Lambda_{\{-1\}}(z),$$

whose unique solutions are given, up-to-type, by

$$\Lambda_{\{+1\}}(z) = [1 + \xi_{\{+1\}} z]_+^{-1/\xi_{\{+1\}}} \quad \text{and} \quad \Lambda_{\{-1\}}(z) = [1 + \xi_{\{-1\}} z]_+^{-1/\xi_{\{-1\}}},$$

where  $(x)_+ = \max(x, 0)$ , respectively characterizing the limit measures  $\nu_{\{+1\}}$  and  $\nu_{\{-1\}}$ .

The connection between the vague convergences (2) and the limiting laws of extremes of a sequence  $\{X_i : i = 1, 2, \dots\}$  of independent and identically distributed random variables from  $F_X$ , comes from the fact that these convergences constitute necessary and sufficient conditions for the sequences of random point measures

$$\sum_{i=1}^n \delta \left[ \left( \frac{X_i - b_n}{a_n}, \frac{i}{n+1} \right) \right] \quad \text{and} \quad \sum_{i=1}^n \delta \left[ \left( \frac{(-X_i) - \beta_n}{\alpha_n}, \frac{i}{n+1} \right) \right]$$

to respectively weakly converge in  $M_p(\overline{\mathbb{E}}_{\xi_{\{+1\}}} \times (0, 1))$  and  $M_p(\overline{\mathbb{E}}_{\xi_{\{-1\}}} \times (0, 1))$ , to Poisson point processes with intensity measures  $\nu_{\{+1\}}(dz)dt$  and  $\nu_{\{-1\}}(dz)dt$ , as  $n \rightarrow \infty$ .

A key aspect of the convergences (2) is that these can be unified under a single theme, allowing us to consider upper and lower extremes simultaneously. Theorem 1 illustrates this unification, which is contingent upon explicitly using the directions along which extremes occur, and shows that the right and left extremes from a random sample from  $\mathbb{P}_{\mathbf{X}}$  become ultimately independent as the sample size approaches infinity. Explicit in the construction below is the transformation of  $X$

into polar coordinates, which has the usual geometric interpretation that the sign of  $X$  is viewed as encoding the direction  $X/|X|$ , while the magnitude  $|X|$  represents the distance of  $X$  from 0.

**Theorem 1.** *Let  $X$  be a real-valued random variable and let  $S$  be the set of all points of the real line, any open neighbourhood of which receives a positive probability mass. Suppose that  $0 \in \text{supp}(\mathbb{P}_X)$ ,  $F_X(\{0\}) = 0$ , and convergences (2) hold true. Let  $\pi = \mathbb{P}(X > 0) = \mathbb{P}(X/|X| = 1)$ ,  $r_n^a(w) = a_{n,\{+1\}} \mathbb{1}_{\{w \in \{+1\}\}} + a_{n,\{-1\}} \mathbb{1}_{\{w \in \{-1\}\}}$  and  $r_n^b(w) = b_{n,\{+1\}} \mathbb{1}_{\{w \in \{+1\}\}} + b_{n,\{-1\}} \mathbb{1}_{\{w \in \{-1\}\}}$ . Let*

$$P_n = \sum_{i=1}^n \delta \left[ \left( \frac{|X_i| - r_n^a(X_i/|X_i|)}{r_n^b(X_i/|X_i|)}, \frac{X_i}{|X_i|}, \frac{i}{n+1} \right) \right].$$

(i) *There exist location and scale constants  $a_{n,\{+1\}} > 0$  and  $b_{n,\{+1\}} \in \mathbb{R}$ , and  $a_{n,\{-1\}} > 0$  and  $b_{n,\{-1\}} \in \mathbb{R}$ , for  $n = 1, 2, \dots$ , such that as  $n \rightarrow \infty$ ,*

$$n\mathbb{P} \left[ (|X| - b_{n,\{+1\}})/a_{n,\{+1\}} \in \cdot \mid X > 0 \right] \xrightarrow{v} \nu_{\{+1\}}(\cdot), \quad \text{in } M_+(\overline{\mathbb{E}}_{\xi_{\{+1\}}}), \quad (3)$$

and

$$n\mathbb{P} \left[ (|X| - b_{n,\{-1\}})/a_{n,\{-1\}} \in \cdot \mid X < 0 \right] \xrightarrow{v} \nu_{\{-1\}}(\cdot), \quad \text{in } M_+(\overline{\mathbb{E}}_{\xi_{\{-1\}}}). \quad (4)$$

(ii) *As  $n \rightarrow \infty$ ,*

$$n\mathbb{P} \left[ \left( \frac{|X| - r_n^b(X/|X|)}{r_n^a(X/|X|)}, X/|X| \right) \in \cdot \right] \xrightarrow{v} \nu(\cdot), \quad (5)$$

*in  $M_+(\overline{\mathbb{E}}^1)$ , where  $\overline{\mathbb{E}}^1 := (\overline{\mathbb{E}}_{\xi_{\{-1\}}} \times \{-1\}) \cup (\overline{\mathbb{E}}_{\xi_{\{+1\}}} \times \{+1\})$  and*

$$\nu = (1 - \pi)\nu_{\{-1\}} \delta_{-1} + \pi\nu_{\{+1\}} \delta_{+1}; \quad (6)$$

(iii) *As  $n \rightarrow \infty$ ,*

$$P_n \xrightarrow{w} P, \quad \text{in } M_p(\overline{\mathbb{E}}^1 \times (0, 1)),$$

*where  $P$  is Poisson point process with intensity measure*

$$\left[ \left\{ (1 + \xi_{\{-1\}}z)_+^{-1-1/\xi_{\{-1\}}} dz \right\} (1 - \pi) \delta_{-1}(dw) + \left\{ (1 + \xi_{\{+1\}}z)_+^{-1-1/\xi_{\{+1\}}} dz \right\} \pi \delta_{+1}(dw) \right] dt. \quad (7)$$

A proof is given in Appendix A.1. The unification presented in Theorem 1 has a simple interpretation in terms of superposition of random point measures. Under this framework, the sequences

$$P_n^+ = \sum_{i=1}^n \delta \left[ \left( \frac{|X_i| - b_{n,\{+1\}}}{a_{n,\{+1\}}}, \frac{i}{n+1} \right) \right] \mathbb{1}_{\{X_i > 0\}} \text{ and } P_n^- = \sum_{i=1}^n \delta \left[ \left( \frac{|X_i| - b_{n,\{-1\}}}{a_{n,\{-1\}}}, \frac{i}{n+1} \right) \right] \mathbb{1}_{\{X_i < 0\}},$$

weakly converge to independent Poisson point processes  $P^+$  and  $P^-$  with intensity measures  $\pi\nu_{\{+1\}}(dz)dt$  and  $(1 - \pi)\nu_{\{-1\}}(dz)dt$  on  $(\overline{\mathbb{E}}_{\xi_{\{+1\}}} \times \{+1\}) \times (0, 1)$  and  $(\overline{\mathbb{E}}_{\xi_{\{-1\}}} \times \{-1\}) \times (0, 1)$ , respectively. This follows directly from (3) and (4) and has a straightforward sampling interpretation. First, we sample  $n$  independent observations from each renormalised conditional distribution. Then, we apply a thinning operation to the resulting independent random point measures

whereby points are probabilistically removed based on the likelihood of observing a positive or negative value of  $X$ , conditionally on retaining  $n$  points in total. Consequently,  $P_n$  is seen as the superposition  $P_n^- + P_n^+$  of the two renormalised random point measures, leading to  $P_n \xrightarrow{w} P$  as  $n \rightarrow \infty$ , where  $P$  is a Poisson point process on the product space between the disjoint union  $(\overline{\mathbb{E}}_{\xi_{\{-1\}}} \times \{-1\}) \cup (\overline{\mathbb{E}}_{\xi_{\{+1\}}} \times \{+1\})$  and  $(0, 1)$ , with intensity measure (7).

Although Proposition (1) assumes  $0 \in \text{supp}(\mathbb{P}_X)$ , we can more generally consider directions relative to any point  $m \in \text{supp}(\mathbb{P}_X)$ , with  $|X - m|$ ,  $(X - m)/|X - m|$ , and  $X - m \leq 0$ , respectively replacing  $|X|$ ,  $X/|X|$ , and  $X \leq 0$ . The assumption  $0 \in \text{supp}(\mathbb{P}_X)$ , however, can be typically met by shifting the origin. While the definition of right and left extremes may vary depending on the application, for generic purposes it may be natural to take  $m$  as a point in  $\text{supp}(\mathbb{P}_X)$  which minimises a well defined measure of extremity relative to any other point in  $\text{supp}(\mathbb{P}_X)$ . For absolutely continuous distributions, whereby  $F_X(\{m\}) = 0$  for any  $m \in \text{supp}(\mathbb{P}_X)$ , there is always a unique such choice of  $m$  (the median of the univariate distribution) which uniquely maximises the population version of halfspace depth. Additionally, the assumption  $F_X(\{m\}) = 0$  can also be relaxed at the cost of adjusting the probabilities  $\pi$  and  $(1 - \pi)$  to new values  $\pi_+ > 0$  and  $\pi_- > 0$ , while ensuring that  $\pi_+ + F_X(\{m\}) + \pi_- = 1$ . In this case, if the median is not well defined, we can select a unique point such as the centroid of the set of values maximizing halfspace depth.

While such generalisations introduce no technical difficulties, here and throughout we opt for the simpler cases for clarity and ease of presentation. Thus, assuming  $0 \in \text{supp}(\mathbb{P}_X)$  with  $F_X(\{0\}) = 0$ , the connection between non-degenerate limit laws that facilitate a simultaneous description of right and left extremes relative to a centre, can be understood through the convergence of the joint distribution of the appropriately renormalised sample minima and maxima.

Let the sample minima and maxima be defined by  $m_n = \min_{i=1, \dots, n}(X_i)$  and  $M_n = \max_{i=1, \dots, n}(X_i)$ , respectively, and fix  $z_-$  and  $z_+$  such that  $-z_- \in \overline{\mathbb{E}}_{\xi_{\{-1\}}}$  and  $z_+ \in \overline{\mathbb{E}}_{\xi_{\{+1\}}}$ . First, we have the relation

$$\mathbb{P} \left( \frac{m_n + b_{n, \{-1\}}}{a_{n, \{-1\}}} > z_-, \frac{M_n - b_{n, \{+1\}}}{a_{n, \{+1\}}} < z_+ \right) = \mathbb{P} (a_{n, \{-1\}} z_- - b_{n, \{-1\}} < X < a_{n, \{+1\}} z_+ + b_{n, \{+1\}})^n.$$

The right-hand side of this relation can be rewritten as

$$\left[ 1 - \frac{1}{n} \{ 1 - \mathbb{P} (a_{n, \{-1\}} z_- - b_{n, \{-1\}} < X < a_{n, \{+1\}} z_+ + b_{n, \{+1\}}) \} \right]^n =: \left[ 1 - \frac{1}{n} n \overline{\mathbb{P}}_n \right]^n, \quad (8)$$

and thus, if  $n \overline{\mathbb{P}}_n$  converges to a non-trivial limit function, then the joint distribution of the renormalised sample minima and maxima converges weakly to a non-degenerate limit distribution.

Assuming convergences (3) and (4) hold, the justification given in Appendix A.2 shows that

$$\lim_{n \rightarrow \infty} \mathbb{P} \left( \frac{m_n + b_{n, \{-1\}}}{a_{n, \{-1\}}} > z_-, \frac{M_n - b_{n, \{+1\}}}{a_{n, \{+1\}}} < z_+ \right) = G_0(-z_-, z_+ | 1 - \pi, \pi), \quad \text{as } n \rightarrow \infty, \quad (9)$$

at continuity points of the limit distribution  $G_0$ , where

$$G_0(-z_-, z_+ | \pi) = \exp[- \{ (1 - \pi) \Lambda_{\{-1\}}(-z_-) + \pi \Lambda_{\{+1\}}(z_+) \} | 1 - \pi, \pi]. \quad (10)$$

Here, we note that one always have the flexibility to change the probability mass function  $(1 - \pi, \pi)$  in (10) to any (not necessarily probability) mass function, through suitable changes in the renormalisation. This can be seen from the fact that for any  $\lambda_-, \lambda_+ > 0$ , we have

$$G_0(-z_-, z_+ | \pi, 1 - \pi) = G_0 \left( -\frac{z_- - \mu_-(1 - \pi, \lambda_-)}{\sigma_-(1 - \pi, \lambda_-)}, \frac{z_+ - \mu_+(\pi, \lambda_+)}{\sigma_+(\pi, \lambda_+)} \mid \lambda_-, \lambda_+ \right)$$

where  $\mu_{\text{sgn}}(x, y) = \{(y/x)^{\xi_{\text{sgn}}} - 1\}/\xi_{\text{sgn}}$  and  $\sigma_{\text{sgn}}(x, y) = (y/x)^{\xi_{\text{sgn}}}$ , for  $x, y > 0$  and  $\text{sgn} \in \{-, +\}$ . Thus, if (9) holds true, then a suitable adaptation of the normalizing constants yields

$$\lim_{n \rightarrow \infty} \mathbb{P} \left( \frac{m_n + b_{n,\{-1\}}^*}{a_{n,\{-1\}}^*} > z_-, \frac{M_n - b_{n,\{+1\}}^*}{a_{n,\{+1\}}^*} < z_+ \right) = G_0(-z_-, z_+ | \lambda_-, \lambda_+), \quad \text{as } n \rightarrow \infty, \quad (11)$$

where

$$b_{n,\text{sgn}}^* = b_{n,\text{sgn}} + \mu_{\text{sgn}}(\pi_{\text{sgn}}, \lambda_{\text{sgn}})a_{n,\text{sgn}} \quad \text{and} \quad a_{n,\text{sgn}}^* = \sigma_{\text{sgn}}(\pi_{\text{sgn}}, \lambda_{\text{sgn}})a_{n,\text{sgn}}, \quad (12)$$

with  $\pi_- = 1 - \pi$  and  $\pi_+ = \pi$ . These steps, alongside the conditions set out in Theorem 1, lead to an extremal types theorem for left and right extremes, presented below by Proposition 1.

**Proposition 1.** *If for some constants  $c_n$  and  $d_n > 0$ , and  $\gamma_n$  and  $\delta_n > 0$ , we have*

$$\mathbb{P} \left( \frac{m_n + \gamma_n}{\delta_n} > z_-, \frac{M_n - c_n}{d_n} < z_+ \right) \xrightarrow{w} G(-z_-, z_+), \quad \text{as } n \rightarrow \infty,$$

for some distribution  $G$ , with non-degenerate margins, then  $G$  is of the same type as  $G_0$  with  $\pi = 1/2$ , that is, there exist location and scale parameters  $\mu_+$  and  $\sigma_+ > 0$ , and  $\mu_-$  and  $\sigma_- > 0$ , such that  $G(-z_-, z_+) = G_0(-(z_- - \mu_-)/\sigma_-, (z_+ - \mu_+)/\sigma_+ | 1/2)$ . Conversely, a distribution function of the same type as  $G_0$  with  $\pi = 1/2$  can appear as such a limit.

The proof of Proposition 1 follows closely the proof of the classical extremal types theorem presented in Section 1.4 in [Leadbetter et al. \(1983\)](#) and is omitted for brevity. However, the form of  $G$  in Proposition 1 has an instructive interpretation: since  $m_n = -\max_{i=1, \dots, n}(-X_i)$ , it follows at once that  $G$  arises as the limiting cumulative distribution function of the appropriately renormalised component-wise sample-maxima of the random sample  $\{(-X_i, X_i) : i = 1, \dots, n\}$ . Thus,  $G$  is a bivariate max-stable distribution, which is confirmed by the identity

$$G(-z_-, z_+)^s = G \left( -\frac{z_- - \mu_{-,s}}{\sigma_{-,s}}, \frac{z_+ - \mu_{+,s}}{\sigma_{+,s}} \right), \quad \text{for any } s > 0, \quad (13)$$

where  $\mu_{\text{sgn},s} = \mu_{\text{sgn}} + \{(s^{\xi_{\text{sgn}}} - 1)/\xi_{\text{sgn}}\}\sigma_{\text{sgn}}$  and  $\sigma_{\text{sgn},s} = s^{\xi_{\text{sgn}}}\sigma_{\text{sgn}}$ . Furthermore, Theorem 1 shows that ultimately, the renormalised sample minima and maxima become independent since  $G(-z_-, z_+) = G_-(-z_-)G_+(z_+)$ , where the marginals of  $G$ , defined by  $G_+(z_+) := G(\infty, z_+)$  and  $G_-(z_-) := G(z_-, \infty)$ , are both generalised extreme value distributions, corresponding to the limiting non-degenerate 1-dimensional distributions of the appropriately renormalised sample maxima drawn from the distribution of  $X$  and  $-X$ , respectively.

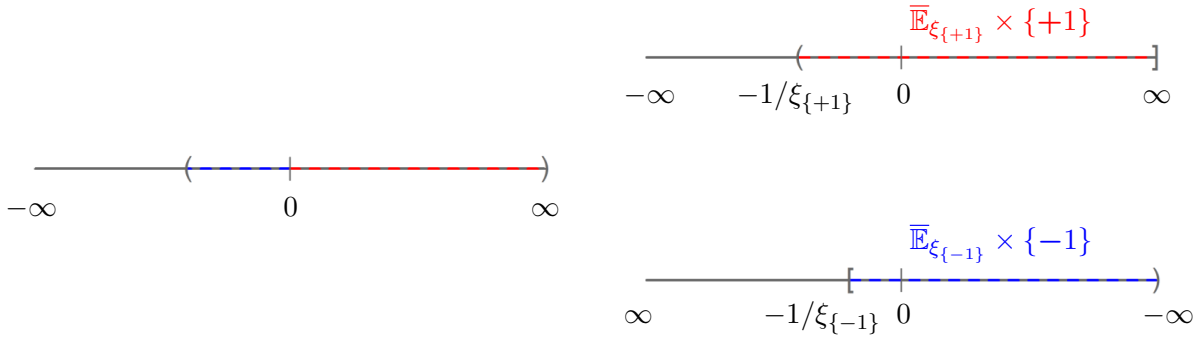


Figure 3: Illustration of  $\bar{\mathbb{E}}_{\xi_{\{+1\}}} \times \{+1\}$  and  $\bar{\mathbb{E}}_{\xi_{\{-1\}}} \times \{-1\}$  using a probability distribution on  $\mathbb{R}$  associated with a random variable  $X$ . In this example, the probability distribution is assumed to have a bounded left lower tail ( $\xi_{\{-1\}} < 0$ ) and a heavy upper tail ( $\xi_{\{+1\}} > 0$ ). The support of  $\mathbb{P}_X$ , containing 0, is the union of the coloured segments shown in the left panel. The red and blue segments, corresponding to positive and negative values of  $X$ , are mapped to  $\bar{\mathbb{E}}_{\xi_{\{+1\}}}$  and  $\bar{\mathbb{E}}_{\xi_{\{-1\}}}$ , respectively, and are oriented according to  $\{+1\}$  and  $\{-1\}$  in the right panel.

While the limiting Poisson point process in Proposition 1 guarantees the convergence of the joint distribution of renormalised sample maxima and minima, as illustrated in Proposition 1, it also yields non-degenerate limiting distributions for suitably rescaled excesses above direction-dependent thresholds. Specifically, we have that as  $q \rightarrow 1$

$$\mathbb{P} \left[ \frac{|X| - r_{1/(1-q)}^a(X/|X|)}{r_{1/(1-q)}^b(X/|X|)} < z, X/|X| = w \mid |X| > r_{1/(1-q)}^a(X/|X|) \right] \xrightarrow{w} H_w(z) f_{X/|X|}(w), \quad z > 0,$$

where  $H_w(y) = 1 - (1 + \xi_w z)_+^{-1/\xi_w}$  is the cumulative distribution function of the standard generalised Pareto distribution with shape parameter  $\xi_w$  and  $f_{X/|X|}(w) = \pi \mathbb{1}_{w \in \{+1\}} + (1 - \pi) \mathbb{1}_{w \in \{-1\}}$ .

We conclude this section by discussing a practical method for identifying candidates for the functions  $r_n^a$  and  $r_n^b$ , and a connection between them, and the transformation  $x \mapsto 2F_X(x) - 1$  based on the *centre-outward distribution function*  $2F_X - 1$ , which pushes  $\mathbb{P}_X$  forward to the uniform distribution on  $(-1, 1)$ , and can be naturally generalised to multivariate distributions (Hallin et al. 2021); see Section 2.4 for a discussion of this transformation to the multivariate setting.

Let  $R = |X|$  and  $W = X/|X|$ . A necessary and sufficient condition for the convergence of each summand in (A.2) is that the functions  $r_n^a$  and  $r_n^b$  in Theorem 1 satisfy

$$\lim_{n \rightarrow \infty} \frac{U_w(nx) - r_n^b(w)}{r_n^a(w)} = \frac{x^{\xi_w} - 1}{\xi_w}, \quad x > 0, \quad (14)$$

where  $U_w(1/(1-q)) = F_{R|W}^{-1}(q | w)$  for  $q \in (0, 1)$ . When the function  $U_w$  satisfies (14), then it follows that we can take without loss of generality,

$$r_n^b(w) = U_w(n), \quad \text{and} \quad r_n^a(w) = U_w(n(1 + \xi_w)^{1/\xi_w}) - U_w(n) \quad \text{whenever } \xi_w \geq -1. \quad (15)$$

This provides with a practical method for finding these functions and neatly shows how information

from the directional variable is encoded in the normalizing constants through the conditional quantile function, which captures the extremity of a point away from  $0 \in S$ , and the probability mass function of the direction, which reflects the propensity to observe right or left extremes.

These two elements carry essential information about  $\mathbb{P}_X$ , which can also be expressed via the centre-outward distribution function. By applying total probability, we obtain the relation

$$2F_X(x) - 1 = \pi [2F_{R|W}(x | 1) - 1] + (1 - \pi) [2\{1 - F_{R|W}(-x | -1)\} - 1], \quad (16)$$

explicitly showing the one-to-one correspondence between the centre-outward distribution function and  $F_{R|W}$  and  $f_W$ , or equivalently,  $F_{R|W}^{-1}$  and  $f_W$ . The centre-outward quantile function  $Q_{\pm} : (-1, 1) \rightarrow \mathbb{R}$  is obtained by inverting  $2F_X(x) - 1 = u$ , with  $u \in (-1, 1)$ . Assuming that the median of the distribution exists and is unique, with 0 corresponding to this median, so that  $\pi = 1/2$ , then (16) gives

$$Q_{\pm}(u) = [F_{R|W}^{-1}(|u| | u/|u|)](u/|u|).$$

The sets

$$C_q = [-F_{R|W}^{-1}(q | -1), +F_{R|W}^{-1}(q | +1)], \quad q \in (0, 1),$$

have the interpretation of *quantile regions* in the sense that  $\mathbb{P}(X \in C_q) = q$  and form a sequence of closed, connected, and nested sets. Similarly, the boundaries of these quantile regions

$$\partial C_q = \{-F_{R|W}^{-1}(q | -1), +F_{R|W}^{-1}(q | +1)\}, \quad q \in (0, 1),$$

have the interpretation of *quantile contours*.

The key advantage of the centre-outward distribution and its associated quantile function compared to traditional quantiles based on the distribution function  $F_X$ , is that it does not rely on the total ordering of  $\mathbb{R}$ . This makes the centre-outward approach much more flexible, as it naturally extends to higher dimensions, where no such total order exist, and is particularly useful for generalizing concepts like quantiles and probability integral transformations in multivariate settings (Hallin et al. 2021). As we move to higher dimensions, however, the relationship of the centre-outward distribution and the conditional quantile function becomes less direct, with additional complexities arising due to the structure of probability distributions on higher-dimensional spaces. Both approaches, working with the conditional distribution of  $R | W$  and the directional variable  $W$ , or with the multivariate analogue of the centre-outward distribution function, offer complementary insights and each viewpoint has its own strengths. The former emphasises how extremes behave relative to fixed directions alongside knowing the frequency of the directions, while the latter provides a broader geometric interpretation of data spread and balance via measure transportation to a target reference distribution.

In Section 2.4, we explore these perspectives in more detail, highlighting their relative strengths and weaknesses in the context of extreme values. By adopting the approach of transforming a random element  $\mathbf{X}$ , arising from a distribution  $\mathbb{P}_{\mathbf{X}}$ , into polar coordinates relative to the centre  $\mathbf{0}$  which is assumed to be an element of  $\text{supp}(\mathbb{P}_{\mathbf{X}})$ , and by using the conditional quantile function, we

introduce a novel definition of quantile sets that closely parallels the quantile regions and quantile contours of [Hallin et al. \(2021\)](#), but has the added benefit of being easily amenable to extrapolation beyond the observed data. Specifically, our definition facilitates the development of new refined limit theory for multivariate extremes via the powerful convergence to the Poisson point process, in a manner akin to the univariate case presented in this section. In Section 2.3 below, we present this theory and establish key properties of the distribution of the limit Poisson point process in association with the renormalisation of the radial component.

### 2.3 Weak convergence to a Poisson point process

In the multivariate setting, a natural extension of convergences (3) and (4) can be obtained by requiring location and scale functions of the direction  $b_n : \mathbb{S}^{d-1} \rightarrow \mathbb{R}_+$  and  $a_n : \mathbb{S}^{d-1} \rightarrow \mathbb{R}_+$ , respectively, and a function  $\xi : \mathbb{S}^{d-1} \rightarrow \mathbb{R}$ , such that as  $n \rightarrow \infty$ ,

$$\nu_{n,\mathbf{w}}(\cdot) := n \mathbb{P} \left( \frac{\|\mathbf{X}\| - b_n(\mathbf{X}/\|\mathbf{X}\|)}{a_n(\mathbf{X}/\|\mathbf{X}\|)} \in \cdot \mid \mathbf{X}/\|\mathbf{X}\| = \mathbf{w} \right) \xrightarrow{v} \nu_{\mathbf{w}}(\cdot) \quad \text{in } M_+(\overline{\mathbb{E}}_{\xi(\mathbf{w})}), \quad \mathbb{P}_{\mathbf{X}/\|\mathbf{X}\|} - a.e., \quad (17)$$

where the limit measure  $\nu_{\mathbf{w}}$  satisfies  $\Lambda_{\xi(\mathbf{w})}(z) = [1 + \xi(\mathbf{w})z]_+^{-1/\xi(\mathbf{w})}$ , with  $\Lambda_{\xi(\mathbf{w})}(z) := \nu_{\mathbf{w}}(z, \sup \mathbb{E}_{\xi(\mathbf{w})}]$ . Unlike the univariate setting, however, where the set of permissible directions is finite – hence the interchange between the limit as  $n \rightarrow \infty$  and the sum over the set of directions in the proof of Theorem 1 is legitimate – in the multivariate setting we have a continuum of directions and convergence (17) alone is not sufficient to guarantee that the mean measure

$$\nu_n(\cdot) := n \mathbb{P} \left[ \left( \frac{\|\mathbf{X}\| - b_n(\mathbf{X}/\|\mathbf{X}\|)}{a_n(\mathbf{X}/\|\mathbf{X}\|)}, \mathbf{X}/\|\mathbf{X}\| \right) \in \cdot \right] \quad (18)$$

vaguely converges in  $M_+(\overline{\mathbb{E}}^d)$  to a non-degenerate limit mean measure  $\nu$ , a condition that is necessary and sufficient for the sequence of renormalised random point measures

$$P_n := \sum_{i=1}^n \delta \left[ \frac{\|\mathbf{X}_i\| - b_n(\mathbf{X}_i/\|\mathbf{X}_i\|)}{a_n(\mathbf{X}_i/\|\mathbf{X}_i\|)}, \mathbf{X}_i/\|\mathbf{X}_i\|, \frac{i}{n+1} \right], \quad n = 1, 2, \dots, \quad (19)$$

to weakly converge in  $M_p(\overline{\mathbb{E}}^d)$  to a non-degenerate Poisson point process  $P$ . Here, the space  $\overline{\mathbb{E}}^d$  is defined in a similar manner to the space  $\overline{\mathbb{E}}$  in Theorem 1, through the disjoint union

$$\overline{\mathbb{E}}^d := \bigcup_{\mathbf{w} \in \text{supp}(\mathbb{P}_{\mathbf{X}/\|\mathbf{X}\|})} (\overline{\mathbb{E}}_{\xi(\mathbf{w})} \times \{\mathbf{w}\}) \subset (-\infty, \infty] \times \mathbb{S}^{d-1}$$

of the family of sets  $(\overline{\mathbb{E}}_{\xi(\mathbf{w})} : \mathbf{w} \in \text{supp}(\mathbb{P}_{\mathbf{X}/\|\mathbf{X}\|}))$ , and each space  $\overline{\mathbb{E}}_{\xi(\mathbf{w})} \times \{\mathbf{w}\} = \{(z, \mathbf{w}) : z \in \overline{\mathbb{E}}_{\xi(\mathbf{w})}\}$  is interpreted as a subset of the extended real line, passing through the origin and oriented in the direction of the unit vector  $\mathbf{w}$ . For simplicity and to avoid overloading the notation, we do not explicitly show the dependence of the space  $\overline{\mathbb{E}}^d$  on the distribution  $\mathbb{P}_{\mathbf{X}}$ , although this dependence is inherent in its definition. An illustration of this construction is presented in Figure 3.

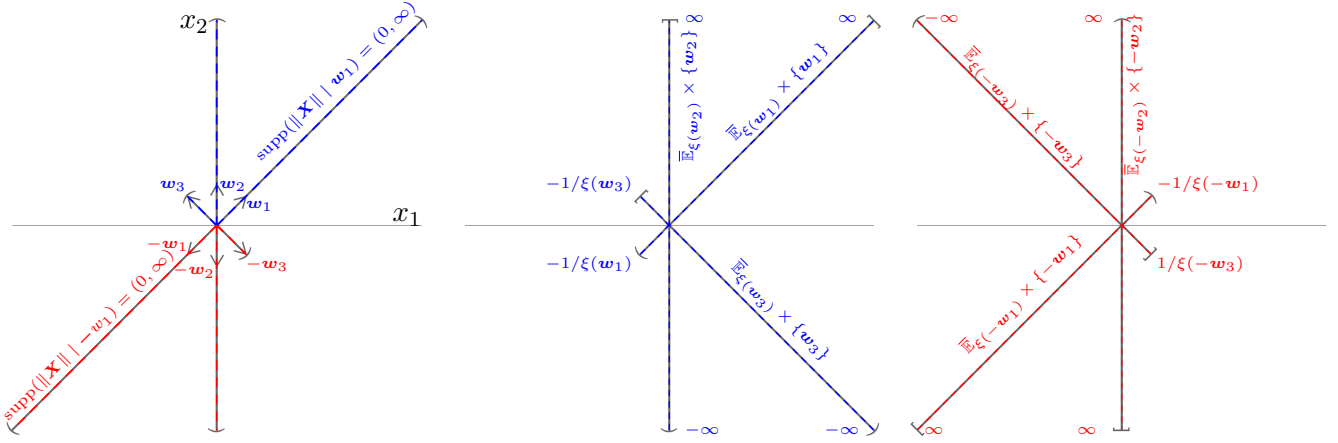


Figure 4: Illustration of a subset of  $\overline{\mathbb{E}}^2$  using a probability distribution on  $\mathbb{R}^2$  associated with a random variable  $\mathbf{X}$  whose support contains  $\mathbf{0}$ . The subset of  $\overline{\mathbb{E}}^2$  is based on the set of directions  $\{\mathbf{w}_1, \mathbf{w}_2, \mathbf{w}_3, -\mathbf{w}_1, -\mathbf{w}_2, -\mathbf{w}_3\}$ , shown in the left panel. In this example, the conditional probability distribution of  $\|\mathbf{X}\| \mid \{\mathbf{X}/\|\mathbf{X}\| = \mathbf{w}\}$  is assumed to have a bounded upper tail ( $\xi(\mathbf{w}) < 0$ ) for  $\mathbf{w} \in \{-\mathbf{w}_1, -\mathbf{w}_3\}$ , a light upper tail ( $\xi(\mathbf{w}) = 0$ ) for  $\mathbf{w} \in \{\mathbf{w}_2, -\mathbf{w}_2\}$  and a heavy upper tail ( $\xi(\mathbf{w}) > 0$ ) for  $\mathbf{w} \in \{\mathbf{w}_1, -\mathbf{w}_1\}$ . The red and blue segments, corresponding to directions  $\mathbf{w}$  and  $-\mathbf{w}$  are mapped to  $\overline{\mathbb{E}}_{\xi(\mathbf{w})}$  and  $\overline{\mathbb{E}}_{\xi(-\mathbf{w})}$ , respectively, and are oriented according to  $\mathbf{w}$  and  $-\mathbf{w}$  in the centre and right panels.

In Assumption 1 below, we strengthen convergence (17) by assuming that the total variation of the signed measure

$$\mu_{n,\mathbf{w}}(\cdot) := n \mathbb{P} \left( \frac{\mathbf{X} - b_n(\mathbf{X}/\|\mathbf{X}\|)}{a_n(\mathbf{X}/\|\mathbf{X}\|)} \in \cdot \mid \mathbf{X}/\|\mathbf{X}\| = \mathbf{w} \right) - \nu_{\mathbf{w}}(\cdot), \quad \mathbf{X} \sim \mathbb{P}_{\mathbf{X}}, \quad (20)$$

is bounded on compact intervals by a function that is integrable with respect to  $\mathbb{P}_{\mathbf{X}/\|\mathbf{X}\|}$ .

**Assumption 1.** *The distribution  $\mathbb{P}_{\mathbf{X}}$  satisfies (17) and there exists a  $\mathbb{P}_{\mathbf{X}/\|\mathbf{X}\|}$ -integrable function  $\Delta : \mathbb{S}^{d-1} \rightarrow \mathbb{R}$ , such that for any  $-\infty < r_{\text{inf}} \leq r_{\text{sup}} \leq \infty$ , there exists  $n_0 = n_0(r_{\text{inf}}, r_{\text{sup}})$  such that*

$$\int_{r_{\text{inf}}}^{r_{\text{sup}}} |\mu_{n,\mathbf{w}}|(dz) \leq \Delta(\mathbf{w}), \quad \text{for all } n \geq n_0,$$

where  $|\mu_{n,\mathbf{w}}|(\cdot) = \mu_{n,\mathbf{w}}^+(\cdot) + \mu_{n,\mathbf{w}}^-(\cdot)$  denotes the total variation measure of  $\mu_{n,\mathbf{w}}$  defined in (20).

The bounding function  $\Delta$  introduced in Assumption 1 serves as dominating function, ensuring sufficient regularity for the vague convergence of  $\nu_n$  to  $\nu$  in  $M_+(\overline{\mathbb{E}}^d)$ , or equivalently, the weak convergence of  $P_n$  to  $P$  in  $M_p(\overline{\mathbb{E}}^d \times (0, 1))$ , as established below in Theorem 2. The function  $\Delta$  need not in general be bounded and may exhibit singularities, meaning that the convergence of  $\nu_n$  need not be uniform on  $\text{supp}(\mathbb{P}_{\mathbf{X}/\|\mathbf{X}\|})$ . On the other hand, when  $\Delta$  is bounded then the convergence is uniform on  $\text{supp}(\mathbb{P}_{\mathbf{X}/\|\mathbf{X}\|})$ .

With Assumption 1 in place, we are now in position to state our main theorem, namely Theorem 2, which concerns the asymptotic behaviour of the radial and directional variables, expressed in terms of a limit Poisson point process, after suitably renormalizing the radius using location

and scale functions of the direction, while preserving the directional variable.

**Theorem 2.** *Let  $\{\mathbf{X}_i : i = 1, \dots, n\}$  be a random sample from  $\mathbb{P}_{\mathbf{X}}$ , where  $\mathbb{P}_{\mathbf{X}}$  satisfies Assumption 1 with  $\mathbf{0} \in \text{supp}(\mathbb{P}_{\mathbf{X}})$ .*

(i) *As  $n \rightarrow \infty$ ,  $\nu_n(\cdot) \xrightarrow{v} \nu(\cdot)$  in  $M_+(\overline{\mathbb{E}}^d)$ , where the limit measure  $\nu$  satisfies*

$$\nu(h) = \iint_{\overline{\mathbb{E}}^d} h(z, \mathbf{w}) \nu_{\mathbf{w}}(dz) \mathbb{P}_{\mathbf{X}/\|\mathbf{X}\|}(d\mathbf{w}),$$

(ii) *As  $n \rightarrow \infty$ ,*

$$P_n \xrightarrow{w} P \quad \text{in } M_p(\overline{\mathbb{E}}^d \times (0, 1)), \quad (21)$$

*where  $P$  is a Poisson point process with intensity measure*

$$\left( [1 + \xi(\mathbf{w})z]_+^{-1-1/\xi(\mathbf{w})} dz \mathbb{P}_{\mathbf{X}/\|\mathbf{X}\|}(d\mathbf{w}) \right) dt.$$

A proof is given in Appendix A.3. Theorem 2, which covers Theorem 1 as a special case, provides a foundation for new asymptotic theory associated with the probabilistic behaviour of multivariate extremes, leading to new insights that stem from limit laws which parallel those typically appearing in extreme value theory, namely the limit laws associated with the renormalised component-wise maxima,  $r$ -largest order statistics and exceedances above high thresholds.

Building on the argument presented in Appendix A.2, Proposition 2 establishes a new limit law from the the void probability of the limit Poisson point process  $P$  in Theorem 2 and naturally generalises Proposition 1, covering the situation where in the limit as  $n \rightarrow \infty$ , all atoms of the renormalised random point measure  $P_n$  fall in a set.

**Proposition 2.** *Let  $\{\mathbf{X}_i : i = 1, \dots, n\}$  be a sequence of independent and identically distributed random variables from  $\mathbb{P}_{\mathbf{X}}$ , where  $\mathbb{P}_{\mathbf{X}}$  satisfies Assumption 1. Then*

$$\mathbb{P} \left[ \left\{ \left( \frac{\|\mathbf{X}_i\| - b_n(\mathbf{X}_i/\|\mathbf{X}_i\|)}{a_n(\mathbf{X}_i/\|\mathbf{X}_i\|)}, \mathbf{X}_i/\|\mathbf{X}_i\| \right) \in B : i = 1, \dots, n \right\} \right] \xrightarrow{w} e^{-\Lambda(B)} \quad \text{in } M_1(\overline{\mathbb{E}}^d), \quad (22)$$

*as  $n \rightarrow \infty$ , where  $\Lambda(B) := \nu((\overline{\mathbb{E}}^d \setminus B) \times (0, 1))$ .*

Unlike the univariate case, the limit law in Proposition 2 is not solely tied to the convergence of renormalised *component-wise* maxima or minima, but encompasses a broader range of scenarios. It can be seen as a special case of Proposition 3, which covers the situation where in the limit as  $n \rightarrow \infty$ , all but finitely many atoms of the renormalised random point measure  $P_n$  fall in a set.

**Proposition 3.** *Let  $\{\mathbf{X}_i : i = 1, \dots, n\}$  be a sequence of independent and identically distributed random variables from  $\mathbb{P}_{\mathbf{X}}$ , where  $\mathbb{P}_{\mathbf{X}}$  satisfies Assumption 1. Then for any  $r = 1, 2, \dots$ ,*

$$\mathbb{P} \left[ \sum_{i=1}^n 1 \left\{ \left( \frac{\|\mathbf{X}_i\| - b_n(\mathbf{X}_i/\|\mathbf{X}_i\|)}{a_n(\mathbf{X}_i/\|\mathbf{X}_i\|)}, \mathbf{X}_i/\|\mathbf{X}_i\| \right) \in B \right\} = n - r + 1 \right] \xrightarrow{w} e^{-\Lambda(B)} \sum_{k=0}^{r-1} \frac{\Lambda(B)^k}{k!} \quad \text{in } M_1(\overline{\mathbb{E}}^d), \quad (23)$$

as  $n \rightarrow \infty$ , where  $\Lambda(B) := \nu((\overline{\mathbb{E}}^d \setminus B) \times (0, 1))$ .

Finally, Proposition 4 focuses on exceedances above directionally-dependent thresholds. It establishes weak convergence in  $M_1(\overline{\mathbb{E}}_+^d)$ , the subset of  $\overline{\mathbb{E}}^d$  restricted to positive elements, that is,

$$\overline{\mathbb{E}}_+^d := \bigcup_{\mathbf{w} \in \text{supp}(\mathbb{P}_{\mathbf{X}/\|\mathbf{X}\|})} ((0, \sup \overline{\mathbb{E}}_{\xi(\mathbf{w})}] \times \{\mathbf{w}\}) \subset \overline{\mathbb{E}}^d.$$

Note that for any  $\xi \in \mathbb{R}$ , 0 is an interior point of  $\overline{\mathbb{E}}_{\xi}$  and thus,  $\overline{\mathbb{E}}_+^d$  is non-empty a.s.. This result highlights the role of thresholds  $b_{1/(1-q)}(\mathbf{X}/\|\mathbf{X}\|)$  and demonstrates how the Poisson point process characterisation extends to such exceedances.

**Proposition 4.** *Let  $\mathbf{X} \sim \mathbb{P}_{\mathbf{X}}$  where  $\mathbb{P}_{\mathbf{X}}$  satisfies Assumption 1. Then*

$$\mathbb{P} \left[ \left( \frac{\|\mathbf{X}\| - b_{1/(1-q)}(\mathbf{X}/\|\mathbf{X}\|)}{a_{1/(1-q)}(\mathbf{X}/\|\mathbf{X}\|)}, \mathbf{X}/\|\mathbf{X}\| \right) \in A \mid \|\mathbf{X}\| > b_{1/(1-q)}(\mathbf{X}/\|\mathbf{X}\|) \right] \xrightarrow{w} \Lambda(\overline{\mathbb{E}}^d \setminus A) \text{ in } M_1(\overline{\mathbb{E}}_+^d),$$

as  $q \rightarrow 1$ , where  $\Lambda(\overline{\mathbb{E}}^d \setminus A) := \nu(A \times (0, 1))$ .

We note that the limit distribution that appears in Proposition 4 is directly expressed in terms of  $\Lambda$  and not in terms of the ratio

$$\frac{\Lambda(\overline{\mathbb{E}}^d \setminus A)}{\Lambda(\overline{\mathbb{E}}^d \setminus \overline{\mathbb{E}}_+^d)} = \frac{\nu(A \times (0, 1))}{\nu(\overline{\mathbb{E}}_+^d \times (0, 1))},$$

because the restriction of  $\nu$  on  $\overline{\mathbb{E}}_+^d \times (0, 1)$  is a probability measure, satisfying  $\nu(\overline{\mathbb{E}}_+^d \times (0, 1)) = 1$ .

These propositions provide a cohesive narrative. They demonstrate how the Poisson point process framework captures multivariate extremes through void probabilities, order statistics, and threshold exceedances. Each result expands upon the classical extreme value theory, offering new insights into the structure and behaviour of multivariate extremes.

In a similar manner to that explained in Section 2.2, one has the flexibility to change the measure  $\mathbb{P}_{\mathbf{X}/\|\mathbf{X}\|}$  in the definition of  $\nu$  in Theorem 2. Here, the intuition is that by applying admissible perturbations in the norming constants  $b_{1/(1-q)}$  and  $a_{1/(1-q)}$ —adjustments that preserve weak convergence under a convergence-to-types argument—alternative norming sequences  $b_{1/(1-q)}^*$  and  $a_{1/(1-q)}^*$  can be selected. Such modifications act on the limit point measure  $\nu$  by thinning it at loci of high directional density and densifying it at loci of low directional density, so that the directional cross-section for the resulting radial-directional intensity is constant. This is explained below in Remark 1.

**Remark 1.** *The probability measure  $\mathbb{P}_{\mathbf{X}/\|\mathbf{X}\|}$  in the definition of  $\nu$  can be changed to some other spherical (not necessarily probability) measure, through suitable changes in the renormalisation. For example, if  $\mathbb{P}_{\mathbf{X}/\|\mathbf{X}\|}$  is mutually absolutely continuous with respect to a probability measure  $\mu$*

on  $\text{supp}(\mathbb{P}_{\mathbf{X}})$ , then the sequence of renormalised random point measures

$$P_n^* := \sum_{i=1}^n \delta \left[ \frac{\|\mathbf{X}_i\| - b_n(\mathbf{X}_i/\|\mathbf{X}_i\|; \mu)}{a_n(\mathbf{X}_i/\|\mathbf{X}_i\|; \mu)}, \mathbf{X}_i/\|\mathbf{X}_i\|, \frac{i}{n+1} \right], \quad n = 1, 2, \dots,$$

converges weakly to  $P^*$  in  $M_p(\overline{\mathbb{E}}^d \times (0, 1))$ , with  $P^*$  a Poisson point process having intensity measure

$$([\{1 + \xi(\mathbf{w})z\}_+^{-1-1/\xi(\mathbf{w})} dz] \mu(d\mathbf{w})) dt,$$

as  $n \rightarrow \infty$ , whenever

$$b_n(\mathbf{w}; \mu) \sim b_n(\mathbf{w}) + [\{\varrho_\mu(\mathbf{w})^{\xi(\mathbf{w})} - 1\}/\xi(\mathbf{w})] a_n(\mathbf{w}), \quad \text{and} \quad (24)$$

$$a_n(\mathbf{w}; \mu) \sim \varrho_\mu(\mathbf{w})^{\xi(\mathbf{w})} a_n(\mathbf{w}), \quad (25)$$

as  $n \rightarrow \infty$ , where  $\varrho_\mu := d\mathbb{P}_{\mathbf{W}}/d\mu$  denotes the Radon–Nikodym derivative of  $\mathbb{P}_{\mathbf{W}}$  with respect to  $\mu$ .

Building on Remark 1, below in Remark 2 we construct a non-linear renormalisation of the exceedances, using the 1-dimensional probability integral transform, producing a limit uniform distribution over the unit ball. This distribution is defined by the product of the uniform distribution over the unit interval of distances to the origin with the uniform distribution over the unit sphere.

**Remark 2.** If  $\|\cdot\|$  denotes the Euclidean norm and  $\mathbb{P}_{\mathbf{X}/\|\mathbf{X}\|}$  is absolutely continuous with respect to the spherical Lebesgue measure, with positive density  $f_{\mathbf{X}/\|\mathbf{X}\|}(\mathbf{w})$ , then

$$(\mathbf{X}/\|\mathbf{X}\|) \mid \{\|\mathbf{X}\| > b_{1/(1-q)}^*(\mathbf{X}/\|\mathbf{X}\|)\}$$

converges in distribution as  $q \rightarrow 1$  to a random variable that follows the uniform distribution on  $\mathbb{S}^{d-1}$ . Here,  $b_n^*(\mathbf{w}) := b_n(\mathbf{w}; \mu^*)$  with  $\mu^*$  being the uniform probability measure on  $\mathbb{S}^{d-1}$ .

Additionally, let  $H_{\mathbf{w}}$  denoting the cumulative distribution function of the standard generalised Pareto distribution with shape parameter  $\xi(\mathbf{w})$ , and define  $a_n^*(\mathbf{w}) = a_n(\mathbf{w}; \mu^*)$ . Then,

$$\left( H_{\mathbf{X}/\|\mathbf{X}\|} \left[ \frac{\|\mathbf{X}\| - b_{1/(1-q)}^*(\mathbf{X}/\|\mathbf{X}\|)}{a_{1/(1-q)}^*(\mathbf{X}/\|\mathbf{X}\|)} \right], \mathbf{X}/\|\mathbf{X}\| \right) \mid \{\|\mathbf{X}\| > b_{1/(1-q)}^*(\mathbf{X}/\|\mathbf{X}\|)\}, \quad \text{as } n \rightarrow \infty,$$

converges in distribution to a random variable following the uniform distribution over the unit ball.

Similarly to the normalising functions (15) in Section 2.2, the functions  $a_n$  and  $b_n$  satisfy

$$b_n(\mathbf{w}) = U_{\mathbf{w}}(n), \quad \text{and} \quad a_n(\mathbf{w}) = U_{\mathbf{w}}(n(1 + \xi(\mathbf{w}))^{1/\xi(\mathbf{w})}) - U_{\mathbf{w}}(n) \quad \text{whenever } \xi(\mathbf{w}) > -1.$$

where  $U_{\mathbf{w}}(1/(1-q)) = F_R^{-1} \mid_{\mathbf{W}}(q \mid \mathbf{w})$ , for  $\mathbf{w} \in \mathbb{S}^{d-1}$ .

In the subsequent Sections 2.4 and 2.5, we discuss these sequences and their link to novel sets offering insightful risk representations in more details.

## 2.4 Correspondence between norming functions and probability sets

Extending the concept of quantiles to probability distributions on spaces beyond the ordinary real line is still being recognised as a major challenge, with apparent difficulties in its formulation. Chernozhukov et al. (2017) ingeniously used measure transportation maps between a distribution of interest on  $\mathbb{R}^d$  and a reference distribution on the  $d$ -dimensional unit ball, to define a new depth concept, termed the *Monge-Kantorovich* depth, which specialises to halfspace depth when  $d = 1$ . Based on this approach, and by leveraging the theory of McCann (1995), Hallin et al. (2021) proposed a *centre-outward* definition of multivariate distributions and quantile functions, along with their empirical counterparts, which is free of any moment assumptions. Central to the aforementioned line of research is the existence of a  $\mathbb{P}_{\mathbf{X}}$ -a.e. unique gradient of a convex function that pushes the distribution  $\mathbb{P}_{\mathbf{X}}$  forward to the uniform distribution over the unit ball, this distribution is defined in Remark 2. That gradient yields a homeomorphism and its inverse naturally qualifies as a quantile function of a probability distribution in  $\mathbb{R}^d$ .

One important consideration behind these approaches can be explained when a well-defined centre in  $\text{supp}(\mathbb{P}_{\mathbf{X}})$  is available for the distribution of  $\mathbf{X}$ , allowing for discussions of its radius and direction, defined by  $(R, \mathbf{W}) = (\|\mathbf{X}\|, \mathbf{X}/\|\mathbf{X}\|)$ , relative to a suitable norm  $\|\cdot\|$ . Specifically, the proposed measure transportation maps of Chernozhukov et al. (2017) and Hallin et al. (2021) do not necessarily preserve the direction  $\mathbf{W}$  since a pair  $(R, \mathbf{W})$  is mapped to the pair  $(U_{(0,1)}, \mathbf{U}_{\mathbb{S}^{d-1}})$ , where  $U_{(0,1)} \sim \text{Unif}((0, 1))$ ,  $\mathbf{U}_{\mathbb{S}^{d-1}} \sim \text{Unif}(\mathbb{S}^{d-1})$ , with  $U_{(0,1)}$  independent of  $\mathbf{U}_{\mathbb{S}^{d-1}}$ . Thus, this approach may not be directly applicable to certain important metric spaces of interest where the Lebesgue measure may not even exist, and hence, where the target uniform distribution is not well-defined. Another limitation in the context of rare event probability estimation is the non-parametric nature of the associated statistical methods, which currently prevent extrapolation beyond the observed data. This is similar to the sample quantile, which cannot estimate quantiles outside the observed range, see *e.g.* Hallin & Konen (2024).

The transformation that we propose maps  $\mathbf{X}$  to  $U\mathbf{W}$ , where  $U = F_{R|\mathbf{W}}(R | \mathbf{W})$  is uniform over the unit interval of distances to the origin and independent of  $\mathbf{W}$ , and where  $F_{R|\mathbf{W}}$  denotes the conditional cumulative distribution function of  $R | \mathbf{W}$ . Unlike the approaches of Chernozhukov et al. (2017) and Hallin et al. (2021), which are indifferent to the radius and direction of  $\mathbf{X}$ , our transformation requires a choice of a norm measuring the size of vectors.

We highlight that the independence of  $U$  and  $\mathbf{W}$ , and the optimality of the transport plan  $F_{R|\mathbf{W}}^{-1}(U | \mathbf{w})$  for each fixed direction  $\mathbf{w}$  under the squared Euclidean distance (Brenier 1991), pushing forward the distribution of  $U$  to the conditional distribution of  $R | \mathbf{W} = \mathbf{w}$ , imply that the map  $U\mathbf{W} \rightarrow F_{R|\mathbf{W}}^{-1}(U | \mathbf{W})\mathbf{W}$  is also an optimal transport plan under the squared Euclidean distance, pushing forward the distribution of  $U\mathbf{W}$  to the distribution of  $\mathbf{X}$ . Hence, it entirely characterises  $\mathbb{P}_{\mathbf{X}}$ . However, unlike typical transport plans, which move a distribution to a known target distribution with full access to its properties, this transport plan relies on having knowledge of the distribution of  $\mathbf{W}$  to optimally transport the distribution of  $U\mathbf{W}$  to that of  $\mathbf{X}$ . This reliance on the distribution of  $\mathbf{W}$  is in fact a key strength, as it enables the derivation of transport plans for a wide range of distributions using only one-dimensional transformations, and facilitates inference

since the distribution of  $\mathbf{W}$  can be estimated directly from data.

Based on these observations, we introduce a novel definition of *probability sets* and *return sets* for a given probability measure  $\mathbb{P}_{\mathbf{X}}$ . Consider a  $\sigma$ -finite measure  $\mu$  such that

$$\mu \ll \mathbb{P}_{\mathbf{W}} \quad \text{and} \quad \mathbb{P}_{\mathbf{W}} \ll \mu. \quad (26)$$

Let

$$q_l(\mathbb{P}_{\mathbf{W}} \parallel \mu) := 1 - \inf \left\{ \frac{d\mathbb{P}_{\mathbf{W}}}{d\mu}(\mathbf{w}) : \mathbf{w} \in \text{supp}(\mathbb{P}_{\mathbf{W}}) \right\}, \quad (27)$$

where  $d\mathbb{P}_{\mathbf{W}}/d\mu$  denotes the Radon–Nikodym derivative of  $\mathbb{P}_{\mathbf{W}}$  with respect to  $\mu$ , which is strictly positive on  $\text{supp}(\mathbb{P}_{\mathbf{W}})$ , due to assumption (26). The range of  $d\mathbb{P}_{\mathbf{W}}/d\mu$  contains values strictly less than 1 if  $\mathbb{P}_{\mathbf{W}} \neq \mu$ , reflecting the fact that at some neighbourhoods on  $\text{supp}(\mathbb{P}_{\mathbf{W}})$  the measure  $\mathbb{P}_{\mathbf{W}}$  assigns less mass than  $\mu$ , while at others it assigns more mass, and is equal to unity if  $\mathbb{P}_{\mathbf{W}} = \mu$ , reflecting that the two measures are identical. Thus, when (26) holds, it follows that  $q_l(\mathbb{P}_{\mathbf{W}} \parallel \mu) \in (0, 1)$ . Define, for all  $q \in (q_l(\mathbb{P}_{\mathbf{W}} \parallel \mu), 1)$ , the radial function

$$r_{\mathcal{Q}_q(\mathbb{P}_{\mathbf{W}} \parallel \mu)}(\mathbf{w}) := \inf \left\{ r \in \mathbb{R} : F_{R|\mathbf{W}}(r \mid \mathbf{w}) \geq 1 - (1 - q) \frac{d\mu}{d\mathbb{P}_{\mathbf{W}}}(\mathbf{w}) \right\}, \quad \mathbf{w} \in \text{supp}(\mathbb{P}_{\mathbf{W}}). \quad (28)$$

**Definition 1.** Suppose that (26) holds. A  $q$ -probability set of  $\mathbb{P}_{\mathbf{X}}$  relative to  $\mu$  is defined by

$$\mathcal{Q}_q(\mathbb{P}_{\mathbf{W}} \parallel \mu) := \bigcup_{\mathbf{w} \in \text{supp}(\mathbb{P}_{\mathbf{W}})} \{(1 - t) \mathbf{0} + t r_{\mathcal{Q}_q(\mathbb{P}_{\mathbf{W}} \parallel \mu)}(\mathbf{w}) \mathbf{w} : t \in [0, 1]\}, \quad \text{for } q \in (q_l(\mathbb{P}_{\mathbf{W}} \parallel \mu), 1).$$

A return set of  $\mathbb{P}_{\mathbf{X}}$  relative to  $\mu$  with return period  $T$  is defined by

$$\mathbf{X}_T(\mathbb{P}_{\mathbf{W}} \parallel \mu) = \text{supp}(\mathbb{P}_{\mathbf{X}}) \setminus \mathcal{Q}_{1-1/T}(\mathbb{P}_{\mathbf{W}} \parallel \mu), \quad T > 1/\{1 - q_l(\mathbb{P}_{\mathbf{W}} \parallel \mu)\}.$$

The justification of the term  $q$ -probability set in Definition 1 comes from the property  $\mathbb{P}[\mathbf{X} \in \mathcal{Q}_q(\mathbb{P}_{\mathbf{W}} \parallel \mu)] = q$ , which is a direct consequence of Proposition 5.

**Proposition 5.** Suppose that condition (26) holds and  $\inf\{\xi(\mathbf{w}) : \mathbf{w} \in \text{supp}(\mathbb{P}_{\mathbf{W}})\} > -1$ . Then,

(i) for all  $q > q_l(\mathbb{P}_{\mathbf{W}} \parallel \mu)$ ,

$$\mathbb{P}[R > r_{\mathcal{Q}_q(\mathbb{P}_{\mathbf{W}} \parallel \mu)}(\mathbf{W})] = 1 - q \quad \text{and} \quad \mathbb{P}[\mathbf{W} \in B \mid R > r_{\mathcal{Q}_q(\mathbb{P}_{\mathbf{W}} \parallel \mu)}(\mathbf{W})] = \mu(B); \quad (29)$$

and

(ii) the  $b_{1/(1-q)}(\mathbf{w}; \mu)$  defined by expression (24) satisfies

$$b_{1/(1-q)}(\mathbf{w}; \mu) \sim r_{\mathcal{Q}_q(\mathbb{P}_{\mathbf{W}} \parallel \mu)}(\mathbf{w}), \quad \mathbf{w} \in \text{supp}(\mathbb{P}_{\mathbf{W}}), \quad \text{as } n \rightarrow \infty,$$

and the function  $a_{1/(1-q)}(\mathbf{w}; \mu)$  defined by expression (25) satisfies

$$a_{1/(1-q)}(\mathbf{w}; \mu) \sim r_{G_q(\mathbb{P}_{\mathbf{W}} \parallel \mu)}(\mathbf{w}), \quad \mathbf{w} \in \text{supp}(\mathbb{P}_{\mathbf{W}}), \quad \text{as } n \rightarrow \infty,$$

where

$$r_{G_q(\mathbb{P}_{\mathbf{W}} \parallel \mu)}(\mathbf{w}) := r_{\mathcal{Q}_q(\mathbb{P}_{\mathbf{W}} \parallel \mu)}(\mathbf{w}) - r_{\mathcal{Q}_q(\mathbb{P}_{\mathbf{W}} \parallel \mu)}(\mathbf{w}) \quad \text{and} \quad q(\mathbf{w}) = 1 - (1 - q)\{1 + \xi(\mathbf{w})\}^{-1/\xi(\mathbf{w})}.$$

A proof is given in Appendix A.4.

**Definition 2.** A quantile set with probability  $q \in (0, 1)$  and a return set with return period  $T > 0$  are respectively defined by

$$\mathcal{Q}_q := \mathcal{Q}_q(\mathbb{P}_{\mathbf{W}} \parallel \mathbb{P}_{\mathbf{W}}) \quad \text{and} \quad \mathbf{X}_T := \mathbf{X}_T(\mathbb{P}_{\mathbf{W}} \parallel \mathbb{P}_{\mathbf{W}}). \quad (30)$$

Suppose that condition (26) holds with  $\mu = \mu^*$ , where  $\mu^*$  denotes the uniform probability measure on  $\text{supp}(\mathbb{P}_{\mathbf{W}})$ . Then for  $q > q_l(\mathbb{P}_{\mathbf{W}} \parallel \mu^*)$ , an isotropic probability set with probability  $q$  and an isotropic return set with return period  $T > 1/\{1 - q_l(\mathbb{P}_{\mathbf{W}} \parallel \mu^*)\}$  are respectively defined by

$$\mathcal{Q}_q^* := \mathcal{Q}_q(\mathbb{P}_{\mathbf{W}} \parallel \mu^*) \quad \text{and} \quad \mathbf{X}_T^* := \mathbf{X}_T(\mathbb{P}_{\mathbf{W}} \parallel \mu^*). \quad (31)$$

## 2.5 Scaling and limit sets

Assumption 1 ensures sufficient regularity of  $\mathbb{P}_{\mathbf{X}}$  for the vague convergence of  $\nu_n$  to  $\nu$  in  $M_+(\overline{\mathbb{E}}^d)$ . However, verifying this assumption directly can be challenging. Proposition 6 provides easily verifiable sufficient conditions for this convergence. These conditions, which hold for a wide range of copulas, especially those with suitably transformed common marginal distributions, rely on the existence of a Lebesgue density  $f_{\mathbf{X}}$  for  $\mathbb{P}_{\mathbf{X}}$ , and guarantee the convergence in distribution of the radially renormalized exceedances, as described in Proposition 4. Our conditions here assume that  $\text{supp}(\mathbb{P}_{\mathbf{X}} \parallel \|\mathbf{X}\|) = \mathbb{S}^{d-1}$  and a constant shape function  $\xi(\mathbf{w}) = \xi \in \mathbb{R}$  for all  $\mathbf{w} \in \mathbb{S}^{d-1}$ . Additionally, our conditions require that the conditional distribution of the radius given the direction is in the domain of *uniform local attraction* (Sweeting 1985), and that the dominating function  $\Delta$  in Assumption 1 is bounded. This is a consequence of the uniform convergence that is assumed in Proposition 6 and can be easily seen to hold when the functional that determines the rate of convergence of the density function to the limit gauge function, presented in Supplementary 2.1, is bounded on  $\mathbb{S}^{d-1}$ .

**Proposition 6.** Suppose that the random vector  $\mathbf{X}$  is absolutely continuous with respect to the Lebesgue measure on  $\mathbb{R}^d$ , admitting a density  $f_{\mathbf{X}}$ . Let  $\mathcal{G} \in \star$  be described by continuous 1-homogeneous gauge function  $g_{\mathcal{G}} : \mathbb{R}^d \rightarrow \mathbb{R}_+$ . Suppose that one of the following conditions holds:

- (i) The limit  $\mathcal{Q}_1 := \lim_{q \rightarrow 1} \mathcal{Q}_q$  exists in  $\star$ ,  $f_{\mathbf{X}}(\mathbf{x}) > 0$  when  $\mathbf{x} \in \mathcal{G}^\circ$ ,  $f_{\mathbf{X}}(\mathbf{x}) = 0$  when  $\mathbf{x} \in \mathcal{G}'$ , and there exists  $\psi_{\mathbf{B}} : \mathbb{R}_+ \rightarrow \mathbb{R}_+$ , and a  $\xi < 0$  such that as  $t \rightarrow \infty$ ,

$$\frac{f_{\mathbf{X}}[\{1 - (\|t\mathbf{y}\|)^{-1}\}r_{\mathcal{Q}_1}(t\mathbf{y})(t\mathbf{y})]}{\psi_{\mathbf{B}}(t)} \rightarrow g_{\mathcal{G}}(\mathbf{y})^{1/\xi+1}, \quad \mathbf{y} \in \mathbb{R}^d \setminus \{\mathbf{0}\}. \quad (32)$$

(ii) There exists  $\psi_L : \mathbb{R}_+ \rightarrow \mathbb{R}_+$ , and a  $\rho > 0$  such that as  $t \rightarrow \infty$ ,

$$-\frac{\log f_{\mathbf{X}}(t\mathbf{y})}{\psi_L(t)} \rightarrow g_{\mathcal{G}}(\mathbf{y})^\rho, \quad \mathbf{y} \in \mathbb{R}^d \setminus \{\mathbf{0}\}. \quad (33)$$

(iii) There exists  $\psi_H : \mathbb{R}_+ \rightarrow \mathbb{R}_+$ , and  $\xi > 0$ , such that as  $t \rightarrow \infty$ ,

$$\frac{f_{\mathbf{X}}(t\mathbf{y})}{\psi_H(t)} \rightarrow g_{\mathcal{G}}(\mathbf{y})^{-(d+\xi^{-1})}, \quad \mathbf{y} \in \mathbb{R}^d \setminus \{\mathbf{0}\}. \quad (34)$$

Further, if the convergence is uniform on  $\mathbb{S}^{d-1}$ , then Proposition 4 holds with  $b_{1/(1-q)} := r_{\mathcal{Q}_q}$  and

(i)  $a_{1/(1-q)} := r_{\mathcal{G}_q}(\mathbf{w})$  where  $r_{\mathcal{G}_q}(\mathbf{w}) = -\xi [r_{\mathcal{Q}_1}(\mathbf{w}) - r_{\mathcal{Q}_q}(\mathbf{w})]$  when  $\xi < 0$ ;

(ii)  $a_{1/(1-q)} := r_{\mathcal{G}_q}(\mathbf{w})$  where  $r_{\mathcal{G}_q}(\mathbf{w}) = r_{\mathcal{G}}(\mathbf{w})^\rho / \psi_L'\{r_{\mathcal{Q}_q}(\mathbf{w})\}$  when  $\xi = 0$ ;

(iii)  $a_{1/(1-q)} := r_{\mathcal{G}_q}(\mathbf{w})$  where  $r_{\mathcal{G}_q}(\mathbf{w}) = \xi r_{\mathcal{Q}_q}(\mathbf{w})$  when  $\xi > 0$ .

A proof is given in Appendix A.5.

**Remark 3.** For the light-tailed case corresponding to case (ii), Assumption 6 guarantees that a suitable sequence of scaling constants  $r_n$  can be found so that the random point-set  $N_n = \{\mathbf{X}_1/r_n, \dots, \mathbf{X}_n/r_n\}$  converges in probability onto a limit set  $\mathcal{G}$  having radial function  $r_{\mathcal{G}}$  (Nolde & Wadsworth 2022). For the heavy tailed-case (iii), our assumption is in a similar spirit to de Haan & Resnick (1987) and guarantees that the distribution of  $\mathbf{X}$  is multivariate regularly varying on  $\mathbb{R}^d \setminus \{\mathbf{0}\}$ . Similarly to the classical theory of univariate extremes, where bounded-tail behaviour is handled by employing power-law tails for the normalised variable through appropriate modifications of the location sequence near the upper endpoint and the scaling sequence, here the multivariate case follows a similar structure. Specifically, the assumption in case (i) corresponds to that in case (iii) after a suitable transformation.

## 2.6 Probability density function of directions

In this section, we introduce useful properties of the direction variable  $\mathbf{W} = \mathbf{X}/\|\mathbf{X}\| \in \mathbb{S}^{d-1}$  in light of its central role in the limiting Poisson Process of appropriately centred and scaled radii, as presented in Section 2.3. The framework presented in that section has the important advantage that it yields a distribution of direction of exceedances of  $\mathcal{Q}_q$  equal to that of directions found in the original variable  $\mathbf{X}$  as exemplified by Corollary 29. Below we present additional properties of the directional variable  $\mathbf{W}$ , including a connection between the distribution of directions and star-bodies, even in cases where  $F_{\mathbf{W}}$  partially depends on the limit set  $\mathcal{G}$ .

For simplicity, we assume throughout that  $F_{\mathbf{W}}$  is absolutely continuous with respect to the spherical Lebesgue measure and that it admits a probability density  $f_{\mathbf{W}}$ . In this setting, we observe that any continuous probability density function on the sphere is in one-to-one correspondence with

a strongly starshaped set  $\mathcal{W}$  with radial function  $r_{\mathcal{W}} = f_{\mathcal{W}}$  defined by

$$\mathcal{W} := \bigcup_{\mathbf{w} \in \text{supp}(\mathbb{P}_{\mathbf{X}}/\|\mathbf{X}\|)} [0 : r_{\mathcal{W}}(\mathbf{w}) \mathbf{w}] \in \star, \quad \mathbf{w} \in \mathbb{S}^{d-1}.$$

Because  $\mathcal{W} \in \star$ , we have  $r_{\mathcal{W}^{1/d}}(\mathbf{w})^d = r_{\mathcal{W}}(\mathbf{w})$ . Thus, from the definition of the volume given in equation (A.15) in Supplementary Material 1.4, for  $f_{\mathcal{W}}$  to be a valid density,  $\mathcal{W}$  must satisfy

$$1 = \int_{\mathbb{S}^{d-1}} f_{\mathcal{W}}(\mathbf{w}) d\mathbf{w} = d \left[ \frac{1}{d} \int_{\mathbb{S}^{d-1}} r_{\mathcal{W}^{1/d}}(\mathbf{w})^d d\mathbf{w} \right] = d|\mathcal{W}^{1/d}|. \quad (35)$$

Hence, to construct any set  $\mathcal{W}$  satisfying condition (35) that  $r_{\mathcal{W}}$ , it suffices to consider

$$\mathcal{W} = \mathcal{L}^d / (d|\mathcal{L}|), \quad (36)$$

for some star-body  $\mathcal{L}$ , which follows from the formula for the volume of a starshaped set.

There are several possible forms for  $\mathcal{L}$ , and hence, for  $\mathcal{W}$ . A first possibility for the form of the set  $\mathcal{L}$  is motivated from the properties of probability density functions that are homothetic with respect to  $\mathcal{G}$  (Balkema & Nolde 2010). Recall that a density is termed homothetic if it has level-sets that are scaled copies of  $\mathcal{G}$ . In the setting where  $f_{\mathbf{X}}$  is homothetic, Proposition 7 explores the one-to-one correspondence between the density of directions and  $\mathcal{G}$ .

**Proposition 7.** *Suppose that  $f_{\mathbf{X}}(\mathbf{x}) = f_0(r_{\mathcal{G}}(\mathbf{x})^{-1})$  for a decreasing, positive, continuous function  $f_0 : [0, \infty) \rightarrow [0, \infty)$  and a radial function  $r_{\mathcal{G}}$  characterizing a set  $\mathcal{G} \in \star$ . Then  $\mathcal{L} = \mathcal{G}$ .*

A proof of Proposition 7 based on the integration by parts method of Balkema & Nolde (Section 3.1, 2010) is given in Appendix A.8. We remark that Proposition 7 is a probabilistic proof for the volume of a star-body in polar coordinates (Klain 1997). As a result, under the homothetic framework, an analytic form of the density of directions can be obtained. Consider the three examples below, all of which have homothetic densities  $f_{\mathbf{X}}$  with common radial function,  $r_{\mathcal{G}}(\mathbf{x}) = (\mathbf{x}^{\top} \mathbf{Q} \mathbf{x})^{-1/2}$  for  $\mathbf{Q}$  is positive, but different generators,  $f_0$ :

**Example 1.** *Suppose  $\mathbf{X} \sim \mathcal{N}_d(\mathbf{0}, \mathbf{Q}^{-1})$ . The margins of  $\mathbf{X}$  are standard-normally distributed. The density  $f_{\mathbf{X}}$  is homothetic with respect to  $r_{\mathcal{G}}$  and  $f_0(r) = C_1 \exp(-r^{-2}/2)$ ,  $r > 0$ , where  $C_1 = [|\mathbf{Q}|^{1/2}/(2\pi)^{d/2}]$ .*

**Example 2.** *Suppose  $\mathbf{X} \sim \text{MVL}(\mathbf{0}, \mathbf{Q}^{-1})$ . The margins of  $\mathbf{X}$  are standard Laplace distributed. The density  $f_{\mathbf{X}}(\mathbf{x})$  is homothetic with respect to  $r_{\mathcal{G}}$  and  $f_0(r) = C_2 r^{-\nu} K_{\nu}(r^{-1})$ ,  $r > 0$ , where  $C_2 = [|\mathbf{Q}|^{1/2}/(2\pi)^{d/2}]$ ,  $K_{\nu}$  is the modified Bessel function of the second kind (Gradshteyn & Ryzhik 2014) and  $\nu = (2 - d)/2$ .*

**Example 3.** *Suppose  $\mathbf{X} \sim t_{\nu}(\mathbf{0}, \mathbf{Q}^{-1})$ . The margins of  $\mathbf{X}$  are Student- $t_{\nu}$  distributed. The density  $f_{\mathbf{X}}(\mathbf{x})$  is homothetic with respect to  $r_{\mathcal{G}}$  and  $f_0(r) = C_3 (1 + r^{-2}/\nu)^{-(\nu+d)/2}$ ,  $r > 0$ , where  $C_3 = [\Gamma\{(\nu + d)/2\}|\mathbf{Q}|^{1/2}/\{(\nu\pi)^{d/2}\Gamma(\nu/2)\}]$ .*

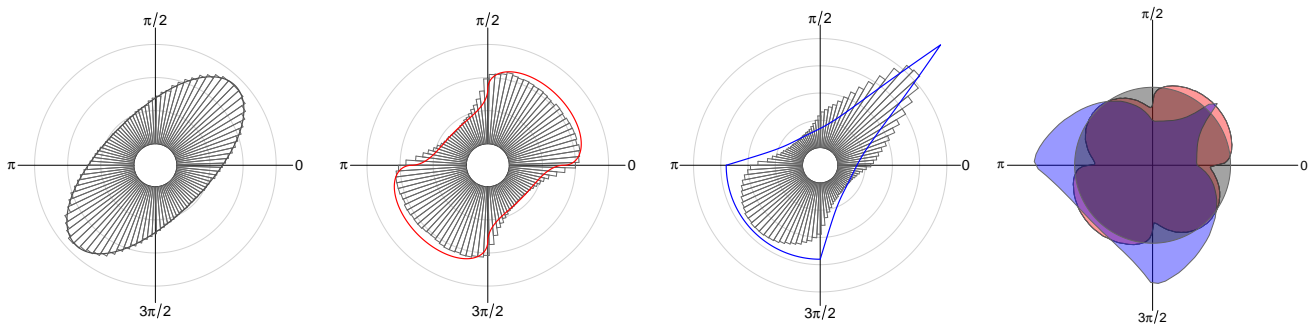


Figure 5: *Left to right*: Circular histogram of  $10^6$  directions sampled from a standard bivariate normal distribution (correlation  $\rho = 0.5$ ) with standard normal margins, standard Laplace margins, and from a bivariate max-stable logistic distribution with Laplace margins (dependence parameter  $\theta = 0.5$ ). A concentric circle corresponds to a leap of 0.1 in the density of directions. Solid lines correspond to the boundary of  $\mathcal{G}^d / (d|\mathcal{G}|)$ , for  $\mathcal{G}$  of the respective distributions. Plot 4: Sets  $[\mathcal{G}^d / (d|\mathcal{G}|)] \cdot \mathcal{W}^{-1}$  corresponding to Plots 1–3.

In each of the above examples, Proposition 7 gives an analytic form for the star set  $\mathcal{W}$ . The set  $\mathcal{W}$  is common to all examples as it is defined by  $r_{\mathcal{G}}^d / (d|\mathcal{G}|)$  for the same  $r_{\mathcal{G}}$  in all examples.

The class of homothetic densities, although rich, serves at best as an idealistic setting. A second option for the form of  $\mathcal{L}$  is revealed when removing the effect of marginal scale to studying the extremal dependence structure of  $\mathbf{X}$ . This is standard practice in extreme value analysis, and is typically achieved by standardising the margins of  $\mathbf{X}$  to a common distribution (see Section 3.1). Consider the map  $\mathbb{R}^d \ni \mathbf{x} \mapsto T(\mathbf{x}) = (\Psi^{\leftarrow}(F_{X_i}(x_i)) : i = 1, \dots, d) \in \mathbb{R}^d$  performing a transformation of the marginal distributions of  $\mathbf{X}$ , so that the  $i$ th element of  $T(\mathbf{X})$  follows  $\Psi$ , a continuous cumulative distribution function on  $\mathbb{R}$ . The transformation preserves the cardinality of the set of input vectors  $\mathbf{X} / \|\mathbf{X}\|$ , ensuring a one-to-one correspondence with the output vector  $T(\mathbf{X}) / \|T(\mathbf{X})\|$ . From a geometric perspective, this means that the densities of  $\mathbf{X} / \|\mathbf{X}\|$  and  $T(\mathbf{X}) / \|T(\mathbf{X})\|$  can be defined over the same set of points. The distribution of directions, however, may change when  $T$  introduces nonlinearities. For example, suppose that  $\mathbf{X}_N$  is distributed according to a multivariate normal distribution with zero mean and covariance matrix  $\mathbf{Q}^{-1}$  where  $\mathbf{Q}$  is such that each marginal follows the standard normal distribution. Let  $\mathbf{X} = F_L^{-1}[\Phi(\mathbf{X}_N)]$ , where  $F_L$  and  $\Phi$  denote the cumulative distribution functions of standard Laplace and standard normal random variables, respectively. While the density of  $\mathbf{X}_N$  is homothetic, thus having uniform rate of convergence is across directions, the density of  $\mathbf{X}$  is not homothetic.

It is worth noting that the asymptotic analysis with Laplace marginals may get complicated, for example through the behaviour of the joint density function along the coordinate axes. Specifically, for the multivariate normal copula in Laplace margins, the standard Mill's ratio approximation breaks down, leading to singularities in the convergence rate. These singularities, however, are resolved when convergence can be established locally uniformly on  $\mathbb{R}^d \setminus \{0\}$ . A refined analysis in Supplementary Material 3.1 for the multivariate normal copula example demonstrates this and highlights that marginal standardisation may not always adversely affect the convergence.

For the multivariate normal copula in Laplace margins, we prove that convergence in (ii) of

Proposition 6 holds uniformly, with  $\mathcal{G}$  determined by

$$r_{\mathcal{G}}(\mathbf{w}) = \left[ \{\text{sgn}(\mathbf{w})|\mathbf{w}|^{1/2}\}^{\top} \mathbf{Q} \{\text{sgn}(\mathbf{w})|\mathbf{w}|^{1/2}\} \right]^{-1}, \quad \mathbf{w} \in \mathbb{S}^{d-1}. \quad (37)$$

where  $\text{sgn}(\mathbf{w})|\mathbf{w}|^{1/2} = (\text{sgn}(w_i)|w_i|^{1/2} : i = 1, \dots, d)$  and  $\text{sgn}(x) = x/|x|$  denotes the signum function. In this case, the star set  $\mathcal{W}$  describing the density of  $\mathbf{X}/\|\mathbf{X}\|$  is no longer a constant scale multiple of  $\mathcal{G}$ , but instead a radial product of  $\mathcal{G}$  with another star-body. Figure 5 also shows the true density (histogram) of  $\mathbf{X}/\|\mathbf{X}\|$  and  $r_{\mathcal{G}}(\mathbf{w})^d/\{d|\mathcal{G}|\}$  (solid curve). The star-body in panel four of the same figure is the ratio between  $\mathcal{W}$  and  $\mathcal{G}^d/\{d|\mathcal{G}|\}$ .

The analysis of the marginal transformation and its effect on the distribution of the directions reveals a case where  $\mathcal{W}$  can depend both on  $\mathcal{G}$  and on some additional star-body  $\mathcal{B}$  independent of  $\mathcal{G}$ . The star-body  $\mathcal{B}$  captures residual directional variation that is not explained by a homothetic density. For instance, assume that  $\mathbf{X}$  follows a bivariate max-stable logistic distribution in standard Laplace margins. From Figure 5, we see that  $\mathcal{W} \neq \mathcal{G}^d/(d|\mathcal{G}|)$ . For the practical case where both  $r_{\mathcal{W}}$  and  $r_{\mathcal{G}}$  are strictly positive on  $\mathbb{S}^{d-1}$ , then  $\mathcal{L} = \mathcal{B} \cdot \mathcal{G}$ ,  $\mathcal{B}, \mathcal{G} \in \star$  with  $\mathcal{B}$  independent of  $\mathcal{G}$ . Hence, in the specific context where  $f$  is homothetic with respect to  $r_{\mathcal{G}}$ ,  $\mathcal{B} = B_1(\mathbf{0})$ .

A third possibility for the set  $\mathcal{L}$ , and consequently the set  $\mathcal{W}$ , is to set  $\mathcal{L} = \mathcal{B}$  for some set  $\mathcal{B}$  independent of  $\mathcal{G}$ , implying a case where  $\mathbf{W}$  is independent of  $\mathcal{G}$ . This can occur within the class of radial generalised Pareto distributions, introduced in the following section. In Supplementary Material 4, we derive closed-form expressions of the distribution of directions  $f_{\mathbf{W}}$  for a number of distributions when the marginal distributions are common and prespecified.

## 2.7 Radial generalised Pareto distributions

We now present a novel family of multivariate distributions, termed radial generalised Pareto (rGP) distributions and detail some of their stability properties making them suitable for extrapolation. They arise as the only non-trivial limits of *radially renormalised* exceedances above a threshold  $\mathcal{Q}_q$ , as detailed in Section 2.3, and enable the modelling of rare events in a much wider set of joint-tail regions of  $\mathbb{R}^d$  than other well-established frameworks of extreme value theory. Radial generalised Pareto distributions are parameterised via members of the class of star bodies  $\star$ .

**Definition 3** (Multivariate radial generalised Pareto distributions). *A random vector  $\mathbf{Z} \in \mathbb{R}^d$  is said to follow the multivariate radial generalised Pareto distribution with location  $\mathcal{M}$ , scale  $\Sigma$ , and shape  $\xi : \mathbb{S}^{d-1} \rightarrow \mathbb{R}$  and directional shape  $\mathcal{W}$ , if for any Borel set  $K \subseteq \mathbb{R}^d \setminus \mathcal{M}$ ,*

$$\mathbb{P}[\mathbf{Z} \in K] = \int_{\mathbb{S}^{d-1}} \int_{\mathbf{0}:\mathbf{w}) \cap K} \left\{ 1 + \xi(\mathbf{w}) \frac{r - r_{\mathcal{M}}(\mathbf{w})}{r_{\Sigma}(\mathbf{w})} \right\}_+^{-1/\xi(\mathbf{w})} r_{\mathcal{W}}(\mathbf{w}) \, dr \, d\mathbf{w}. \quad (38)$$

The radial generalised Pareto distribution presented in Definition 3 possesses stability properties detailed in Propositions 8 and 9, where Proposition 9 is concerned with the special case of the when  $\xi(\mathbf{w}) = 0$  for all  $\mathbf{w} \in \mathbb{S}^{d-1}$ , corresponding to a radial exponential distribution.

**Proposition 8.** Let  $\mathbf{Z} \in \mathbb{R}^d$  follow a radial generalised Pareto distribution with location  $\mathcal{M}$ , scale  $\Sigma$ , shape  $\xi : \mathbb{S}^{d-1} \rightarrow \mathbb{R}$ , and directional shape  $\mathcal{W}$ , then the quantile and isotropic probability sets of  $\mathbf{Z}$  are respectively

$$\mathcal{Q}_q = \mathcal{M} + \xi^{-1}\{B_{1-q}(\mathbf{0})^{-\xi} - B_1(\mathbf{0})\} \cdot \Sigma, \quad q \in (0, 1), \quad (39)$$

$$\mathcal{Q}_q^* = \mathcal{Q}_q + \xi^{-1}[\{\mathcal{W} \cdot B_{|\mathbb{S}^{d-1}|}(\mathbf{0})\}^\xi - B_1(\mathbf{0})] \cdot \Sigma, \quad q \in (q_l(\mathbb{P}_{\mathbf{Z}/\|\mathbf{Z}\|} \|\mu^*\), 1), \quad (40)$$

where  $q_l$  is defined in expression (27), and where  $\mathcal{B}^\xi$  for  $\mathcal{B} \in \star$  is interpreted as  $r_{\mathcal{B}}(\mathbf{w})^{\xi(\mathbf{w})}$ , for all  $\mathbf{w} \in \text{supp}(\mathbb{P}_{\mathbf{Z}/\|\mathbf{Z}\|})$ . Further, if  $\xi$  is constant,  $\mathbf{Z}$  satisfies the radial stability property

$$\mathbb{P}[\mathbf{Z} \in \{\mathcal{M} + B_{r_1+r_2}(\mathbf{0}) \cdot \Sigma\}' \mid \mathbf{Z} \in \{\mathcal{M} + B_{r_1}(\mathbf{0}) \cdot \Sigma\}'] = \mathbb{P}\left[\mathbf{Z} \in \left\{\mathcal{M} + \frac{B_{r_2}(\mathbf{0}) \cdot \Sigma}{B_1(\mathbf{0}) + B_\xi(\mathbf{0}) \cdot B_{r_1}(\mathbf{0})}\right\}'\right]. \quad (41)$$

**Proposition 9.** Let  $\mathbf{Z} \in \mathbb{R}^d$  follow a radial exponential distribution with location  $\mathcal{M}$ , scale  $\Sigma$ , and directional shape  $\mathcal{W}$ , then the quantile and isotropic probability sets of  $\mathbf{Z}$  are respectively given by

$$\mathcal{Q}_q = \mathcal{M} + B_{-\log(1-q)}(\mathbf{0}) \cdot \Sigma, \quad q \in (0, 1), \quad (42)$$

$$\mathcal{Q}_q^* = \mathcal{Q}_q + \log\{\mathcal{W} \cdot B_{|\mathbb{S}^{d-1}|}(\mathbf{0})\} \cdot \Sigma, \quad q \in (q_l(\mathbb{P}_{\mathbf{Z}/\|\mathbf{Z}\|} \|\mu^*\), 1). \quad (43)$$

Further,  $\mathbf{Z}$  satisfies the radial memoryless property that

$$\mathbb{P}[\mathbf{Z} \in [\mathcal{M} + B_{r_1+r_2}(\mathbf{0}) \cdot \Sigma]' \mid \mathbf{Z} \in \{\mathcal{M} + B_{r_1}(\mathbf{0}) \cdot \Sigma\}'] = \mathbb{P}[\mathbf{Z} \in \{\mathcal{M} + B_{r_2}(\mathbf{0}) \cdot \Sigma\}']. \quad (44)$$

Proofs of stability properties (39) and (42) are given in Appendix A.6 and A.7. We note that in equation (44), equality holds when replacing the location  $\mathcal{M}$  by any  $K \in \star$  with  $K \subseteq \mathcal{M}$ .

Given a probability set  $\mathcal{Q}_q$  of a random vector  $\mathbf{Z}$ , the stability properties established above allow extrapolation to probability sets with probability  $q' \geq q$ . If  $\mathbf{Z}$  follows a radial generalised Pareto distribution as in Proposition 8, then  $\mathbf{Z} \mid \mathbf{Z} \notin \mathcal{Q}_q$  follows a radial generalised Pareto distribution with scale  $\Sigma' = \Sigma + \xi \cdot (\mathcal{Q}_q - \mathcal{M})$ , and for  $q' \geq q$ ,

$$\mathcal{Q}_{q'} = \mathcal{Q}_q + \{B_{(1-q)/(1-q')}(\mathbf{0})^\xi - B_1(\mathbf{0})\} \cdot \Sigma'/\xi, \quad (45)$$

and  $\mathcal{Q}_{q'}^*$  is obtained according to equality (40). Similarly, if  $\mathbf{Z}$  follows a radial exponential distribution as in Proposition 9, then  $\mathbf{Z} \mid \mathbf{Z} \notin \mathcal{Q}_q$  follows a radial exponential distribution with same scale  $\Sigma$ , and for  $q' \geq q$ ,

$$\mathcal{Q}_{q'} = \mathcal{Q}_q + B_{\lceil \log\{(1-q)/(1-q')\} \rceil}(\mathbf{0}) \cdot \Sigma, \quad (46)$$

and  $\mathcal{Q}_{q'}^*$  obtained according to equality (43).

In Section 3, we propose a statistical inference method utilising the family of radial generalised Pareto distributions to extrapolate to extreme regions lying beyond the range of observed data.

### 3 Statistical inference

#### 3.1 Standardisation of margins

Suppose that  $\mathbf{o}_1, \dots, \mathbf{o}_n$ , are observations drawn randomly from the distribution of the random variable  $\mathbf{O} = (O_1, \dots, O_d)^\top$ . When the tails of the original distribution decay exponentially, we have the flexibility to model a broader range of extremal dependence structures, not only allowing for both asymptotic independence and asymptotic dependence, but also allowing for more complex types of dependencies such as when some coordinates exhibit positive extremal dependence while others exhibit negative extremal dependence (Keef et al. 2013, Nolde & Wadsworth 2022). When  $\mathbf{O}$  does not have exponential decay, the transformation  $X_j = F_L^{-1}(\widehat{F}_j(O_j))$  must be applied for  $j = 1, \dots, d$ , where  $F_L^{-1}$  is the distribution function of the standard Laplace distribution, and

$$\widehat{F}_j(o) = \begin{cases} \left[ 1 - \left\{ 1 - \xi_{j,-} \left( \frac{o - u_{j,-}}{\sigma_{j,-}} \right) \right\}_+^{-1/\xi_{j,-}} \right] \widetilde{F}_j(u_{j,-}) & o \leq u_{j,-} \\ \widetilde{F}_j(o) & u_{j,-} < o \leq u_{j,+} \\ 1 - [1 - \widetilde{F}(u_{j,+})] \left\{ 1 + \xi_{j,+} \left( \frac{o - u_{j,+}}{\sigma_{j,+}} \right) \right\}_+^{-1/\xi_{j,+}} & o > u_{j,+} \end{cases} \quad (47)$$

$\widetilde{F}_j(o) = (n+1)^{-1} \sum_{i=1}^n \mathbb{1}[o_{ij} \leq o]$ , and  $(\widehat{\sigma}_1, \widehat{\xi}_1)$  and  $(\widehat{\sigma}_{j,-}, \widehat{\xi}_{j,-})$  and  $(\widehat{\sigma}_{j,+}, \widehat{\xi}_{j,+})$  are scale and shape parameters of generalised Pareto distributions for the lower and upper tail of the  $j^{\text{th}}$  margin, which are used to model the tail decay below and above the thresholds  $u_{j,-}$  and  $u_{j,+}$ , respectively.

In practice, the thresholds  $u_{j,-}$  and  $u_{j,+}$  can be modelled as quantiles of the marginal distribution. By adopting a Bayesian approach, we can assign a posterior distribution to the joint distribution of these quantiles. This posterior enables us to sample candidate thresholds, above which separate GP models are implemented for the tails. This approach naturally accounts for uncertainty in the marginal distributions' parameters, as the posterior distribution of the quantiles propagates this uncertainty forward into the tail modelling process. Adopting a Frequentist approach, we can estimate GP parameters using maximum likelihood to the exceedances above empirical quantiles, and propagate the uncertainty in the quantile estimate and the corresponding GP parameters forward using a bootstrap approach.

#### 3.2 Quantile regression

Quantile regression methods are typically implemented using a pinball loss function (Koenker 2005) and often without a distributional model for the density. Although Yu & Moyeed (2001) propose the use of the asymmetric Laplace distribution for the model density due to the equivalence of the negative log density of the asymmetric Laplace with the pinball loss function, naively treating the asymmetric Laplace as an adequate model for the data is precarious in a Bayesian setting. For example, Waldmann et al. (2013) show that the resulting posterior prediction intervals have poor frequentist calibration properties, and this is especially pronounced for tail quantiles, which are essential in our setup. Second, the scale parameter of the asymmetric Laplace distribution is

arbitrary in a Bayesian framework and even maximum likelihood based estimators are known to lead to inaccurate quantile estimates, see [Fasiolo et al. \(2021\)](#).

We adopt a *generalised linear model* based approach for quantile regression, requiring an adequate distributional model for the density of  $R \mid \mathbf{W}$ . In particular, we assume that  $R \mid \mathbf{W} = \mathbf{w}$  follows a Gamma distribution and model the logarithm of its conditional  $q$ -quantile  $\log r_{\mathcal{Q}_q}(\mathbf{w})$  using a finite-dimensional continuously specified Gaussian process prior on  $\mathbb{S}^{d-1}$  (see Supplementary Material 5.1). We model the logarithms of the radial function  $r_{\mathcal{Q}_q}$  by approximations of Matérn Gaussian fields on  $\mathbb{S}^{d-1}$  using the stochastic partial differential equation approach by [Lindgren et al. \(2011\)](#), with  $\alpha = 2$  (see their Equation (2)) which is also the default option in the R-INLA package ([www.r-inla.org](http://www.r-inla.org)).

There are at least two strengths behind this choice. First, due to Proposition 11, the Gamma distribution serves as a good approximation for the density in the tail region of the distribution of  $R \mid \mathbf{W}$ . Since estimators of high quantiles are not influenced by the bulk of the distribution, a likely misspecification between our choice and the true density of  $R \mid \mathbf{W}$  in the body of the distribution is not of concern. Second, our choice exploits the form of the decay of the conditional density and allows for Bayesian inference for the conditional quantile under a model that can adequately describe the behaviour in the tail. In this paper, we adopt a Gamma quantile regression models due to the simplicity that it affords, but remark that further improvements may be achieved by using, for example, a truncated Gamma distribution, so as to further eliminate effects from the body of the distribution of  $R \mid \mathbf{W}$  ([Wadsworth & Campbell 2024](#)).

Given i.i.d. observations  $\mathbf{o}_1, \dots, \mathbf{o}_n$  from a random vector  $\mathbf{O}$ , we obtain the standardised data  $\mathbf{x} = \{\mathbf{x}_1, \dots, \mathbf{x}_n\}$  via  $\mathbf{x}_i = (F^{-1}(\tilde{F}_1(o_{i,1})), \dots, F^{-1}(\tilde{F}_d(o_{i,d})))$  as described in Section 3.1. To infer the quantile set  $\mathcal{Q}_q$  of  $\mathbf{X}$ , we treat  $\mathbf{y} = \{(r_i, \mathbf{w}_i) : i = 1, \dots, n\}$ , with  $(r_i, \mathbf{w}_i) = (\|\mathbf{x}_i\|, \mathbf{x}_i/\|\mathbf{x}_i\|)$ , as observations from  $(R, \mathbf{W})$  and apply the Gamma quantile regression method detailed above.

### 3.3 Conditional likelihood function

Given that  $\mathbf{X}$  has standard Laplace margins, we assume that exceedances of  $\mathcal{Q}_q$  follow a radial GP distribution with location  $\mathcal{Q}_q$ , scale  $\mathcal{G}$ , radial shape  $\xi$ , and directional shape  $\mathcal{W}$ . Below we describe a likelihood-based statistical inference approach for these parameters.

We recall from equation (36) that the set  $\mathcal{W}$  can be expressed as  $f_{\mathbf{W}}(\mathbf{w}) = r_{\mathcal{L}}(\mathbf{w})^d / (d|\mathcal{L}|)$ , where  $\mathcal{L}$  is a star-body. Based on Section 2.6, we motivate three models for  $\mathcal{W}$  given by

$$M_1 : \mathcal{L} = \mathcal{B}, \quad M_2 : \mathcal{L} = \mathcal{G}, \quad M_3 : \mathcal{L} = \mathcal{B} \cdot \mathcal{G}, \quad (48)$$

for  $\mathcal{B} \in \star$  independent of  $\mathcal{G}$ . We note that the latent star-bodies  $\mathcal{B}$  in models  $M_1$  and  $M_3$  do not have the same interpretation, but the slight abuse of notation allows to simplify the notation for the parameter space in later sections without loss of interpretation. The nested structure of model  $M_2$  within the parameter space of model  $M_3$  translates into a bias-variance trade-off as the latter offers additional flexibility at the cost of a possibly increased variance for the latent set  $\mathcal{G}$ . A similar trade-off occurs for  $\mathcal{G}$  between models  $M_1$  and  $M_3$  since the former ignores possible information

contained in the observed directions.

Conditionally on the quantile set  $\mathcal{Q}_q$  and the data  $\mathbf{y}$ , the likelihood of  $\boldsymbol{\theta} = (\mathcal{G}, \mathcal{L}, \xi)$ , is given by  $L(\boldsymbol{\theta} \mid \mathcal{Q}_q, \mathbf{y}) := \prod_{i=1}^n f_{R, \mathbf{W}}(r_i, \mathbf{w}_i \mid \boldsymbol{\theta}, \mathcal{Q}_q)$ . Letting  $\mathcal{S}_q := \{i \in \{1, \dots, n\} : r_i > r_{\mathcal{Q}_q}(\mathbf{w}_i)\}$  denote the set of random indices corresponding to exceedances of  $\mathcal{Q}_q$ , and  $\mathcal{S}'_q := \{1, \dots, n\} \setminus \mathcal{S}_q$ ,  $L$  can be expressed in terms of contributions of the radii  $\{r_1, \dots, r_n\}$  above and below  $r_{\mathcal{Q}_q}$  via

$$L(\boldsymbol{\theta} \mid \mathcal{Q}_q, \mathbf{y}) = \left[ \prod_{i \in \mathcal{S}'_q} f_{R|R \leq r_{\mathcal{Q}_q}(\mathbf{w}), \mathbf{W}}(r_i) f_{\mathbf{W}}(\mathbf{w}_i) \right] \left[ \prod_{i \in \mathcal{S}_q} f_{R|R > r_{\mathcal{Q}_q}(\mathbf{w}), \mathbf{W}}(r_i) f_{\mathbf{W}}(\mathbf{w}_i) \right]. \quad (49)$$

Under the assumption that  $\mathbf{y}$  is a random sample, Corollary 29 suggests that all directions  $\{\mathbf{w}_1, \dots, \mathbf{w}_n\}$  may be used in the likelihood for the inference of  $f_{\mathbf{W}} = r_{\mathcal{L}}^d / (d|\mathcal{L}|)$  used to model  $\mathbf{W} \mid R > r_{\mathcal{Q}_q}(\mathbf{W})$ . In particular, when models  $M_1$  or  $M_3$  are used, substantial gains in the inference for  $\mathcal{G}$  can be attained by also including in inference the directions at which non-exceedances occur, as illustrated in the simulation study of Supplementary Material 6. Based on Theorem 2, non-exceedance radii  $\{r_i : i \in \mathcal{S}'_q\}$  are assumed not to carry information about  $\mathcal{G}$  and  $\mathcal{L}$ ; we pose that  $\mathcal{L}$  is constant with respect to them. Denoting by  $\mathcal{S}_w$  the set of indices of at least all exceedances and at most all observations—or  $\mathcal{S}_q \subseteq \mathcal{S}_w \subseteq \{1, \dots, n\}$ —the likelihood thus reduces to

$$\begin{aligned} L(\boldsymbol{\theta} \mid \mathcal{Q}_q, \mathbf{y}) &\propto \prod_{i \in \mathcal{S}_q} f_{R|R > r_{\mathcal{Q}_q}(\mathbf{w}), \mathbf{W}}(r_i \mid \mathbf{w}_i) \prod_{i \in \mathcal{S}_w} f_{\mathbf{W}}(\mathbf{w}_i) \\ &= \exp\{-|\mathcal{S}_w| \log(d|\mathcal{L}|\}\} \prod_{i \in \mathcal{S}_q} f_{R_E|\mathbf{W}}((r_i - r_{\mathcal{Q}_q}(\mathbf{w}_i))/r_{\mathcal{G}_q}(\mathbf{w}_i) \mid \mathbf{w}_i) \prod_{i \in \mathcal{S}_w} r_{\mathcal{L}}(\mathbf{w}_i)^d, \end{aligned} \quad (50)$$

where  $f_{R_E|\mathbf{W}}(z \mid \mathbf{w}) = [1 + \xi(\mathbf{w})z]_+^{-1/\xi(\mathbf{w})-1} / r_{\mathcal{G}}(\mathbf{w})$ . The likelihood function (50) is amenable to standard likelihood based inference using either frequentist or Bayesian methods when parametric models are selected for  $\mathcal{W}$  and  $\mathcal{G}$ . When interest is in semi-parametric models, a key complication arises when using the likelihood in expression (50). Evaluating the likelihood function (50) requires computing the constant  $d|\mathcal{L}|$  which ensures the density of  $\mathbf{W}$  integrates to one. This normalising constant is in several cases difficult to compute exactly, which makes inference difficult. However, using the *Poisson transform* (Baker 1994), we can map the likelihood into an *equivalent* likelihood function  $L(\boldsymbol{\theta}, \beta \mid \mathcal{Q}_q, \mathbf{y})$  of a Poisson point process defined in an expanded space given by

$$L(\boldsymbol{\theta}, \beta) = \exp[-|\mathcal{S}_w| e^\beta (d|\mathcal{L}|)] \prod_{i \in \mathcal{S}_q} f_{R_E|\mathbf{W}}((r_i - r_{\mathcal{Q}_q}(\mathbf{w}_i))/r_{\mathcal{G}_q}(\mathbf{w}_i) \mid \mathbf{w}_i) \prod_{i \in \mathcal{S}_w} e^\beta r_{\mathcal{L}}(\mathbf{w}_i)^d, \quad (51)$$

where the latent variable  $\beta$  estimates the normalising constant  $d|\mathcal{L}|$ ; it is inferred as another parameter at no loss of information (Barthelmé & Chopin 2015). It is worth noting that through this approach, we still need to compute the volume of  $\mathcal{L}$ . However, since our parametrisation assumes that  $\log r_{\mathcal{L}}$  is linear within,  $|\mathcal{L}|$  can be estimated numerically in a stable and efficient manner based on the method introduced by Simpson et al. (2016), see also Yuan et al. (2017), Arce Guillen et al. (2023) and Papastathopoulos et al. (2023) for further applications of this method. Inference can be performed either using frequentist methods or in a fully Bayesian manner, that is, by assigning

suitable prior distributions on  $\mathcal{G}$ ,  $\mathcal{L}$ , and  $\beta$  (Arce Guillen et al. 2023). More details on statistical inference for the latent variables and on how the fitted models can be used to perform rare event probability estimation are found in Supplementary Material 5.

### 3.4 Assessment of convergence to limit distribution

In this section, we outline a novel diagnostic, allowing assessment of the weak convergence in Theorem 2. Following Remarks 1 and 2, observe that under the conditions of Theorem 2 we have

$$H_{\mathbf{W}} \left( \frac{R - r_{\mathcal{Q}_q^*}(\mathbf{W})}{r_{\mathcal{G}_q^*}(\mathbf{W})} \right)^{1/d} \mathbf{W} \mid \{R > r_{\mathcal{Q}_q^*}(\mathbf{W})\} \xrightarrow{d} \mathbf{U}_{B_1(\mathbf{0})}, \quad \text{as } q \rightarrow 1,$$

where  $\mathbf{U}_{B_1(\mathbf{0})}$  is a random variable with a uniform distribution *in* the  $d$ -dimensional unit ball  $B_1(\mathbf{0})$ , that is,  $\mathbb{P}_{\mathbf{U}_{B_1(\mathbf{0})}}(A) = |A \cap B_1(\mathbf{0})|/|\mathbb{S}^{d-1}|$  for any Borel set  $A \subseteq B_1(\mathbf{0})$ . Here,  $r_{\mathcal{Q}_q^*} := b_{1/(1-q)}^*$  and  $r_{\mathcal{G}_q^*} := a_{1/(1-q)}^*$ , where  $b_{1/(1-q)}^*$  and  $a_{1/(1-q)}^*$  are given by the functions (24) and (25), that is,

$$r_{\mathcal{Q}_q^*}(\mathbf{w}) = r_{\mathcal{Q}_q}(\mathbf{w}) + r_{\mathcal{G}_q}(\mathbf{w})[\{|\mathbb{S}^{d-1}|r_{\mathcal{W}}(\mathbf{w})\}^\xi - 1]/\xi \quad \text{and} \quad r_{\mathcal{G}_q^*}(\mathbf{w}) = r_{\mathcal{G}_q}(\mathbf{w})\{|\mathbb{S}^{d-1}|r_{\mathcal{W}}(\mathbf{w})\}^\xi,$$

for  $\mathbf{w} \in \mathbb{S}^{d-1}$  and  $q$  such that  $\inf\{r_{\mathcal{Q}_q^*}(\mathbf{w}) : \mathbf{w} \in \mathbb{S}^{d-1}\} \geq 0$ .

We note the power  $1/d$  used in the transformation of the renormalised radius as this transformation results in the aforementioned limit distribution, possessing particularly convenient features that allow us to build a simple diagnostic based on the second order properties (Ripley 1976, 1977) of a stationary random point measure. Here, stationarity means that the distribution of  $P^*$  is invariant under rotations in  $\mathbb{R}^d$ . In particular, the stationary random point measure

$$P^* := \sum_{i=1}^n \delta \left[ H_{\mathbf{W}_i} \left( \frac{R_i - r_{\mathcal{Q}_q^*}(\mathbf{W}_i)}{r_{\mathcal{G}_q^*}(\mathbf{W}_i)} \right)^{1/d} \mathbf{W}_i \right] \mathbb{1}_{R_i > r_{\mathcal{Q}_q^*}(\mathbf{W}_i)}, \quad (52)$$

has size  $n^* := \sum_{i=1}^n \mathbb{1}_{\|\mathbf{x}_i\| > r_{\mathcal{Q}_q^*}(\mathbf{x}_i/\|\mathbf{x}_i\|)}$ . In what follows, we develop a method to assess if it is statistically distinguishable from a random point measure with constant intensity on  $B_1(\mathbf{0})$ .

For a random point measure  $\Pi_{n^*} := \sum_{i=1}^{n^*} \delta_{\mathbf{U}_i}$  on  $B_1(\mathbf{0})$ , we define the normalised reduced second-order measures  $K_B$  and  $K_C$  by

$$K_B(r) = \lambda^{-1} \mathbb{E} \left[ \sum_{j \neq i} \mathbb{1}_{\mathbf{U}_j} \{B_r(\mathbf{U}_i)\} \right] \quad \text{and} \quad K_C(r) = \lambda^{-1} \mathbb{E} \left[ \sum_{j \neq i} \mathbb{1}_{\mathbf{U}_j} \{C_r(\mathbf{U}_i)\} \right], \quad (53)$$

where  $\lambda$  is the average intensity of the point measure over  $B_1(\mathbf{0})$ ,  $B_r(\mathbf{U}_j)$  is the ball of radius  $r$  centred at  $\mathbf{U}_j$ , and  $C_r(\mathbf{U}_j)$  is the spherical sector with apex at  $\mathbf{0}$ , extending outwards in the direction of  $\mathbf{U}_j$ , with half aperture angle  $r$ . The specific geometries of  $B_r$  and  $C_r$  are chosen such that they reveal regions of deviation from constant intensity of an underlying random point measure occurring in radial-directional and strictly directional neighbourhoods, respectively. In particular, if  $\{\mathbf{U}_i : i = 1, \dots, n^*\}$  is a random sample of uniformly distributed directions arising from the

distribution of  $U_{B_1(\mathbf{0})}$ , then we have

$$K_B(r) = \int_{B_1(\mathbf{0})} \frac{|B_r(\mathbf{x}) \cap B_1(\mathbf{0})|}{|B_1(\mathbf{0})|} d\mathbf{x} \quad \text{and} \quad K_C(r) = \int_{B_1(\mathbf{0})} \frac{|C_r(\mathbf{x}) \cap B_1(\mathbf{0})|}{|B_1(\mathbf{0})|} d\mathbf{x}. \quad (54)$$

Hence, given an observed point pattern  $P^*$  obtained via transformation (52) of a random sample from  $\mathbb{P}_{\mathbf{X}}$  and a sample from the posterior distribution of  $\mathcal{Q}_q^*$  and  $\mathcal{G}_q^*$ , we can compare the functions  $K_B$  and  $K_C$  given by expression (54) with the empirical estimates of the measures (53),

$$\widehat{K}_B(r | P^*) = \frac{|B_1(\mathbf{0})|}{(n^*)^2} \sum_{\substack{\mathbf{u}_i, \mathbf{u}_j \in P^* \\ \mathbf{u}_i \neq \mathbf{u}_j}} \mathbb{1}_{\mathbf{u}_j} \{B_r(\mathbf{u}_i)\} \quad \text{and} \quad \widehat{K}_C(r | P^*) = \frac{|B_1(\mathbf{0})|}{(n^*)^2} \sum_{\substack{\mathbf{u}_i, \mathbf{u}_j \in P^* \\ \mathbf{u}_i \neq \mathbf{u}_j}} \mathbb{1}_{\mathbf{u}_j} \{C_r(\mathbf{u}_i)\}. \quad (55)$$

To evaluate the variability of the function  $\widehat{K}_S(\cdot | \Pi_{n^*})$ , where  $S$  represents the sets  $B$  or  $C$ , on random point measures  $\Pi_{n^*}$  with constant intensity on  $B_1(\mathbf{0})$ , we construct a  $(1 - \alpha)$ -envelope denoted by  $\mathcal{E}_{S, n^*}(r) = [\mathcal{E}_{S, n^*}^{\text{low}}(r), \mathcal{E}_{S, n^*}^{\text{upp}}(r)]$  which satisfies, for  $I_B = [0, 2]$  and  $I_C = [0, \pi]$ , that

$$\mathbb{P} \left[ \left\{ \mathcal{E}_{S, n^*}^{\text{low}}(r) \leq \widehat{K}_S(r | \Pi_{n^*}) \leq \mathcal{E}_{S, n^*}^{\text{upp}}(r) : r \in I_S \right\} \right] = 1 - \alpha. \quad (56)$$

The envelope bounds are estimated using Monte-Carlo simulation. Specifically, we draw  $m$  independent samples of size  $n^*$  from the distribution  $\mathbb{P}_{U_{B_1(\mathbf{0})}}$ , say  $\{\Pi_{n^*}^{(j)} : j = 1, \dots, m\}$ , each corresponding to a realisation of a random point measure with constant intensity in  $B_1(\mathbf{0})$ . For each sample  $\Pi_{n^*}^{(j)}$ , we compute the discretised estimates  $\widehat{K}_S(\cdot | \Pi_{n^*}^{(j)})$  at a predefined sequence of  $r$  values. The lower and upper bounds of the envelope are defined in a manner akin to [Bolin & Lindgren \(2018\)](#), that is, as the empirical  $(\rho/2)$ - and  $(1 - \rho/2)$ -quantiles of the  $m$  values of  $\{\widehat{K}_S(r | \Pi_{n^*}^{(j)}) : j = 1, \dots, m\}$ , where  $\rho \in (0, 1)$  is chosen such that  $100(1 - \alpha)\%$  of the  $m$  discretised function estimates lie entirely within the envelope. Then, evidence against the assumption that  $P^*$  has constant intensity—observed whenever the estimates  $\widehat{K}_B(\cdot | P^*)$  or  $\widehat{K}_C(\cdot | P^*)$  do not lie entirely within their  $(1 - \alpha)$ -envelopes—suggests evidence against the validity of the approximation of the distribution of the observed extremes via the limit distribution of Theorem 2.

More details on model selection and validation, on classical goodness-of-fit methods, and on simultaneous uncertainty bands are found in the Supplementary Material 5.3.

## 4 Newlyn wave heights data analysis

We apply our methodology to a dataset of dimension  $d = 3$  consisting of hourly measurements of wave height  $O_H$ , in meters, wave period  $O_P$ , in seconds, and surge  $O_S$ , in meters, measured over the period 1971–1977 at the Newlyn port in south-west England. The dataset was first analysed in [Coles & Tawn \(1994\)](#) in the case where asymptotic dependence was assumed between all three variables. Although a typical assumption, [Wadsworth & Campbell \(2024\)](#) show that asymptotic independence is a more reasonable assumption. Here, we revisit this data with a more flexible approach also enabling the modelling of negative dependence. Following previous literature, we analyse componentwise

maxima over 15-hour periods, resulting in a dataset of  $n = 2,894$  observations. The margins  $O_H, O_P, O_S$  of the data are unknown and we thus standardise them to standard Laplace using methods from Section 3.1, resulting in observations  $\tilde{\mathbf{x}} := \{\mathbf{x}_i = (x_{H,i}, x_{P,i}, x_{S,i}) : i = 1, \dots, n\}$  interpreted as random draws from  $\mathbf{X} = (X_H, X_P, X_S)$ .

We begin by fitting to  $\tilde{\mathbf{x}}$  the hierarchical Bayesian gamma quantile regression model for the quantile set  $\mathcal{Q}_q$  at the  $q = 0.9$  probability level. For each of 20 samples  $\{\mathcal{Q}_{q,i} : i = 1, \dots, 20\}$  from the posterior distribution of  $\mathcal{Q}_q$ , we assume that the exceedances of  $\mathcal{Q}_{q,i}$  follow a radial exponential distribution exactly, and fit the models  $M_1, M_2$ , and  $M_3$  to them. For each model and  $\mathcal{Q}_{q,i}$ , we sample 50 observations  $\{(\mathcal{G}_{j,i}, \mathcal{W}_{j,i}) : j = 1, \dots, 50\}$  from the posterior distribution of  $\mathcal{G}, \mathcal{W} \mid \mathcal{Q}_{q,i}$ . It is deemed via model checks that  $M_2$  fitted on exceedance directions only provides the best overall joint fit (see Supplementary Material 7.2).

Figure 6 shows the posterior mean of  $\mathcal{Q}_q, \mathcal{G}$  and  $\mathcal{W}$  obtained from model  $M_2$ , as well as the posterior means of extrapolated  $\mathcal{Q}_{0.95}$  and  $\mathcal{Q}_{0.95}^*$ , corresponding to complement return sets with return period  $T = 300$ -hour. The probability sets  $\mathcal{Q}_{0.95}$  and  $\mathcal{Q}_{0.95}^*$  were inferred via expressions (46), using the assumption that a radial exponential distribution holds exactly above  $\mathcal{Q}_q$ .

The model captures the extremal dependence structure of our dataset well as observed through the correspondence between the posterior mean of  $\mathcal{G}$  and the scaled sample cloud. Figure 6 also shows the directions of exceedances of the posterior means of  $\mathcal{Q}_{0.95}$  and  $\mathcal{Q}_{0.95}^*$  which, as expected, seem to respectively follow  $\mathcal{W}$  and the uniform density on  $\mathbb{S}^2$  well.

To assess model adequacy, we use the method developed in Section 3.4. We apply transformation (52) to  $\tilde{\mathbf{x}}$  for each of the posterior samples  $(\mathcal{Q}_{q,i}, \mathcal{G}_{i,j}, \mathcal{W}_{i,j})$ , with  $i = 1, \dots, 20$  and  $j = 1, \dots, 50$ , resulting in 1000 associated observed point patterns  $P_{i,j}^*$ . Variability in the posterior samples entails varying numbers of atoms  $n_{i,j}^*$  in each  $P_{i,j}^*$ ; to enable a global comparison under a single 0.95-envelope, we thin each  $P_{i,j}^*$  by removing uniformly at random the number of atoms needed to reach  $\min_{i,j} n_{i,j}^*$ . Each thinned  $P_{i,j}^*$  is then used to compute  $\hat{K}_B(r \mid P_{i,j}^*)$  and  $\hat{K}_C(r \mid P_{i,j}^*)$ , the estimates (55), at a sequence of distances and half aperture angles  $r$ . These are shown in Figure 7. A vast majority of these function estimates stay entirely within the the 0.95-envelopes created from a uniform sample of size  $\min_{i,j} n_{i,j}^*$ , thus providing evidence that the weak convergence given in Theorem 2 may hold well for the data at hand. Furthermore, the QQ plots in Figures 34 in Supplementary Material 7.2 show that there is good agreement with the empirical and model-based estimates in their abilities to extrapolate exceedances to extreme values. Figure 35 in Supplementary Material 7.2 shows PP plots for directions generated from the posterior distribution of  $r_{\mathcal{W}}$  have good agreement with the empirical distribution of the directions. Via plots of posterior mean and prediction intervals for  $\chi_q(A)$ ,  $A \subseteq \{H, P, S\}$ , Supplementary 7.2 also shows the strong ability of our model to estimate joint tail probabilities.

Coles & Tawn (1994) introduce a structure variable  $Q(v; \mathbf{O})$ , interpreted as the volume of water (in cubic meters,  $m^3$ ) overtopping the sea-wall per unit length (in meters,  $m$ ) over a fixed duration (in seconds,  $s$ ), and measured in  $m^3 s^{-1} m^{-1}$  for a sea-wall  $v$  meters in height. More precisely,

$$Q(v; \mathbf{O}) = a_1 O_S O_P \exp\{a_2 (v - O_S - l) / (O_P O_H^{*1/2})\}.$$

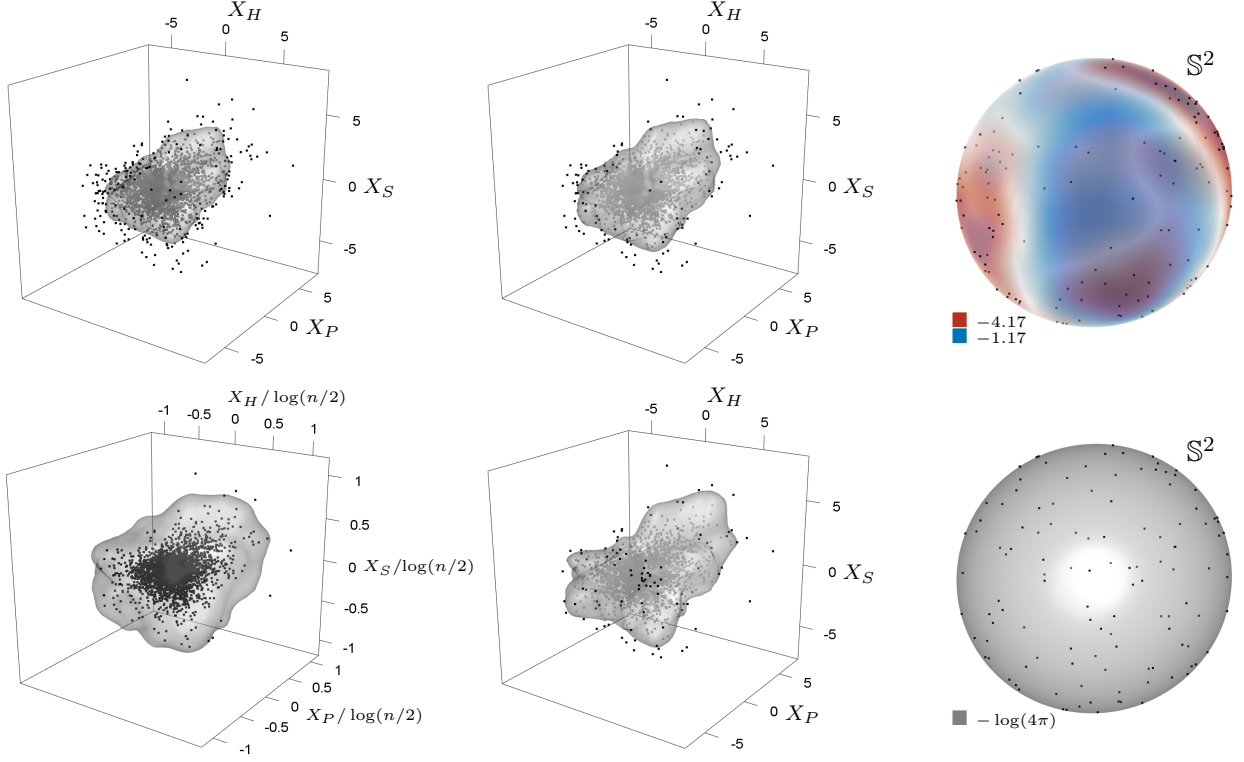


Figure 6: Posterior means of model variables for the Newlyn wave data. *Top-left*: quantile set  $\mathcal{Q}_{0.9}$ . *Bottom-left*: boundary of the scaling set  $\mathcal{G}$ . *Top-centre*: quantile set  $\mathcal{Q}_q$ . *Bottom-centre*: isotropic probability set  $\mathcal{Q}_q^*$ . *Top-right*: log-density of  $\mathbf{W} \mid R > r_{\mathcal{Q}_q}$  plotted over  $\mathbb{S}^2$  with observations in  $\mathbf{X}_{1/(1-q)}$  projected onto  $\mathbb{S}^2$ . *Bottom-right*: logarithm of the density of the uniform distribution on  $\mathbb{S}^2$  with observations in  $\mathbf{X}_{1/(1-q)}^*$  projected onto  $\mathbb{S}^2$ . The probability level  $q$  is set to 0.95.

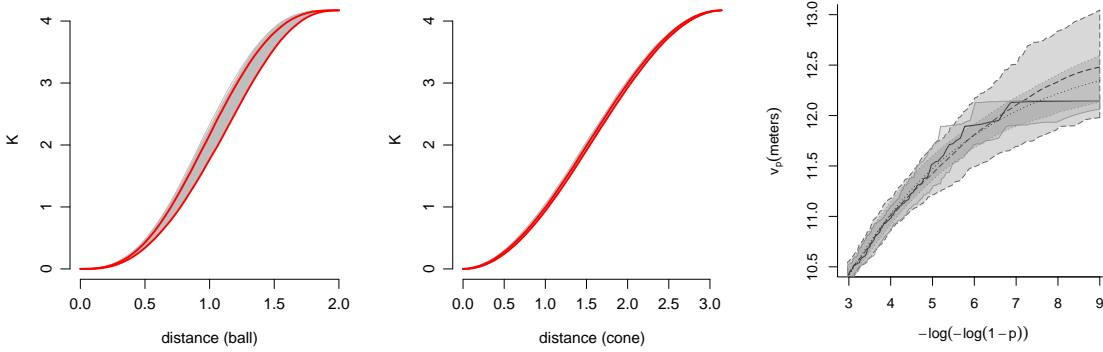


Figure 7: *Left and centre*: Score values  $K_B(r)$  and  $K_C(r)$  from 1000 posterior values of  $r_{\mathcal{Q}^*}(\mathbf{w})$  and  $r_{\mathcal{G}^*}(\mathbf{w})$  for increasing distances  $r$ , with simultaneous 95% prediction intervals in red. *Right*: Estimated return levels for sea-wall height. Presented are results from empirical fits (solid black line), GP (dotted black line), and our semi-parametric method (dashed black line). Grey regions correspond to 95% confidence bands.

The wave height component  $O_H^*$  is a calibration of the wave height marginal variable  $O_H$  to approximate the off-shore wave height, since measurements are taken on-shore. We estimate the

sea-wall height structure variable  $v_p$  (in meters,  $m$ ) for which the discharge rate value  $Q(v_p; \mathbf{O})$  is expected to exceed the design standard of  $0.002m^3s^{-1}m^{-1}$  with probability  $p$ . Setting  $V = Q^{-1}(0.002; \mathbf{O})$ ,  $v_p$  is the solution to  $\mathbb{P}(V > v_p) = p$ . As in [Bortot et al. \(2000\)](#), we fix the sea-wall design feature constants to  $a_1 = 0.25$ ,  $a_2 = 26$ , and tidal level relative to the seabed to  $l = 4.3$ .

We obtain three separate estimates for  $v_p$  at a range of  $p$  values. First, an empirical estimate of  $v_p$  is obtained by using the empirical quantile function on values of the structure variable  $V$  computed from the dataset. Second, a GP model is fitted using the dataset’s computed values of  $V$  obtained from the dataset, and quantiles are then obtained for  $v_p$ . Finally, we compare these with prediction intervals for  $v_p$  obtained from our fitted model  $M_2$  via the procedure described below.

The method consists in sampling a collection  $\{\tilde{\mathbf{O}}_k = \{\mathbf{O}_{1,k}, \dots, \mathbf{O}_{n,k}\} : k = 1, \dots, l\}$  of new datasets, each comprising  $n = 2,894$  observations, to collect a sample of wall heights  $\{v_{p,k} : k = 1, \dots, l\}$  where each  $v_{p,k}$  is the  $p$ -quantile of  $\{V_{j,k} = Q^{-1}(0.002; \mathbf{O}_{j,k}) : j = 1, \dots, n\}$ . For a sequence of  $p \in (0.9, 1)$ , we consider the  $p$ -wise mean as well as the 95% prediction intervals based on equal-tailed quantiles of the sample of sea wall heights.

To generate a new data set  $\tilde{\mathbf{O}}_k$ , we randomly sample one of the 20 realisations from the posterior distribution of  $\mathcal{Q}_q$ , label it  $\mathcal{Q}_{q,k}$ , as well as one of the 50 realisations from the conditional distribution of  $\mathcal{G}, \mathcal{W} \mid \mathcal{Q}_{q,k}$ , and label it  $(\mathcal{G}_k, \mathcal{W}_k)$ . The new sample  $\tilde{\mathbf{X}}_k$  is then constructed by sampling with replacement  $nq$  observations from the original observations falling in  $\mathcal{Q}_{q,k}$ , and  $n(1 - q)$  observations from a radial exponential distribution with location  $\mathcal{Q}_{q,k}$ , scale  $\mathcal{G}_k$ , and directional shape  $\mathcal{W}_k$ , before transforming the sample to original margins using the probability integral transform via the standard Laplace distribution function and then inverse transform via the inverse marginal model specified in Section 3.1.

Figure 7 includes the resulting estimates of  $v_p$  plotted against  $-\log(-\log(1 - p))$  for a range of  $p$  values. Compared to the empirical and GP distribution fit approach, our method accurately estimates the sea-wall height variable  $v_p$  across all values of  $p \in (0, 0.10)$ . The larger prediction intervals corresponding to our method can be attributed to our more holistic account of uncertainty via a joint model for extreme events, in contrast with a structured variable approach; our method hence reveals that risk may have been underestimated by such previous methods.

## 5 Discussion

This work introduces a framework for defining probability sets and return sets in multivariate extremes, emphasizing the role of these sets in capturing the geometry of extreme events. Central to this framework is the identification of the isotropic return set under a radial-directional decomposition, which balances exceedances across all directions and provides a natural representation of the geometry of a sample cloud. Importantly, in our framework these return sets arise through equivalence classes of normalising functions that lead to the weak convergence of radially renormalised sample clouds to a novel Poisson point process, further refining recent results on the convergence of scaled sample clouds and allowing for extrapolation of these sets.

Our construction of probability sets shares conceptual similarities to other constructions, such

as the total probability sets and environmental contours (Mackay & Haselsteiner 2021), which have been used in structural reliability and risk assessment. These sets have been motivated by the multivariate probability integral transform of Rosenblatt (1952), which may be burdensome to implement in high-dimensional settings due to its reliance on sequential conditioning, and recent efforts have focussed on methods that bypass this transformation, see for example Mackay & de Hauteclocque (2023). In a similar spirit, our framework simplifies implementation by relying on a one-dimensional probability integral transform under a radial-directional decomposition, making it more computationally tractable in multivariate extremes. This is already evidenced by the work of Campbell & Wadsworth (2024), which leverage piece-wise linear models for the radial functions of the limit set, the quantile set and the directional set, to infer probabilities of rare events in dimensions  $d = 4$  and  $d = 5$ , with statistical guarantees. Additionally, our approach shares conceptual similarities with the framework of Hallin et al. (2021) for optimal transport-based center-outward ranks, where a probability integral transform that does not rely on sequential conditioning, pushes the multivariate distribution forwards to the uniform distribution over unit ball. However, while this method focusses on center-outward ordering, our work leverages related ideas in the context of extremes to define isotropic return sets that can reflect the geometry of extreme multivariate events and facilitates their extrapolation beyond the observed data.

In parallel to our work, Simpson & Tawn (2024b) developed a pair of environmental contours under a radial-directional decomposition, termed “new environmental contours”. While their paper acknowledges that our framework appeared on *arXiv* during the review of their manuscript, it is important to clarify that this approach defines only two contours, one of which coincides with the *quantile set* introduced in our framework, which also appeared in Mackay & Jonathan (2024). In contrast, here we provide a general definition of an infinite class of return sets, which includes the isotropic return set, exhibiting particularly desirable properties by aligning closely with the structure of the underlying sample. By integrating a new probabilistic theory with geometric insights, our work establishes a foundation that advances existing state-of-the-art theory, opening pathways for innovation in statistical inference and risk assessment.

## Acknowledgments

We thank Jennifer L. Wadsworth for insightful discussions on the framework of geometric extremes, and Finn Lindgren for guidance with the `inlabru` and `excursions` packages in the **R** computing language. Part of this paper was written during a visit of IP and LDM at King Abdullah University of Science and Technology and during a visit of RC at the University of Edinburgh. LDM acknowledges funding by the School of Mathematics, University of Edinburgh. RC acknowledges funding by the EPSRC DTP EP/W523811/1 fund at Lancaster University, with additional funding provided by NSERC PGS D (Canada), and the FRQNT doctoral fund (Québec).

## References

- Arce Guillen, R., Lindgren, F., Muff, S., Glass, T. W., Breed, G. A. & Schlägel, U. E. (2023), ‘Accounting for unobserved spatial variation in step selection analyses of animal movement via spatial random effects’, *Methods in Ecology and Evolution* **14**(10), 2639–2653.
- Baker, S. G. (1994), ‘The multinomial-Poisson transformation’, *J. Roy. Statist. Soc., D* **43**(4), 495–504.
- Balkema, A. A. & de Haan, L. (1974), ‘Residual life time at great age’, *Ann. Probab.* **2**(5), 792–804.
- Balkema, G. & Nolde, N. (2010), ‘Asymptotic independence for unimodal densities’, *Adv. Appl. Probab.* **42**(2), 411–432.
- Barnett, V. (1976), ‘The ordering of multivariate data (with discussion)’, *J. Roy. Statist. Soc., A* **139**(3), 318–355.
- Barthelmé, S. & Chopin, N. (2015), ‘The Poisson transform for unnormalised statistical models’, *Stat. Comput.* **25**(4), 767–780.
- Billingsley, P. (2008), *Probability and Measure*, 3rd edn, John Wiley & Sons.
- Bolin, D. & Lindgren, F. (2015), ‘Excursion and contour uncertainty regions for latent Gaussian models’, *J. Roy. Statist. Soc., B* **77**(1), 85–106.
- Bolin, D. & Lindgren, F. (2017), ‘Quantifying the uncertainty of contour maps’, *Journal of Computational and Graphical Statistics* **26**(3), 513–524.
- Bolin, D. & Lindgren, F. (2018), ‘Calculating probabilistic excursion sets and related quantities using excursions’, *J. Stat. Softw.* **86**(5), 1–20.
- Bortot, P., Coles, S. & Tawn, J. (2000), ‘The multivariate Gaussian tail model: An application to oceanographic data’, *J. Roy. Statist. Soc., C* **49**(1), 31–049.
- Brenier, Y. (1991), ‘Polar factorization and monotone rearrangement of vector-valued functions’, *Communications on Pure and Applied Mathematics* **44**(4), 375–417.
- Campbell, R. & Wadsworth, J. (2024), ‘Piecewise-linear modeling of multivariate geometric extremes’, [arXiv:2412.05195](https://arxiv.org/abs/2412.05195).
- Chernozhukov, V., Galichon, A., Hallin, M. & Henry, M. (2017), ‘Monge–Kantorovich depth, quantiles, ranks and signs’, *Ann. Stat.* **45**(1), 223 – 256.
- Coles, S. G. (2001), *An Introduction to Statistical Modeling of Extreme Values*, Springer–Verlag, London.
- Coles, S. G. & Tawn, J. A. (1991), ‘Modelling extreme multivariate events’, *J. Roy. Statist. Soc., B* **53**, 377–392.

- Coles, S. G. & Tawn, J. A. (1994), ‘Statistical methods for multivariate extremes: an application to structural design’, *J. Roy. Statist. Soc., C* **43**(1), 1–31.
- Davison, A. C. & Smith, R. L. (1990), ‘Models for exceedances over high thresholds (with discussion)’, *J. Roy. Statist. Soc., B* **52**(3), 393–442.
- de Haan, L. (1984), ‘A spectral representation for max-stable processes’, *Ann. Probab.* **12**(3), 1194–1204.
- de Haan, L. & Ferreira, A. (2006), *Extreme Value Theory: An Introduction*, Vol. 21 of *Springer Series in Operations Research & Financial Engineering*, Springer, New York.
- de Haan, L. & Resnick, S. (1987), ‘On regular variation of probability densities’, *Stochastic processes and their applications* **25**, 83–93.
- de Haan, L. & Resnick, S. I. (1977), ‘Limit theory for multivariate sample extremes’, *Z. Wahrsch. Theor.* **40**(4), 317–337.
- de Haan, L. & Stadtmüller, U. (1996), ‘Generalized regular variation of second order’, *Journal of the Australian Mathematical Society* **61**(3), 381–395.
- Engelke, S. & Hitz, A. S. (2020), ‘Graphical models for extremes (with discussion)’, *J. Roy. Statist. Soc. Ser. B*.
- Fasiolo, M., Wood, S. N., Zaffran, M., Nedellec, R. & Goude, Y. (2021), ‘Fast calibrated additive quantile regression’, *J. Am. Stat. Assoc.* **116**(535), 1402–1412.
- Gradshteyn, I. S. & Ryzhik, I. M. (2014), *Table of Integrals, Series, and Products*, Academic Press.
- Hallin, M., del Barrio, E., Cuesta-Albertos, J. & Matrán, C. (2021), ‘Distribution and quantile functions, ranks and signs in dimension  $d$ : A measure transportation approach’, *Ann. Stat.* **49**(2), 1139 – 1165.
- Hallin, M. & Konen, D. (2024), Multivariate quantiles: Geometric and measure-transportation-based contours, in V. Kreinovich, W. Yamaka & S. Leurcharusmee, eds, ‘Applications of Optimal Transport to Economics and Related Topics’, Springer Nature Switzerland, Cham, pp. 61–78.
- Hansen, G., Herbrut, I., Martini, H. & Moszyńska, M. (2020), ‘Starshaped sets’, *Aequationes mathematicae* **94**, 1001–1092.
- Heffernan, J. E. & Tawn, J. A. (2004), ‘A conditional approach for multivariate extreme values (with discussion)’, *J. Roy. Statist. Soc., B* **66**(3), 1–34.
- Keef, C., Papastathopoulos, I. & Tawn, J. A. (2013), ‘Estimation of the conditional distribution of a multivariate variable given that one of its components is large: additional constraints for the Heffernan and Tawn model’, *J. Mult. Anal* **115**, 396–404.

- Kiriliouk, A., Rootzén, H., Segers, J. & Wadsworth, J. L. (2019), ‘Peaks over thresholds modeling with multivariate generalized Pareto distributions’, *Technometrics* **61**(1), 123–135.
- Klain, D. A. (1997), ‘Invariant valuations on star-shaped sets’, *Advances in Mathematics* **125**(1), 95–113.
- Koenker, R. (2005), *Quantile Regression*, Vol. 38, Cambridge University Press.
- Kotz, S., Kozubowski, T. J. & Podgorski, K. (2001), ‘The laplace distribution and generalizations’, *(No Title)*.
- Leadbetter, M. R., Lindgren, G. & Rootzén, H. (1983), *Extremes and Related Properties of Random Sequences and Series*, Springer–Verlag, New York.
- Ledford, A. W. & Tawn, J. A. (1996), ‘Statistics for near independence in multivariate extreme values’, *Biometrika* **83**(1), 169–187.
- Ledford, A. W. & Tawn, J. A. (1997), ‘Modelling dependence within joint tail regions’, *J. Roy. Statist. Soc., B* **59**(1), 475–499.
- Lindgren, F., Rue, H. & Lindström, J. (2011), ‘An explicit link between Gaussian fields and Gaussian Markov random fields: the stochastic partial differential equation approach (with discussion)’, *J. Roy. Statist. Soc., B* **73**(4), 423–498.
- Lutwak, E. (1988), ‘Intersection bodies and dual mixed volumes’, *Advances in Mathematics* **71**(2), 232–261.
- Mackay, E. & de Hauteclocque, G. (2023), ‘Model-free environmental contours in higher dimensions’, *Ocean Engineering* **273**, 113959.
- Mackay, E. & Haselsteiner, A. F. (2021), ‘Marginal and total exceedance probabilities of environmental contours’, *Marine Structures* **75**, 102863.
- Mackay, E. & Jonathan, P. (2024), ‘Modelling multivariate extremes through angular-radial decomposition of the density function’, *arXiv:2310.12711*.
- Majumder, R., Shaby, B. A., Reich, B. J. & Cooley, D. (2023), ‘Semiparametric estimation of the shape of the limiting multivariate point cloud’, *arXiv:2306.13257*.
- Maulik, K. & Resnick, S. (2004), ‘Characterizations and examples of hidden regular variation’, *Extremes* **7**(1), 31–67.
- McCann, R. J. (1995), ‘Existence and uniqueness of monotone measure-preserving maps’, *Duke Mathematical Journal* **80**(2), 309 – 323.
- Nolde, N. (2014), ‘Geometric interpretation of the residual dependence coefficient’, *J. Mult. Anal.* **123**, 85–95.

- Nolde, N. & Wadsworth, J. L. (2022), ‘Linking representations for multivariate extremes via a limit set’, *Adv. Appl. Probab.* **54**(3), 688–717.
- Papastathopoulos, I., Auld, G., Lindgren, F., Gerlei, K. Z. & Nolan, M. F. (2023), ‘Bayesian inference of grid cell firing patterns using Poisson point process models with latent oscillatory Gaussian random fields’, *arXiv:2303.17217*.
- Papastathopoulos, I. & Paulin, D. (2023), ‘Markov random tail fields and extended multivariate regularly varying functions’. Unpublished research.
- Papastathopoulos, I. & Tawn, J. A. (2013), ‘A generalised Student’s  $t$ -distribution’, *Stat. Probabil. Lett.* **83**, 70–77.
- Pickands, J. (1975), ‘Statistical inference using extreme order statistics’, *Ann. Stat.* **3**(1), 119–131.
- Resnick, S. I. (1987), *Extreme Values, Regular Variation and Point Processes*, Springer–Verlag, New York.
- Resnick, S. I. (2007), *Heavy-tail phenomena: probabilistic and statistical modeling*, Springer Science & Business Media, New York.
- Ripley, B. D. (1976), ‘The second-order analysis of stationary point processes’, *J. Appl. Probab.* **13**(2), 255–266.
- Ripley, B. D. (1977), ‘Modelling spatial patterns (with discussion)’, *J. Roy. Statist. Soc., B* **39**(2), 172–192.
- Rootzén, H. & Tajvidi (2006), ‘The multivariate generalized Pareto distribution’, *Bernoulli* **12**, 917–930.
- Rosenblatt, M. (1952), ‘Remarks on a multivariate transformation’, *The Annals of Mathematical Statistics* **23**(3), 470–472.
- Seneta, E. (1976), *Regularly Varying Functions*, Vol. 508 of *Lecture Notes in Mathematics*, Springer Berlin, Heidelberg.
- Simpson, D., Illian, J. B., Lindgren, F., Sørbye, S. H. & Rue, H. (2016), ‘Going off grid: computationally efficient inference for log-Gaussian Cox processes’, *Biometrika* **103**(1), 49–70.
- Simpson, E. S. & Tawn, J. A. (2024a), ‘Estimating the limiting shape of bivariate scaled sample clouds: With additional benefits of self-consistent inference for existing extremal dependence properties’, *EJS* **18**(2), 4582 – 4611.
- Simpson, E. S. & Tawn, J. A. (2024b), ‘Inference for new environmental contours using extreme value analysis’, *JABES*.

- Soms, A. P. (1976), ‘An asymptotic expansion for the tail area of the t-distribution’, *J. Am. Stat. Assoc.* **71**(355), 728–730.
- Sweeting, T. J. (1985), ‘On Domains of Uniform Local Attraction in Extreme Value Theory’, *The Annals of Probability* **13**(1), 196 – 205.
- Wadsworth, J. L. & Campbell, R. (2024), ‘Statistical inference for multivariate extremes via a geometric approach’, *J. Roy. Statist. Soc., B* **86**(5), 1243–1265.
- Wadsworth, J. & Tawn, J. (2013), ‘A new representation for multivariate tail probabilities’, *Bernoulli* **19**(5B), 2689–2714.
- Waldmann, E., Kneib, T., Yue, Y. R., Lang, S. & Flexeder, C. (2013), ‘Bayesian semiparametric additive quantile regression’, *Stat. Model.* **13**(3), 223–252.
- Wood, S. N. (2017), *Generalized Additive Models: an Introduction with R*, CRC press, New York.
- Yu, K. & Moyeed, R. A. (2001), ‘Bayesian quantile regression’, *Stat. Probabil. Lett.* **54**(4), 437–447.
- Yuan, Y., Bachl, F. E., Lindgren, F., Borchers, D. L., Illian, J. B., Buckland, S. T., Rue, H. & Gerrodette, T. (2017), ‘Point process models for spatio-temporal distance sampling data from a large-scale survey of blue whales’, *Ann. Appl. Stat.* **11**(4), 2270–2297.

# APPENDIX

## A Proofs

### A.1 Proof of Theorem 1

The fact that (2) imply (3) and (4) follows from Assumption 0  $\in S$ , which implies that  $\pi = \mathbb{P}(X > 0) \in (0, 1)$  and  $1 - \pi = \mathbb{P}(X < 0) \in (0, 1)$ , and convergence of types (Theorem 1.4.2 in Billingsley 2008), with normalizing sequences satisfying

$$\begin{aligned} b_{n,\{+1\}} &\sim (b_n - m) + [(\pi^{-\xi_{\{+1\}}} - 1)/\xi_{\{+1\}}]a_n & \text{and} & & a_{n,\{+1\}} &\sim a_n \pi^{-\xi_{\{+1\}}}, \\ b_{n,\{-1\}} &\sim (\beta_n - m) + [((1 - \pi)^{-\xi_{\{-1\}}} - 1)/\xi_{\{-1\}}]\alpha_n & \text{and} & & a_{n,\{-1\}} &\sim \alpha_n (1 - \pi)^{-\xi_{\{-1\}}} \end{aligned}$$

as  $n \rightarrow \infty$ . To show that the sequence of mean measures in expression (5) converges vaguely in  $M_+(\overline{\mathbb{E}}_{\xi_{\{-1\}}} \times \{-1\}) \cup (\overline{\mathbb{E}}_{\xi_{\{+1\}}} \times \{+1\})$ , we need to show that for any  $h \in C_K^+(\overline{\mathbb{E}}_{\xi_{\{-1\}}} \times \{-1\}) \cup (\overline{\mathbb{E}}_{\xi_{\{+1\}}} \times \{+1\})$

$$\begin{aligned} &\lim_{n \rightarrow \infty} \int_{(\overline{\mathbb{E}}_{\xi_{\{-1\}}} \times \{-1\}) \cup (\overline{\mathbb{E}}_{\xi_{\{+1\}}} \times \{+1\})} h(z, w) n \mathbb{P} \left[ \left( \frac{|X| - r_n^a(X/|X|)}{r_n^b(X/|X|)}, X/|X| \right) \in dz \times dw \right] \quad (\text{A.1}) \\ &= \int_{(\overline{\mathbb{E}}_{\xi_{\{-1\}}} \times \{-1\}) \cup (\overline{\mathbb{E}}_{\xi_{\{+1\}}} \times \{+1\})} h(z, w) \Lambda(dz \times dw), \end{aligned}$$

with  $\Lambda$  defined in expression (6). Note that because  $(\overline{\mathbb{E}}_{\xi_{\{-1\}}} \times \{-1\}) \cup (\overline{\mathbb{E}}_{\xi_{\{+1\}}} \times \{+1\})$  is a disjoint union, then  $h(z, w) = h_{\{-1\}}(z) \mathbb{1}_{\{w=-1\}} + h_{\{+1\}}(z) \mathbb{1}_{\{w=1\}}$ , with  $h_{\{-1\}} \in C_K^+(\overline{\mathbb{E}}_{\xi_{\{-1\}}})$  and  $h_{\{+1\}} \in C_K^+(\overline{\mathbb{E}}_{\xi_{\{+1\}}})$ . Using total probability, the integral in expression (A.1) equals

$$\begin{aligned} &(1 - \pi) \int_{\overline{\mathbb{E}}_{\xi_{\{-1\}}} h_{\{-1\}}(z) n \mathbb{P} \left[ \left( \frac{|X| - r_n^a(X/|X|)}{r_n^b(X/|X|)} \in dz \mid X/|X| = -1 \right) \right] + \\ &+ \pi \int_{\overline{\mathbb{E}}_{\xi_{\{+1\}}} h_{\{+1\}}(z) n \mathbb{P} \left[ \left( \frac{|X| - r_n^a(X/|X|)}{r_n^b(X/|X|)} \in dz \mid X/|X| = +1 \right) \right]. \end{aligned}$$

Convergences (3) and (4) guarantee that as  $n \rightarrow \infty$ , the latter expression converges to

$$(1 - \pi) \int_{\overline{\mathbb{E}}_{\xi_{\{-1\}}} h_{\{-1\}} d\nu_{\{-1\}} + \pi \int_{\overline{\mathbb{E}}_{\xi_{\{+1\}}} h_{\{+1\}} d\nu_{\{+1\}} = \int_{(\overline{\mathbb{E}}_{\xi_{\{-1\}}} \times \{-1\}) \cup (\overline{\mathbb{E}}_{\xi_{\{+1\}}} \times \{+1\})} h d\Lambda,$$

completing the proof.

## A.2 Convergence in distribution of renormalised sample minimum and maximum

By replacing 1 with  $\pi + (1 - \pi)$  in  $1 - \mathbb{P}_n := \bar{\mathbb{P}}_n$  and by applying the law of total probability to  $\mathbb{P}_n$ , we average the conditional probabilities given  $\{X \geq 0\}$  and  $\{X < 0\}$  over  $\pi$  and  $1 - \pi$  and note that, due to conditions (3) and (4), which guarantee that both  $a_{n,\{+1\}}z_+ + b_{n,\{+1\}}$  and  $a_{n,\{-1\}}(-z_-) + b_{n,\{-1\}}$  are ultimately positive, we find that

$$n\bar{\mathbb{P}}_n = (1 - \pi)n\mathbb{P}\left(\frac{|X| - b_{n,\{-1\}}}{a_{n,\{-1\}}} > -z_- \mid X < 0\right) + \pi n\mathbb{P}\left(\frac{|X| - b_{n,\{+1\}}}{a_{n,\{+1\}}} > z_+ \mid X > 0\right), \quad (\text{A.2})$$

for all sufficiently large  $n$ . Thus, the convergences (3) and (4) lead to

$$\lim_{n \rightarrow \infty} \mathbb{P}\left(\frac{m_n + b_{n,\{-1\}}}{a_{n,\{-1\}}} > z_-, \frac{M_n - b_{n,\{+1\}}}{a_{n,\{+1\}}} < z_+\right) = G_0(-z_-, z_+ \mid \pi), \quad \text{as } n \rightarrow \infty, \quad (\text{A.3})$$

at continuity points of the limit distribution  $G_0$  given by expression (10).

## A.3 Convergence to Poisson point process

*Proof of Theorem 2.* To prove the weak convergence of the random point measure to the stated limit Poisson random measure, we need to show that for any  $h \in C_K^+(\cup_{\mathbf{w} \in \mathbb{S}^{d-1}} \bar{\mathbb{E}}_{\xi(\mathbf{w})} \times \{\mathbf{w}\})$

$$\nu_n(h) := \int_{\mathbb{S}^{d-1}} \int_{\bar{\mathbb{E}}_{\xi(\mathbf{w})}} h(z, \mathbf{w}) \nu_{n,\mathbf{w}}(dz) \mathbb{P}_{\mathbf{X}/\|\mathbf{X}\|}(d\mathbf{w}) \rightarrow \int_{\mathbb{S}^{d-1}} \int_{\bar{\mathbb{E}}_{\xi(\mathbf{w})}} h(z, \mathbf{w}) \nu_{\mathbf{w}}(dz) \mathbb{P}_{\mathbf{X}/\|\mathbf{X}\|}(d\mathbf{w}) =: \nu(h),$$

as  $n \rightarrow \infty$ . It suffices to show that  $|\nu_n(h) - \nu(h)| \rightarrow 0$  as  $n \rightarrow \infty$ . Since  $h$  is continuous on a compact set, say  $K_h \subset \bar{\mathbb{E}}^d$ , we can find a compact cover  $\mathbb{S}^{d-1} \times [r_{\text{inf}}, r_{\text{sup}}] \supset K_h$ , with  $r_{\text{inf}} = \inf\{\|\mathbf{x}\| : \mathbf{x} \in K_h\}$  and  $r_{\text{sup}} = \sup\{\|\mathbf{x}\| : \mathbf{x} \in K_h\}$ , such that

$$\begin{aligned} |\nu_n(h) - \nu(h)| &\leq \int_{\mathbb{S}^{d-1}} \|h\|_{\infty}(\mathbf{w}) |\mu_{n,\mathbf{w}}|([r_{\text{inf}}, r_{\text{sup}}]) \mathbb{P}_{\mathbf{X}/\|\mathbf{X}\|}(\mathbf{w}), \\ &\leq \int_{\mathbb{S}^{d-1}} \|h\|_{\infty}(\mathbf{w}) \Delta(\mathbf{w}) \mathbb{P}_{\mathbf{X}/\|\mathbf{X}\|}(d\mathbf{w}) \quad \text{for all } n > n_0, \end{aligned}$$

where  $\|h\|_{\infty}(\mathbf{w}) = \sup\{h(z, \mathbf{w}) : z \in \bar{\mathbb{E}}_{\xi(\mathbf{w})}\} < \infty$ . Since

$$\lim_{n \rightarrow \infty} (\nu_{n,\mathbf{w}}(h) - \nu_{\mathbf{w}}(h)) = 0,$$

dominated convergence gives that  $|\nu_n(h) - \nu(h)| \rightarrow 0$  as  $n \rightarrow \infty$ .  $\square$

## A.4 Properties of probability sets

*Proof of Proposition 5.* (i) Using total probability and the change of the integrating measure  $\mathbb{P}_{\mathbf{W}}$  to  $\mu$ , we have

$$\mathbb{P}(R > r_{\mathcal{Q}_q(\mathbb{P}_{\mathbf{W}} \parallel \mu)}(\mathbf{W})) = \int_{\text{supp}(\mathbb{P}_{\mathbf{X}/\|\mathbf{X}\|})} \mathbb{P}(R > r_{\mathcal{Q}_q(\mathbb{P}_{\mathbf{W}} \parallel \mu)}(\mathbf{w}) \mid \mathbf{W} = \mathbf{w}) \frac{d\mathbb{P}_{\mathbf{W}}}{d\mu}(\mathbf{w}) \mu(d\mathbf{w})$$

Multiplication and division by  $1/(1-q)$  gives

$$\mathbb{P}(R > r_{\mathcal{Q}_q(\mathbb{P}_{\mathbf{W}} \parallel \mu)}(\mathbf{W})) = (1-q) \int_{\text{supp}(\mathbb{P}_{\mathbf{W}})} \frac{\mathbb{P}(R > r_{\mathcal{Q}_q(\mathbb{P}_{\mathbf{W}} \parallel \mu)}(\mathbf{w}) \mid \mathbf{W} = \mathbf{w})}{1-q} \frac{d\mathbb{P}_{\mathbf{W}}}{d\mu}(\mathbf{w}) \mu(d\mathbf{w}).$$

From the definition (28) of  $r_{\mathcal{Q}_q(\mathbb{P}_{\mathbf{W}} \parallel \mu)}(\mathbf{w})$ , we have that for any  $q > q_l(\mathbb{P}_{\mathbf{W}} \parallel \mu^*)$ ,

$$\frac{\mathbb{P}(R > r_{\mathcal{Q}_q(\mathbb{P}_{\mathbf{W}} \parallel \mu)}(\mathbf{w}) \mid \mathbf{W} = \mathbf{w})}{1-q} = \left( \frac{d\mathbb{P}_{\mathbf{W}}}{d\mu}(\mathbf{w}) \right)^{-1}.$$

Thus, since  $\mu$  is a probability measure on  $\text{supp}(\mathbb{P}_{\mathbf{W}})$ ,

$$\mathbb{P}[R > r_{\mathcal{Q}_q(\mathbb{P}_{\mathbf{W}} \parallel \mu)}(\mathbf{W})] = (1-q) \int_{\text{supp}(\mathbb{P}_{\mathbf{W}})} \mu(d\mathbf{w}) = (1-q).$$

Next, we consider the conditional distribution of  $\mathbf{W}$  given  $R > r_{\mathcal{Q}_q(\mathbb{P}_{\mathbf{W}} \parallel \mu)}(\mathbf{W})$ . For any measurable set  $B \subset \text{supp}(\mathbb{P}_{\mathbf{W}})$ , we have

$$\mathbb{P}(\mathbf{W} \in B \mid R > r_{\mathcal{Q}_q(\mathbb{P}_{\mathbf{W}} \parallel \mu)}(\mathbf{W})) = \mathbb{P}(R > r_{\mathcal{Q}_q(\mathbb{P}_{\mathbf{W}} \parallel \mu)}(\mathbf{W}), \mathbf{W} \in B) / \mathbb{P}(R > r_{\mathcal{Q}_q(\mathbb{P}_{\mathbf{W}} \parallel \mu)}(\mathbf{W}))$$

Because  $\mathbb{P}[R > r_{\mathcal{Q}_q(\mathbb{P}_{\mathbf{W}} \parallel \mu)}(\mathbf{W})] = (1-q)$ , it follows that for any  $q > q_l(\mathbb{P}_{\mathbf{W}} \parallel \mu^*)$ ,

$$\begin{aligned} \mathbb{P}(\mathbf{W} \in B \mid R > r_{\mathcal{Q}_q(\mathbb{P}_{\mathbf{W}} \parallel \mu)}(\mathbf{W})) &= (1-q)^{-1} \int_B \mathbb{P}(R > r_{\mathcal{Q}_q(\mathbb{P}_{\mathbf{W}} \parallel \mu)}(\mathbf{w}) \mid \mathbf{W} = \mathbf{w}) \mathbb{P}_{\mathbf{W}}(d\mathbf{w}) \\ &= (1-q)^{-1} \int_B (1-q) \frac{d\mu}{\mathbb{P}_{\mathbf{W}}}(\mathbf{w}) \mathbb{P}_{\mathbf{W}}(d\mathbf{w}) \\ &= \int_B \mu(\mathbf{w}) = \mu(B), \end{aligned}$$

which completes the proof of (i).

(ii) For each  $z$  in some open interval  $(a, b)$  that is a continuity point of the limit measure  $\nu_{\mathbf{w}}$ , we have by Assumption that 1

$$\lim_{n \rightarrow \infty} n \mathbb{P} \left[ \frac{R - b_n(\mathbf{W})}{a_n(\mathbf{W})} > z \mid \mathbf{W} = \mathbf{w} \right] \varrho_{\mu}(\mathbf{w}) = [1 + \xi(\mathbf{w})z]_+^{-1/\xi(\mathbf{w})} \varrho_{\mu}(\mathbf{w}), \quad (\text{A.4})$$

for  $\mathbf{w} \in \text{supp}(\mathbb{P}_{\mathbf{W}})$ , where  $\varrho_{\mu} = d\mathbb{P}_{\mathbf{W}}/d\mu > 0$ . Convergence (A.4) is equivalent to  $\lim f_n(z; \mathbf{w}) =$

$g(z; \mathbf{w})$  for  $\mathbf{w} \in \text{supp}(\mathbb{P}_{\mathbf{W}})$ , where

$$f_n(z; \mathbf{w}) := 1 / \left( n \mathbb{P} \left[ \frac{R - b_n(\mathbf{W})}{a_n(\mathbf{W})} > z \mid \mathbf{W} = \mathbf{w} \right] \varrho_\mu(\mathbf{w}) \right) \quad (\text{A.5})$$

$$g(z; \mathbf{w}) = [1 + \xi(\mathbf{w})z]_+^{1/\xi(\mathbf{w})} / \varrho_\mu(\mathbf{w}), \quad (\text{A.6})$$

for  $\mathbf{w} \in \text{supp}(\mathbb{P}_{\mathbf{W}})$ . Since a sequence of non-decreasing functions in  $z$  converges to a limit function that is non-decreasing in  $z$ , Lemma 1.1.1 in [de Haan & Ferreira \(2006\)](#) applies and for each  $y \in (g(a; \mathbf{w}), g(a; \mathbf{w}))$  that is a continuity point of  $g^{-1}$ , we have  $\lim_{n \rightarrow \infty} f_n^{-1}(y; \mathbf{w}) = g^{-1}(y; \mathbf{w})$ , where  $f_n^{-1}$  and  $g^{-1}$  denote the left-continuous inverses of  $f_n$  and  $g$ , respectively. That is,

$$\lim_{n \rightarrow \infty} \frac{V_{\mathbf{w}}(ny; \mu) - b_n(\mathbf{w})}{a_n(\mathbf{w})} = \frac{\{y \varrho_\mu(\mathbf{w})\}^{\xi(\mathbf{w})} - 1}{\xi(\mathbf{w})}, \quad \mathbf{w} \in \text{supp}(\mathbb{P}_{\mathbf{W}}),$$

where

$$V_{\mathbf{w}}(y; \mu) = \inf \{ z \in \mathbb{R} : (n \mathbb{P}(R > z \mid \mathbf{W} = \mathbf{w}) \varrho_\mu(\mathbf{w}))^{-1} \geq y \},$$

is defined for  $y > 1$ . Note that the function  $V_{\mathbf{w}}(n; \mu)$  satisfies  $V_{\mathbf{w}}(1/(1-q); \mu) = r_{\mathcal{Q}_q(\mathbb{P}_{\mathbf{W}} \parallel \mu)}(\mathbf{w})$ .

Since  $\inf \{ \xi(\mathbf{w}) : \mathbf{w} \in \text{supp}(\mathbb{P}_{\mathbf{X}/\|\mathbf{X}\|}) \} > -1$ , it suffices to show that

$$\lim_{n \rightarrow \infty} \frac{V_{\mathbf{w}}(ny; \mu) - V_{\mathbf{w}}(n; \mu)}{V_{\mathbf{w}}(n\{1 + \xi(\mathbf{w})\}^{1/\xi(\mathbf{w})}; \mu) - V_{\mathbf{w}}(n; \mu)} = \frac{y^{\xi(\mathbf{w})} - 1}{\xi(\mathbf{w})}, \quad \mathbf{w} \in \text{supp}(\mathbb{P}_{\mathbf{W}}). \quad (\text{A.7})$$

The left-hand side of expression (A.7) equal

$$\begin{aligned} & \frac{\frac{V_{\mathbf{w}}(ny; \mu) - b_n(\mathbf{w})}{a_n(\mathbf{w})} - \frac{V_{\mathbf{w}}(n; \mu) - b_n(\mathbf{w})}{a_n(\mathbf{w})}}{\frac{V_{\mathbf{w}}(n\{1 + \xi(\mathbf{w})\}^{1/\xi(\mathbf{w})}; \mu) - b_n(\mathbf{w})}{a_n(\mathbf{w})} - \frac{V_{\mathbf{w}}(n; \mu) - b_n(\mathbf{w})}{a_n(\mathbf{w})}} \\ &= \frac{\frac{\{y \varrho_\mu(\mathbf{w})\}^{\xi(\mathbf{w})} - 1}{\xi(\mathbf{w})} - \frac{\varrho_\mu(\mathbf{w})^{\xi(\mathbf{w})} - 1}{\xi(\mathbf{w})}}{\frac{\{(1 + \xi(\mathbf{w}))^{1/\xi(\mathbf{w})} \varrho_\mu(\mathbf{w})\}^{\xi(\mathbf{w})} - 1}{\xi(\mathbf{w})} - \frac{\varrho_\mu(\mathbf{w})^{\xi(\mathbf{w})} - 1}{\xi(\mathbf{w})}} \\ &= \frac{\rho_\mu(\mathbf{w})^{\xi(\mathbf{w})} (y^{\xi(\mathbf{w})} - 1) / \xi(\mathbf{w})}{\varrho_\mu(\mathbf{w})^{\xi(\mathbf{w})}} = \frac{y^{\xi(\mathbf{w})} - 1}{\xi(\mathbf{w})}, \quad \mathbf{w} \in \text{supp}(\mathbb{P}_{\mathbf{W}}). \end{aligned}$$

□

## A.5 Density convergence of rescaled radial excess variable

Below, we use Lemma 1, a direct consequence of the Corollary 3.3 of [de Haan & Resnick \(1987\)](#).

**Lemma 1** (Potter bounds). *Let  $V : \mathbb{R}^d \rightarrow \mathbb{R}$  and suppose there exist  $\rho \in \mathbb{R}$ ,  $h : \mathbb{R}_+ \rightarrow \mathbb{R}_+$ , and  $\mathcal{G} \in \star$  such that  $\lim_{t \rightarrow \infty} V(t\mathbf{x})/h(t) = g_{\mathcal{G}}(\mathbf{x})^\rho$  uniformly on  $\mathbb{S}^{d-1}$ . Then, for any  $\varepsilon > 0$ , there exists  $t_0 = t_0(\varepsilon) > 0$  such that for all  $t > t_0$ ,*

$$(1 - \varepsilon)\|\mathbf{x}\|^{-\varepsilon}g_{\mathcal{G}}(\mathbf{x})^\rho \leq \frac{V(t\mathbf{x})}{h(t)} \leq (1 + \varepsilon)\|\mathbf{x}\|^\varepsilon g_{\mathcal{G}}(\mathbf{x})^\rho, \quad \forall \mathbf{x} \in \mathbb{R}^d \setminus \{\mathbf{0}\}.$$

*Proof of Proposition 6.* Consider the following relation

$$\frac{\partial}{\partial z} \mathbb{P} \left[ \frac{R - r_{\mathcal{Q}_q}(\mathbf{w})}{r_{\mathcal{G}_q}(\mathbf{w})} \leq z \mid R > r_{\mathcal{Q}_q}(\mathbf{W}), \mathbf{W} = \mathbf{w} \right] = \frac{r_{\mathcal{G}_q}(\mathbf{w})z_q(\mathbf{w})^{d-1}f_{\mathbf{X}}(z_q(\mathbf{w})\mathbf{w})}{\int_{r_{\mathcal{Q}_q}(\mathbf{w})}^{r_{\mathcal{Q}_1}(\mathbf{w})} f_{R, \mathbf{W}}(s, \mathbf{w}) ds}, \quad (\text{A.8})$$

where  $z_q(\mathbf{w}) = r_{\mathcal{Q}_q}(\mathbf{w}) + r_{\mathcal{G}_q}(\mathbf{w})z$ ,  $z \in [0, \{r_{\mathcal{Q}_1}(\mathbf{w}) - r_{\mathcal{Q}_q}(\mathbf{w})\}/r_{\mathcal{G}_q}(\mathbf{w})]$ , and  $\mathbf{w} \in \mathbb{S}^{d-1}$ .

(i) Write the integral in expression (A.8) using the change of variable  $s = \{1 - (t\|\mathbf{w}\|)^{-1}\}r_{\mathcal{Q}_1}(\mathbf{w})$ , with  $L_q(\mathbf{w}) := r_{\mathcal{Q}_1}(\mathbf{w})/\{r_{\mathcal{Q}_1}(\mathbf{w}) - r_{\mathcal{Q}_q}(\mathbf{w})\}$ , as

$$\int_{r_{\mathcal{Q}_q}(\mathbf{w})}^{r_{\mathcal{Q}_1}(\mathbf{w})} f_{R, \mathbf{W}}(s, \mathbf{w}) ds = r_{\mathcal{Q}_1}(\mathbf{w})^d \int_{L_q(\mathbf{w})}^{\infty} (1 - 1/t)^{d-1} t^{-2} \{f_{\mathbf{X}}[(1 - 1/t)r_{\mathcal{Q}_1}(\mathbf{w})\mathbf{w}]/\psi_{\mathbf{B}}(t)\} \psi_{\mathbf{B}}(t) dt.$$

Due to convergence (i), the map  $(0, \infty) \ni s \mapsto f_{\mathbf{X}}[(1 - 1/s)r_{\mathcal{Q}_1}(\mathbf{w})\mathbf{w}]/\psi_{\mathbf{B}}(s) \in \mathbb{R}^+$  is slowly varying at  $\infty$ . Additionally, convergence (i) implies that  $\psi_{\mathbf{B}}(s) \in \text{RV}_{1+1/\xi}^\infty$ , hence there exists  $l_{\mathbf{B}} \in \text{RV}_0^\infty$  such that  $\psi_{\mathbf{B}}(s) = l_{\mathbf{B}}(s)s^{1+1/\xi}$ . Thus, by Karamata's theorem (Theorem 2.1 Resnick 2007),

$$\frac{\int_{r_{\mathcal{Q}_q}(\mathbf{w})}^{r_{\mathcal{Q}_1}(\mathbf{w})} f_{R, \mathbf{W}}(s, \mathbf{w}) ds}{\{r_{\mathcal{Q}_1}(\mathbf{w}) - r_{\mathcal{Q}_q}(\mathbf{w})\}f_{R, \mathbf{W}}[r_{\mathcal{Q}_q}(\mathbf{w}), \mathbf{w}]} = -\xi\{1 + o(1)\}, \quad \text{as } q \rightarrow 1.$$

Using the assumption that  $f_{\mathbf{X}}(r\mathbf{w}) \sim \psi_{\mathbf{B}}[r_{\mathcal{Q}_1}(\mathbf{w})/\{r_{\mathcal{Q}_1}(\mathbf{w}) - r\}]g_{\mathcal{G}}(\mathbf{w})^{1+1/\xi}$  as  $r \rightarrow r_{\mathcal{Q}_1}(\mathbf{w})$ , and setting  $r_{\mathcal{G}_q}(\mathbf{w}) = -\xi\{r_{\mathcal{Q}_1}(\mathbf{w}) - r_{\mathcal{Q}_q}(\mathbf{w})\}$ , expression (A.8) converges to

$$\begin{aligned} & \frac{r_{\mathcal{G}_q}(\mathbf{w})z_q(\mathbf{w})^{d-1}f_{\mathbf{X}}[z_q(\mathbf{w})\mathbf{w}]}{-\xi\{r_{\mathcal{Q}_1}(\mathbf{w}) - r_{\mathcal{Q}_q}(\mathbf{w})\}r_{\mathcal{Q}_q}(\mathbf{w})^{d-1}f_{\mathbf{X}}[r_{\mathcal{Q}_q}(\mathbf{w})\mathbf{w}]} \{1 + o(1)\} = \\ & = \frac{z_q(\mathbf{w})^{d-1}}{r_{\mathcal{Q}_q}(\mathbf{w})^{d-1}} \left[ \frac{r_{\mathcal{Q}_1}(\mathbf{w}) - z_q(\mathbf{w})}{r_{\mathcal{Q}_1}(\mathbf{w}) - r_{\mathcal{Q}_q}(\mathbf{w})} \right]^{-1-1/\xi} \{1 + o(1)\} \rightarrow (1 + \xi z)_+^{-1-1/\xi}, \quad \text{as } q \rightarrow 1. \end{aligned}$$

(ii) Consider first the integral term in expression (A.8). The integral is equal to

$$\int_{r_{\mathcal{Q}_q}(\mathbf{w})}^{\infty} s^{d-1} f_{\mathbf{X}}(s\mathbf{w}) ds = \int_{r_{\mathcal{Q}_q}(\mathbf{w})}^{\infty} s^{d-1} \exp[-\psi_{\mathbf{L}}(s)\{-\{\log f_{\mathbf{X}}(s\mathbf{w})\}/\psi_{\mathbf{L}}(s)\}] ds.$$

Due to Lemma 1 with  $V(\mathbf{x}) = -\log f_{\mathbf{X}}(\mathbf{x})$  and  $h = \psi$ , for all  $\varepsilon > 0$  there exists  $q_0 > q$  such that

$$\int_{r_{\mathcal{Q}_q}(\mathbf{w})}^{\infty} s^{d-1} \exp[-(1 + \varepsilon)\psi_{\mathbf{L}}(s)g_{\mathcal{G}}(\mathbf{w})^\rho] ds \leq \int_{r_{\mathcal{Q}_q}(\mathbf{w})}^{\infty} s^{d-1} f_{\mathbf{X}}(s\mathbf{w}) ds \leq \int_{r_{\mathcal{Q}_q}(\mathbf{w})}^{\infty} \exp[-(1 - \varepsilon)\psi_{\mathbf{L}}(s)g_{\mathcal{G}}(\mathbf{w})^\rho] ds.$$

Since  $\varepsilon$  can be made arbitrarily small, we have

$$\int_{r_{\mathcal{Q}_q(\mathbf{w})}}^{\infty} s^{d-1} f_{\mathbf{X}}(s\mathbf{w}) \, ds \sim \int_{r_{\mathcal{Q}_q(\mathbf{w})}}^{\infty} s^{d-1} \exp[-\psi_{\mathbf{L}}(s)g_{\mathcal{G}}(\mathbf{w})^{\rho}] \, ds$$

Without loss,  $\psi_{\mathbf{L}}$  can be taken smooth (Lemma 1.4, [Seneta \(1976\)](#)) so that  $d^k \psi_{\mathbf{L}}(t)/dt^k$  exists for all  $t > 0$  and  $k \in \mathbb{N}$ . Therefore,

$$\begin{aligned} \int_{r_{\mathcal{Q}_q(\mathbf{w})}}^{\infty} s^{d-1} f_{\mathbf{X}}(s\mathbf{w}) \, ds &\sim \int_{r_{\mathcal{Q}_q(\mathbf{w})}}^{\infty} s^{d-1} \left[ \frac{\frac{d}{ds} \exp[-\psi_{\mathbf{L}}(s)g_{\mathcal{G}}(\mathbf{w})^{\rho}]}{-g_{\mathcal{G}}(\mathbf{w})^{\rho} \psi'_{\mathbf{L}}(s)} \right] \, ds \\ &= r_{\mathcal{Q}_q(\mathbf{w})}^{d-1} \left[ \frac{\exp[-\psi_{\mathbf{L}}(r_{\mathcal{Q}_q(\mathbf{w})})g_{\mathcal{G}}(\mathbf{w})^{\rho}]}{g_{\mathcal{G}}(\mathbf{w})^{\rho} \psi'_{\mathbf{L}}(r_{\mathcal{Q}_q(\mathbf{w})})} \right] \{1 + o(1)\}, \quad \text{as } q \rightarrow 1. \end{aligned}$$

Using Lemma 1 again, we have that equation (A.8) converges to

$$\begin{aligned} &\frac{r_{\mathcal{G}_q(\mathbf{w})} z_q(\mathbf{w})^{d-1}}{r_{\mathcal{Q}_q(\mathbf{w})}^{d-1}} g_{\mathcal{G}}(\mathbf{w})^{\rho} \psi'_{\mathbf{L}}(r_{\mathcal{Q}_q(\mathbf{w})}) \exp[-g_{\mathcal{G}}(\mathbf{w})^{\rho} \{\psi_{\mathbf{L}}(z_q(\mathbf{w})) - \psi_{\mathbf{L}}(r_{\mathcal{Q}_q(\mathbf{w}))}\}] \{1 + o(1)\} \\ &= r_{\mathcal{G}_q(\mathbf{w})} g_{\mathcal{G}}(\mathbf{w})^{\rho} \psi'_{\mathbf{L}}(r_{\mathcal{Q}_q(\mathbf{w})}) \exp[-g_{\mathcal{G}}(\mathbf{w})^{\rho} \{\psi_{\mathbf{L}}(z_q(\mathbf{w})) - \psi_{\mathbf{L}}(r_{\mathcal{Q}_q(\mathbf{w}))}\}] \{1 + o(1)\}, \quad \text{as } q \rightarrow 1. \end{aligned}$$

A Taylor expansion of  $\psi_{\mathbf{L}}(z_q(\mathbf{w}))$  about  $r_{\mathcal{Q}_q}$  and local uniform convergence give  $\psi_{\mathbf{L}}(z_q(\mathbf{w})) = \psi_{\mathbf{L}}(r_{\mathcal{Q}_q(\mathbf{w})}) + \psi'_{\mathbf{L}}(r_{\mathcal{Q}_q(\mathbf{w})})r_{\mathcal{G}_q(\mathbf{w})} + o(1)$ . Thus,

$$\begin{aligned} &r_{\mathcal{G}_q(\mathbf{w})} g_{\mathcal{G}}(\mathbf{w})^{\rho} \psi'_{\mathbf{L}}(r_{\mathcal{Q}_q(\mathbf{w})}) \exp[-g_{\mathcal{G}}(\mathbf{w})^{\rho} \{\psi'_{\mathbf{L}}(r_{\mathcal{Q}_q(\mathbf{w})})r_{\mathcal{G}_q(\mathbf{w})} + o(1)\}] \{1 + o(1)\} \\ &= r_{\mathcal{G}_q(\mathbf{w})} g_{\mathcal{G}}(\mathbf{w})^{\rho} \psi'_{\mathbf{L}}(r_{\mathcal{Q}_q(\mathbf{w})}) \exp[-g_{\mathcal{G}}(\mathbf{w})^{\rho} \{\psi'_{\mathbf{L}}(r_{\mathcal{Q}_q(\mathbf{w})})r_{\mathcal{G}_q(\mathbf{w})}\}] \{1 + o(1)\} \rightarrow \exp(-z), \quad \text{as } q \rightarrow 1, \end{aligned}$$

whenever  $r_{\mathcal{G}_q(\mathbf{w})} \sim \{\psi'_{\mathbf{L}}(r_{\mathcal{Q}_q(\mathbf{w})})g_{\mathcal{G}}(\mathbf{w})^{\rho}\}^{-1}$ .

(iii) Consider first the integral term in expression (A.8). The integral is equal to

$$\int_{r_{\mathcal{Q}_q(\mathbf{w})}}^{\infty} f_{R,\mathbf{W}}(s, \mathbf{w}) \, ds = \int_{r_{\mathcal{Q}_q(\mathbf{w})}}^{\infty} s^{d-1} \{f_{\mathbf{X}}(s\mathbf{w})/\psi_{\mathbf{H}}(s)\} \{\psi_{\mathbf{H}}(s)/s^{1-d}\} \, ds.$$

Due to convergence (iii), the map  $(0, \infty) \ni s \mapsto \{f_{\mathbf{X}}(s\mathbf{w})/\psi_{\mathbf{H}}(s)\} \in \mathbb{R}^+$  is slowly varying at  $\infty$  for any  $\mathbf{w} \in \mathbb{S}^{d-1}$ . Further, convergence (iii) implies that  $\psi_{\mathbf{H}}(s) \in \text{RV}_{-(d+\xi-1)}^{\infty}$ , hence there exists  $l_{\mathbf{H}} \in \text{RV}_0^{\infty}$  such that  $\psi_{\mathbf{H}}(s) = l_{\mathbf{H}}(s)s^{-\{d+(1/\xi)\}}$ . By Karamata's theorem (Theorem 2.1 [Resnick 2007](#)),

$$\frac{\int_{r_{\mathcal{Q}_q(\mathbf{w})}}^{\infty} f_{R,\mathbf{W}}(s, \mathbf{w}) \, ds}{r_{\mathcal{Q}_q(\mathbf{w})} f_{R,\mathbf{W}}(r_{\mathcal{Q}_q(\mathbf{w})}, \mathbf{w})} = \xi \{1 + o(1)\}, \quad \text{as } q \rightarrow 1.$$

Thus, when  $r_{\mathcal{G}_q(\mathbf{w})} = \xi r_{\mathcal{Q}_q(\mathbf{w})}$  and as  $q \rightarrow 1$ , expression (A.8) converges to

$$\frac{1}{\xi} \frac{r_{\mathcal{G}_q(\mathbf{w})}}{r_{\mathcal{Q}_q(\mathbf{w})}} \left[ \frac{z_q(\mathbf{w})}{r_{\mathcal{Q}_q(\mathbf{w})}} \right]^{d-1} \frac{f_{\mathbf{X}}[z_q(\mathbf{w})\mathbf{w}]}{f_{\mathbf{X}}[r_{\mathcal{Q}_q(\mathbf{w})}\mathbf{w}]} \{1 + o(1)\} = \left[ 1 + \frac{r_{\mathcal{G}_q(\mathbf{w})} z}{r_{\mathcal{Q}_q(\mathbf{w})}} \right]^{-1-1/\xi} \{1 + o(1)\} \rightarrow (1 + \xi z)_+^{-1-1/\xi}.$$

□

## A.6 Stability of the radial Exponential distribution

*Proof of stability equation (44).* Let the random vector  $\mathbf{Z} \in \mathbb{R}^d$  follow an rExp distribution with location  $\mathcal{M}$ , scale  $\Sigma$ , and directional component  $\mathcal{W}$ . Then,

$$\begin{aligned} \mathbb{P}[\mathbf{Z} \in [\mathcal{M} + B_{r_1+r_2}(\mathbf{0}) \cdot \Sigma]' \mid \mathbf{Z} \in \{\mathcal{M} + B_{r_1}(\mathbf{0}) \cdot \Sigma\}'] &= \frac{\mathbb{P}[\mathbf{Z} \in \{\mathcal{M} + B_{r_1+r_2}(\mathbf{0}) \cdot \Sigma\}']}{\mathbb{P}[\mathbf{Z} \in \{\mathcal{M} + B_{r_1}(\mathbf{0}) \cdot \Sigma\}']} \\ &= \frac{\mathbb{P}[\{\|\mathbf{Z}\| - r_{\mathcal{M}}(\mathbf{Z}/\|\mathbf{Z}\|)\}/r_{\Sigma}(\mathbf{Z}/\|\mathbf{Z}\|) > r_1 + r_2]}{\mathbb{P}[\{\|\mathbf{Z}\| - r_{\mathcal{M}}(\mathbf{Z}/\|\mathbf{Z}\|)\}/r_{\Sigma}(\mathbf{Z}/\|\mathbf{Z}\|) > r_1]} = \exp\{-r_2\} = \mathbb{P}[\mathbf{Z} \in \{\mathcal{M} + B_{r_2}(\mathbf{0})\}' \cdot \Sigma]. \end{aligned}$$

□

## A.7 Stability of the radial generalised Pareto distribution

*Proof of stability equation (41).* Let the random vector  $\mathbf{Z} \in \mathbb{R}^d$  follow an rGP distribution with location  $\mathcal{M}$ , scale  $\Sigma$ , shape  $\xi \in \mathbb{R}$ , and directional component  $\mathcal{W}$ . Then,

$$\begin{aligned} \mathbb{P}[\mathbf{Z} \in [\mathcal{M} + B_{r_1+r_2}(\mathbf{0}) \cdot \Sigma]' \mid \mathbf{Z} \in \{\mathcal{M} + B_{r_1}(\mathbf{0}) \cdot \Sigma\}'] &= \frac{\mathbb{P}[\mathbf{Z} \in \{\mathcal{M} + B_{r_1+r_2}(\mathbf{0}) \cdot \Sigma\}']}{\mathbb{P}[\mathbf{Z} \in \{\mathcal{M} + B_{r_1}(\mathbf{0}) \cdot \Sigma\}']} \\ &= \frac{\mathbb{P}[\{\|\mathbf{Z}\| - r_{\mathcal{M}}(\mathbf{Z}/\|\mathbf{Z}\|)\}/r_{\Sigma}(\mathbf{Z}/\|\mathbf{Z}\|) > r_1 + r_2]}{\mathbb{P}[\{\|\mathbf{Z}\| - r_{\mathcal{M}}(\mathbf{Z}/\|\mathbf{Z}\|)\}/r_{\Sigma}(\mathbf{Z}/\|\mathbf{Z}\|) > r_1]} = \frac{[1 + \xi(r_1 + r_2)]_+^{-1/\xi}}{[1 + \xi r_1]_+^{-1/\xi}} = \left[1 + \xi \frac{r_2}{1 + \xi r_1}\right]^{-1/\xi} \\ &= \mathbb{P}\left[\mathbf{Z} \in \left\{\mathcal{M} + \frac{B_{r_2}(\mathbf{0}) \cdot \Sigma}{B_1(\mathbf{0}) + B_{\xi}(\mathbf{0}) \cdot B_{r_1}(\mathbf{0})}\right\}'\right]. \end{aligned}$$

□

## A.8 Marginal density of directional variable under homothetic density

*Proof of Proposition (7).* Suppose that  $f(\mathbf{x}) = f_0(g_{\mathcal{G}}(\mathbf{x}))$ ,  $\mathbf{x} \in \mathbb{R}^d$ . Then,

$$f_{\mathbf{W}}(\mathbf{w}) = \int_0^{\infty} f_{R, \mathbf{W}}(r, \mathbf{w}) \, dr = \frac{1}{g_{\mathcal{G}}(\mathbf{w})^d} \int_0^{\infty} s^{d-1} f_0(s) \, ds = \frac{1}{d |\mathcal{G}| g_{\mathcal{G}}(\mathbf{w})^d}, \quad (\text{A.9})$$

where the last equality follows from [Balkema & Nolde \(2010, see Section 3.1\)](#). □

# Supplementary Material for “Statistical inference for radially-stable generalized Pareto distributions and return level-sets in geometric extremes”

## 1 Technical background

### 1.1 Vague convergence

For a detailed exposition of the concept of vague convergence, see [Resnick \(2007\)](#). Let  $\mathcal{E}$  be a locally compact metric space with countable base (e.g.,  $\mathbb{R}^d$ ) and let  $M_+(\mathcal{E})$  be the class of nonnegative Radon measures on Borel subsets of  $\mathcal{E}$ . If  $\mu_n \in M_+(\mathcal{E})$  for  $n \geq 0$ , then we say that  $\mu_n$  converges vaguely to  $\mu$  (presented as  $\mu_n \xrightarrow{v} \mu$ ) if

$$\lim_{n \rightarrow \infty} \int_{\mathcal{E}} f d\mu_n = \int_{\mathcal{E}} f d\mu.$$

for all bounded continuous functions  $f$  with compact support.

### 1.2 Multivariate regular variation

To understand radial stability properties in a  $d$ -dimensional setup, we revisit classical multivariate extreme value theory through consideration of multivariate regular variation (MRV). Given a random vector  $\mathbf{X} \in \mathbb{R}^d$ , a common assumption is that its margins follow the same univariate distribution. If this is not guaranteed, standardisation is required through the probability integral transform with the true distribution function and the desired target quantile function. When the true distribution function is not known, the empirical distribution function is used in the bulk of the data, while the Generalised Pareto distribution function with fitted parameters is used outside of high left and right thresholds to avoid issues that arise when using the empirical distribution function in the tail ([Coles & Tawn 1991](#)). Under the choice of standard exponential margins, a random vector  $\mathbf{X}$  is multivariate regularly varying on the cone  $\mathcal{E} = [-\infty, \infty]^d \setminus \{-\infty\}^d$  if there exists a limit measure  $\nu_{\text{MRV}}$  such that as  $n \rightarrow \infty$

$$n \mathbb{P}[\mathbf{X} - (\log n)\mathbf{1} \in \cdot] \xrightarrow{v} \nu_{\text{MRV}}(\cdot), \quad \text{in } M_+(\mathcal{E}), \quad (\text{A.10})$$

A consequence of convergence (A.10) is that  $\nu_{\text{MRV}}(t\mathbf{1} + B) = \exp(-t)\nu_{\text{MRV}}(B)$ , implying domain of attraction properties for the distribution of  $\mathbf{X}$ . For instance, after appropriate recentering, the distribution function of the componentwise maxima  $\mathbf{M}_n := (\max_{i=1, \dots, n} X_{ij} : j = 1, \dots, d)$  of a random sample  $\mathbf{X}_i = (X_{ij} : j = 1, \dots, d)$ ,  $i = 1, \dots, n$ , from the distribution of  $\mathbf{X}$ , converges weakly to

$$\mathbb{P}(\mathbf{M}_n - (\log n)\mathbf{1} \leq \mathbf{z}) = \mathbb{P}\{\mathbf{X}_i - (\log n)\mathbf{1} \in [-\infty, \mathbf{z}] : i = 1, \dots, n\} \xrightarrow{w} \exp[-\Lambda_{\text{MRV}}(\mathbf{z})],$$

where the exponent function  $\Lambda_{\text{MRV}}(\mathbf{z}) := \nu_{\text{MRV}}([-\infty, \mathbf{z}]')$ . The measure  $\Lambda_{\text{MRV}}$  is in one-to-one correspondence with a Radon measure  $H_{\text{MRV}}$  on the unit-simplex  $\Delta_+^{d-1} = \{\boldsymbol{\omega} \in \mathbb{R}_+^d : \|\boldsymbol{\omega}\|_1 = 1\}$ , where  $\|\mathbf{x}\|_p = (\sum_{i=1}^d |x_i|^p)^{1/p}$  for  $\mathbf{x} = (x_1, \dots, x_d) \in \mathbb{R}^d$ , termed the spectral measure, satisfying the mass-moment constraint  $H_{\text{MRV}}(\Delta_+^{d-1}) = d$  and  $\int_{\Delta_+^{d-1}} w_i H(d\boldsymbol{\omega}) = 1$ , for  $i = 1, \dots, d$ . The correspondence is given by

$$\Lambda_{\text{MRV}}(B) = \int_{\Delta_+^{d-1}} \max[\boldsymbol{\omega} \exp(-\mathbf{x})] H_{\text{MRV}}(d\boldsymbol{\omega}),$$

where vector algebra is interpreted component-wise. Similarly, the vector of renormalised threshold exceedances converges in distribution to a multivariate Pareto distribution. That is,

$$\lim_{r \rightarrow \infty} \mathbb{P}[\mathbf{X} - r\mathbf{1} \in [-\infty, \mathbf{x}] \mid \max \mathbf{X} > r] = \frac{\Lambda_{\text{MRV}}(\mathbf{x} \wedge \mathbf{0}) - \Lambda_{\text{MRV}}(\mathbf{x})}{\Lambda_{\text{MRV}}(\mathbf{0})},$$

at continuity points  $\mathbf{x} \in \mathcal{E}$  of the limit distribution function of the multivariate generalised Pareto distribution, where  $\Lambda_{\text{MRV}}(\mathbf{x}) = \nu_{\text{MRV}}([-\infty, \mathbf{x}]')$ . Multivariate generalised Pareto distributions arise as the only non-trivial limit distributions when renormalised multivariate exceedances are considered (Rootzén & Tajvidi 2006). These distributions possess appealing theoretical and practical properties Engelke & Hitz (2020) and are often thought to be the multivariate analogue of the generalised Pareto distribution Pickands (1975) by being the only threshold-stable multivariate distributions (Kiriliouk et al. 2019). The practical importance of their threshold-stability lies in the preservation of the model's distributional type at higher levels, which is advantageous for extrapolation into the joint tail region of the distribution.

Both component-wise maxima and multivariate threshold exceedance approaches can be unified under a single theme. Let  $r_q$  be the  $q$ -th quantile of the distribution of  $\|\mathbf{X}\|_1$ . Then the overarching assumption that unifies these approaches is that as  $q \rightarrow 1$ , the point process of recentered exceedances  $\mathbf{X}_i - r_q \mathbf{1} \mid \|\mathbf{X}_i\|_1 > r_q$ , converges in distribution to a Poisson point process on  $(0, \infty] \times \Delta_+^{d-1}$  with mean measure

$$\lim_{q \rightarrow 1} \mathbb{P} \left[ \|\mathbf{X}\|_1 - r_q > z, \frac{\mathbf{X}}{\|\mathbf{X}\|_1} \in B \mid \|\mathbf{X}\|_1 > r_q \right] = \exp(-z) H_{\text{MRV}}(B), \quad z > 0, B \subset \Delta_+^{d-1} \quad (\text{A.11})$$

In practice, convergence (A.11) is typically assumed to hold with  $H_{\text{MRV}}$  placing mass in the interior of the unit-simplex  $\Delta_+^{d-1}$ ,  $(\Delta_+^{d-1})^\circ := \{\boldsymbol{\omega} \in \mathbb{R}_+^d : \min_i \omega_i > 0, \|\boldsymbol{\omega}\|_1 = 1\}$ . Although useful for theoretical investigations,  $H_{\text{MRV}}$  placing mass in  $(\Delta_+^{d-1})^\circ$  as a *dependence assumption* can be inadequate in practice since it imposes a strong form of dependence in the joint tail, which may not be supported by the data at hand, see for example Section 4.

### 1.3 Background on starshaped sets

An expository review and survey of material about the fundamental mathematical notion of star-shaped sets, emphasising their geometric, analytical, combinatorial, and topological properties, is

given by Hansen et al. (2020) and references therein.

If  $\mathbf{a}$  and  $\mathbf{b}$  are different elements of  $\mathbb{R}^d$ , then  $[\mathbf{a} : \mathbf{b}] = \{(1-t)\mathbf{a} + t\mathbf{b} : 0 \leq t \leq 1\}$  denotes the segment with endpoints  $\mathbf{a}$  and  $\mathbf{b}$ ,  $[\mathbf{a} : \mathbf{b}) = \{(1-t)\mathbf{a} + t\mathbf{b} : t \geq 0\}$  denotes the half-line with origin  $\mathbf{a}$  through  $\mathbf{b}$ ,  $(\mathbf{a} : \mathbf{b}] = \{(1-t)\mathbf{a} + t\mathbf{b} : 0 \leq t \in \mathbb{R}\}$  denotes the line through  $\mathbf{a}$  and  $\mathbf{b}$ ,  $] \mathbf{a} : \mathbf{b} = \{(1-t)\mathbf{a} + t\mathbf{b} : 0 < t \leq 1\}$  denotes the segment  $[\mathbf{a} : \mathbf{b}]$  without its endpoint  $\mathbf{a}$ ,  $[\mathbf{a} : \mathbf{b}[ = \{(1-t)\mathbf{a} + t\mathbf{b} : 0 \leq t < 1\}$  denotes the segment  $[\mathbf{a} : \mathbf{b}]$  without its endpoint  $\mathbf{b}$  and  $] \mathbf{a} : \mathbf{b} = \{(1-t)\mathbf{a} + t\mathbf{b} : t > 0\}$  denotes the ray  $[\mathbf{a}, \mathbf{b})$  without its origin  $\mathbf{a}$ . A set  $G \subset \mathbb{R}^d$  is called starshaped if there exists  $\mathbf{x} \in G$  such that every point  $\mathbf{y} \in G$  is visible from  $\mathbf{x}$  in the sense that  $[\mathbf{x} : \mathbf{y}] \subset G$ . If  $G$  is a set and  $\mathbf{x} \in G$ , the star of  $\mathbf{x}$  in  $G$  is the set of all points in  $G$  that are visible from  $\mathbf{x}$ , that is,  $\text{st}(\mathbf{x} : G) = \{\mathbf{y} \in G : [\mathbf{x} : \mathbf{y}] \subset G\}$ . A set  $G$  is starshaped if and only if there exists  $\mathbf{x} \in G$  such that  $\text{st}(\mathbf{x} : G) = G$ . The kernel of a set  $G$ , denoted by  $\ker G$ , is the convex set of all of its star centres, that is,  $\ker G = \{\mathbf{x} \in G : \text{st}(\mathbf{x} : G) = G\}$ . A star set is called a star-body if it is a compact set on a regular domain, that is if  $G$  is a compact starshaped set such that  $G^\circ$  is connected and  $G = \overline{G^\circ}$ . Let  $G$  be a closed proper subset of  $\mathbb{R}^d$  with non-empty interior. Then  $G$  is said to be strongly starshaped at  $\mathbf{a}$  whenever there exists  $\mathbf{a} \in \mathbb{R}^d$  such that for every  $\mathbf{w} \in \mathbb{S}^{d-1}$ , the halfline  $\mathbf{a} + [\mathbf{0} : \mathbf{w})$  does not intersect the boundary  $\partial G$  of  $G$  more than once. A strongly starshaped set at  $\mathbf{a}$  is a starshaped set with  $\mathbf{a} \in \ker G$ . A set  $G$  is said to be strongly starshaped if it is strongly starshaped at  $\mathbf{0}$ . We write  $\Delta_{\mathbf{w}}$  for the half-line through the origin  $[\mathbf{0} : \mathbf{w})$  passing through  $\mathbf{w} \in \mathbb{S}^{d-1}$ . If  $G$  is starshaped at  $\mathbf{m} \in \ker G$ , we say that  $\mathbf{z} \in G$  is the last point of a ray  $[\mathbf{m} : \mathbf{x})$  in  $G$  if  $\mathbf{z} \in [\mathbf{m} : \mathbf{x})$  and there is no point  $\mathbf{y} \in [\mathbf{m} : \mathbf{x}) \cap G$  such that  $\mathbf{y} \notin [\mathbf{m} : \mathbf{z}]$ . Let  $G$  be a starshaped set such that  $(\ker G)^\circ \neq \emptyset$ . If  $\mathbf{m} \in (\ker G)^\circ$  and  $\mathbf{x} \in \overline{G}$ , then  $[\mathbf{m} : \mathbf{x}[ \subset G$ . If  $G$  is a closed starshaped set such that  $(\ker G)^\circ \neq \emptyset$ , then  $G^\circ$  is connected and  $G = \overline{(G^\circ)}$ , whence a regular domain.

## 1.4 Radial addition and gauges of starshaped sets

If  $G$  is a closed starshaped set,  $\mathbf{m} \in \ker G$  and  $\mathbf{w} \in \mathbb{S}^{d-1}$ , then there are two cases. There exists a last point  $\mathbf{p}$  of  $\mathbf{m} + \Delta_{\mathbf{w}}$  in  $G$  or  $\mathbf{m} + \Delta_{\mathbf{w}} \subset G$ . In the first case, let

$$\rho_{\mathbf{m},G}(\mathbf{w}) = \sup\{\lambda \in \mathbb{R} : \mathbf{m} + \lambda\mathbf{w} \in G\}.$$

The *radial function* of  $G$  at  $\mathbf{m}$  is the function  $r_{\mathbf{m},G} : \mathbb{S}^{d-1} \rightarrow \mathbb{R}_+$  defined by

$$r_{\mathbf{m},G}(\mathbf{w}) = \begin{cases} \rho_{\mathbf{m},G}(\mathbf{w}) & \mathbf{m} + \Delta_{\mathbf{w}} \not\subseteq G \\ +\infty & \mathbf{m} + \Delta_{\mathbf{w}} \subseteq G. \end{cases}$$

We have the equivalence  $\mathbf{m} \in (\ker G)^\circ \Leftrightarrow r_{\mathbf{m},G} > 0$ . Also, if  $G$  is compact and  $\mathbf{m} \in (\ker G)^\circ$ , then  $r_{\mathbf{m},G}$  is a Lipschitz function.

Let  $\star$  denote the space of star-bodies in  $\mathbb{R}^d$  and  $+, \cdot : \star \times \star \rightarrow \star$  be the operators of *radial*

*addition* and *radial multiplication* respectively, defined by means of radial functions as as

$$\rho_{G_1+G_2}(\mathbf{w}) = \rho_{G_1}(\mathbf{w}) + \rho_{G_2}(\mathbf{w}), \quad G_1, G_2 \in \star, \quad (\text{A.12})$$

$$(\text{A.13})$$

$$\rho_{G_1 \cdot G_2}(\mathbf{w}) = \rho_{G_1}(\mathbf{w})\rho_{G_2}(\mathbf{w}), \quad G_1, G_2 \in \star, \quad (\text{A.14})$$

as illustrated in Figure 8. Multiplication of a set  $G \in \star$  by a nonnegative scalar  $c$  is equivalent to radial multiplication of  $G$  by  $B_c(\mathbf{0})$ , that is,  $cG := B_c(\mathbf{0}) \cdot G$ ,  $c \geq 0$ . The set  $\star$  equipped with the binary operation  $+$  is a commutative monoid. In other words,  $(\star, +)$  satisfies the following.

**Identity element:** There exists an element  $\mathbf{0} \in \star$  such that  $\mathbf{0} + G = G + \mathbf{0} = G \forall G \in \star$ .

**Commutative law:** For  $G_1$  and  $G_2$  in  $\star$ ,  $G_1 + G_2 = G_2 + G_1$ .

Additionally, we have

**Scalar Multiplication Closure:** The result of  $\cdot$  between a compact star set and a non-negative scalar remains within the space of compact star sets.

**Distributive Laws:** The operations  $+$  and  $\cdot$  obey distributive laws similar to those in a ring. For example,  $(G_1 + G_2) \cdot B_c(\mathbf{0}) = G_1 \cdot B_c(\mathbf{0}) + G_2 \cdot B_c(\mathbf{0})$ .

**Associativity:** Both  $+$  and  $\cdot$  are associative operations. For example,  $(G_1 + G_2) + G_3 = G_1 + (G_2 + G_3)$ .

The monoid  $(\star, +)$  is endowed with its algebraic preordering  $\leq$  defined by  $G_1 \leq G_2$  whenever there exists  $H \in \star$  such that  $G_1 + H = G_2$ . In this case, we define radial subtraction  $H = G_2 - G_1$  through ordinary difference of radial functions.

The algebraic structure on the space of compact star sets with the operations  $+$  and  $\cdot$  provides a mathematical framework to explore relationships, transformations, and compositions of these sets. This algebraic approach facilitates the development of consistent theories and methodologies when dealing with operations involving compact star sets.

Last, let  $G_1$  and  $G_2$  be two star-bodies such that  $\rho_{S_i}$  is continuous on  $\mathbb{S}^{d-1}$ . Then the dual Brunn-Minkowski inequality (Lutwak 1988) yields

$$|G_1 + G_2|^{1/d} \leq |G_1|^{1/d} + |G_2|^{1/d},$$

and equality holds if  $d = 1$  or  $d \geq 2$  and  $G_2 = rG_1$ , for some  $r > 0$ . If  $G$  is compact and strongly starshaped, then the volume of  $G$  can be expressed by the formula

$$|G| = \frac{1}{d} \int_{\mathbb{S}^{d-1}} r_G(\mathbf{w})^d d\mathbf{w}, \quad (\text{A.15})$$

see Klain (1997). The reciprocal of the radial function of a set  $G$  starshaped at  $\mathbf{0}$  is called the gauge function  $g_G : \mathbb{R}^d \setminus \{\mathbf{0}\} \rightarrow \mathbb{R}_+$ , defined by  $g_G(\mathbf{x}) = \inf\{t \geq 0 : \mathbf{x} \in tG\}$  for  $\mathbf{x} \in \mathbb{R}^d \setminus \{\mathbf{0}\}$ .

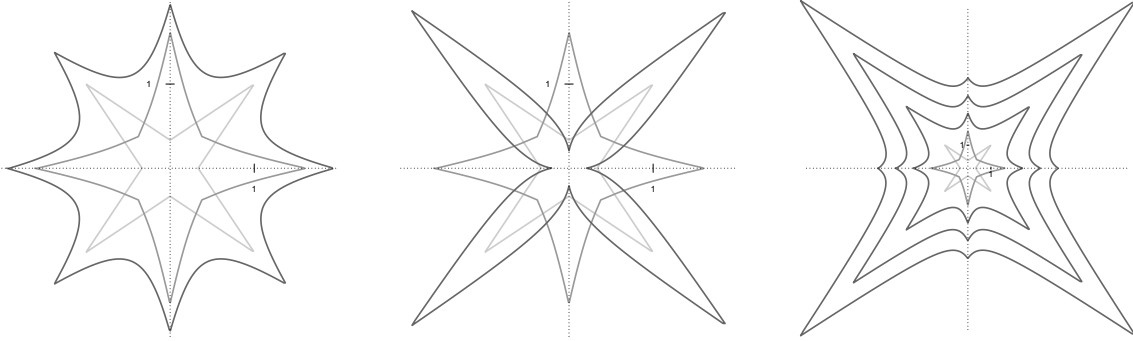


Figure 8: Left:  $\mathcal{M} + \mathcal{G}$ . Centre:  $\mathcal{M}/\mathcal{G}$ . Right:  $\mathcal{M} + B_{-\log(1-q)}(\mathbf{0}) \cdot \mathcal{G}$ , for  $B_r(\mathbf{x})$  the ball of radius  $r$  centred at  $\mathbf{x}$ , and  $q \in \{0.9, 0.99, 0.999\}$ .  $\mathcal{M}$  in lightest grey,  $\mathcal{G}$  in mid grey, result of operations in dark grey.

## 2 Remainder term and quality of convergence

### 2.1 Rates of convergence

Let

$$f_{[L]}(t\mathbf{x}) = \exp\{-g_{\mathcal{G}_L}(t\mathbf{x}) + \text{remainder}\}(1 + o(1)), \quad \text{as } t \rightarrow \infty, \quad (\text{A.16})$$

where the remainder is interpreted as the evaluation  $u(t\mathbf{x})$  of a function  $u : \mathbb{K} \rightarrow \mathbb{R}$  at  $t\mathbf{x} \in \mathbb{K}$ . The domain of the function  $u$  is assumed to be a solid cone  $\mathbb{K}$  in  $\mathbb{R}^d \setminus \{\mathbf{0}\}$ . A characterisation of the map  $u$  under second-order conditions (de Haan & Stadtmüller 1996) is given in Section 2.1. A functional  $u : \mathbb{R}^d \setminus \{\mathbf{0}\} \rightarrow \mathbb{R}$  is said to determine the rate of convergence to  $g_{\mathcal{G}}$  in expression (33) if it satisfies

$$f_{[L]}(t\mathbf{x}) = \exp(-[tg_{\mathcal{G}}(\mathbf{x})\{1 + o(1)\}]) = \exp[-\{g_{\mathcal{G}}(t\mathbf{x}) + u(t\mathbf{x})\}\{1 + o(1)\}], \quad \mathbf{x} \in \mathbb{R}^d \setminus \{\mathbf{0}\}, \quad (\text{A.17})$$

as  $t \rightarrow \infty$ . Two functionals  $u_1$  and  $u_2$  that determine the rate of convergence to  $g_{\mathcal{G}}$  are asymptotically equivalent, that is,  $\lim_{t \rightarrow \infty} u_1(t\mathbf{x})/u_2(t\mathbf{x}) = 1$ ,  $\forall \mathbf{x} \in \mathbb{R}^d \setminus \{\mathbf{0}\}$ . As such, the set of all functionals  $u$  satisfying expression (A.17) forms an equivalence class. To better understand the properties of the members of this class, it is helpful to consider the special case where the leading order term of  $u$  is equal to the product of a positive scaling function  $l_1(t)$  and a function  $u_1(\mathbf{x})$ , that is, when  $u(t\mathbf{x}) = O(l_1(t)u_1(\mathbf{x}))$  as  $t \rightarrow \infty$ , for  $\mathbf{x} \in \mathbb{R}^d \setminus \{\mathbf{0}\}$ . Assumption 2 delineates a sufficient condition subject to which the rate of convergence has such a behaviour.

**Assumption 2.** *Suppose that condition (ii) of Proposition 6 holds. There exists a non-decreasing function  $l_1 : (0, \infty) \rightarrow (0, \infty)$  and a function  $u_1 : \mathbb{R}^d \setminus \{\mathbf{0}\} \rightarrow \mathbb{R}$  which is not everywhere zero, such that*

$$\lim_{r \rightarrow \infty} \frac{\{-\log f_{[L]}(t\mathbf{x})/t\} - g_{\mathcal{G}}(\mathbf{x})}{a_1(t)} = u_1(\mathbf{x}), \quad (\text{A.18})$$

where  $a_1(t) = l_1(t)/t$  for  $t > 0$ .

Due to condition (ii) of Proposition 6 we have that the scale sequence  $a_1(t) = o(1)$  as  $t \rightarrow$

$\infty$ . This implies that  $l_1(t) = o(t)$  as  $t \rightarrow \infty$ . Also Assumption (2) requires that  $-\log f_{[L]}$  is a *multivariate extended regularly varying* function in the sense of Definition 1 of Papastathopoulos & Paulin (2023). To be precise, convergence (A.18) is equivalent to assuming that there exists  $p_1 : \mathbb{R}^d \setminus \{\mathbf{0}\} \rightarrow \mathbb{R}$  which is not everywhere zero, such that

$$\lim_{t \rightarrow \infty} \frac{[-\log f_{[L]}(t\mathbf{x})/g_{\mathcal{G}}(t\mathbf{x})] - [-\log f_{[L]}(t\mathbf{1})/g_{\mathcal{G}}(t\mathbf{1})]}{a_1(t)} = p_1(\mathbf{x}), \quad \mathbf{x} \in \mathbb{R}^d \setminus \{\mathbf{0}\}. \quad (\text{A.19})$$

The correspondence between the two limit functions in (A.18) and (A.19) is  $p_1(\mathbf{x}) = [u_1(\mathbf{x})/g_{\mathcal{G}}(\mathbf{x})] - [u_1(\mathbf{1})/g_{\mathcal{G}}(\mathbf{1})]$ . From this, it immediately follows that  $p_1(\mathbf{1}) = 0$ . Also, it is known that the only possible non-trivial limit functions that can arise from convergence (A.19) are those that satisfy the functional equation

$$[p_1(t\mathbf{x}) - p_1(t\mathbf{1})]/t^{\gamma-1} = p_1(\mathbf{x}), \quad t > 0, \quad \mathbf{x} \in \mathbb{R}^d \setminus \{\mathbf{0}\},$$

for some  $\gamma \in \mathbb{R}$ , see Theorem 2 of Papastathopoulos & Paulin (2023) for a proof. These observations lead to Proposition 10 which identifies the key properties of the scaling function  $a_1(t) = l_1(t)/t$  and of the limit function  $u_1(\mathbf{x})$  under Assumption (2).

**Proposition 10.** *Suppose that Assumption 2 holds. There exists  $\gamma < 1$  such that  $a_1(t) \in \mathbf{RV}_{\gamma-1}^{\infty}$  and  $u_1$  is  $\gamma$ -homogeneous, that is,  $u_1(t\mathbf{x}) = t^{\gamma}u_1(\mathbf{x}) \forall t > 0$  and  $\mathbf{x} \in \mathbb{R}^d \setminus \{\mathbf{0}\}$ .*

From Proposition 10 we obtain  $l_1(t) \in \mathbf{RV}_{\gamma}^{\infty}$ . Because Assumption 2 requires  $l_1(t)$  to be a non-decreasing function, it suffices to consider the following two cases. First, the case when  $l_1(t)$  converges to a constant  $K \in (0, \infty)$  and second, the case when  $l_1(t)$  grows without bound. For the former case we consider without loss of generality the case  $l_1(t) = 1 \forall t > 0$ . This is because positive real constants can be absorbed in the limit function  $u_1$ . Below, we treat the two cases in turn.

First, when  $l_1(t) = 1$ , the leading order term of  $u(t\mathbf{x})$  is constant in  $t$  which implies that the rate of convergence is determined by the function  $u_1$ , that is,  $u(t\mathbf{x}) = u_1(t\mathbf{x}) + o(1)$ , as  $t \rightarrow \infty$ . Also, because  $l_1 \in \mathbf{RV}_0^{\infty}$ , Proposition 10 yields that  $u_1$  is a 0-homogeneous function. Consequently,

$$f_{[L]}(t\mathbf{x}) = \exp[-\{tg_{\mathcal{G}}(\mathbf{x}) + u_1(\mathbf{x})\}]\{1 + o(1)\}, \quad \text{as } t \rightarrow \infty. \quad (\text{A.20})$$

This special case gives a characterisation of the rate of convergence which is independent of the distance from the origin  $t$ . This behaviour is specific to the case  $l(t) = 1$  and is waived when  $l_1(t)$  grows without bound because in the latter case, the rate of convergence may have non-negligible remainder terms.

Using the same working principle as in Assumption 2, below in Assumption 3 we outline a sufficient condition subject to which the rate of convergence exhibits a so-called *second-order* behaviour (de Haan & Stadtmüller 1996, Papastathopoulos & Paulin 2023).

**Assumption 3.** *Suppose that Assumption 2 holds with  $\lim_{t \rightarrow \infty} l_1(t) = \infty$ . There exists a non-decreasing function  $l_2$  and a function  $u_2 : \mathbb{R}^d \setminus \{\mathbf{0}\} \rightarrow \mathbb{R}$  which is not equal to the product of  $u_1$*

and a 0-homogeneous function on  $\mathbb{R}^d \setminus \{\mathbf{0}\}$ , such that for  $a_2(t) = l_2(t)/l_1(t)$

$$\lim_{t \rightarrow \infty} \frac{([\{-\log f_L(t\mathbf{x})/t\} - g_{\mathcal{G}}(\mathbf{x})]/a_1(t)) - u_1(\mathbf{x})}{a_2(t)} = u_2(\mathbf{x}). \quad (\text{A.21})$$

It is clear that when Assumption 3 holds with  $l_2(t) = 1$ , then

$$f_{[L]}(t\mathbf{x}) = \exp[-\{tg_{\mathcal{G}}(\mathbf{x}) + l_1(t)u_1(\mathbf{x}) + u_2(\mathbf{x})\}\{1 + o(1)\}], \quad \text{as } t \rightarrow \infty. \quad (\text{A.22})$$

More generally, we can construct an asymptotic expansion of  $-\log f_{[L]}(t\mathbf{x})$  of the form

$$-\log f_{[L]}(t\mathbf{x}) = g_{\mathcal{G}}(t\mathbf{x}) + \sum_{j=1}^{\infty} l_j(t)u_j(\mathbf{x}), \quad \text{as } t \rightarrow \infty. \quad (\text{A.23})$$

for a sequence of positive scale functions  $\{l_j\}_{j=1}^M$  with  $M \in \mathbb{N} \cup \{\infty\}$ , satisfying  $l_j(t) = o(l_{j+1}(t))$  as  $t \rightarrow \infty$ , and a sequence of functions  $\{u_j\}_{j=1}^M$  mapping  $\mathbb{R}^d \setminus \{\mathbf{0}\}$  into  $\mathbb{R}$ . The function  $u_j$  captures the contribution of  $-\log f_{[L]}(t\mathbf{x})$  at a given order of the series and  $l_j$  is the scaling factor associated with this term. The  $j$ -th term  $l_j(t)u_j(\mathbf{x})$  in the sum represents the  $j$ -th approximation to  $-\log f_{[L]}(t\mathbf{x})$  as  $t \rightarrow \infty$ , and the scaling factors  $l_j$  determine the rate of convergence to  $u_{j-1}$ , with  $u_0(\mathbf{x}) := g_{\mathcal{G}}(\mathbf{x})$ .

**Proposition 11.** *Suppose that Assumption 3 holds for the random vector  $\mathbf{X}_L$ . There exists  $\gamma < 1$  and  $\rho \leq 0$  such that*

$$u_2(t\mathbf{x}) = t^\gamma u_2(\mathbf{x}) + ct^\gamma \frac{t^\rho - 1}{\rho} u_1(\mathbf{x}).$$

and the solution of this functional equation is

$$u_2(\mathbf{x}) = \|\mathbf{x}\|^{\gamma+\rho} h\left(\frac{\mathbf{x}}{\|\mathbf{x}\|}\right) + c\|\mathbf{x}\|^\gamma \log\|\mathbf{x}\| u_1\left(\frac{\mathbf{x}}{\|\mathbf{x}\|}\right), \quad \mathbf{x} \in \mathbb{R}^d \setminus \{\mathbf{0}\}. \quad (\text{A.24})$$

for a measurable function  $h$  that maps  $\mathbb{S}^{d-1}$  into  $\mathbb{R}$ .

Proposition 11 provides key insight into the rate of convergence to the limit function in Proposition 6 (ii). This result is shown to hold in Appendix 3 for certain known copulas in Examples 3.1, 3.2, and 3.8. We note that a similar approach can be used to study the rate of convergence in Proposition 6 (i) and (iii) for light- and heavy-tailed distributions.

*Proof of Proposition 10.* The homogeneity of  $u_1$  follows directly from the correspondence between  $u_1$  and  $p_1$  and the fact that  $p_1$  is  $(\gamma - 1)$ -homogeneous. It remains to show that  $a_1 \in \text{RV}_{\gamma-1}^\infty$ . For any  $a > 0$  and  $\mathbf{x} \in \mathbb{R}^d \setminus \{\mathbf{0}\}$  we have

$$\frac{[-\log f_{[L]}(\{t(a\mathbf{x})\}/t) - g_{\mathcal{G}}(a\mathbf{x})]}{a_1(t)} = a \frac{[-\log f_{[L]}(\{(at)\mathbf{x}\}/(at)) - g_{\mathcal{G}}(\mathbf{x})]}{a_1(at)} \frac{a_1(at)}{a_1(t)}.$$

By Assumption 2, the LHS converges to  $u_1(a\mathbf{x})$  as  $t \rightarrow \infty$  and the second factor of the RHS converges to  $u_1(\mathbf{x})$  as  $t \rightarrow \infty$ . Hence, the third factor of RHS must converge as  $t \rightarrow \infty$  which

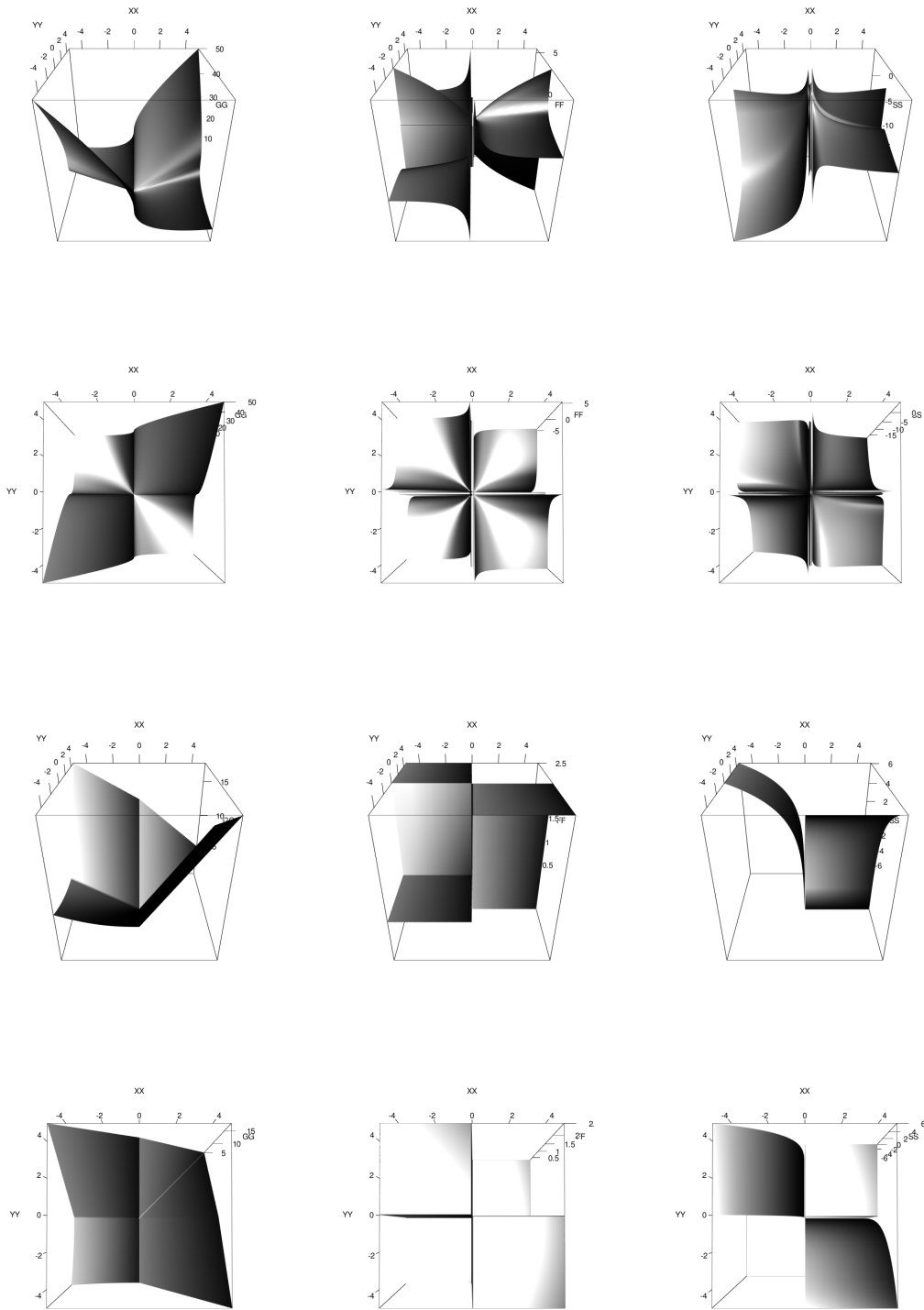


Figure 9: Limit functions in asymptotic expansion of the logarithm of the density of the multivariate normal copula with Laplace marginals. *Left:* gauge function  $g_{\mathcal{G}}$  of limit set  $\mathcal{G}$ . *Centre:* limit function  $u_1$ . *Right:* Limit function  $u_2$ . *Bottom:* alternative viewing angle obtained by rotating the images shown in top row by  $60^\circ$  about  $x$  axis

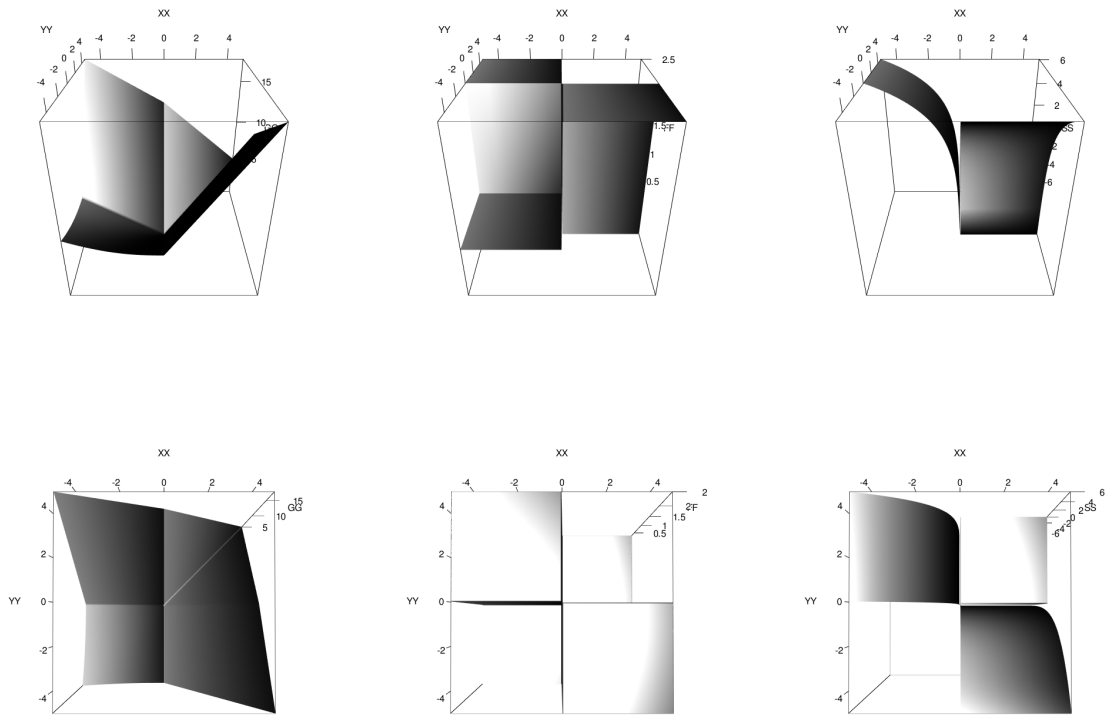


Figure 10: Limit functions in asymptotic expansion of the logarithm of the density of the bivariate max-stable copula with logistic dependence and Laplace marginal distributions. *Left*: gauge function  $g_{\mathcal{G}}$  of limit set  $\mathcal{G}$ . *Centre*: limit function  $u_1$ . *Right*: Limit function  $u_2$ . *Bottom*: alternative viewing angle obtained by rotating the images shown in top row by  $60^\circ$  about  $x$  axis

implies that there exists  $\gamma \in \mathbb{R}$  such that  $a_1 \in \text{RV}_{\gamma-1}^\infty$ . The case  $\gamma > 1$  is not admissible due to homogeneity of  $g_{\mathcal{G}}$  as the latter ensures that the rate of convergence  $u(t\mathbf{x})$  is not growing faster than  $g_{\mathcal{G}}(t\mathbf{x})$ , that is,  $\lim_{t \rightarrow \infty} u(t\mathbf{x})/g_{\mathcal{G}}(t\mathbf{x}) = 0$  for all  $\mathbf{x} \in \mathbb{R}^d \setminus \{\mathbf{0}\}$ . When  $\gamma = 1$  we have  $a_1 \in \text{RV}_0^\infty$ , which implies that  $l_1(t) \in \text{RV}_0^\infty$ . Thus, the case  $\gamma = 1$  is not admissible because it requires  $l_1(t) \rightarrow 0$  as  $t \rightarrow \infty$  for  $u(t\mathbf{x})/g_{\mathcal{G}}(t\mathbf{x})$  to converge to zero for all  $\mathbf{x} \in \mathbb{R}^d \setminus \{\mathbf{0}\}$ , which contradicts the assumption that  $l_1$  is a non-decreasing function.  $\square$

*Proof of Proposition 11.* Since for any  $a > 0$  we have

$$\begin{aligned} & \frac{-t^{-1} \log f_{[L]} \{t(a\mathbf{x})\} - g_{\mathcal{G}}(a\mathbf{x})}{a_1(t)} - u_1(a\mathbf{x}) \\ & \frac{-(at)^{-1} \log f_{[L]} \{(at)\mathbf{x}\} - g_{\mathcal{G}}(\mathbf{x})}{a_1(at)} - a^\gamma u_1(\mathbf{x}) \\ & \frac{a_2(at)}{a_2(t)} = \frac{a_2(at)}{a_2(t)} \frac{-(at)^{-1} \log f_{[L]} \{(at)\mathbf{x}\} - g_{\mathcal{G}}(\mathbf{x})}{a_1(at)} - a^\gamma u_1(\mathbf{x}) \\ & = \frac{a_2(at)}{a_2(t)} a^\gamma \frac{-(at)^{-1} \log f_{[L]} \{(at)\mathbf{x}\} - g_{\mathcal{G}}(\mathbf{x})}{a_1(at)} \\ & \quad + a \frac{\left(\frac{a_1(at)}{a_1(t)} - a^{\gamma-1}\right) - (at)^{-1} \log f_{[L]} \{(at)\mathbf{x}\} - g_{\mathcal{G}}(\mathbf{x})}{a_2(t) a_1(at)}, \end{aligned}$$

it follows that

$$u_2(a\mathbf{x}) = \lim_{t \rightarrow \infty} \frac{a_2(at)}{a_2(t)} a^\gamma u_2(\mathbf{x}) + a \lim_{t \rightarrow \infty} \frac{\left(\frac{a_1(at)}{a_1(t)} - a^{\gamma-1}\right)}{a_2(t)} u_1(\mathbf{x}).$$

Suppose there exist  $a > 0$ , and sequences  $t_n, t'_n$  such that

$$\lim_{t_n \rightarrow \infty} \frac{a_2(at_n)}{a_2(t_n)} = A, \quad \lim_{t'_n \rightarrow \infty} \frac{a_2(at'_n)}{a_2(t'_n)} = A', \quad \lim_{t_n \rightarrow \infty} \frac{\left(\frac{a_1(at_n)}{a_1(t_n)} - a^{\gamma-1}\right)}{a_2(t_n)} = B \quad \text{and} \quad \lim_{t'_n \rightarrow \infty} \frac{\left(\frac{a_1(at'_n)}{a_1(t'_n)} - a^{\gamma-1}\right)}{a_2(t'_n)} = B',$$

with  $A \neq A'$  and  $B \neq B'$ . Then, for all  $\mathbf{x} \in \mathbb{R}^d \setminus \{\mathbf{0}\}$ ,

$$0 = (A - A') a^\gamma u_2(\mathbf{x}) + a(B - B') u_1(\mathbf{x})$$

By assumption,  $u_2$  is not equal to the product of  $u_1$  and a 0-homogeneous functional. Hence,  $A = A'$  and  $B = B'$ . This implies that there exists  $\rho \leq 0$  and  $c \in \mathbb{R}$  such that

$$\lim_{t \rightarrow \infty} \frac{a_2(tx)}{a_2(t)} = x^\rho \quad \text{and} \quad \lim_{t \rightarrow \infty} \frac{\left(\frac{a_1(at)}{a_1(t)} - a^{\gamma-1}\right)}{a_2(t)} = cx^{\gamma-1} \frac{x^\rho - 1}{\rho}, \quad \forall x > 0,$$

for a proof see [de Haan & Stadtmüller \(1996\)](#). Consequently, we arrive at the functional equation

$$u_2 \left( \|\mathbf{x}\| \frac{\mathbf{x}}{\|\mathbf{x}\|} \right) = \|\mathbf{x}\|^{\gamma+\rho} u_2 \left( \frac{\mathbf{x}}{\|\mathbf{x}\|} \right) + c \|\mathbf{x}\|^\gamma \frac{\|\mathbf{x}\|^\rho - 1}{\rho} u_1 \left( \frac{\mathbf{x}}{\|\mathbf{x}\|} \right), \quad \mathbf{x} \in \mathbb{R}^d \setminus \{\mathbf{0}\}. \quad (\text{A.25})$$

where  $u_1$  is a  $\gamma$ -homogeneous functional on  $\mathbb{R}^d \setminus \{\mathbf{0}\}$  and  $u_2$  is an unknown function. Let

$$u_2^\star(\mathbf{x}) = \|\mathbf{x}\|^{\gamma+\rho} \tilde{\lambda}_2 \left( \frac{\mathbf{x}}{\|\mathbf{x}\|} \right) + c \|\mathbf{x}\|^\gamma \frac{\|\mathbf{x}\|^\rho - 1}{\rho} u_1 \left( \frac{\mathbf{x}}{\|\mathbf{x}\|} \right), \quad \mathbf{x} \in \mathbb{R}^d \setminus \{\mathbf{0}\}, \quad (\text{A.26})$$

where  $\tilde{\lambda}_2$  be an arbitrary map from  $\mathbb{R}^d \setminus \{\mathbf{0}\}$  into  $\mathbb{R}$ . A simple calculation shows that the function  $u_2^\star$  satisfies the functional equation (A.25). This proves that the general solution of the functional equation (A.25) is  $u_2^\star$ . Last, by Assumption 3 we have  $a_2(t) = o(a_1(t))$  as  $t \rightarrow \infty$ . □

## 3 Convergence to gauge functions for $d$ -dimensional copulas

### 3.1 Multivariate normal copula

The negative logarithm of the probability density function of the standard  $d$ -dimensional normal copula with standard Laplace margins and positive-definite precision matrix  $\mathbf{Q}$  is standard  $d$ -dimensional normal copula with standard Laplace margins and positive-definite precision matrix  $\mathbf{Q}$  is

$$-\log f(t\mathbf{x}) = -\frac{1}{2} \log |\mathbf{Q}| + d \log 2 + t \sum_{i=1}^d |x_{t,i}| + \frac{1}{2} \mathbf{H}(t, \mathbf{x})^\top (\mathbf{Q} - I) \mathbf{H}(t, \mathbf{x}) \quad (\text{A.27})$$

where  $\mathbf{H} : \mathbb{R}_+ \times \mathbb{R}^d \rightarrow \mathbb{R}^d$  is defined by  $\mathbf{H}(t, \mathbf{x}) = (H(t, x_i) : i = 1, \dots, d)$ , with  $H(t, y) := \Phi^{-1}\{F_L(ty)\}$ , for  $t > 0$  and  $y \in \mathbb{R}$ . By Mill's ratio, each individual component of  $\mathbf{H}(t, \mathbf{x})$  admits the asymptotic expansion

$$H(t, x_i) = \begin{cases} 0 & x_i = 0 \\ \text{sgn}(x_i) [2(\log 2 + |tx_i|) - \log\{4\pi(\log 2 + |tx_i|)\}]^{1/2} + o(t^{-1/2}) & \text{otherwise,} \end{cases} \quad (\text{A.28})$$

as  $t \rightarrow \infty$ , also implying that

$$H(t, x_i)^2 = \begin{cases} 0 & x_i = 0 \\ 2(\log 2 + |tx_i|) - \log\{4\pi(\log 2 + |tx_i|)\} + o(1) & \text{otherwise,} \end{cases} \quad (\text{A.29})$$

as  $t \rightarrow \infty$ .

Suppose that  $x_i \neq 0$  for all  $i \in \{1, \dots, d\}$ . Since

$$2(\log 2 + |tx_i|) > \log\{4\pi(\log 2 + |tx_i|)\}$$

for all sufficiently large  $t$ , the binomial series gives that as  $t \rightarrow \infty$ ,

$$H(t, x_i) = \operatorname{sgn}(x_i) \sum_{k=0}^{\infty} a_k(t, x_i) + o(t^{-1/2}). \quad (\text{A.30})$$

where

$$a_k(t, x_i) = \frac{\binom{1/2}{k} (-1)^k [\log\{4\pi(\log 2 + t|x_i|)\}]^k}{\{2(\log 2 + t|x_i|)\}^{k-(1/2)}}$$

Let  $\mathbf{A} = \mathbf{Q} - \mathbf{I}$  and consider the quadratic form in expression (A.27)

$$\begin{aligned} \frac{1}{2} \mathbf{H}(t, \mathbf{x})^\top \mathbf{A} \mathbf{H}(t, \mathbf{x}) &= \\ &= \frac{1}{2} \sum_{k=0}^{\infty} [\operatorname{sgn}(\mathbf{x}) \mathbf{a}_k(t, \mathbf{x})]^\top \mathbf{A} [\operatorname{sgn}(\mathbf{x}) \mathbf{a}_k(t, \mathbf{x})] + \sum_{k=0}^{\infty} \sum_{k'=k+1}^{\infty} [\operatorname{sgn}(\mathbf{x}) \mathbf{a}_k(t, \mathbf{x})]^\top \mathbf{A} [\operatorname{sgn}(\mathbf{x}) \mathbf{a}_{k'}(t, \mathbf{x})] \end{aligned} \quad (\text{A.31})$$

where  $\mathbf{a}_k(t, \mathbf{x}) = (a_k(t, x_i) : i = 1, \dots, d)^\top$  is a column vector with  $d$  rows, satisfying

$$\mathbf{a}_k(t, \mathbf{x}) = \begin{cases} (2t|\mathbf{x}|)^{1/2} + (2t|\mathbf{x}|)^{-1/2} \log 2 + O(t^{-3/2}), & k = 0 \\ -[\{(\log t)/(2t|\mathbf{x}|)^{1/2}\} + \{\log(4\pi|\mathbf{x}|)/(2t|\mathbf{x}|)^{1/2}\}] + O(t^{-3/2} \log t), & k = 1 \\ (\log t)^k / (2t|\mathbf{x}|)^{k-(1/2)} + O((\log t)^{k-1} / t^{k-(1/2)}) & k \geq 2, \end{cases}$$

as  $t \rightarrow \infty$ . Here, all 1-dimensional real-valued terms are recycled to match the length of the vector  $\mathbf{x}$ , and vector algebra is interpreted as elementwise.

We consider each summand of the two terms in expression (A.31) separately. The summand associated with  $k = 0$  in the first term is

$$\begin{aligned} & \frac{1}{2} \left[ \left\{ (2t|\mathbf{x}|)^{1/2} + \frac{\log 2}{(2t|\mathbf{x}|)^{1/2}} + O(t^{-3/2}) \right\} \operatorname{sgn}(\mathbf{x}) \right]^\top \mathbf{A} \left[ \left\{ (2t|\mathbf{x}|)^{1/2} + \frac{\log 2}{(2t|\mathbf{x}|)^{1/2}} + O(t^{-3/2}) \right\} \operatorname{sgn}(\mathbf{x}) \right] = \\ &= t \left[ \operatorname{sgn}(\mathbf{x}) |\mathbf{x}|^{1/2} + \operatorname{sgn}(\mathbf{x}) \frac{\log 2}{2t(|\mathbf{x}|)^{1/2}} \right]^\top \mathbf{A} \left[ \operatorname{sgn}(\mathbf{x}) |\mathbf{x}|^{1/2} + \operatorname{sgn}(\mathbf{x}) \frac{\log 2}{2t(|\mathbf{x}|)^{1/2}} \right] + O(t^{-1/2}) \\ &= t [\operatorname{sgn}(\mathbf{x}) |\mathbf{x}|^{1/2}]^\top \mathbf{A} [\operatorname{sgn}(\mathbf{x}) |\mathbf{x}|^{1/2}] + \{\operatorname{sgn}(\mathbf{x}) |\mathbf{x}|^{1/2}\}^\top \mathbf{A} \left\{ \operatorname{sgn}(\mathbf{x}) \frac{\log 2}{|\mathbf{x}|^{1/2}} \right\} + O(t^{-1/2}) \\ &= t \{\operatorname{sgn}(\mathbf{x}) |\mathbf{x}|^{1/2}\}^\top \mathbf{Q} \{\operatorname{sgn}(\mathbf{x}) |\mathbf{x}|^{1/2}\} - t \sum_{i=1}^d |x_i| + \{\operatorname{sgn}(\mathbf{x}) |\mathbf{x}|^{1/2}\}^\top \mathbf{A} \left\{ \operatorname{sgn}(\mathbf{x}) \frac{\log 2}{|\mathbf{x}|^{1/2}} \right\} + O(t^{-1/2}). \end{aligned}$$

and a similar calculation shows that the terms associated with  $k \geq 1$  decays to zero according to

$O\{(\log t)^{2k}/t^{2k-1}\}$ . Now, we consider the second term in (A.31). Here, the summand associated with  $(k, k') = (0, 1)$

$$\begin{aligned} & \left[ \{2(\log 2 + t|\mathbf{x}|)\}^{1/2} \text{sgn}(\mathbf{x}) \right]^\top \mathbf{A} \left[ -\frac{\log\{4\pi(\log 2 + t|\mathbf{x}|)\}}{2\{2(\log 2 + t|\mathbf{x}|)\}^{1/2}} \text{sgn}(\mathbf{x}) \right] = \\ & = -\log t \left\{ \text{sgn}(\mathbf{x})|\mathbf{x}|^{1/2} \right\}^\top \mathbf{A} \left\{ \text{sgn}(\mathbf{x})(2|\mathbf{x}|^{1/2})^{-1} \right\} - \\ & \quad -\frac{1}{2} \left\{ \text{sgn}(\mathbf{x})|\mathbf{x}|^{1/2} \right\}^\top \mathbf{A} \left\{ \text{sgn}(\mathbf{x}) \log(4\pi|\mathbf{x}|)|\mathbf{x}|^{-1/2} \right\} + O(t^{-1}) \end{aligned}$$

Thus,

$$-\log f(t\mathbf{x}) = tg(\mathbf{x}) + (\log t)u_1(\mathbf{x}) + u_2(\mathbf{x}) + o(1) \quad \text{as } t \rightarrow \infty, \quad (\text{A.32})$$

where

$$\begin{aligned} g(\mathbf{x}) &= \left[ \text{sgn}(\mathbf{x})|\mathbf{x}|^{1/2} \right]^\top \mathbf{Q} \left[ \text{sgn}(\mathbf{x})|\mathbf{x}|^{1/2} \right] \quad (\text{A.33}) \\ u_1(\mathbf{x}) &= -\frac{1}{2} \left[ \text{sgn}(\mathbf{x})|\mathbf{x}|^{1/2} \right]^\top (\mathbf{Q} - \mathbf{I}) \left[ \text{sgn}(\mathbf{x})|\mathbf{x}|^{-1/2} \right] \\ u_2(\mathbf{x}) &= \left[ \text{sgn}(\mathbf{x})|\mathbf{x}|^{1/2} \right]^\top (\mathbf{Q} - \mathbf{I}) \left[ \text{sgn}(\mathbf{x}) \log 2|\mathbf{x}|^{-1/2} \right] - \\ & \quad -\frac{1}{2} \left[ \text{sgn}(\mathbf{x})|\mathbf{x}|^{1/2} \right]^\top (\mathbf{Q} - \mathbf{I}) \left[ \text{sgn}(\mathbf{x}) \log(4\pi|\mathbf{x}|)|\mathbf{x}|^{-1/2} \right] - \frac{1}{2} \log |\mathbf{Q}| + d \log 2 \quad (\text{A.34}) \end{aligned}$$

The asymptotic expansion in (A.32) is valid for large  $t$  when all  $x_i \neq 0$ , and loses validity when at least one  $x_i$  is equal to 0. This is a result of the asymptotic expansion of (A.28) and (A.29), both depending on  $t$  and  $x_i$ , resulting in nonuniform behavior. When  $x_i = 0$ , the expansions (A.28) and (A.29) collapse to zero, while for  $x_i \neq 0$ , the leading term grows as  $t^{1/2}$  with logarithmic corrections. This difference in growth rates reflects the nonuniformity in  $x_i$ , as the expansion behaves differently near the origin and away from it, complicating the asymptotic analysis of  $-\log f(t\mathbf{x})$  whenever  $\mathbf{x}$  is near an axis.

In what follows, we show that a uniform asymptotic expansion exists, by proving  $-\log f(t\mathbf{x})/t$  converges locally uniformly to a continuous gauge function via the method of continuous convergence (Resnick 2007). That is, we prove that  $-\log f(t\mathbf{x})/t \rightarrow g(\mathbf{x})$  as  $t \rightarrow \infty$ , uniformly on compact sets in the variable  $\mathbf{x} \in \mathbb{R}^d$ , by showing that  $-\log f(t\mathbf{x}_t)/t$  converges to  $g(\mathbf{x})$  whenever  $\mathbf{x}_t \rightarrow \mathbf{x} \in \mathbb{R}^d$ . Consequently, because  $\mathbb{S}^{d-1}$  is compact, the convergence is uniform on  $\mathbb{S}^{d-1}$  and therefore, the conditions of Proposition 6 are satisfied. To prove this assertion, it suffices to consider three disjoint index sets  $A, B, C \subseteq \{1, \dots, d\} \cup \{\emptyset\}$  such that  $A \cup B \cup C = \{1, \dots, d\}$ , and

- (i)  $x_{t,i} \rightarrow x_i$  and  $|tx_{t,i}| \rightarrow \infty$ , where  $x_i \neq 0$ , as  $t \rightarrow \infty$  for  $i \in A$ .
- (ii)  $x_{t,i} \rightarrow 0$  and  $|tx_{t,i}| \rightarrow \infty$ , as  $t \rightarrow \infty$  for  $i \in B$ .
- (iii)  $x_{t,i} \rightarrow 0$  and  $|tx_{t,i}| \rightarrow c_i$ , where  $c_i \in \mathbb{R}$ , as  $t \rightarrow \infty$  for  $i \in C$ .

Decomposing the quadratic form in expression (A.27) based on this partition, leads to

$$\mathbf{H}(t, \mathbf{x}_t)^\top \mathbf{A} \mathbf{H}(t, \mathbf{x}_t)$$

$$\begin{aligned}
&= \mathbf{H}(t, \mathbf{x}_{A,t})^\top \mathbf{A}_{AA} \mathbf{H}(t, \mathbf{x}_{A,t}) + \mathbf{H}(t, \mathbf{x}_{B,t})^\top \mathbf{A}_{BB} \mathbf{H}(t, \mathbf{x}_{B,t}) + \mathbf{H}(t, \mathbf{x}_{C,t})^\top \mathbf{A}_{CC} \mathbf{H}(t, \mathbf{x}_{C,t}) \\
&\quad + 2\mathbf{H}(t, \mathbf{x}_{A,t})^\top \mathbf{A}_{AB} \mathbf{H}(t, \mathbf{x}_{B,t}) + 2\mathbf{H}(t, \mathbf{x}_{A,t})^\top \mathbf{A}_{AC} \mathbf{H}(t, \mathbf{x}_{C,t}) + 2\mathbf{H}(t, \mathbf{x}_{B,t})^\top \mathbf{A}_{BC} \mathbf{H}(t, \mathbf{x}_{C,t}),
\end{aligned}$$

where  $\mathbf{A}_{MM'} = (\mathbf{A}_{ij})_{i \in M, j \in M'}$  is the submatrix of  $\mathbf{A}$  with rows indexed by  $M$  and columns indexed by  $M'$ . In what follows, we derive the growth rates of each term in this decomposition separately. By using equations (A.28) and (A.29) and the binomial series, we obtain

$$\frac{1}{2} \mathbf{H}(t, \mathbf{x}_{A,t})^\top \mathbf{A}_{AA} \mathbf{H}(t, \mathbf{x}_{A,t}) \quad (\text{A.35})$$

$$\begin{aligned}
&= \frac{1}{2} \sum_{k=0}^{\infty} [\text{sgn}(\mathbf{x}_{A,t}) \mathbf{a}_k(t, \mathbf{x}_{A,t})]^\top \mathbf{A}_{AA} [\text{sgn}(\mathbf{x}_{A,t}) \mathbf{a}_k(t, \mathbf{x}_{A,t})] \\
&\quad + \sum_{k=0}^{\infty} \sum_{k'=k+1}^{\infty} [\text{sgn}(\mathbf{x}_{A,t}) \mathbf{a}_k(t, \mathbf{x}_{A,t})]^\top \mathbf{A}_{AA} [\text{sgn}(\mathbf{x}_{A,t}) \mathbf{a}_{k'}(t, \mathbf{x}_{A,t})]
\end{aligned} \quad (\text{A.36})$$

where  $\mathbf{a}_k(t, \mathbf{x}_{A,t}) = (a_k(t, x_{t,i}) : i = 1, \dots, d)^\top$  is a column vector with  $|A|$  rows, defined in a similar manner to  $\mathbf{a}_k(t, \mathbf{x})$  in expression (A.31), restricted to the subset  $A$ . The summand associated with  $k = 0$  in the first term of expression (A.36) is

$$\begin{aligned}
&\frac{1}{2} \left[ \left\{ (2t|\mathbf{x}_{A,t}|)^{1/2} + \frac{\log 2}{(2t|\mathbf{x}_{A,t}|)^{1/2}} + O(t^{-3/2}) \right\} \text{sgn}(\mathbf{x}_{A,t}) \right]^\top \mathbf{A}_{AA} \left[ \left\{ (2t|\mathbf{x}_{A,t}|)^{1/2} + \frac{\log 2}{(2t|\mathbf{x}_{A,t}|)^{1/2}} + O(t^{-3/2}) \right\} \text{sgn}(\mathbf{x}) \right] \\
&= t \left[ \text{sgn}(\mathbf{x}_{A,t}) |\mathbf{x}_{A,t}|^{1/2} + \text{sgn}(\mathbf{x}_{A,t}) \frac{\log 2}{2t(|\mathbf{x}_{A,t}|)^{1/2}} \right]^\top \mathbf{A}_{AA} \left[ \text{sgn}(\mathbf{x}_{A,t}) |\mathbf{x}_{A,t}|^{1/2} + \text{sgn}(\mathbf{x}_{A,t}) \frac{\log 2}{2t(|\mathbf{x}_{A,t}|)^{1/2}} \right] + O(t^{-1/2}) \\
&= t \left[ \text{sgn}(\mathbf{x}_{A,t}) |\mathbf{x}_{A,t}|^{1/2} \right]^\top \mathbf{A}_{AA} \left[ \text{sgn}(\mathbf{x}_{A,t}) |\mathbf{x}_{A,t}|^{1/2} \right] + \left\{ \text{sgn}(\mathbf{x}_{A,t}) |\mathbf{x}_{A,t}|^{1/2} \right\}^\top \mathbf{A}_{AA} \left\{ \text{sgn}(\mathbf{x}_{A,t}) \frac{\log 2}{|\mathbf{x}_{A,t}|^{1/2}} \right\} + O(t^{-1/2}) \\
&= t \left\{ \text{sgn}(\mathbf{x}_{A,t}) |\mathbf{x}_{A,t}|^{1/2} \right\}^\top \mathbf{Q}_{AA} \left\{ \text{sgn}(\mathbf{x}_{A,t}) |\mathbf{x}_{A,t}|^{1/2} \right\} - t \sum_{i \in A} |x_{t,i}| + \left\{ \text{sgn}(\mathbf{x}_{A,t}) |\mathbf{x}_{A,t}|^{1/2} \right\}^\top \mathbf{A}_{AA} \left\{ \text{sgn}(\mathbf{x}_{A,t}) \frac{\log 2}{|\mathbf{x}_{A,t}|^{1/2}} \right\} + O(t^{-1/2}),
\end{aligned}$$

and the  $k$ th summand in the first term of expression (A.36), with  $k \geq 1$ , decays to zero with rate  $O\{(\log t)^{2k}/t^{2k-1}\}$ . Likewise, the first summand in the second term of expression (A.36), associated with  $k = 0$  and  $k' = 1$ , is

$$\begin{aligned}
&\left[ \{2(\log 2 + t|\mathbf{x}_{A,t}|)\}^{1/2} \text{sgn}(\mathbf{x}_{A,t}) \right]^\top \mathbf{A}_{AA} \left[ -\frac{\log\{4\pi(\log 2 + t|\mathbf{x}_{A,t}|)\}}{2\{2(\log 2 + t|\mathbf{x}_{A,t}|)\}^{1/2}} \text{sgn}(\mathbf{x}_{A,t}) \right] \\
&= -\log t \left\{ \text{sgn}(\mathbf{x}_{A,t}) |\mathbf{x}_{A,t}|^{1/2} \right\}^\top \mathbf{A}_{AA} \left\{ \text{sgn}(\mathbf{x}_{A,t}) (2|\mathbf{x}_{A,t}|^{1/2})^{-1} \right\} \\
&\quad - \frac{1}{2} \left\{ \text{sgn}(\mathbf{x}_{A,t}) |\mathbf{x}_{A,t}|^{1/2} \right\}^\top \mathbf{A}_{AA} \left\{ \text{sgn}(\mathbf{x}_{A,t}) |\mathbf{x}_{A,t}|^{-1/2} \log(4\pi|\mathbf{x}_{A,t}|) \right\} + O(t^{-1}).
\end{aligned}$$

Putting this together, obtain

$$\begin{aligned}
&\frac{1}{2} \mathbf{H}(t, \mathbf{x}_{A,t})^\top \mathbf{A}_{AA} \mathbf{H}(t, \mathbf{x}_{A,t}) \\
&= t \left\{ \text{sgn}(\mathbf{x}_{A,t}) |\mathbf{x}_{A,t}|^{1/2} \right\}^\top \mathbf{Q}_{AA} \left\{ \text{sgn}(\mathbf{x}_{A,t}) |\mathbf{x}_{A,t}|^{1/2} \right\} - t \sum_{i \in A} |x_{t,i}| \\
&\quad - \log t \left\{ \text{sgn}(\mathbf{x}_{A,t}) |\mathbf{x}_{A,t}|^{1/2} \right\}^\top \mathbf{A}_{AA} \left\{ \text{sgn}(\mathbf{x}_{A,t}) (2|\mathbf{x}_{A,t}|^{1/2})^{-1} \right\} -
\end{aligned}$$

$$\begin{aligned}
& + \left\{ \operatorname{sgn}(\mathbf{x}_{A,t}) |\mathbf{x}_{A,t}|^{1/2} \right\}^\top \mathbf{A}_{AA} \left\{ \operatorname{sgn}(\mathbf{x}_{A,t}) \frac{\log 2}{|\mathbf{x}_{A,t}|^{1/2}} \right\} \\
& - \frac{1}{2} \left\{ \operatorname{sgn}(\mathbf{x}_{A,t}) |\mathbf{x}_{A,t}|^{1/2} \right\}^\top \mathbf{A}_{AA} \left\{ \operatorname{sgn}(\mathbf{x}_{A,t}) |\mathbf{x}_{A,t}|^{-1/2} \log(4\pi |\mathbf{x}_{A,t}|) \right\} + O(t^{1/2})
\end{aligned}$$

Since  $|tx_{t,i}| \rightarrow \infty$  for all  $i \in B$  as  $t \rightarrow \infty$ , a similar analysis based the Mill's ratio approximation yields

$$\begin{aligned}
& \frac{1}{2} \mathbf{H}(t, \mathbf{x}_{B,t})^\top \mathbf{A}_{BB} \mathbf{H}(t, \mathbf{x}_{B,t}) \\
& = t \left\{ \operatorname{sgn}(\mathbf{x}_{B,t}) |\mathbf{x}_{B,t}|^{1/2} \right\}^\top \mathbf{Q}_{BB} \left\{ \operatorname{sgn}(\mathbf{x}_{B,t}) |\mathbf{x}_{B,t}|^{1/2} \right\} - t \sum_{i \in B} |x_{t,i}| \\
& \quad - \log t \left\{ \operatorname{sgn}(\mathbf{x}_{B,t}) |\mathbf{x}_{B,t}|^{1/2} \right\}^\top \mathbf{A}_{BB} \left\{ \operatorname{sgn}(\mathbf{x}_{B,t}) (2|\mathbf{x}_{B,t}|^{1/2})^{-1} \right\} - \\
& \quad + \left\{ \operatorname{sgn}(\mathbf{x}_{B,t}) |\mathbf{x}_{B,t}|^{1/2} \right\}^\top \mathbf{A}_{BB} \left\{ \operatorname{sgn}(\mathbf{x}_{B,t}) \frac{\log 2}{|\mathbf{x}_{B,t}|^{1/2}} \right\} \\
& \quad - \frac{1}{2} \left\{ \operatorname{sgn}(\mathbf{x}_{B,t}) |\mathbf{x}_{B,t}|^{1/2} \right\}^\top \mathbf{A}_{BB} \left\{ \operatorname{sgn}(\mathbf{x}_{B,t}) |\mathbf{x}_{B,t}|^{-1/2} \log(4\pi |\mathbf{x}_{B,t}|) \right\} + O(t^{1/2})
\end{aligned}$$

And finally note that  $\mathbf{H}(t, \mathbf{x}_{C,t})^\top \mathbf{A}_{CC} \mathbf{H}(t, \mathbf{x}_{C,t}) \rightarrow \Phi^{-1}\{F_L(\mathbf{x}^C)\}^\top \mathbf{A}_{CC} \Phi^{-1}\{F_L(\mathbf{x}^C)\}$  as  $t \rightarrow \infty$ . For the mixed quadratic arguments of (A.27), start with the expansion using Mill's ratio.

$$\begin{aligned}
& \mathbf{H}(t, \mathbf{x}_{A,t})^\top \mathbf{A}_{AB} \mathbf{H}(t, \mathbf{x}_{B,t}) \\
& = \sum_{k=0}^{\infty} [\operatorname{sgn}(\mathbf{x}_{A,t}) \mathbf{a}_k(t, \mathbf{x}_{A,t})]^\top \mathbf{A}_{AB} [\operatorname{sgn}(\mathbf{x}_{B,t}) \mathbf{a}_k(t, \mathbf{x}_{B,t})] \\
& \quad + \sum_{k, k' \geq 0, k \neq k'} [\operatorname{sgn}(\mathbf{x}_{A,t}) \mathbf{a}_k(t, \mathbf{x}_{A,t})]^\top \mathbf{A}_{AB} [\operatorname{sgn}(\mathbf{x}_{B,t}) \mathbf{a}_{k'}(t, \mathbf{x}_{B,t})] \\
& = t \left\{ \operatorname{sgn}(\mathbf{x}_{A,t}) |\mathbf{x}_{A,t}|^{1/2} \right\}^\top \mathbf{Q}_{AB} \left\{ \operatorname{sgn}(\mathbf{x}_{B,t}) |\mathbf{x}_{B,t}|^{1/2} \right\} \\
& \quad - t \left\{ \operatorname{sgn}(\mathbf{x}_{A,t}) |\mathbf{x}_{A,t}|^{1/2} \right\}^\top \left\{ \operatorname{sgn}(\mathbf{x}_{B,t}) |\mathbf{x}_{B,t}|^{1/2} \right\} \\
& \quad - \log t \left\{ \operatorname{sgn}(\mathbf{x}_{A,t}) |\mathbf{x}_{A,t}|^{-1/2} \right\}^\top \mathbf{A}_{AB} \left\{ \operatorname{sgn}(\mathbf{x}_{B,t}) |\mathbf{x}_{B,t}|^{1/2} \right\} \\
& \quad - \log t \left\{ \operatorname{sgn}(\mathbf{x}_{A,t}) |\mathbf{x}_{A,t}|^{1/2} \right\}^\top \mathbf{A}_{AB} \left\{ \operatorname{sgn}(\mathbf{x}_{B,t}) |\mathbf{x}_{B,t}|^{-1/2} \right\} \\
& \quad + \log 2 \left\{ \operatorname{sgn}(\mathbf{x}_{A,t}) |\mathbf{x}_{A,t}|^{-1/2} \right\}^\top \mathbf{A}_{AB} \left\{ \operatorname{sgn}(\mathbf{x}_{B,t}) |\mathbf{x}_{B,t}|^{1/2} \right\} \\
& \quad + \log 2 \left\{ \operatorname{sgn}(\mathbf{x}_{A,t}) |\mathbf{x}_{A,t}|^{1/2} \right\}^\top \mathbf{A}_{AB} \left\{ \operatorname{sgn}(\mathbf{x}_{B,t}) |\mathbf{x}_{B,t}|^{-1/2} \right\} \\
& \quad - \left\{ \log(4\pi |\mathbf{x}_{A,t}|) \operatorname{sgn}(\mathbf{x}_{A,t}) |\mathbf{x}_{A,t}|^{-1/2} \right\}^\top \mathbf{A}_{AB} \left\{ \operatorname{sgn}(\mathbf{x}_{B,t}) |\mathbf{x}_{B,t}|^{1/2} \right\} \\
& \quad - \left\{ \operatorname{sgn}(\mathbf{x}_{A,t}) |\mathbf{x}_{A,t}|^{1/2} \right\}^\top \mathbf{A}_{AB} \left\{ \log(4\pi |\mathbf{x}_{B,t}|) \operatorname{sgn}(\mathbf{x}_{B,t}) |\mathbf{x}_{B,t}|^{-1/2} \right\} + O(t^{1/2})
\end{aligned}$$

We note that Mill's ratio is suitable here, as  $|tx_{t,i}| \rightarrow \infty$  as  $t \rightarrow \infty$  for  $i \in A, B$ . Next, we consider the term  $\mathbf{H}(t, \mathbf{x}_{A,t})^\top \mathbf{A}_{AC} \mathbf{H}(t, \mathbf{x}_{C,t})$ , only applying Mill's ratio to components in  $A$ ,

$$\mathbf{H}(t, \mathbf{x}_{A,t})^\top \mathbf{A}_{AC} \mathbf{H}(t, \mathbf{x}_{C,t})$$

$$\begin{aligned}
&= \sum_{k=0}^{\infty} [\text{sgn}(\mathbf{x}_{A,t}) \mathbf{a}_k(t, \mathbf{x}_{A,t})]^\top \mathbf{A}_{AC} H(t, \mathbf{x}_{C,t}) \\
&= \left\{ \text{sgn}(\mathbf{x}_{A,t}) (2t |\mathbf{x}_{A,t}|)^{1/2} + \text{sgn}(\mathbf{x}_{A,t}) \log 2 (2t |\mathbf{x}_{A,t}|)^{-1/2} + O(t^{-3/2}) \right\}^\top \mathbf{A}_{AC} H(t, \mathbf{x}_{C,t}) \\
&\quad + \left\{ -\text{sgn}(\mathbf{x}_{A,t}) \frac{\log t}{(2t |\mathbf{x}_{A,t}|)^{1/2}} - \text{sgn}(\mathbf{x}_{A,t}) \frac{\log(4\pi |\mathbf{x}|)}{(2t |\mathbf{x}_{A,t}|)^{1/2}} + O(t^{-3/2} \log t) \right\}^\top \mathbf{A}_{AC} H(t, \mathbf{x}_{C,t}) \\
&= \left\{ \text{sgn}(\mathbf{x}_{A,t}) (2t |\mathbf{x}_{A,t}|)^{1/2} \right\}^\top \mathbf{A}_{AC} H(t, \mathbf{x}_{C,t}) + \left\{ \text{sgn}(\mathbf{x}_{A,t}) \log 2 (2t |\mathbf{x}_{A,t}|)^{-1/2} \right\}^\top \mathbf{A}_{AC} H(t, \mathbf{x}_{C,t}) \\
&\quad - t^{-1/2} \log t \left\{ \text{sgn}(\mathbf{x}_{A,t}) (2 |\mathbf{x}_{A,t}|)^{-1/2} \right\}^\top \mathbf{A}_{AC} H(t, \mathbf{x}_{C,t}) - \left\{ \text{sgn}(\mathbf{x}_{A,t}) \frac{\log(4\pi |\mathbf{x}|)}{(2t |\mathbf{x}_{A,t}|)^{1/2}} \right\}^\top \mathbf{A}_{AC} H(t, \mathbf{x}_{C,t}) \\
&\quad + o(1)
\end{aligned}$$

Similarly, we have

$$\begin{aligned}
&\mathbf{H}(t, \mathbf{x}_{B,t})^\top \mathbf{A}_{BC} \mathbf{H}(t, \mathbf{x}_{C,t}) \\
&= \left\{ \text{sgn}(\mathbf{x}_{B,t}) (2t |\mathbf{x}_{B,t}|)^{1/2} \right\}^\top \mathbf{A}_{BC} H(t, \mathbf{x}_{C,t}) + \left\{ \text{sgn}(\mathbf{x}_{B,t}) \log 2 (2t |\mathbf{x}_{B,t}|)^{-1/2} \right\}^\top \mathbf{A}_{BC} H(t, \mathbf{x}_{C,t}) \\
&\quad - t^{-1/2} \log t \left\{ \text{sgn}(\mathbf{x}_{B,t}) (2 |\mathbf{x}_{B,t}|)^{-1/2} \right\}^\top \mathbf{A}_{BC} H(t, \mathbf{x}_{C,t}) - \left\{ \text{sgn}(\mathbf{x}_{B,t}) \frac{\log(4\pi |\mathbf{x}|)}{(2t |\mathbf{x}_{B,t}|)^{1/2}} \right\}^\top \mathbf{A}_{BC} H(t, \mathbf{x}_{C,t}) \\
&\quad + o(1)
\end{aligned}$$

Combining all terms together leads to

$$-\frac{\log f(t\mathbf{x}_t)}{t} \rightarrow g(\mathbf{x}) \quad \text{whenever } \mathbf{x}_t \rightarrow \mathbf{x},$$

where  $g$  is defined in expression (A.33).

### 3.2 Multivariate Laplace copula

The joint density of the  $d$ -variate Laplace distribution in standard Laplace margins with positive definite precision matrix  $\mathbf{Q}$  is

$$f_{[L]}(t\mathbf{x}) = \frac{2^{1+\frac{d}{2}} |\mathbf{Q}|^{1/2}}{(2\pi)^{d/2}} t^v \left( \frac{1}{2^2} \mathbf{x}^\top \mathbf{Q} \mathbf{x} \right)^{v/2} K_v \left\{ t (\mathbf{x}^\top \mathbf{Q} \mathbf{x})^{1/2} \right\}$$

for  $t > 0$ , where  $v = (2 - d)/2$  and  $K_v$  is the modified Bessel function of the second kind (Kotz et al. 2001). Therefore,  $-\log f_{[L]}(t\mathbf{x}) =$

$$= - \left( 1 + \frac{d}{2} \right) \log 2 + \frac{d}{2} \log(2\pi) - \frac{1}{2} \log |\mathbf{Q}| + v \log(2/t) - \frac{v}{2} \log(\mathbf{x}^\top \mathbf{Q} \mathbf{x}) - \log \left[ K_v \left\{ t (\mathbf{x}^\top \mathbf{Q} \mathbf{x})^{1/2} \right\} \right]$$

Asymptotically, we have  $K_v(z) \sim (\pi/2z)^{1/2} e^{-z} (1 + O(z^{-1}))$  as  $z \rightarrow \infty$  (GradshTEYN & Ryzhik 2014). Applying the negative logarithm, obtain

$$-\log K_v(z) \sim -\frac{1}{2} \log \left( \frac{\pi}{2} \right) + \frac{1}{2} \log z + z + O(z^{-1}).$$

Substituting this in the expression for  $-\log f_{[L]}(t\mathbf{x})$ , obtain

$$\begin{aligned} -\log f_{[L]}(t\mathbf{x}) &\sim -\left(1 + \frac{d}{2}\right) \log 2 + \frac{d}{2} \log 2\pi - \frac{1}{2} |\mathbf{Q}| - v \log t + v \log 2 - \frac{v}{2} \log (\mathbf{x}^\top \mathbf{Q} \mathbf{x}) \\ &\quad - \frac{1}{2} \log \left( \frac{\pi}{2} \right) + \frac{1}{2} \log t + \frac{1}{4} \log (\mathbf{x}^\top \mathbf{Q} \mathbf{x}) + t (\mathbf{x}^\top \mathbf{Q} \mathbf{x})^{1/2} + O(t^{-1}) \\ &= t g_G(\mathbf{x}) + (\log t) u_1(\mathbf{x}) + u_2(\mathbf{x}) + O(t^{-1}), \end{aligned}$$

for  $t \rightarrow \infty$ , where the gauge function is  $g_G(\mathbf{x}) = (\mathbf{x}^\top \mathbf{Q} \mathbf{x})^{1/2}$ . The higher order terms are given by  $u_1(\mathbf{x}) = \frac{1}{2} - v$  and  $u_2(\mathbf{x}) = -\left(1 + \frac{d}{2} - v\right) \log 2 + \frac{d}{2} \log 2\pi - \frac{1}{2} \log |\mathbf{Q}| - \frac{1}{2} \log \left( \frac{\pi}{2} \right) + \left( \frac{1}{4} - \frac{v}{2} \right) \log (\mathbf{x}^\top \mathbf{Q} \mathbf{x})$ .

### 3.3 Multivariate max-stable Logistic distribution with standard Fréchet marginal distributions

For positive entries  $\mathbf{x} \in \mathbb{R}_+^d$ , the joint density in standard Fréchet margins is

$$f(\mathbf{x}) = \left( \sum_{\pi \in \Pi} (-1)^{|\pi|} \prod_{s \in \pi} V_s(\mathbf{x}) \right) \exp \{-V(\mathbf{x})\}$$

where  $V(\mathbf{x}) = \left( \sum_{j=1}^d x_j^{-1/\theta} \right)^\theta$  is a  $-1$ -homogeneous exponent function with dependence parameter  $\theta \in (0, 1)$ , and

$$V_s(\mathbf{x}) = (-\theta)^{-|s|} \left[ \prod_{k=0}^{|s|-1} (\theta - k) \right] \left( \prod_{k \in s} x_k \right)^{-\frac{1}{\theta} - 1} \left( \sum_{j=1}^d x_j^{-1/\theta} \right)^{\theta - |s|}$$

is the  $-(|s| + 1)$ -homogeneous  $|s|$ -order partial derivative of  $V$  with respect to inputs whose indices are in  $s$ . Using the intuition in Proposition 6 (iii) and setting  $\psi(t) = t^{-(d+1)}$ , we have the following convergence

$$\frac{f(t\mathbf{x})}{t^{-(d+1)}} \rightarrow (-1)^d V_{\{1, \dots, d\}}(\mathbf{x}) = g(\mathbf{x})^{-(d+1)}$$

as  $t \rightarrow \infty$ , where  $V_{\{1, \dots, d\}}$  is the partial derivative of the exponent function with respect to all  $d$  components. Note that in the context of Proposition 6 (iii), this convergence implied that  $\xi = 1$ .

In the logistic setting, the expression of  $g$  is therefore given by

$$g(\mathbf{x}) = (-\theta)^{-d} \left[ \prod_{k=0}^{d-1} (\theta - k) \right] \left( \prod_{k=1}^d x_k \right)^{-\frac{1}{\theta}-1} \left( \sum_{j=1}^d x_j^{-1/\theta} \right)^{\theta-d}$$

Higher-order terms are given by

$$\begin{aligned} u_k(\mathbf{w}) &= \frac{f(t\mathbf{x}) - t^{-(d+1)}g(\mathbf{x})^{-(d+1-1)} - \sum_{i=1}^{k-1} t^{-\sum_{\ell=i+1}^k \sum_{j=1}^{\ell} (d+j)} u_i(\mathbf{x})}{t^{-\sum_{j=1}^{k+1} (d+j)}} \\ &\rightarrow \sum_{\pi \in \Pi(d+1+k)} (-1)^{|\pi|} \prod_{s \in \pi} V_s(\mathbf{x}) ; t \rightarrow \infty \end{aligned}$$

for  $k = 1, \dots, d-1$ , where  $\Pi^{(n)} \subset \Pi$  is such that for all  $\pi \in \Pi^{(n)}$ ,  $\sum_{s \in \pi} |s| = n$  for  $n \in \{d+2, d+3, \dots, 2d\}$ .

### 3.4 Multivariate inverted max-stable distributions, standard exponential margins

The class of multivariate inverted max-stable distributions is usually represented in exponential margins, and has a joint distribution function

$$F(\mathbf{x}) = e^{-\ell(\mathbf{x})}$$

where  $\ell$  is the 1-homogeneous *stable tail dependence function*, and is defined by the  $-1$ -homogeneous exponent function  $V$ , introduced in Supplementary Material 3.3, through the relation  $\ell(\mathbf{x}) = V(1/\mathbf{x})$ . The joint density in exponential margins is given by

$$f(\mathbf{x}) = \left( \sum_{\pi \in \Pi} (-1)^{|\pi|} \prod_{s \in \pi} \ell_s(\mathbf{x}) \right) \exp \{-\ell(\mathbf{x})\}$$

where  $\ell_s(\mathbf{x}) = V_s(1/\mathbf{x})(-1)^{|s|} \prod_{j \in s} x_j^{-2}$  is  $(1-|s|)$ -homogeneous. Here, we use the limiting behaviour in Proposition 6 (ii) to see limiting behaviour

$$-\log f(t\mathbf{x}) = tg(\mathbf{x}) + u(\mathbf{x})$$

where the gauge function is given by  $g(\mathbf{x}) = \ell(\mathbf{x})$  and higher order term

$$u(\mathbf{x}) = -\log \left[ (-1)^d \prod_{j=1}^d \ell_{\{j\}}(\mathbf{x}) + o(1) \right]$$

as  $t \rightarrow \infty$ .

### 3.5 Multivariate max-stable and inverted max-stable copula, logistic dependence

The joint density function in Fréchet margins is

$$f_F(\mathbf{z}) = \left( \sum_{\pi \in \Pi} (-1)^{|\pi|} \prod_{s \in \pi} V_s(\mathbf{z}) \right) \exp \{-V(\mathbf{z})\}$$

where  $V(\mathbf{z}) = \left( \sum_{j=1}^d z_j^{-1/\theta} \right)^\theta$  is a  $-1$ -homogeneous exponent function with dependence parameter  $\theta \in (0, 1)$ , and  $V_s$  is the  $|s|$ -order partial derivative of  $V$  with respect to inputs whose indices are in  $s$ . Let  $\Pi$  be the set of all partitions of the set of indices  $\{1, \dots, d\}$ , and let  $\pi$  be the set of all partitions of an arbitrary element in  $\Pi$ . To obtain the joint density in Laplace margins, change of variables is implemented.

Suppose  $z_t(x_j) = z(tx_j)$  for  $t > 0$  and  $j \in \{1, \dots, d\}$ . If  $x_j < 0$  (or  $z_t(x_j) < (\log 2)^{-1}$ ), then we perform the change of variables from Fréchet to Laplace margins

$$z_t(x_j) = \left( -\log \left( \frac{1}{2} e^{tx_j} \right) \right)^{-1} = (-tx_j)^{-1} (1 - \log 2 (-tx_j)^{-1} + O(t^{-2}))$$

with derivative given by

$$\frac{d}{d(tx_j)} z_t(x_j) = (-tx_j)^{-2} (1 - 2 \log 2 (-tx_j)^{-1} + O(t^{-2})).$$

If  $x_j > 0$  (or  $z_t(x_j) > (\log 2)^{-1}$ ), then

$$z_t(x_j) = \left( -\log \left( 1 - \frac{1}{2} e^{-tx_j} \right) \right)^{-1} = 2e^{tx_j} - \frac{1}{2} + O(e^{-tx_j})$$

with derivative given by

$$\frac{d}{d(tx_j)} z_t(x_j) = 2e^{tx_j} + O(e^{-tx_j}).$$

Lastly, if  $x_j = 0$ , then  $z_t(x_j) = (\log 2)^{-1}$ . By the inverse function and chain rules,

$$\frac{d}{d(tx_j)} z_t(x_j) = \frac{f_L(tx_j)}{f_F(F_F^{-1}(F_L(tx_j)))} = \begin{cases} \frac{e^{-t|x_j|}}{e^{tx_j} (\log(\frac{1}{2} e^{tx_j}))^2} & ; x_j < 0 \\ \frac{\frac{1}{2} e^{-t|x_j|}}{(1 - \frac{1}{2} e^{-tx_j}) (\log(1 - \frac{1}{2} e^{-tx_j}))^2} & ; x_j > 0 \end{cases} \xrightarrow{x_j \rightarrow 0} (\log 2)^{-2}$$

For a vector  $\mathbf{x} = (x_1, \dots, x_d)^\top$ , let  $A, B, C \subset \{1, \dots, d\}$  be the set of indices such that  $x_j$  is positive, negative, and zero for  $j \in A, B, C$ , respectively such that  $|A| + |B| + |C| = d$ . By change of variables, the joint density for the max-stable distribution with logistic dependence in Laplace

margins is

$$\begin{aligned}
f_L(t\mathbf{x}) &= \left| \prod_{j=1}^d \frac{d}{d(tx_j)} z_t(x_j) \right| f_F(z(tx_1), \dots, z(tx_d)) \\
&= (-1)^{d+1} \left\{ \prod_{\ell=0}^{d-1} \left(1 - \frac{\ell}{\theta}\right) \right\} 2^{-\frac{|A|}{\theta}} t^{\left(\frac{1}{\theta}-1\right)|B|+1-\frac{d}{\theta}} (\log 2)^{-2|C|} \left( \prod_{k \in B} (-x_k)^{\frac{1}{\theta}-1} \right) \left( \sum_{k \in B} (-x_k)^{1/\theta} \right)^{\theta-d} \\
&\quad \times \exp \left\{ -t \left[ \frac{1}{\theta} \sum_{j \in A} x_j + \left( \sum_{k \in B} (-x_k)^{1/\theta} \right)^\theta \left( 1 + O\left(e^{-\frac{t}{\theta} \min_{j \in A} x_j}\right) + O(t^{-1}) \right) \right] \right\} (1 + o(1))
\end{aligned}$$

Applying the negative logarithm, obtain the following expression

$$\begin{aligned}
-\log f_L(t\mathbf{x}) &= -\log \left[ (-1)^{d+1} \left\{ \prod_{\ell=0}^{d-1} \left(1 - \frac{\ell}{\theta}\right) \right\} 2^{-\frac{|A|}{\theta}} (\log 2)^{-2|C|} \right] - \left(\frac{1}{\theta} - 1\right) \sum_{k \in B} \log(-x_k) \\
&\quad - (\theta - d) \log \left( \sum_{k \in B} (-x_k)^{1/\theta} \right) + \left\{ -\left(\frac{1}{\theta} - 1\right) |B| - 1 + \frac{d}{\theta} \right\} \log t \\
&\quad + t \left[ \frac{1}{\theta} \sum_{j \in A} x_j + \left\{ \sum_{k \in B} (-x_k)^{1/\theta} \right\}^\theta \left\{ 1 + O\left(e^{-\frac{t}{\theta} \min_{j \in A} x_j}\right) + O(t^{-1}) \right\} \right] + o(1) \\
&= tg(\mathbf{x}) + (\log t)u_1(\mathbf{x}) + u_2(\mathbf{x})
\end{aligned}$$

where, when letting  $t \rightarrow \infty$ , the gauge function is

$$g(\mathbf{x}) = \frac{1}{\theta} \sum_{j \in A} x_j + \left\{ \sum_{k \in B} (-x_k)^{1/\theta} \right\}^\theta$$

the higher order terms are given by

$$u_1(\mathbf{x}) = -\left(\frac{1}{\theta} - 1\right) |B| - 1 + \frac{d}{\theta}$$

and

$$u_2(\mathbf{x}) = -\log \left[ \frac{(-1)^{d+1} 2^{-\frac{|A|}{\theta}} \left\{ \prod_{\ell=0}^{d-1} \left(1 - \frac{\ell}{\theta}\right) \right\}}{(\log 2)^{-2|C|}} \right] - \left(\frac{1}{\theta} - 1\right) \sum_{k \in B} \log(-x_k) - (\theta - d) \log \left\{ \sum_{k \in B} (-x_k)^{1/\theta} \right\}$$

There are 2 special cases to consider:

- **special case 1:** Suppose  $x_j > 0 \forall j \in \{1, \dots, d\}$  and let  $x_{(d)} = \min_{j=1, \dots, d} x_j$ . Here, the joint

log-density is

$$-\log f_L(t\mathbf{x}) = -\log \left[ 2^{-1}(-1)^d \left\{ \prod_{\ell=1}^{d-1} \left( 1 - \frac{\ell}{\theta} \right) \right\} \right] + t \left\{ \frac{1}{\theta} \sum_{j=1}^d x_j + \left( 1 - \frac{d}{\theta} \right) x_{(d)} \right\} + 2^{-1} e^{-tx_{(d)}} (1 + o(1)) + o(1) = tg(\mathbf{x}) + u_1(\mathbf{x}) + o(1)$$

where the gauge function is

$$g(\mathbf{x}) = \frac{1}{\theta} \sum_{j=1}^d x_j + \left( 1 - \frac{d}{\theta} \right) \min_{k=1, \dots, d} x_k$$

and the higher order term is

$$u_1(\mathbf{x}) = -\log \left[ 2^{-1}(-1)^{d+1} \left\{ \prod_{\ell=1}^{d-1} \left( 1 - \frac{\ell}{\theta} \right) \right\} \right], \quad \text{as } t \rightarrow \infty.$$

- **special case 2:** Suppose  $x_j < 0 \forall j \in \{1, \dots, d\}$ . Here, we have

$$-\log f_L(t\mathbf{x}) = tg(\mathbf{x}) + (\log t)u_1(\mathbf{x}) + u_2(\mathbf{x}) + o(1)$$

where the gauge function is

$$g(\mathbf{x}) = \left\{ \sum_{j=1}^d (-x_j)^{1/\theta} \right\}^\theta$$

the higher order terms are given by

$$u_1(\mathbf{x}) = d - 1$$

and

$$u_2(\mathbf{x}) = -\log \left[ (-1)^{d+1} \left\{ \prod_{\ell=0}^{d-1} \left( 1 - \frac{\ell}{\theta} \right) \right\} \left\{ \prod_{j=1}^d (-x_j) \right\}^{\frac{1}{\theta}-1} \left\{ \sum_{j=1}^d (-x_j)^{1/\theta} \right\}^{\theta-d} \right], \quad \text{as } t \rightarrow \infty.$$

To study the case of **inverted logistic dependence**, first recall the definition of the joint distribution function in Fréchet margins

$$F_F(\mathbf{z}) = \exp \{-V(\mathbf{z})\}$$

By evaluating at the univariate Fréchet quantile function, get the Logistic copula

$$C_{log.}(u_1, \dots, u_d) = F_F \left( -\frac{1}{\log u_1}, \dots, -\frac{1}{\log u_d} \right) = \exp \left\{ -V \left( -\frac{1}{\log u_1}, \dots, -\frac{1}{\log u_d} \right) \right\}$$

where  $V$  is specified to be the exponent function commonly associated with logistic dependence. The survival copula associated with the inverted logistic distribution is therefore given by

$$\bar{C}_{inv.log.}(u_1, \dots, u_d) = C_{log.}(1 - u_1, \dots, 1 - u_d) = \exp \left\{ -V \left( -\frac{1}{\log(1 - u_1)}, \dots, -\frac{1}{\log(1 - u_d)} \right) \right\}$$

So  $x_j > 0$  (or  $u_j > 1/2$ ) in the logistic case corresponds to  $x_j < 0$  (or  $u_j < 1/2$ ) in the inverted logistic case. This leads to the decomposition of the log-joint density in Laplace margins  $-\log f_L(t\mathbf{x}) = tg(\mathbf{x}) + (\log t)u_1(\mathbf{x}) + g_0^*(\mathbf{x})$  where the gauge function is

$$g(\mathbf{x}) = \left( \sum_{j \in A} x_j^{1/\theta} \right)^\theta + \frac{1}{\theta} \sum_{k \in B} (-x_k)$$

the higher-order terms are given by

$$u_1(\mathbf{x}) = - \left( \frac{1}{\theta} - 1 \right) |A| - 1 + \frac{d}{\theta}$$

and

$$u_2(\mathbf{x}) = -\log \left[ (-1)^{d+1} \left\{ \prod_{\ell=0}^{d-1} \left( 1 - \frac{\ell}{\theta} \right) \right\} 2^{-\frac{|B|}{\theta}} (\log 2)^{-2|C|} \right] - \left( \frac{1}{\theta} - 1 \right) \sum_{j \in A} \log(x_j) - (\theta - d) \log \left( \sum_{j \in A} x_j^{1/\theta} \right)$$

In the case where  $x_j > 0 \forall j \in \{1, \dots, d\}$  we have  $-\log f_L(t\mathbf{x}) = tg(\mathbf{x}) + (\log t)u_1(\mathbf{x}) + u_2(\mathbf{x}) + o(1)$  where the gauge function is

$$g(\mathbf{x}) = \left( \sum_{j=1}^d x_j^{1/\theta} \right)^\theta$$

with higher-order terms given by

$$u_1(\mathbf{x}) = d - 1$$

and

$$u_2(\mathbf{x}) = -\log \left[ (-1)^{d+1} \left\{ \prod_{\ell=0}^{d-1} \left( 1 - \frac{\ell}{\theta} \right) \right\} \left( \prod_{j=1}^d x_j \right)^{\frac{1}{\theta}-1} \left( \sum_{j=1}^d x_j^{1/\theta} \right)^{\theta-d} \right]$$

as  $t \rightarrow \infty$ . In the case where  $x_j < 0 \forall j \in \{1, \dots, d\}$  we have

$$-\log f_L(t\mathbf{x}) = tg(\mathbf{x}) + u_1(\mathbf{x}) + o(1)$$

where the gauge function is

$$g(\mathbf{x}) = \frac{1}{\theta} \sum_{j=1}^d (-x_j) + \left( 1 - \frac{d}{\theta} \right) \min_{k=1, \dots, d} |x_k|$$

and the higher order term is

$$u_1(\mathbf{x}) = -\log \left[ 2^{-1}(-1)^d \left\{ \prod_{\ell=1}^{d-1} \left( 1 - \frac{\ell}{\theta} \right) \right\} \right], \quad \text{as } t \rightarrow \infty.$$

The joint density function in Fréchet margins is

$$f_F(\mathbf{z}) = \left( \sum_{\pi \in \Pi} (-1)^{|\pi|} \prod_{s \in \pi} V_s(\mathbf{z}) \right) \exp \{-V(\mathbf{z})\}$$

where  $V(\mathbf{z}) = \left( \sum_{j=1}^d z_j^{-1/\theta} \right)^\theta$  is a  $-1$ -homogeneous exponent function with dependence parameter  $\theta \in (0, 1)$ , and  $V_s$  is the  $|s|$ -order partial derivative of  $V$  with respect to inputs whose indices are in  $s$ . Let  $\Pi$  be the set of all partitions of the set of indices  $\{1, \dots, d\}$ , and let  $\pi$  be the set of all partitions of an arbitrary element in  $\Pi$ . To obtain the joint density in Laplace margins, change of variables is implemented.

Suppose  $z_t(x_j) = z(tx_j)$  for  $t > 0$  and  $j \in \{1, \dots, d\}$ . If  $x_j < 0$  (or  $z_t(x_j) < (\log 2)^{-1}$ ), then we perform the change of variables from Fréchet to Laplace margins

$$z_t(x_j) = \left( -\log \left( \frac{1}{2} e^{tx_j} \right) \right)^{-1} = (-tx_j)^{-1} (1 - \log 2 (-tx_j)^{-1} + O(t^{-2}))$$

with derivative given by

$$\frac{d}{d(tx_j)} z_t(x_j) = (-tx_j)^{-2} (1 - 2 \log 2 (-tx_j)^{-1} + O(t^{-2})).$$

If  $x_j > 0$  (or  $z_t(x_j) > (\log 2)^{-1}$ ), then

$$z_t(x_j) = \left( -\log \left( 1 - \frac{1}{2} e^{-tx_j} \right) \right)^{-1} = 2e^{tx_j} - \frac{1}{2} + O(e^{-tx_j})$$

with derivative given by

$$\frac{d}{d(tx_j)} z_t(x_j) = 2e^{tx_j} + O(e^{-tx_j}).$$

Lastly, if  $x_j = 0$ , then  $z_t(x_j) = (\log 2)^{-1}$ . By the inverse function and chain rules,

$$\frac{d}{d(tx_j)} z_t(x_j) = \frac{f_L(tx_j)}{f_F(F_F^{-1}(F_L(tx_j)))} = \begin{cases} \frac{e^{-t|x_j|}}{e^{tx_j} (\log(\frac{1}{2} e^{tx_j}))^2} & ; x_j < 0 \\ \frac{\frac{1}{2} e^{-t|x_j|}}{(1 - \frac{1}{2} e^{-tx_j}) (\log(1 - \frac{1}{2} e^{-tx_j}))^2} & ; x_j > 0 \end{cases} \xrightarrow{x_j \rightarrow 0} (\log 2)^{-2}$$

For a vector  $\mathbf{x} = (x_1, \dots, x_d)^\top$ , let  $A, B, C \subset \{1, \dots, d\}$  be the set of indices such that  $x_j$  is positive, negative, and zero for  $j \in A, B, C$ , respectively such that  $|A| + |B| + |C| = d$ . By change of variables, the joint density for the max-stable distribution with logistic dependence in Laplace

margins is

$$\begin{aligned}
f_L(t\mathbf{x}) &= \left| \prod_{j=1}^d \frac{d}{d(tx_j)} z_t(x_j) \right| f_F(z(tx_1), \dots, z(tx_d)) \\
&= (-1)^{d+1} \left\{ \prod_{\ell=0}^{d-1} \left(1 - \frac{\ell}{\theta}\right) \right\} 2^{-\frac{|A|}{\theta}} t^{\left(\frac{1}{\theta}-1\right)|B|+1-\frac{d}{\theta}} (\log 2)^{-2|C|} \left( \prod_{k \in B} (-x_k)^{\frac{1}{\theta}-1} \right) \left( \sum_{k \in B} (-x_k)^{1/\theta} \right)^{\theta-d} \\
&\quad \times \exp \left\{ -t \left[ \frac{1}{\theta} \sum_{j \in A} x_j + \left( \sum_{k \in B} (-x_k)^{1/\theta} \right)^\theta \left( 1 + O\left(e^{-\frac{t}{\theta} \min_{j \in A} x_j}\right) + O(t^{-1}) \right) \right] \right\} (1 + o(1))
\end{aligned}$$

Applying the negative logarithm, obtain the following expression

$$\begin{aligned}
-\log f_L(t\mathbf{x}) &= -\log \left[ (-1)^{d+1} \left\{ \prod_{\ell=0}^{d-1} \left(1 - \frac{\ell}{\theta}\right) \right\} 2^{-\frac{|A|}{\theta}} (\log 2)^{-2|C|} \right] - \left(\frac{1}{\theta} - 1\right) \sum_{k \in B} \log(-x_k) \\
&\quad - (\theta - d) \log \left( \sum_{k \in B} (-x_k)^{1/\theta} \right) + \left\{ -\left(\frac{1}{\theta} - 1\right) |B| - 1 + \frac{d}{\theta} \right\} \log t \\
&\quad + t \left[ \frac{1}{\theta} \sum_{j \in A} x_j + \left\{ \sum_{k \in B} (-x_k)^{1/\theta} \right\}^\theta \left\{ 1 + O\left(e^{-\frac{t}{\theta} \min_{j \in A} x_j}\right) + O(t^{-1}) \right\} \right] + o(1) \\
&= tg(\mathbf{x}) + (\log t)u_1(\mathbf{x}) + u_2(\mathbf{x})
\end{aligned}$$

where, when letting  $t \rightarrow \infty$ , the gauge function is

$$g(\mathbf{x}) = \frac{1}{\theta} \sum_{j \in A} x_j + \left\{ \sum_{k \in B} (-x_k)^{1/\theta} \right\}^\theta$$

the higher order terms are given by

$$u_1(\mathbf{x}) = -\left(\frac{1}{\theta} - 1\right) |B| - 1 + \frac{d}{\theta}$$

and

$$u_2(\mathbf{x}) = -\log \left[ \frac{(-1)^{d+1} 2^{-\frac{|A|}{\theta}} \left\{ \prod_{\ell=0}^{d-1} \left(1 - \frac{\ell}{\theta}\right) \right\}}{(\log 2)^{-2|C|}} \right] - \left(\frac{1}{\theta} - 1\right) \sum_{k \in B} \log(-x_k) - (\theta - d) \log \left\{ \sum_{k \in B} (-x_k)^{1/\theta} \right\}$$

There are 2 special cases to consider:

- **special case 1:** Suppose  $x_j > 0 \forall j \in \{1, \dots, d\}$  and let  $x_{(d)} = \min_{j=1, \dots, d} x_j$ . Here, the joint

log-density is

$$-\log f_L(t\mathbf{x}) = -\log \left[ 2^{-1}(-1)^d \left\{ \prod_{\ell=1}^{d-1} \left( 1 - \frac{\ell}{\theta} \right) \right\} \right] + t \left\{ \frac{1}{\theta} \sum_{j=1}^d x_j + \left( 1 - \frac{d}{\theta} \right) x_{(d)} \right\} + 2^{-1} e^{-tx_{(d)}} (1 + o(1)) + o(1) = tg(\mathbf{x}) + u_1(\mathbf{x}) + o(1)$$

where the gauge function is

$$g(\mathbf{x}) = \frac{1}{\theta} \sum_{j=1}^d x_j + \left( 1 - \frac{d}{\theta} \right) \min_{k=1, \dots, d} x_k$$

and the higher order term is

$$u_1(\mathbf{x}) = -\log \left[ 2^{-1}(-1)^{d+1} \left\{ \prod_{\ell=1}^{d-1} \left( 1 - \frac{\ell}{\theta} \right) \right\} \right], \quad \text{as } t \rightarrow \infty.$$

- **special case 2:** Suppose  $x_j < 0 \forall j \in \{1, \dots, d\}$ . Here, we have

$$-\log f_L(t\mathbf{x}) = tg(\mathbf{x}) + (\log t)u_1(\mathbf{x}) + u_2(\mathbf{x}) + o(1)$$

where the gauge function is

$$g(\mathbf{x}) = \left\{ \sum_{j=1}^d (-x_j)^{1/\theta} \right\}^\theta$$

the higher order terms are given by

$$u_1(\mathbf{x}) = d - 1$$

and

$$u_2(\mathbf{x}) = -\log \left[ (-1)^{d+1} \left\{ \prod_{\ell=0}^{d-1} \left( 1 - \frac{\ell}{\theta} \right) \right\} \left\{ \prod_{j=1}^d (-x_j) \right\}^{\frac{1}{\theta}-1} \left\{ \sum_{j=1}^d (-x_j)^{1/\theta} \right\}^{\theta-d} \right], \quad \text{as } t \rightarrow \infty.$$

To study the case of **inverted logistic dependence**, first recall the definition of the joint distribution function in Fréchet margins

$$F_F(\mathbf{z}) = \exp \{-V(\mathbf{z})\}$$

By evaluating at the univariate Fréchet quantile function, get the Logistic copula

$$C_{log.}(u_1, \dots, u_d) = F_F \left( -\frac{1}{\log u_1}, \dots, -\frac{1}{\log u_d} \right) = \exp \left\{ -V \left( -\frac{1}{\log u_1}, \dots, -\frac{1}{\log u_d} \right) \right\}$$

where  $V$  is specified to be the exponent function commonly associated with logistic dependence. The survival copula associated with the inverted logistic distribution is therefore given by

$$\bar{C}_{inv.log.}(u_1, \dots, u_d) = C_{log.}(1 - u_1, \dots, 1 - u_d) = \exp \left\{ -V \left( -\frac{1}{\log(1 - u_1)}, \dots, -\frac{1}{\log(1 - u_d)} \right) \right\}$$

So  $x_j > 0$  (or  $u_j > 1/2$ ) in the logistic case corresponds to  $x_j < 0$  (or  $u_j < 1/2$ ) in the inverted logistic case. This leads to the decomposition of the log-joint density in Laplace margins  $-\log f_L(t\mathbf{x}) = tg(\mathbf{x}) + (\log t)u_1(\mathbf{x}) + g_0^*(\mathbf{x})$  where the gauge function is

$$g(\mathbf{x}) = \left( \sum_{j \in A} x_j^{1/\theta} \right)^\theta + \frac{1}{\theta} \sum_{k \in B} (-x_k)$$

the higher-order terms are given by

$$u_1(\mathbf{x}) = - \left( \frac{1}{\theta} - 1 \right) |A| - 1 + \frac{d}{\theta}$$

and

$$u_2(\mathbf{x}) = -\log \left[ (-1)^{d+1} \left\{ \prod_{\ell=0}^{d-1} \left( 1 - \frac{\ell}{\theta} \right) \right\} 2^{-\frac{|B|}{\theta}} (\log 2)^{-2|C|} \right] - \left( \frac{1}{\theta} - 1 \right) \sum_{j \in A} \log(x_j) - (\theta - d) \log \left( \sum_{j \in A} x_j^{1/\theta} \right)$$

In the case where  $x_j > 0 \forall j \in \{1, \dots, d\}$  we have  $-\log f_L(t\mathbf{x}) = tg(\mathbf{x}) + (\log t)u_1(\mathbf{x}) + u_2(\mathbf{x}) + o(1)$  where the gauge function is

$$g(\mathbf{x}) = \left( \sum_{j=1}^d x_j^{1/\theta} \right)^\theta$$

with higher-order terms given by

$$u_1(\mathbf{x}) = d - 1$$

and

$$u_2(\mathbf{x}) = -\log \left[ (-1)^{d+1} \left\{ \prod_{\ell=0}^{d-1} \left( 1 - \frac{\ell}{\theta} \right) \right\} \left( \prod_{j=1}^d x_j \right)^{\frac{1}{\theta}-1} \left( \sum_{j=1}^d x_j^{1/\theta} \right)^{\theta-d} \right]$$

as  $t \rightarrow \infty$ . In the case where  $x_j < 0 \forall j \in \{1, \dots, d\}$  we have

$$-\log f_L(t\mathbf{x}) = tg(\mathbf{x}) + u_1(\mathbf{x}) + o(1)$$

where the gauge function is

$$g(\mathbf{x}) = \frac{1}{\theta} \sum_{j=1}^d (-x_j) + \left( 1 - \frac{d}{\theta} \right) \min_{k=1, \dots, d} |x_k|$$

and the higher order term is

$$u_1(\mathbf{x}) = -\log \left[ 2^{-1}(-1)^d \left\{ \prod_{\ell=1}^{d-1} \left( 1 - \frac{\ell}{\theta} \right) \right\} \right], \quad \text{as } t \rightarrow \infty.$$

### 3.6 Multivariate Student- $t_\nu$ copula, Student- $t_\nu$ margins, $\nu > 0$

Suppose  $\mathbf{Q}$  positive definite and  $\nu > 0$ . The joint density can be expressed as  $f(\mathbf{x}) = f_0(g_{\mathcal{G}}(\mathbf{x}))$ , where the homothetic function  $f_0$  and gauge function is given by

$$\begin{aligned} f_0(s) &= k_{\nu, \mathbf{Q}} (1 + \nu^{-1} s^2)^{-\frac{1}{2}(\nu+d)}, \\ g_{\mathcal{G}}(\mathbf{x}) &= (\mathbf{x}^\top \mathbf{Q} \mathbf{x})^{1/2}, \end{aligned}$$

where  $k_{\nu, \mathbf{Q}} = \Gamma\left(\frac{\nu+d}{2}\right) / \left\{ \Gamma\left(\frac{\nu}{2}\right) \nu^{d/2} \pi^{d/2} |\mathbf{Q}|^{-1/2} \right\}$ . By the third condition of Proposition 6, setting  $\psi(t) = k_{\nu, \mathbf{Q}} \nu^{\frac{1}{2}(\nu+d)} t^{-(\nu+d)}$ , and for  $t > 0$  large, the higher-order term is

$$\begin{aligned} u(\mathbf{x}) &= \frac{\frac{f(t\mathbf{x})}{\psi(t)} - g(\mathbf{x})^{-(\nu+d)}}{t^{-2}} \\ &= t^2 \left[ \psi(t)^{-1} k_{\nu, \mathbf{Q}} \nu^{\frac{1}{2}(\nu+d)} t^{-(\nu+d)} g_{\mathcal{G}}(\mathbf{x})^{-(\nu+d)} \left\{ 1 + \nu t^{-2} g_{\mathcal{G}}(\mathbf{x})^{-2} \right\}^{-\frac{1}{2}(\nu+d)} - g_{\mathcal{G}}(\mathbf{x})^{-(\nu+d)} \right] \\ &= t^2 \left[ g_{\mathcal{G}}(\mathbf{x})^{-(\nu+d)} \left\{ 1 - \frac{1}{2}(\nu+d) \nu t^{-2} g_{\mathcal{G}}(\mathbf{x})^{-2} + O(t^{-4}) \right\} - g_{\mathcal{G}}(\mathbf{x})^{-(\nu+d)} \right] \\ &= -\frac{1}{2}(\nu+d) \nu g_{\mathcal{G}}(\mathbf{x})^{-2-(\nu+d)} + O(t^{-2}) \\ &= -\frac{1}{2}(\nu+d) \nu g_{\mathcal{G}}(\mathbf{x})^{-2-(\nu+d)} + o(1) \end{aligned}$$

### 3.7 Multivariate Student- $t_\nu$ copula, Student- $t_\nu$ margins, $\nu < 0$

Suppose  $\mathbf{Q}$  positive definite and  $\nu < 0$  and  $\nu < 2 - d$  (Papastathopoulos & Tawn 2013). For support  $\{\mathbf{x} \in \mathbb{R}^d : 1 + \nu^{-1} \mathbf{x}^\top \mathbf{Q} \mathbf{x} > 0\}$ , the joint density is given by

$$f(\mathbf{x}) = k_{\nu, \mathbf{Q}} (1 + \nu^{-1} \mathbf{x}^\top \mathbf{Q} \mathbf{x})^{-\frac{1}{2}(\nu+d)}$$

where  $k_{\nu, \mathbf{Q}} = \pi^{-d/2} |\mathbf{Q}|^{1/2} |\nu|^{1-\frac{d}{2}} (|\nu| - d)^{-1} \Gamma\left(\frac{|\nu|}{2}\right) \Gamma\left(\frac{|\nu|-d}{2}\right)^{-1}$ . Note the homothetic form  $f(\mathbf{x}) = f_0(g_{\mathcal{G}}(\mathbf{x}))$ , where  $f_0(s) = k_{\nu, \mathbf{Q}} (1 - s^2)^{-\frac{1}{2}(\nu+d)}$  for  $s \in (-1, 1)$ . Therefore, we extract the gauge function

$$g_{\mathcal{G}}(\mathbf{x}) = (-\nu^{-1} \mathbf{x}^\top \mathbf{Q} \mathbf{x})^{1/2}$$

Therefore,  $r_{\mathcal{G}}(\cdot) = g_{\mathcal{G}}(\cdot)^{-1}$  is a  $-1$ -homogeneous radial function, and  $r_{\mathcal{G}}(\mathbf{x})\mathbf{x}$  lies on the boundary of the support (i.e.,  $f\{r_{\mathcal{G}}(\mathbf{x})\mathbf{x}\} = 0$ ). Using the transformation of the density function incondition

in Proposition 6 (i), we have the rate of convergence black

$$\begin{aligned}
f \{r_{\mathcal{G}}(\mathbf{x}) (\mathbf{x} - t^{-1}\mathbf{1})\} &= k_{\nu, \mathbf{Q}} \left[ 1 - r_{\mathcal{G}} \{r_{\mathcal{G}}(\mathbf{x}) (\mathbf{x} - t^{-1}\mathbf{1})\} \right]_+^{-\frac{1}{2}(\nu+d)} \\
&= k_{\nu, \mathbf{Q}} \left[ 1 - r_{\mathcal{G}}(\mathbf{x})^2 r_{\mathcal{G}}(\mathbf{x} - t^{-1}\mathbf{1}) \right]_+^{-\frac{1}{2}(\nu+d)} \\
&= k_{\nu, \mathbf{Q}} \left[ 1 - r_{\mathcal{G}}(\mathbf{x})^2 \{r_{\mathcal{G}}(\mathbf{x}) - \nabla r_{\mathcal{G}}(\mathbf{x})t^{-1} + O(t^{-2})\} \right]_+^{-\frac{1}{2}(\nu+d)} \\
&= k_{\nu, \mathbf{Q}} t^{\frac{1}{2}(\nu+d)} \left\{ -\frac{2}{r_{\mathcal{G}}(\mathbf{x})} \nabla r_{\mathcal{G}}(\mathbf{x}) + O(t^{-1}) \right\}
\end{aligned}$$

Therefore,

$$\frac{f \{r_{\mathcal{G}}(\mathbf{x}) (\mathbf{x} - t^{-1}\mathbf{1})\}}{k_{\nu, \mathbf{Q}} t^{\frac{1}{2}(\nu+d)}} = -\frac{2}{r_{\mathcal{G}}(\mathbf{x})} \nabla r_{\mathcal{G}}(\mathbf{x}) + o(1)$$

### 3.8 Multivariate Student- $t_{\nu}$ copula, $\nu > 0$ , Laplace margins

The multivariate t-distribution with positive definite precision matrix  $\mathbf{Q} = (q_{ij})_{i,j=1}^d$  and with univariate t-distribution margins with  $\nu$  degrees of freedom is given has joint density

$$f(\mathbf{z}) = k_{\nu, \mathbf{Q}} \left( 1 + \frac{1}{\nu} \sum_{j=1}^d q_{jj} z_j^2 + \frac{2}{\nu} \sum_{1 \leq j < k \leq d} q_{jk} z_j z_k \right)^{-\frac{1}{2}(\nu+d)}$$

where  $k_{\nu, \mathbf{Q}} = \Gamma(\frac{\nu+d}{2}) / \left\{ \Gamma(\frac{\nu}{2}) \nu^{d/2} \pi^{d/2} |\mathbf{Q}|^{-1/2} \right\}$ . Perform the change of variables to the standard Laplace distribution, where we take advantage of a univariate t-distribution analog of Mill's ratio (Soms 1976). Let  $f_{t_{\nu}}$  and  $F_{t_{\nu}}$  be the density and distribution functions of the univariate t-distribution with  $\nu$  degrees of freedom, respectively.

Suppose  $z = z(tx) > 0$  (or  $x > 0$ ), then for  $t > 0$  large, the change of variables from the t-distribution to the standard Laplace distribution

$$tx = -\log [2 \{1 - F_{t_{\nu}}(z(tx))\}] = -\log \left[ \frac{2\Gamma(\frac{\nu+1}{2}) \nu^{\frac{1-\nu}{2}}}{\Gamma(\frac{\nu}{2}) \sqrt{\nu\pi}} \right] + \nu \log z(tx) + O(z(tx)^{-2}).$$

Inverting this transformation, obtain

$$z(tx) = c_{\nu} e^{\frac{t}{\nu}x} \left( 1 + O\left(e^{-\frac{2t}{\nu}}\right) \right),$$

with partial derivative with respect to  $tx$  given by

$$\frac{d}{dtx} z(tx) = \frac{c_{\nu}}{\nu} e^{\frac{t}{\nu}x} \left( 1 + O\left(e^{-\frac{2t}{\nu}}\right) \right),$$

where  $c_\nu = \left\{ 2\Gamma\left(\frac{\nu+1}{2}\right) \nu^{\left(\frac{1-\nu}{2}\right)} \Gamma\left(\frac{\nu}{2}\right)^{-1} (\nu\pi)^{-1/2} \right\}^{1/\nu}$ . When  $z(tx) < 0$  (or  $x < 0$ ), the transformation to Laplace margins is

$$tx = \log [2F_{t_\nu}(z(tx))] = \log 2 + \log [1 - F_{t_\nu}(-z(tx))].$$

Negating,

$$-tx = -\log 2 - \log (1 - F_{t_\nu}(-z(tx))) = -\log \left[ \frac{2\Gamma\left(\frac{\nu+1}{2}\right) \nu^{\left(\frac{1-\nu}{2}\right)}}{\Gamma\left(\frac{\nu}{2}\right) \sqrt{\nu\pi}} \right] + \nu \log(-z(tx)) + O(z(tx)^{-2}).$$

Inverting this transformation,

$$z(tx) = -c_\nu e^{\frac{t}{\nu}|x|} \left( 1 + O\left(e^{\frac{-2t}{\nu}}\right) \right),$$

with partial derivative

$$\frac{d}{dtx} z(tx) = \frac{c_\nu}{\nu} e^{\frac{t}{\nu}|x|} \left( 1 + O\left(e^{\frac{-2t}{\nu}}\right) \right).$$

Therefore, by change of variables, obtain the joint density in Laplace margins

$$\begin{aligned} f_L(\mathbf{t}\mathbf{x}) &= \left| \prod_{j=1}^d \frac{d}{d(tx_j)} z(tx_j) \right| f(z(tx_1), \dots, z(tx_d)) \\ &= \frac{c_\nu^d k_{\nu, \mathbf{Q}}}{\nu^d} \exp \left\{ \frac{t}{\nu} \sum_{j=1}^d |x_j| \right\} \frac{q_{j^* j^*} c_\nu^2}{\nu} \exp \left\{ -t \left( 1 + \frac{d}{\nu} \right) \max_{j=1, \dots, d} |x_j| \right\} (1 + o(1)), \end{aligned}$$

where  $j^*$  is the index such that  $|x_{j^*}| = \max_{j=1, \dots, d} |x_j|$ . Taking the negative logarithm, we obtain

$$-\log f_L(\mathbf{t}\mathbf{x}) = tg(\mathbf{x}) + u_1(\mathbf{x}) + o(1),$$

where the gauge function is

$$g(\mathbf{x}) = -\frac{1}{\nu} \sum_{j=1}^d |x_j| + \left( 1 + \frac{d}{\nu} \right) \max_{j=1, \dots, d} |x_j|,$$

and the higher order term is

$$u_1(\mathbf{x}) = -\log \left( \frac{c_\nu^{d+2} k_{\nu, \mathbf{Q}} q_{j^* j^*}}{\nu^{d+1}} \right).$$

### 3.9 Wishart distribution

For a  $d \times d$  positive definite matrix  $\mathbf{X}$ , the Wishart distribution with  $\nu$  degrees of freedom and positive definite scale matrix  $\mathbf{V}$  has density function

$$f_{\mathbf{X}}(\mathbf{X}) = 2^{-(\nu d)/2} \det(\mathbf{V})^{-\nu/2} \Gamma_d(\nu/2)^{-1} \det(\mathbf{X})^{\frac{1}{2}(\nu-d-1)} e^{-\frac{1}{2}\text{tr}(\mathbf{V}^{-1}\mathbf{X})}$$

Thus,

$$-\log f_{\mathbf{X}}(t\mathbf{X}) = tg(\mathbf{X}) + (\log t)u_1(\mathbf{X}) + u_2(\mathbf{X})$$

where  $g(\mathbf{X}) = \frac{1}{2}\text{tr}(\mathbf{V}^{-1}\mathbf{X})$  is 1-homogeneous, and  $u_1(\mathbf{X}) = (-\frac{d}{2}(\nu - d - 1))$  and  $u_2(\mathbf{X}) = -\frac{1}{2}(\nu - d - 1) \log \det(\mathbf{X}) + \log (2^{-(\nu d)/2} \det(\mathbf{V})^{-\nu/2} \Gamma_d(\nu/2)^{-1})$  are higher-order terms.

## 4 Directional densities

### 4.1 Multivariate normal distribution, standard normal margins

The joint density can be written in the form  $f(\mathbf{x}) = f_0(g_{\mathcal{G}}(\mathbf{x}))$ , where  $f(s) = (2\pi)^{-d/2} |\mathbf{Q}|^{1/2} \exp\{-s^2/2\}$ . By (A.9),

$$\begin{aligned} f_{\mathbf{W}}(\mathbf{w}) &= g_{\mathcal{G}}(\mathbf{x})^{-d} \int_0^{\infty} s^{d-1} f_0(s) ds = (2\pi)^{-d/2} |\mathbf{Q}|^{1/2} (\mathbf{w}^{\top} \mathbf{Q} \mathbf{w})^{-d/2} \int_0^{\infty} s^{d-1} e^{-\frac{1}{2}s^2} ds \\ &= \Gamma(d/2) 2^{\frac{d}{2}-1} (2\pi)^{-d/2} |\mathbf{Q}|^{1/2} (\mathbf{w}^{\top} \mathbf{Q} \mathbf{w})^{-d/2} = \Gamma(d/2) 2^{-1} \pi^{-d/2} |\mathbf{Q}|^{1/2} (\mathbf{w}^{\top} \mathbf{Q} \mathbf{w})^{-d/2} \end{aligned}$$

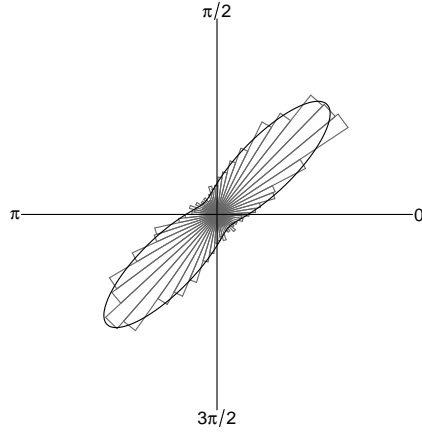


Figure 11: Directional density for the bivariate Gaussian distribution, standard Gaussian margins, with  $\mathbf{Q}_{11}^{-1} = \mathbf{Q}_{22}^{-1} = 1$ ,  $\mathbf{Q}_{12}^{-1} = \mathbf{Q}_{21}^{-1} = 0.8$ , plotted over an empirical sample

### 4.2 Multivariate Laplace distribution, standard Laplace margins

We have  $f_{[L]}(\mathbf{x}) = f_0(g_{\mathcal{G}}(\mathbf{x}))$ , where  $f_0(s) = |\mathbf{Q}|^{1/2} (2\pi)^{-d/2} s^v K_v(s)$ . By (A.9), the density of angles is

$$\begin{aligned} f_{\mathbf{W}}(\mathbf{w}) &= \int_0^{\infty} r^{d-1} f_0(r g_{\mathcal{G}}(\mathbf{w})) dr = g_{\mathcal{G}}(\mathbf{w})^{-d} \int_0^{\infty} s^{d-1} f_0(s) ds \\ &= |\mathbf{Q}|^{1/2} (2\pi)^{-d/2} (\mathbf{w}^{\top} \mathbf{Q} \mathbf{w})^{-d/2} \int_0^{\infty} s^{d+v-1} K_v(s) ds = \Gamma(d/2) 2^{\frac{d}{2}-1} (2\pi)^{-d/2} |\mathbf{Q}|^{1/2} (\mathbf{w}^{\top} \mathbf{Q} \mathbf{w})^{-d/2} \\ &= \Gamma(d/2) 2^{-1} \pi^{-d/2} |\mathbf{Q}|^{1/2} (\mathbf{w}^{\top} \mathbf{Q} \mathbf{w})^{-d/2} \end{aligned}$$

where the expression for the integral can be found in Sections 6.5–6.7 of [Gradshteyn & Ryzhik \(2014\)](#).

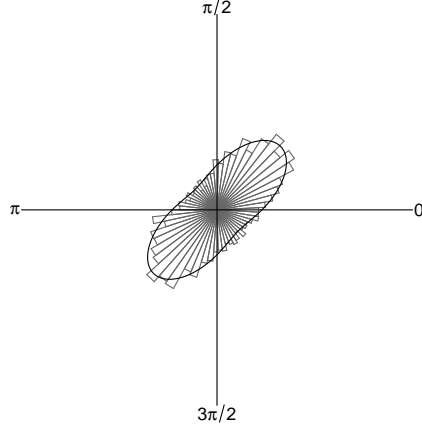


Figure 12: Directional density for the bivariate Laplace distribution, standard Laplace margins, with  $\mathbf{Q}_{11}^{-1} = \mathbf{Q}_{22}^{-1} = 1$ ,  $\mathbf{Q}_{12}^{-1} = \mathbf{Q}_{21}^{-1} = 0.5$ , plotted over an empirical sample

### 4.3 Multivariate Student $t_\nu$ distribution, Student $t_\nu$ margins, $\nu > 0$

We have  $f(\mathbf{x}) = f_0(g_{\mathcal{G}}(\mathbf{x}))$ , where  $f_0(s) = k_{\nu, \mathbf{Q}} (1 + \nu^{-1}s^2)^{-\frac{1}{2}(\nu+d)}$ . By (A.9), the density of angles is

$$\begin{aligned}
f_{\mathbf{W}}(\mathbf{w}) &= \int_0^\infty r^{d-1} f_0(r g_{\mathcal{G}}(\mathbf{w})) dr = g_{\mathcal{G}}(\mathbf{w})^{-d} \int_0^\infty s^{d-1} f_0(s) ds \\
&= k_{\nu, \mathbf{Q}} (\mathbf{w}^\top \mathbf{Q} \mathbf{w})^{-d/2} \int_0^\infty s^{d-1} (1 + \nu^{-1}s^2)^{-\frac{1}{2}(\nu+d)} ds \\
&= \Gamma\left(\frac{\nu+d}{2}\right) \Gamma\left(\frac{\nu}{2}\right)^{-1} \nu^{-d/2} \pi^{-d/2} |\mathbf{Q}|^{1/2} (\mathbf{w}^\top \mathbf{Q} \mathbf{w})^{-d/2} \nu^{-1+d/2} \Gamma\left(\frac{\nu+d}{2}\right)^{-1} \Gamma\left(\frac{\nu}{2}\right) \Gamma\left(1 + \frac{\nu}{2}\right) \\
&= \Gamma\left(\frac{d}{2}\right) 2^{-1/2} \pi^{-d/2} |\mathbf{Q}|^{1/2} (\mathbf{w}^\top \mathbf{Q} \mathbf{w})^{-d/2}
\end{aligned}$$

### 4.4 Multivariate max-stable distribution, standard Fréchet margins

For a general  $-1$ -homogeneous exponent function,

$$\begin{aligned}
f_{\mathbf{W}}(\mathbf{w}) &= \int_0^\infty r^{d-1} f(r\mathbf{w}) dr \\
&= \int_0^\infty r^{d-1} \left[ \sum_{\pi \in \Pi} (-1)^{|\pi|} \prod_{s \in \pi} V_s(r\mathbf{w}) \right] e^{-V(r\mathbf{w})} dr
\end{aligned}$$

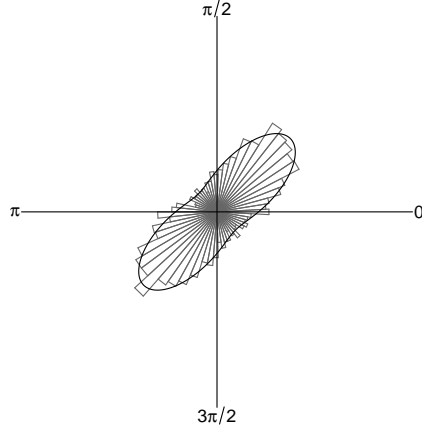


Figure 13: Directional density for the bivariate Student  $t_\nu$  distribution,  $t_\nu$  margins, with  $\nu = 5$  and  $Q_{11}^{-1} = Q_{22}^{-1} = 1$ ,  $Q_{12}^{-1} = Q_{21}^{-1} = 0.6$ , plotted over an empirical sample

$$\begin{aligned}
 &= \sum_{\pi \in \Pi} (-1)^{|\pi|} \left[ \prod_{s \in \pi} V_s(\mathbf{w}) \right] \int_0^\infty r^{d - \sum_{s \in \pi} (1 + |s|) - 1} e^{-r^{-1} V(\mathbf{w})} dr \\
 &= \sum_{\pi \in \Pi} (-1)^{|\pi|} \left[ \prod_{s \in \pi} V_s(\mathbf{w}) \right] \Gamma \left\{ \sum_{s \in \pi} (1 + |s|) - d \right\} V(\mathbf{w})^{\sum_{s \in \pi} (1 + |s|) - d}
 \end{aligned}$$

Suppose we fix  $d = 2$ , and we assume we have logistic dependence and Fréchet margins, then the exponent function is given by  $V(x, y) = (x^{-1/\theta} + y^{-1/\theta})^\theta$ , and the true directional density  $f_{\mathbf{W}}$  can be plotted against an empirical sample of angles (see Figure 14).

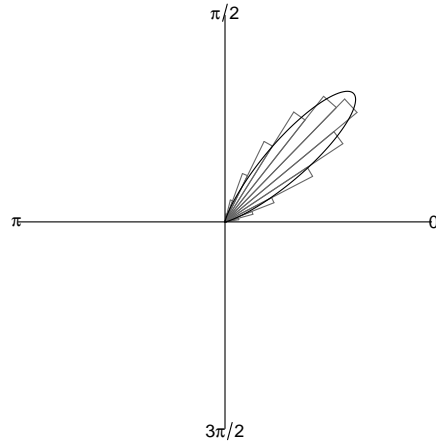


Figure 14: Directional density for the bivariate max-stable logistic distribution, standard Fréchet margins, with dependence parameter  $\theta = 0.3$ , plotted over an empirical sample

## 4.5 Multivariate inverted max-stable distributions, standard exponential margins

Recall, from subsection 3.4 that the first order gauge function for inverted max-stable distributions in exponential margins is given by the 1-homogeneous stable tail dependence function,  $g(\mathbf{x}) = \ell(\mathbf{x})$ . With this in mind, the density of angles in this setting is given by

$$\begin{aligned}
 f_{\mathbf{w}}(\mathbf{w}) &= \int_0^{\infty} r^{d-1} f(r\mathbf{w}) dr \\
 &= \int_0^{\infty} r^{d-1} \left[ \sum_{\pi \in \Pi} (-1)^{|\pi|} \prod_{s \in \pi} \ell_s(r\mathbf{w}) \right] e^{-\ell(r\mathbf{w})} dr \\
 &= \sum_{\pi \in \Pi} (-1)^{|\pi|} \left[ \prod_{s \in \pi} \ell_s(\mathbf{w}) \right] \int_0^{\infty} r^{d + \sum_{s \in \pi} (1-|s|) - 1} e^{-r\ell(\mathbf{w})} dr \\
 &= \sum_{\pi \in \Pi} (-1)^{|\pi|} \left[ \prod_{s \in \pi} \ell_s(\mathbf{w}) \right] \Gamma \left\{ d + \sum_{s \in \pi} (1 - |s|) \right\} \ell(\mathbf{w})^{d + \sum_{s \in \pi} (1-|s|)} \\
 &= \left[ \sum_{\pi \in \Pi} (-1)^{|\pi|} \left[ \prod_{s \in \pi} \ell_s(\mathbf{w}) \right] \Gamma \left\{ d + \sum_{s \in \pi} (1 - |s|) \right\} g(\mathbf{w})^{\sum_{s \in \pi} (1-|s|)} \right] g(\mathbf{w})^d,
 \end{aligned}$$

thus following the expression given in equation (36) from Section 2.6. Suppose we fix  $d = 2$ , and we assume we have logistic dependence and standard exponential margins, then the exponent function is given by  $\ell(x, y) = (x^{1/\theta} + y^{1/\theta})^\theta$ , and the true directional density  $f_{\mathbf{w}}$  can be plotted against an empirical sample of angles (see Figure 15).

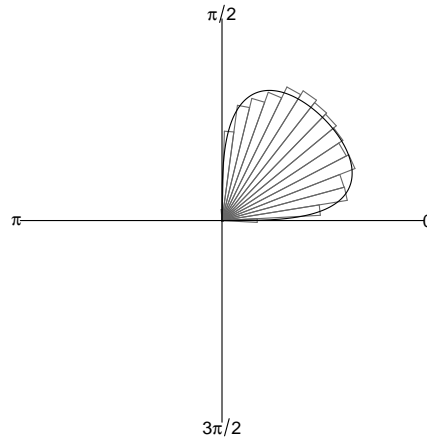


Figure 15: Directional density for the bivariate inverted max-stable logistic distribution, standard exponential margins, with dependence parameter  $\theta = 0.7$ , plotted over an empirical sample

## 4.6 Wishart distribution

The density of angles is computed using

$$f_{\mathbf{W}}(\mathbf{W}) = \int_0^\infty r^{d-1} f_{\mathbf{X}}(r\mathbf{W}) dr$$

$$= 2^{-(\nu d)/2} \det(\mathbf{V})^{-\nu/2} \Gamma_d(\nu/2)^{-1} \det(\mathbf{W})^{\frac{1}{2}(\nu-d-1)} \Gamma\left(\frac{d}{2}(1+\nu-d)\right) \left(\frac{1}{2}\text{tr}(\mathbf{V}^{-1}\mathbf{W})\right)^{-\frac{d}{2}(1+\nu-d)}$$

where in this setting, radii and angles are defined using a matrix norm;  $R = \|\mathbf{X}\|$ ,  $\mathbf{W} = \mathbf{X}/\|\mathbf{X}\|$ .

## 5 Statistical inference

### 5.1 Inference for latent variables

Given  $n$  independent observations  $\mathbf{y} := \{r_1\mathbf{w}_1, \dots, r_n\mathbf{w}_n\}$  from  $\mathbf{X} = R\mathbf{W} \in \mathbb{R}^d$ , the latent quantities of interest are the set  $\mathcal{G}$ , the quantile set  $\mathcal{Q}_q$  and the set  $\mathcal{L}$ . In what follows, we detail the procedure to obtain realisations from the joint posterior distribution of these quantities.

We model the logarithms of the random radial functions  $r_{\mathcal{Q}_q}$ ,  $r_{\mathcal{G}_q}$  and  $r_{\mathcal{L}}$  as Matérn (Gaussian) fields on  $\mathbb{S}^{d-1}$  using the stochastic partial differential equation (SPDE) approach by Lindgren et al. (2011), using  $\alpha = 2$  (see their Equation (2)) which is also the default option in the R-INLA package ([www.r-inla.org](http://www.r-inla.org)). We denote the respective random intercepts  $\beta_{\mathcal{Q}}, \beta_{\mathcal{G}}, \beta_{\mathcal{L}} \in \mathbb{R}$  as well as their stochastic weights in the finite element representation (Lindgren et al. 2011, Equation (9)) as  $\mathbf{z}_{\mathcal{Q}}, \mathbf{z}_{\mathcal{G}}, \mathbf{z}_{\mathcal{L}} \in \mathbb{R}^p$ . We denote by  $\boldsymbol{\theta} = (\beta_{\mathcal{Q}}, \mathbf{z}_{\mathcal{Q}}, \beta_{\mathcal{G}}, \mathbf{z}_{\mathcal{G}}, \beta_{\mathcal{L}}, \mathbf{z}_{\mathcal{L}}) \in \mathbb{R}^{3p+3}$  the set of all latent variables for our models, and it follows that the joint posterior distribution of  $\boldsymbol{\theta}$  fully determines that of  $\mathcal{Q}_q$ ,  $\mathcal{G}$  and  $\mathcal{L}$ . Due to the hierarchical structure of all proposed models detailed in Sections 3.2 and 3.3, the joint posterior density of  $\boldsymbol{\theta}$  factorises according to  $\pi[\boldsymbol{\theta} | \mathbf{y}] = \pi[\beta_{\mathcal{G}}, \mathbf{z}_{\mathcal{G}}, \beta_{\mathcal{L}}, \mathbf{z}_{\mathcal{L}} | \beta_{\mathcal{Q}}, \mathbf{z}_{\mathcal{Q}}, \mathbf{y}] \pi[\beta_{\mathcal{Q}}, \mathbf{z}_{\mathcal{Q}} | \mathbf{y}]$ . We first fit the Bayesian Gamma log-linear quantile regression model described in Section 3.2 for a fixed probability  $q$  to all observations  $\mathbf{y}$ . Samples  $\{(\beta_{\mathcal{Q},i}, \mathbf{z}_{\mathcal{Q},i}) : i = 1, \dots, n_{\mathcal{Q}}\}$  from the posterior density  $\pi[\beta_{\mathcal{Q}}, \mathbf{z}_{\mathcal{Q}} | \mathbf{y}]$  map to a set of radial functions  $\{r_{\mathcal{Q},i} : i = 1, \dots, n_{\mathcal{Q}}\}$  which are then interpreted as candidate radial functions of a  $q$ -th quantile set. Given a radial function  $r_{\mathcal{Q},i}$ , we define a set of exceedances through

$$\mathcal{Y}_i = \{(r_j, \mathbf{w}_j) \in (0, \infty) \times \mathbb{S}^{d-1} : r_j > r_{\mathcal{Q},i}(\mathbf{w}_j), r_j\mathbf{w}_j \in \mathbb{R}^d, j = 1, \dots, n\}. \quad (\text{A.37})$$

We then fit model M<sub>1</sub>, M<sub>2</sub>, or M<sub>3</sub> to each collection of exceedances  $\mathcal{Y}_i$ , as detailed in Section 3.3, and also possibly include angles from non-exceedance data in the likelihood. This procedure yields a conditional posterior density  $\pi[\beta_{\mathcal{G}}, \mathbf{z}_{\mathcal{G}}, \beta_{\mathcal{L}}, \mathbf{z}_{\mathcal{L}} | \beta_{\mathcal{Q},i}, \mathbf{z}_{\mathcal{Q},i}, \mathbf{y}]$  for each  $i = 1, \dots, n_{\mathcal{Q}}$ . Sampling  $n_{\mathcal{G}\mathcal{L}}$  realisations jointly from each  $\pi[\beta_{\mathcal{G}}, \mathbf{z}_{\mathcal{G}}, \beta_{\mathcal{L}}, \mathbf{z}_{\mathcal{L}} | \beta_{\mathcal{Q},i}, \mathbf{z}_{\mathcal{Q},i}, \mathbf{y}]$  provides an assembled sample of  $n_{\mathcal{Q}} \cdot n_{\mathcal{G}\mathcal{L}}$  realisations from the joint posterior distribution of  $\boldsymbol{\theta}$ ,

$$\{\boldsymbol{\theta}_{i,j} = (\beta_{\mathcal{Q},i}, \mathbf{z}_{\mathcal{Q},i}, \beta_{\mathcal{G},(i,j)}, \mathbf{z}_{\mathcal{G},(i,j)}, \beta_{\mathcal{L},(i,j)}, \mathbf{z}_{\mathcal{L},(i,j)}) \in \Theta : i = 1, \dots, n_{\mathcal{Q}}, j = 1, \dots, n_{\mathcal{G}\mathcal{L}}\}. \quad (\text{A.38})$$

For simplicity and without loss, we re-index the sample (A.38) from the posterior distribution of  $\boldsymbol{\theta}$  to  $\{\boldsymbol{\theta}_i : i = 1, \dots, n_{\boldsymbol{\theta}}\}$  with  $n_{\boldsymbol{\theta}} := n_{\mathcal{Q}} \cdot n_{\mathcal{G}\mathcal{L}}$  and use this notation in the next sections. We shall also refer to the sampled latent functions  $r_{\mathcal{Q}_q, i}$ ,  $r_{\mathcal{G}_q, i}$ , and  $r_{\mathcal{L}, i}$  constructed from  $\boldsymbol{\theta}_i$ .

Interval estimation for the latent fields  $r_{\mathcal{Q}_q}$ ,  $r_{\mathcal{G}_q}$ , and  $r_{\mathcal{L}}$  is accomplished via prediction intervals (see Bolin & Lindgren 2018). A  $(1 - \alpha)$  prediction-interval for the value of a random field  $Y : \Omega \rightarrow \mathbb{R}^{\mathbb{S}^{d-1}}$  at an angle  $\boldsymbol{w} \in \mathbb{S}^{d-1}$  is the closed line segment  $[q_{\alpha}(\boldsymbol{w})\boldsymbol{w} : q_{1-\alpha}(\boldsymbol{w})\boldsymbol{w}]$  where  $q_{\alpha}(\boldsymbol{w})$  is the  $\alpha$ -quantile of the distribution of  $Y(\boldsymbol{w})$ . A  $(1 - \alpha)$  prediction interval for the process  $Y$  defined on  $\mathbb{S}^{d-1}$  consists of the strip  $R_{1-\alpha} := \cup_{\boldsymbol{w} \in \mathbb{S}^{d-1}} R_{1-\alpha}(\boldsymbol{w})$  defined through  $R_{1-\alpha}(\boldsymbol{w}) := [q_{\rho}(\boldsymbol{w})\boldsymbol{w} : q_{1-\rho}(\boldsymbol{w})\boldsymbol{w}]$  for some  $\rho$  such that  $q_{\rho}(\boldsymbol{w})$  and  $q_{1-\rho}(\boldsymbol{w})$  satisfy

$$\mathbb{P}[q_{\rho}(\boldsymbol{w}) \leq Y(\boldsymbol{w}) \leq q_{1-\rho}(\boldsymbol{w}), \boldsymbol{w} \in \mathbb{S}^{d-1}] = 1 - \alpha.$$

In the context of our latent fields  $r_{\mathcal{Q}_q}$ ,  $r_{\mathcal{G}_1}$ , and  $r_{\mathcal{L}}$ ,  $(1 - \alpha)$  prediction intervals consist of sets withing within which the true functions lie entirely with probability  $1 - \alpha$ . Prediction intervals can be obtained from a sample from the posterior distribution of a parameter of interest using the `excursions` package in `{+1}`. (Bolin & Lindgren 2015, 2017).

## 5.2 Rare event probability estimation

Given  $n$  independent observations  $\boldsymbol{y} := \{r_1\boldsymbol{w}_1, \dots, r_n\boldsymbol{w}_n\}$  from  $\boldsymbol{X} = R\boldsymbol{W} \in \mathbb{R}^d$ , interest lies in the estimation of the probability that a new draw from  $R\boldsymbol{W}$  falls within some Borel set  $B \in \mathbb{R}^d \setminus \{\mathbf{0}\}$  far enough from the origin ( $\mathbf{0} \in \mathbb{R}^d$ ). We provide a statistical inference framework for  $\mathbb{P}_{B|\boldsymbol{y}} := \mathbb{P}[R\boldsymbol{W} \in B \mid \boldsymbol{y}]$ . In practice, common types of sets of interest are boxes  $\{\boldsymbol{x} \in \mathbb{R}^d : \boldsymbol{a} \leq \boldsymbol{x} \leq \boldsymbol{b}, \boldsymbol{a}, \boldsymbol{b} \in \mathbb{R}^d\}$  and sets of the form  $\{r\boldsymbol{w} : r > h(\boldsymbol{w}) > 0, r \in (0, \infty), \boldsymbol{w} \in \mathbb{S}^{d-1}\}$  for some positive function  $h$  defined on  $\mathbb{S}^{d-1}$ , both starshaped at  $\mathbf{0}$ . This is useful in our setting as it allows for an exact probability calculation with respect to our model specification for exceedances. Simple adaptations can be made to consider more complex sets.

For a set  $B \in \mathbb{R}^d \setminus \{\mathbf{0}\}$  starshaped at  $\mathbf{0}$ , define  $S_B := \{\boldsymbol{w} \in \mathbb{S}^{d-1} : r\boldsymbol{w} \in B, r \in (0, \infty)\} \subseteq \mathbb{S}^{d-1}$  and consider, for any  $\boldsymbol{w} \in S_B$ , the partition  $I_{\text{inf}}(\boldsymbol{w}) \cup I_B(\boldsymbol{w}) \cup I_{\text{sup}}(\boldsymbol{w})$  of  $(0, \infty)$ , where  $I_{\text{inf}}(\boldsymbol{w}) := (0, r_{B_{\text{inf}}}(\boldsymbol{w}))$ ,  $I_B(\boldsymbol{w}) := [r_{B_{\text{inf}}}(\boldsymbol{w}), r_B(\boldsymbol{w})]$ , and  $I_{\text{sup}}(\boldsymbol{w}) := (r_B(\boldsymbol{w}), \infty)$  for the radial function  $r_B(\boldsymbol{w})$  of  $B$  and the function  $r_{B_{\text{inf}}}(\boldsymbol{w}) = \inf\{r > 0 : r\boldsymbol{w} \in B\}$ . Then,

$$\mathbb{P}_{B|\boldsymbol{y}} = \mathbb{P}[R \in I_B(\boldsymbol{W}), \boldsymbol{W} \in S_B \mid \boldsymbol{y}], \quad (\text{A.39})$$

The posterior predictive distribution in (A.39) is given from the posterior density of  $\boldsymbol{\theta}$  via

$$\mathbb{P}_{B|\boldsymbol{y}} = \int_{\mathbb{R}^{3p+3}} \mathbb{P}[R \in I_B(\boldsymbol{W}), \boldsymbol{W} \in S_B \mid \boldsymbol{\theta}] \pi[\boldsymbol{\theta} \mid \boldsymbol{y}] d\boldsymbol{\theta}, \quad (\text{A.40})$$

where  $\pi[\boldsymbol{\theta} \mid \boldsymbol{y}]$  is obtained following the procedure described in Section 5.1. Since  $\mathcal{Q}_q$  is a latent variable,  $r_{\mathcal{Q}_q}(\boldsymbol{w})$  intersects with  $I_{\text{inf}}(\boldsymbol{w})$ ,  $I_B(\boldsymbol{w})$ , or  $I_{\text{sup}}(\boldsymbol{w})$  with non-zero probability for all  $\boldsymbol{w} \in S_B$ .

Hence, from total probability,  $\mathbb{P}_{B|\boldsymbol{\theta}} := \mathbb{P}[R \in I_B(\mathbf{W}), \mathbf{W} \in S_B | \boldsymbol{\theta}]$  of (A.40) satisfies

$$\mathbb{P}_{B|\boldsymbol{\theta}} = \mathbb{P}[R\mathbf{W} \in B, R > r_{\mathcal{Q}_q}(\mathbf{W}) | \boldsymbol{\theta}] + \mathbb{P}[R\mathbf{W} \in B, R \leq r_{\mathcal{Q}_q}(\mathbf{W}) | \boldsymbol{\theta}], \quad (\text{A.41})$$

and our model is best suited for sets  $B$  such that the second term in the equation (A.41) is small. The first term in equation (A.41) decomposes into

$$\begin{aligned} \mathbb{P}[R\mathbf{W} \in B, R > r_{\mathcal{Q}_q}(\mathbf{W}) | \boldsymbol{\theta}] &= \mathbb{P}[R \in I_B(\mathbf{W}) | \mathbf{W} \in S_B, R > r_{\mathcal{Q}_q}(\mathbf{W}), \boldsymbol{\theta}] \times \\ &\times \mathbb{P}[\mathbf{W} \in S_B | R > r_{\mathcal{Q}_q}(\mathbf{W}), \boldsymbol{\theta}] \mathbb{P}[R > r_{\mathcal{Q}_q}(\mathbf{W}) | \boldsymbol{\theta}]. \end{aligned} \quad (\text{A.42})$$

By the assumptions detailed in Section 3.2, the last term  $\mathbb{P}[R > r_{\mathcal{Q}_q}(\mathbf{W}) | \boldsymbol{\theta}]$  in equation (A.42) equals  $1 - q$  for all  $\boldsymbol{\theta} \sim \pi[\boldsymbol{\theta} | \mathbf{y}]$ . Following our model formulation for  $\mathbf{W}$ , the second term in equation (A.42) corresponds to the predictive distribution of the angles given  $\boldsymbol{\theta}$  and is given by

$$\mathbb{P}[\mathbf{W} \in S_B | R > r_{\mathcal{Q}_q}(\mathbf{W}), \boldsymbol{\theta}] = \int_{S_B} \tilde{f}_{\mathbf{W}|\boldsymbol{\theta}}(\mathbf{w} | \boldsymbol{\theta}) d\mathbf{w} \Big/ \int_{\mathbb{S}^{d-1}} \tilde{f}_{\mathbf{W}|\boldsymbol{\theta}}(\mathbf{w} | \boldsymbol{\theta}) d\mathbf{w}, \quad (\text{A.43})$$

where  $\tilde{f}_{\mathbf{W}}$  is chosen from  $M_1, M_2$ , or  $M_3$  (see Section 2.6). The integrals in (A.43) are computed efficiently via numerical integration for  $d = 2$  or  $3$ . The first term in (A.42) is obtained through

$$\mathbb{P}[R \in I_B(\mathbf{W}) | \mathbf{W} \in S_B, R > r_{\mathcal{Q}_q}(\mathbf{W}), \boldsymbol{\theta}] = \mathbb{E}_{\mathbf{W}|\mathbf{W} \in S_B, \mathbf{y}}(\mathbb{P}[R \in I_B(\mathbf{W}) | R > r_{\mathcal{Q}_q}(\mathbf{W}), \boldsymbol{\theta}]), \quad (\text{A.44})$$

where  $\mathbb{P}[R \in I_B(\mathbf{w}) | \mathbf{W} = \mathbf{w}, R > r_{\mathcal{Q}_q}(\mathbf{w}), \boldsymbol{\theta}]$ , needed for the expectation calculation in equation (A.44), equals

$$F_{R_E|\mathbf{W}} \left[ \frac{\max \{r_B(\mathbf{w}), r_{\mathcal{Q}_q}(\mathbf{w})\} - r_{\mathcal{Q}_q}(\mathbf{w})}{r_{\mathcal{G}_q}(\mathbf{w})} \Big| \mathbf{w} \right] - F_{R_E|\mathbf{W}} \left[ \frac{\max \{r_{B_{\text{inf}}}(\mathbf{w}), r_{\mathcal{Q}_q}(\mathbf{w})\} - r_{\mathcal{Q}_q}(\mathbf{w})}{r_{\mathcal{G}_q}(\mathbf{w})} \Big| \mathbf{w} \right], \quad (\text{A.45})$$

with  $F_{R_E|\mathbf{W}}(z | \mathbf{w}) = 1 - [1 + \xi(\mathbf{w})z]_+^{-1/\xi(\mathbf{w})}$ . We approximate expectation (A.44) through Monte-Carlo integration by sampling angles  $\{\tilde{\mathbf{w}}_1, \dots, \tilde{\mathbf{w}}_{n_w}\}$  from  $f_{\mathbf{W}}$  restricted to the set  $S_B$  via

$$n_w^{-1} \sum_{i=1}^{n_w} \mathbb{P}[R \in I_B(\tilde{\mathbf{w}}_i) | R > r_{\mathcal{Q}_q}(\tilde{\mathbf{w}}_i), \boldsymbol{\theta}] \rightarrow \mathbb{P}[R \in I_B(\mathbf{W}) | \mathbf{W} \in S_B, R > r_{\mathcal{Q}_q}(\mathbf{W}), \boldsymbol{\theta}], \quad (\text{A.46})$$

as  $n_w \rightarrow \infty$ . The second term in equation (A.41),  $\mathbb{P}[R\mathbf{W} \in B, R \leq r_{\mathcal{Q}_q}(\mathbf{W}) | \boldsymbol{\theta}] =: p$ , corresponds to a probability over a region in which our model is not specified. We hence consider it as the success probability of the binomial random variable describing the number of observations falling in the set  $\mathcal{Q}_q \cap B$ . For each  $i \in \{1, \dots, n_{\boldsymbol{\theta}}\}$ , we impose a binomial likelihood and beta prior for the parameter  $p$ , leading to a closed form beta posterior distribution. When  $\mathcal{Q}_q \cap B \neq \emptyset$ , we sample a probability from the posterior distribution of  $p$  and add it accordingly in equation (A.41).

In practice, inference for  $\mathbb{P}_{B|\mathbf{y}}$  is performed by first collecting a sample  $\{\boldsymbol{\theta}_1, \dots, \boldsymbol{\theta}_{n_{\boldsymbol{\theta}}}\}$  from  $\pi[\boldsymbol{\theta} | \mathbf{y}]$  through the procedure described in Section 5.1, and then calculating  $\mathbb{P}_{B|\boldsymbol{\theta}_i}$  for each

$i \in \{1, \dots, n_\theta\}$ . A *posteriori* mean estimates corresponding to the Monte-Carlo integration

$$n_\theta^{-1} \sum_{i=1}^{n_\theta} \mathbb{P}_{B|\theta_i} \rightarrow \mathbb{P}_{B|\mathbf{y}}, \quad \text{as } n_\theta \rightarrow \infty, \quad (\text{A.47})$$

approximating equation (A.40). Equal-tailed credible intervals from the sample  $\{\mathbb{P}_{B|\theta_i} : i = 1, \dots, n_\theta\}$  hence complete the inference procedure for  $\mathbb{P}_{B|\mathbf{y}}$ .

### 5.3 Model selection and validation

Our model formulation gives rise to various modelling choices needing to be assessed and validated. For instance, as discussed in Section 3.3, selecting the most appropriate model within the set of candidate models  $M_1$ ,  $M_2$ , and  $M_3$  given observed data amounts to analysing the properties of the distribution of  $R, \mathbf{W} \mid R > r_{\mathcal{Q}_q}(\mathbf{W})$  with respect to the association between  $g_{\mathcal{G}}$  and  $f_{\mathbf{W}}$ . Another modelling choice requiring assessment is that of the set of angles contributing to likelihood (51) since it translates into a bias-variance trade-off for  $\mathcal{G}$  and  $\mathcal{L}$ . Further, hyper-parameters values imposed on the prior distributions of  $\mathcal{Q}_q$ ,  $\mathcal{G}$ , and  $\mathcal{L}$  imply *a priori* information on the differentiability properties of their boundaries (see Section 5.1), and their impact on the posterior may need assessment. Finally, the usual concern of the sensitivity of the posterior distribution of the latent variables to the return period for the latent threshold function  $r_{\mathcal{Q}_q}$  (Section 3.2) remains. We detail possible methods for model selection and validation below.

The nested structure of model  $M_2$  within the parameter space of model  $M_3$  raises the question of whether model  $M_2$  can serve as a sensible simplification of model  $M_3$  given observed data  $\mathbf{y} = \{r_1 \mathbf{w}_1, \dots, r_n \mathbf{w}_n\}$ . As discussed in Section 3.3, evidence for a constant  $r_B$  in model  $M_3$  points to evidence that  $M_2$  can serve as an sensible simplification of  $M_3$ , or equivalently that the observed data  $\mathbf{y}$  may come from a process following a homothetic density with respect to its gauge function  $g_{\mathcal{G}}$ . Given a sample of random functions  $\{\psi(\mathbf{w})^\top \mathbf{z}_{B,i} : i = 1, \dots, n_\theta\}$  from the posterior distribution of the latent random field  $\psi(\mathbf{w})^\top \mathbf{z}_B$ , we obtain a 0.95 prediction interval,  $R_{0.95}$ , for  $\psi(\mathbf{W})^\top \mathbf{z}_B$  through the procedure described in Section 5.1. We say there is evidence against a homothetic underlying density whenever there is some non-empty subset  $S_0 \subset \mathbb{S}^{d-1}$  such that  $0 \notin R_{0.95}(\mathbf{w})$  for  $\mathbf{w} \in S_0$ .

The sensitivity of the posterior distributions of the latent parameters to the remaining modelling choices discussed in the beginning of this section can be assessed through the quality of the calibration of the posterior predictive distribution to the observed data. Given a set of observed exceedances  $\mathcal{Y}_i$  of a sampled latent function  $r_{\mathcal{Q}_q,i}$  (see expression (A.37)), we wish to assess the calibration of the predictive distribution for the excess variable  $R - r_{\mathcal{Q}_q,i}(\mathbf{W}) \mid R > r_{\mathcal{Q}_q,i}(\mathbf{W})$ . We thus compare each observed excess  $r_j - r_{\mathcal{Q}_q,i}(\mathbf{w}_j)$  with the quantile of the Exponential( $r_{\mathcal{G}_q}(\mathbf{w}_j)$ ), with  $\log r_{\mathcal{G}_q}(\mathbf{w}) = \beta_{\mathcal{G}} + \psi(\mathbf{w})^\top \mathbf{z}_{\mathcal{G}}$  and  $(\beta_{\mathcal{G}}, \mathbf{z}_{\mathcal{G}}) \sim \pi[\beta_{\mathcal{G}}, \mathbf{z}_{\mathcal{G}} \mid \beta_{\mathcal{Q}_q,i}, \mathbf{z}_{\mathcal{Q}_q,i}, \mathbf{y}]$ . We draw exceedance radii  $\{\tilde{r}_1, \dots, \tilde{r}_{n_s}\}$  from their predictive distribution  $\text{Exp}(r_{\mathcal{G}_q}(\mathbf{w}_j))$ , and define the empirical distribution function  $F_{\mathbf{w}_j, n_s}(r) := n_s^{-1} \sum_{k=1}^{n_s} \mathbb{1}[\tilde{r}_k \leq r]$ , for  $r \in (0, \infty)$ . A probability-probability (PP) plot for

the exceedances  $\mathcal{Y}_i$  is then given by

$$\left\{ \left( \frac{j}{|\mathcal{Y}_i| + 1}, p_{(j)} \right) : j = 1, \dots, |\mathcal{Y}_i| \right\}, \quad (\text{A.48})$$

where  $p_{(j)}$  denotes the  $j$ -th order statistic of the sample  $\{F_{\mathbf{w}_j, n_s}(r_j - r_{\mathcal{Q}, i}(\mathbf{w}_j)) : j = 1, \dots, |\mathcal{Y}_i|\}$ . A quantile-quantile (QQ) plot in unit exponential margins for the exceedances  $\mathcal{Y}_i$  is then easily obtained via probability-probability (PP) plot for the exceedances  $\mathcal{Y}_i$  via

$$\left\{ \left( -\log \left( 1 - \frac{j}{|\mathcal{Y}_i| + 1} \right), -\log (1 - p_{(j)}) \right) : j = 1, \dots, |\mathcal{Y}_i| \right\}. \quad (\text{A.49})$$

In a similar fashion, we can obtain PP plots for the predictive distribution of  $\mathbf{W} \mid R > r_{\mathcal{Q}, i}(\mathbf{W})$ . This is achieved by sampling angles  $\{\tilde{\mathbf{w}}_1, \dots, \tilde{\mathbf{w}}_{n_s}\}$  from the predictive density  $f_{\mathbf{W} \mid \beta_{\mathcal{G}}, \mathbf{z}_{\mathcal{G}}, \beta_{\mathcal{B}}, \mathbf{z}_{\mathcal{B}}, \mathbf{y}}$  where  $(\beta_{\mathcal{G}}, \mathbf{z}_{\mathcal{G}}, \beta_{\mathcal{B}}, \mathbf{z}_{\mathcal{B}}) \sim \pi[\beta_{\mathcal{G}}, \mathbf{z}_{\mathcal{G}}, \beta_{\mathcal{B}}, \mathbf{z}_{\mathcal{B}} \mid \beta_{\mathcal{Q}, i}, \mathbf{z}_{\mathcal{Q}, i}, \mathbf{y}]$ . We transform the sampled angles and the observed angles from  $\mathcal{Y}$  to spherical coordinates, respectively denoted  $\{\tilde{\boldsymbol{\varphi}}_j = (\tilde{\varphi}_{1,j}, \dots, \tilde{\varphi}_{d-1,j}) \in \Phi : j = 1, \dots, n_s\}$  and  $\{\boldsymbol{\varphi}_j = (\varphi_{1,j}, \dots, \varphi_{d-1,j}) \in \Phi : j = 1, \dots, |\mathcal{Y}_i|\}$ , and consider the empirical distribution function  $F_{n_s}(\boldsymbol{\varphi}) := n_s^{-1} \sum_{k=1}^{n_s} \mathbb{1}[\tilde{\boldsymbol{\varphi}}_k \leq \boldsymbol{\varphi}]$ . A PP plot for the calibration of the predictive distribution of angles to the observed angles in  $\mathcal{Y}_i$  is then given by expression (A.48) with  $p_{(j)}$  denoting the  $j$ -th order statistic of the sample  $\{F_{n_s}(\boldsymbol{\varphi}_j) : j = 1, \dots, |\mathcal{Y}_i|\}$ .

## 6 Simulation study

### 6.1 Setting

We here describe the setting of a simulation study performed using samples from classical parametric bivariate copulas. We provide a brief summary of the properties of these distributions.

A random variable  $\mathbf{X}_L$  is said to follow a bivariate Laplace distribution with precision matrix  $\mathbf{Q} = \Sigma^{-1}$  for a positive definite covariance  $\Sigma$ —with unit diagonal terms and a correlation value  $\rho \in [-1, 1]$  on the remaining off-diagonal terms. The parameter  $\rho$  hence fully determines a member of the family of the bivariate normal distribution as well as its extremal properties and in the subsequent sections, we use  $\rho = 0.5$ .

A random vector  $\mathbf{X} \in \mathbb{R}^2$  has a bivariate normal distribution with Laplace marginal distributions and precision matrix  $\mathbf{Q} = \Sigma^{-1}$  for a positive definite covariance  $\Sigma$ —with unit diagonal terms and a correlation value  $\rho \in [-1, 1]$  on the remaining off-diagonal terms. In what follows, we use the bivariate normal distribution as an instance of asymptotically independent distribution and draw samples using the value  $\rho = 0.8$ .

A random vector  $\mathbf{X} \in \mathbb{R}^2$  has a bivariate max-stable logistic distribution with Laplace margins parametrised by an exponent function  $V(x_1, \dots, x_d) = \left(\sum_{j=1}^d x_j^{-1/\theta}\right)^\theta$  where the dependence parameter  $\theta \in (0, 1]$ . The max-stable logistic distribution belongs the class of asymptotic dependent distributions provided  $\theta \neq 1$ . For any  $\theta \in (0, 1)$ ,  $\alpha_{|i} = 1$  and  $\eta = 1$ . We carry the simulation study using  $\theta = 0.3$ . Table 1 presents, for each family of distributions, the values of extremal coefficients associated with fixed parameters.

Extremal coefficient	Laplace	Normal	Max-stable logistic
$\alpha_{ i}$	$\rho = 0.5$	$\rho^2 = 0.64$	1
$\eta$	$\sqrt{(1 - \rho^2)/(2 - 2\rho)} \approx 0.866$	$(1 + \rho)/2 = 0.9$	1

Table 1: Values of the extremal coefficients  $\alpha_{|i}$  and  $\eta$  for the bivariate Laplace, normal, and max-stable logistic distributions with specified parameters.

### 6.2 Posterior distribution of latent variables

We perform a simulation study to obtain realisations from the posterior distribution of the latent sets  $\mathcal{Q}_q$ ,  $\mathcal{L}$ , and  $\mathcal{G}$ , as well as from the posterior predictive distribution of  $R$  and  $\mathbf{W}$ . We centre the simulation study on the bivariate Laplace, normal, and max-stable logistic families of distributions. The bivariate Laplace distribution is chosen for the homothetic structure of its density with respect to its gauge function  $g_{\mathcal{G}}$ , implying that its marginal density of the angles is exactly that assumed by model  $M_2$ . The bivariate max-stable logistic and normal distributions are chosen respectively for their asymptotic dependence and independence properties. From each of these distributions, we generate 100 samples of size  $n_1 = 1000$  and 100 samples of size  $n_2 = 10000$ , resulting in six cases (600 samples) with which we carry our analyses.

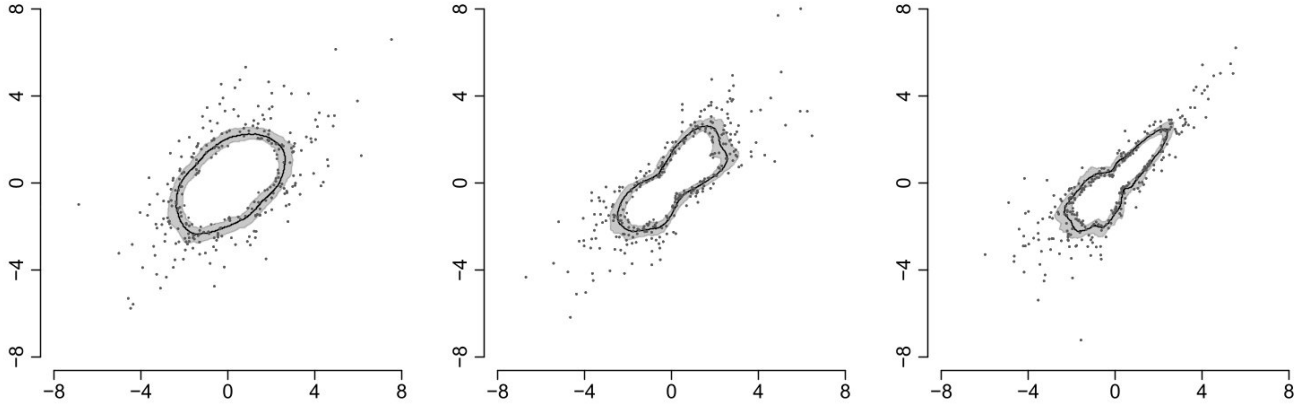


Figure 16: Angle-wise posterior mean and 0.95 prediction intervals for 100 samples from the posterior distribution of  $r_{Q_{0.8}}$  obtained from  $n_1$  draws from a bivariate Laplace (left), normal (centre), max-stable logistic (right) distributions in Laplace margins. Points correspond to exceedances of at least one sampled posterior  $r_{Q_{0.8}}$ .

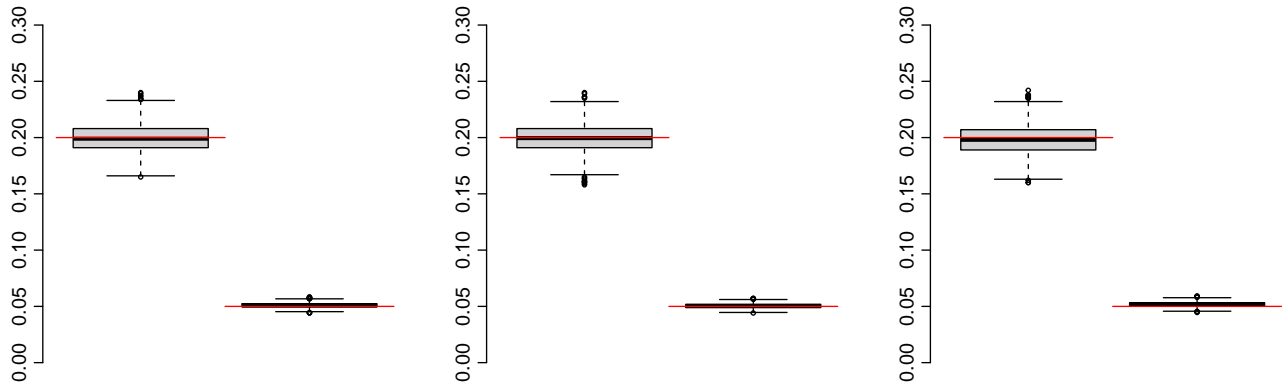


Figure 17: Boxplots of the proportion of data assigned as exceedances by each realisation from the posterior distribution of  $r_{Q_q}$  for  $n$  draws from the bivariate Laplace (left), normal (centre), max-stable logistic (right) distributions in Laplace margins. Within panels:  $n_1$ ,  $1 - q_1 = 0.2$  (left),  $n_2$ ,  $1 - q_2 = 0.05$  (right). Red segments: values of  $1 - q_k$  used in the fitting procedure.

Following the posterior sampling procedure described in Section 5.1, we first fit a bayesian Gamma quantile regression to each of the 600 samples described above using  $q_1 = 0.8$  for each sample of size  $n_1$  and  $q_2 = 0.98$  for each samples of size  $n_2$ . Here,  $q_1$  and  $q_2$  are chosen such that the expected number of exceedances of  $\mathcal{Q}_{q_k}$ ,  $n_k \cdot \mathbb{P}[R\mathbf{W} \in \mathcal{Q}'_{q_k} \mid \mathbf{y}]$ , equals 200 for  $k = \{1, 2\}$ . Again for each sample, we obtain 20 realisations  $\{r_{\mathcal{Q}_{q_k,i}} : i = 1, \dots, 20\}$  from the posterior distribution of  $r_{\mathcal{Q}_{q_k}}$  and define 20 sets of exceedances accordingly. Figure 16 displays the angle-wise posterior mean and 0.95 prediction intervals for  $r_{\mathcal{Q}_{0.8}}$  resulting from fitting quantile regressions to one sample of  $n_1$  draws from each of the three distributions of interest. Figure 16 also displays the data points defined as exceedances for at least one realisation from the posterior distribution of  $r_{\mathcal{Q}_{0.8}}$ . A brief assessment of the performance of the quantile regression is made through Figure 17, which consists of boxplots of the number of exceedances of each realisation from the posterior distribution of  $r_{\mathcal{Q}_{q_k}}$  for each of the 600 samples described above grouped by family of distributions and sample size.

Given the satisfying properties of the posterior distribution of  $r_{\mathcal{Q}_{q_k}}$ , we proceed with the investigation of the joint model for  $R$  and  $\mathbf{W}$ . Following the procedure described in Section 5.1, we obtain realisations from the posterior distributions of  $r_{\mathcal{G}}$  and  $r_{\mathcal{L}}$ —say  $\{r_{\mathcal{G}_i} : i = 1, \dots, n_{\theta}\}$  and  $\{r_{\mathcal{L}_i} : i = 1, \dots, n_{\theta}\}$  for  $n_{\theta} = n_{\mathcal{Q}}n_{\mathcal{G}\mathcal{L}} = 20 \cdot 50$ —using each model  $M_1$ ,  $M_2$ , and  $M_3$  on each sample described above. Due to expression (29), we consider the two cases of including only the angles of exceedances of the sampled quantile sets  $\mathcal{Q}_{q_k,i}$  and including all observed angles  $(\mathbf{w}_1, \dots, \mathbf{w}_n)$  in the model likelihood. Figure 18 provides a comparison of the posterior predictive density of angles  $\pi[\mathbf{W} \mid \mathcal{G}, \mathcal{L}, \mathbf{y}]$  output by models  $M_1$ ,  $M_2$ , and  $M_3$  fitted on samples of sizes  $n_1$  and  $n_2$  from a multivariate Laplace distribution in Laplace margins. As discussed in Section 2.6, the marginal density of angles for the multivariate Laplace distribution is known exactly given the homothetic structure of its density with respect to its gauge function  $g_{\mathcal{G}}$ . This allows for validation of the performance of  $M_1$ ,  $M_2$ , and  $M_3$ . It is clear from Figure 18 that all three models recover the true or the empirical marginal density of angles of the multivariate Laplace distribution well. As expected, including all angles in the fitting procedure and increasing the sample size both lead to reduction in the uncertainty of the posterior predictive density  $\pi[\mathbf{W} \mid \mathcal{G}, \mathcal{L}, \mathbf{y}]$ .

The max-stable logistic distribution is an instance of family of distributions for which  $M_2$  is known to be a wrong model for the marginal density of the angles. However, it is observed from Figure 19—which displays the mean of the posterior predictive density  $\pi[\mathbf{W} \mid \mathcal{G}, \mathcal{L}, \mathbf{y}]$  as well as its 0.95 prediction interval—that all three models possess the ability to capture the empirical distribution of angles when incorporating all sampled angles in the model likelihood. Figure 20 depicts some consequences of this. When the number of data used to fit  $\pi[\mathbf{W} \mid \mathcal{G}, \mathcal{L}, \mathbf{y}]$  is greater than the number of exceedances of  $\mathcal{Q}_{q_k}$ , the posterior distribution of the gauge function  $g_{\mathcal{G}}$  obtained from  $M_2$  is allowed to over-fit to the directional component of the model. This generates bias and over-confidence in the posterior distribution of the gauge function  $g_{\mathcal{G}}$  and of its associated limit boundary  $\partial\mathcal{G}$ . Under  $M_1$ , the decoupling of the dependence of the density of angles  $\pi[\mathbf{W} \mid \mathcal{G}, \mathcal{L}, \mathbf{y}]$  on the gauge function  $g_{\mathcal{G}}$  (so that  $\pi[\mathbf{W} \mid \mathcal{G}, \mathcal{L}, \mathbf{y}] = \pi[\mathbf{W} \mid \mathbf{y}]$ ) is expected to remove potential bias in  $g_{\mathcal{G}}$  coming from the observed angles. A clear consequence, however, is the increase in the variance of the posterior distribution of  $g_{\mathcal{G}}$ .

Figure 21 provides, for each of the modelling choices detailed in the beginning of this Section,

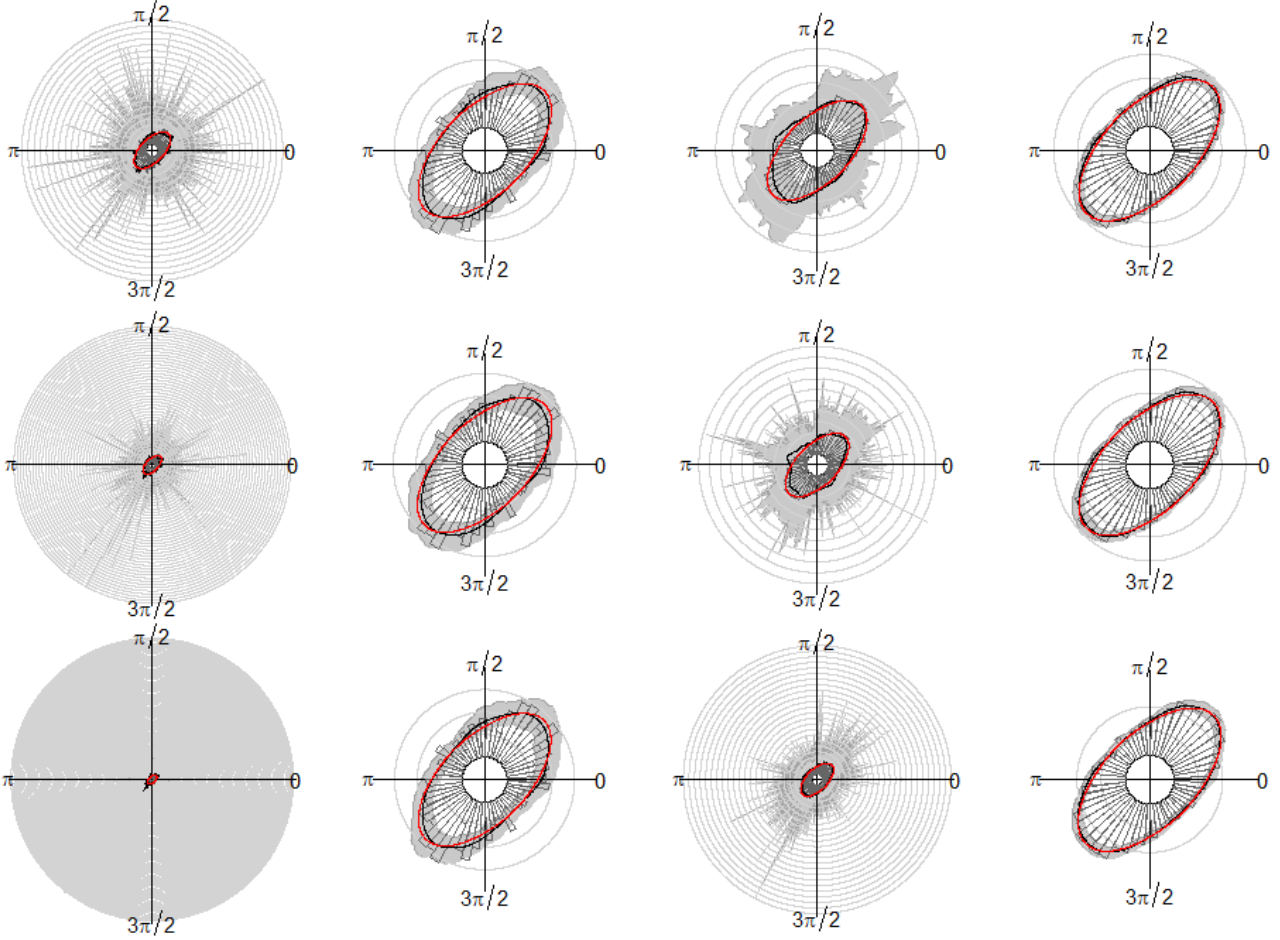


Figure 18: Histogram of the angles  $\{\varphi_j \in [0, 2\pi] : \mathbf{w}_j = (\cos \varphi_j, \sin \varphi_j), j = 1, \dots, n_k\}$  from a sample of  $n$  observations from a bivariate Laplace distribution with angle-wise posterior mean of  $\pi[\mathbf{W} \mid \mathcal{G}, \mathcal{L}, \mathbf{y}]$  (black line), 0.95 prediction interval for  $\pi[\mathbf{W} \mid \mathcal{G}, \mathcal{L}, \mathbf{y}]$  (grey band) output from model  $\mathcal{M}_i$ , and the true density  $f_{\mathbf{W}}$  for the bivariate Laplace (red line). Rows from top to bottom:  $\mathcal{M}_1$ ,  $\mathcal{M}_2$ , and  $\mathcal{M}_3$ . First column:  $\pi[\mathbf{W} \mid \mathcal{G}, \mathcal{L}, \mathbf{y}]$  fitted using exceedances of  $\mathcal{Q}_{0.8}$  only (sample size  $n_1$ ). Second column:  $\pi[\mathbf{W} \mid \mathcal{G}, \mathcal{L}, \mathbf{y}]$  fitted using all sampled angles (sample size  $n_1$ ). Third column:  $\pi[\mathbf{W} \mid \mathcal{G}, \mathcal{L}, \mathbf{y}]$  fitted using exceedances of  $\mathcal{Q}_{0.98}$  only (sample size  $n_2$ ). Fourth column:  $\pi[\mathbf{W} \mid \mathcal{G}, \mathcal{L}, \mathbf{y}]$  fitted using all sampled angles (sample size  $n_2$ ).

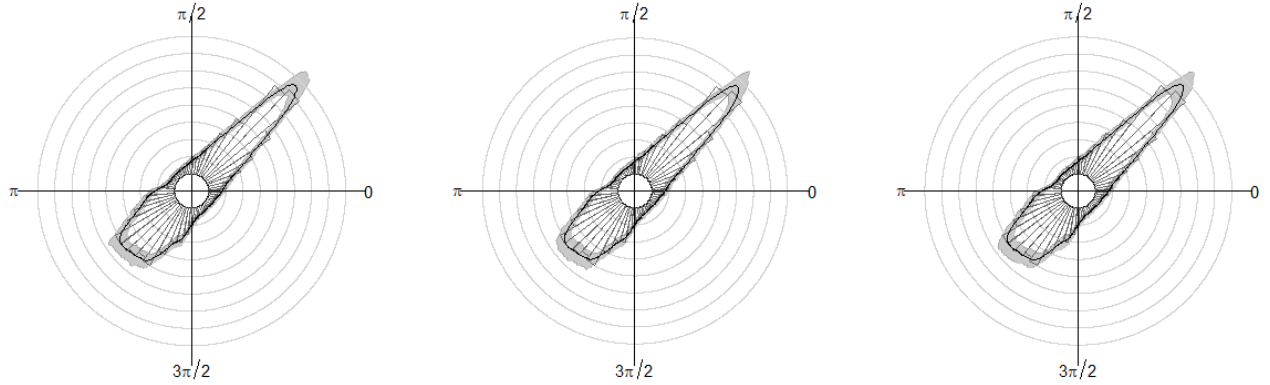


Figure 19: Histogram of the angles  $\{\varphi_j \in [0, 2\pi] : \mathbf{w}_j = (\cos \varphi_j, \sin \varphi_j), j = 1, \dots, n_2\}$  of  $n_2$  draws from a bivariate max-stable logistic distribution, with angle-wise posterior mean (black line) and 0.95 prediction intervals (grey) for the marginal distribution of angles  $\pi[\mathbf{W} \mid \mathcal{G}, \mathcal{L}, \mathbf{y}]$ . From left to right: outputs of  $M_1$ ,  $M_2$ , and  $M_3$ .

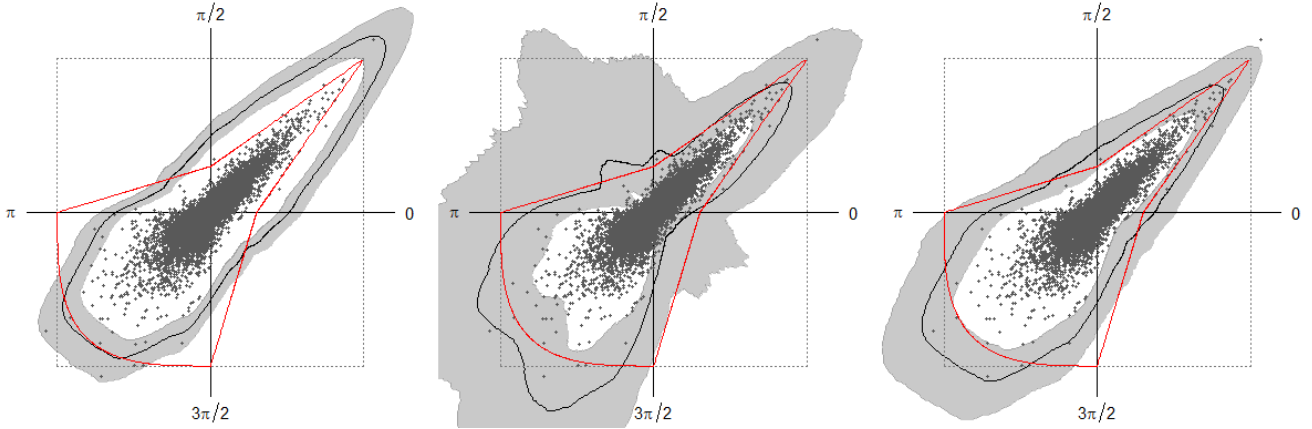


Figure 20: Estimated limit sets from  $n_2$  draws from a scaled bivariate max-stable logistic distribution, with posterior mean (black line), 0.95 prediction interval (grey), and true limit set (red line). From left to right: outputs of  $M_1$ ,  $M_2$ , and  $M_3$ .

a boxplot of the mean of the mean integrated square distance (MISD) from each realisation of the posterior of  $\partial\mathcal{G}$ . Model  $M_3$ , in all cases, seems to be the best—or approximately as valid as the best—model in terms of MISD. Figure 22 presents the angle-wise mean of the posterior distribution

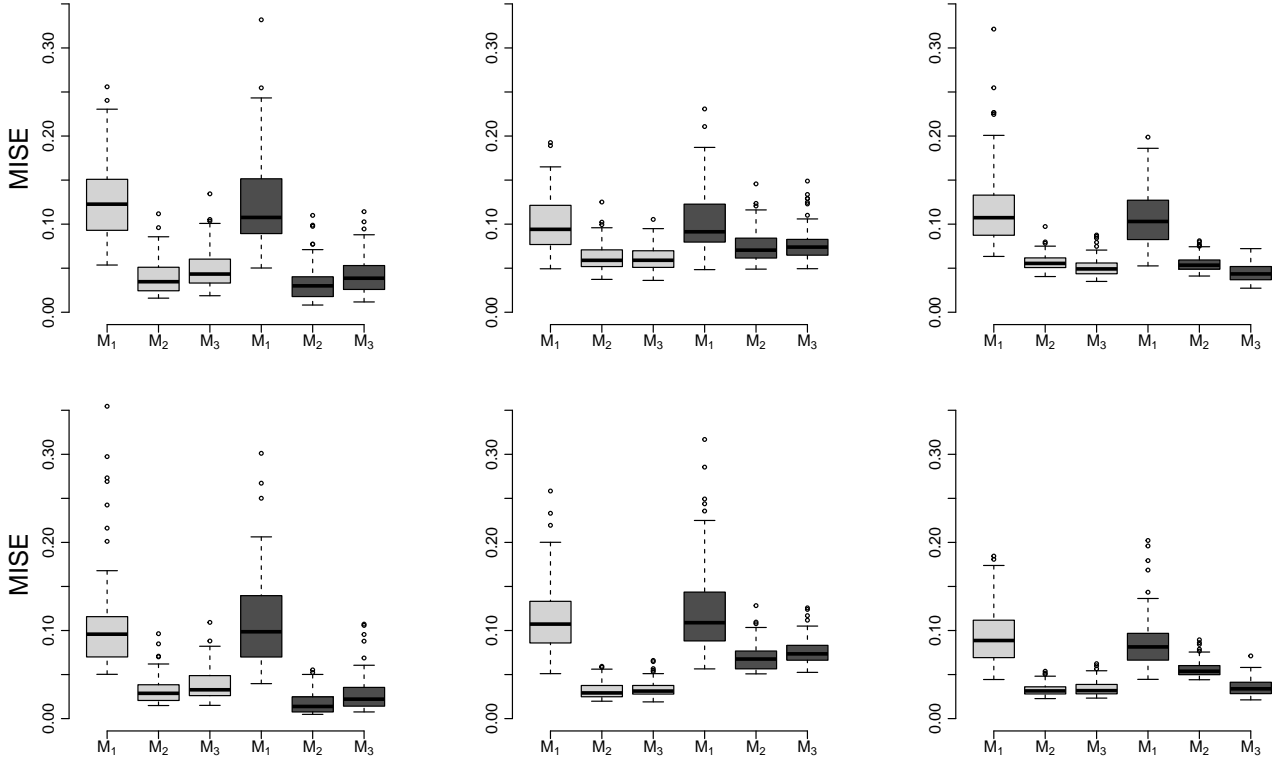


Figure 21: Boxplots of the means of the mean integrated squared error (MISE) from each posterior realisations of  $\partial\mathcal{G}$  from each of the 600 samples to the true limit sets. From top to bottom rows:  $n_1$ ,  $n_2$ . From left to right columns: Bivariate Laplace, normal, and max-stable logistic distributions. Within panels: Results for models  $M_1$ ,  $M_2$ , and  $M_3$  using only angles of exceedances (light grey) and using all angles (dark grey).

of the limit boundaries  $\partial\mathcal{G}$  estimated from  $M_3$  with the associated 0.95 prediction interval. As expected, increasing the sample size decreases uncertainty in the estimated limit boundaries. One may also infer that when it is reasonable to assume that observed extremes come from the same data generating mechanism as all other observations, including all sampled angles into the likelihood provides smoother estimates of  $\partial\mathcal{G}$  than a procedure using only the exceedances of  $Q_{q_k}$ . We argue that while there may be valid reasons to select  $M_1$  or  $M_2$ —respectively for evidence of a homothetic data generating mechanism or of a poor matching between the density of angles  $\pi[\mathbf{W} \mid \mathcal{G}, \mathcal{L}, \mathbf{y}]$  and the homothetic density  $\mathcal{G}^d/|\mathcal{G}^d|$ —,  $M_3$  generally provides a better-behaved and more balanced choice.

### 6.3 Estimating rare event probabilities

Based on the results of Figures 21 and 22, we carry the remainder of this simulation study under the framework of model  $M_3$  and use all observed angles for the cases of the bivariate Laplace and

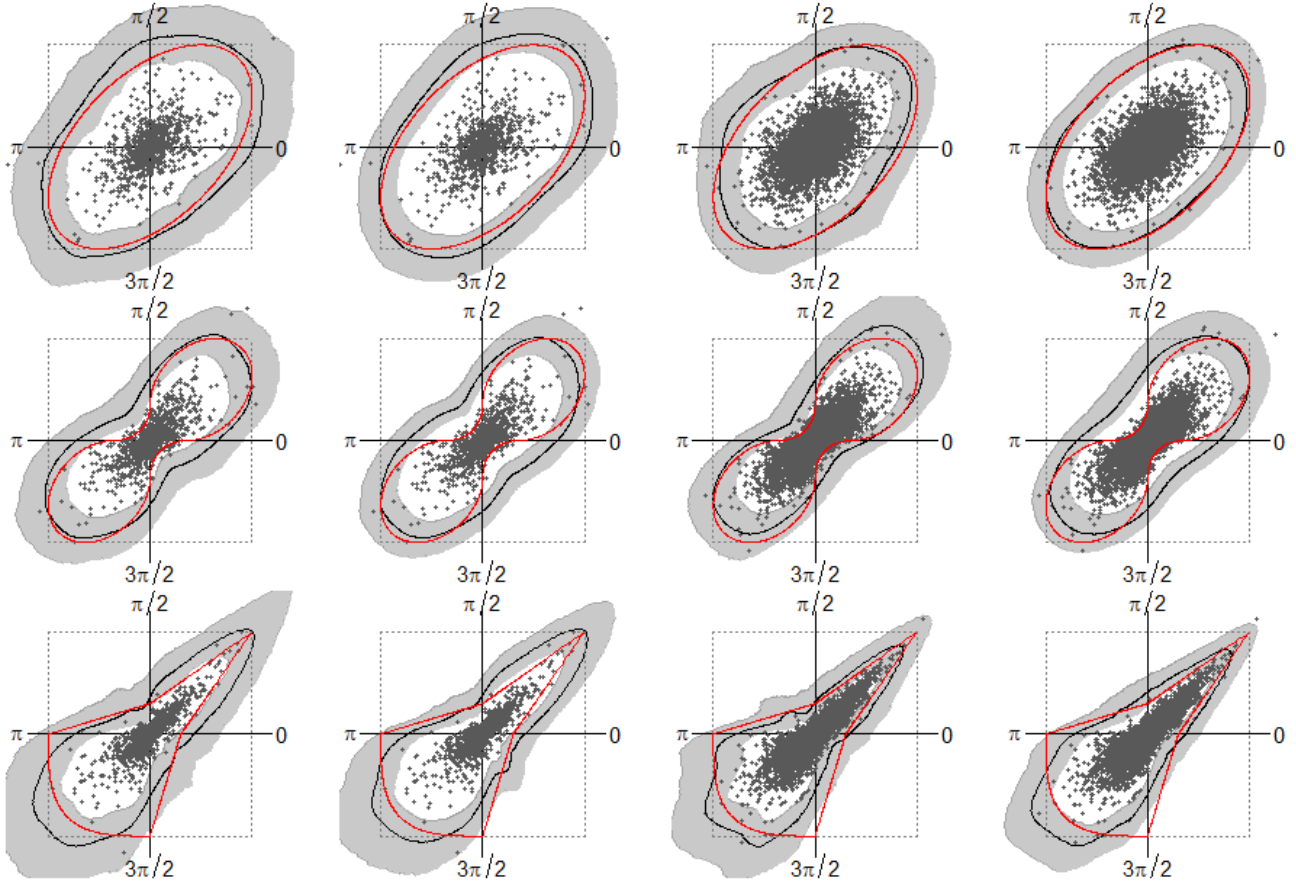


Figure 22: Limit set estimated from samples of size  $n$  by  $M_3$  via the posterior mean of  $\partial\mathcal{G}$  (black line) and 0.95 prediction interval (grey bands) with true limit set (red line) and unit square (dotted grey). Rows from top to bottom rows: Draws from the bivariate normal, max stable logistic, and multivariate Laplace distributions. Columns from left to right:  $M_3$  fitted only exceedances of  $r_{\mathcal{Q}_{0.8}}$  (sample size  $n_1$ ),  $M_3$  fitted using all angles (sample size  $n_1$ ),  $M_3$  fitted only exceedances of  $r_{\mathcal{Q}_{0.98}}$  (sample size  $n_2$ ),  $M_3$  fitted using all angles (sample size  $n_2$ ).

max-stable logistic distributions and only those of exceedances of  $Q_{q_k}$  for the bivariate normal distribution. For each of the 600 samples defined in Section 6.2, we obtain realisations from the posterior distribution of  $\mathbb{P}_{B_i|\mathbf{y}}$  according to the procedure described in Section 5.1 to estimate the probability that a new observation  $R\mathbf{W}$  falls within extreme sets  $B_1$ ,  $B_2$ , and  $B_3$  as defined in Figure 23. Figure 24 displays boxplots of the log-mean of the realisations from the posterior predictive distribution of each set  $B_i$  and each sample. It is clear that the mean of predictive

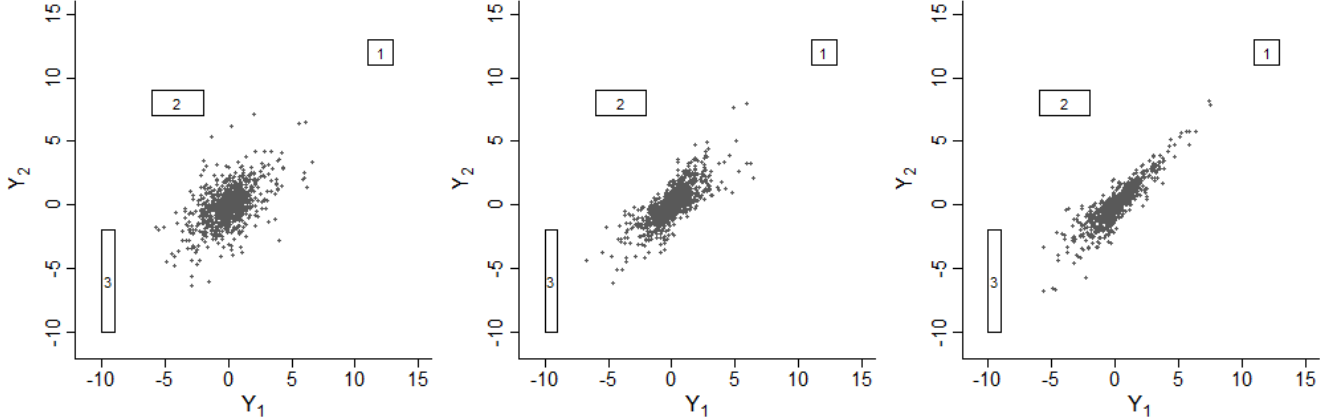


Figure 23: Regions  $B_1 = [11, 13] \times [11, 13]$ ,  $B_2 = [-6, -2] \times [7, 9]$ , and  $B_3 = [-10, -9] \times [-2, -10]$  for probability estimation superposed with samples of size  $n_1$  for the Gaussian (left), logistic (centre), and multivariate Laplace (right) distributions in Laplace margins.

posterior distribution is well-behaved for the sets  $B_i$  corresponding to directional subsets of  $\mathbb{S}$  where the posterior distribution of the limit sets presented in Section 6.2 is itself well-behaved. Table 2 details the coverage obtained from 100 samples for the probability that a new observation  $R\mathbf{W}$  falls within the sets  $B_1$ ,  $B_2$ , and  $B_3$  based on 0.95 prediction intervals based on the quantile method for the posterior predictive distributions. The coverage properties of the prediction intervals seem to be satisfying, except for the set  $B_2$  where the true probability is on the order of  $10^{-16}$  and  $10^{-14}$  for the bivariate normal and max-stable logistic distributions respectively. We again note that these correspond to regions in which the posterior distributions of  $r_{\mathcal{G}}$  are biased in the case of the bivariate normal distribution. We argue that reasonable coverage properties are obtained in other cases.

Bivariate distribution	Laplace		Normal		Max-stable logistic	
$n$	1000	10000	1000	10000	1000	10000
Coverage for $\mathbb{P}_{B_1 \mathbf{y}}$	0.97	0.94	0.99	0.97	0.56	0.57
Coverage for $\mathbb{P}_{B_2 \mathbf{y}}$	0.96	0.88	0.13	0.70	0.89	0.85
Coverage for $\mathbb{P}_{B_3 \mathbf{y}}$	0.98	0.97	0.97	0.94	0.92	0.92

Table 2: Coverage study of the 0.95 prediction intervals from the posterior predictive distribution  $\mathbb{P}_{B_i|\mathbf{y}}$  for the bivariate Laplace, normal, and max-stable logistic distributions.

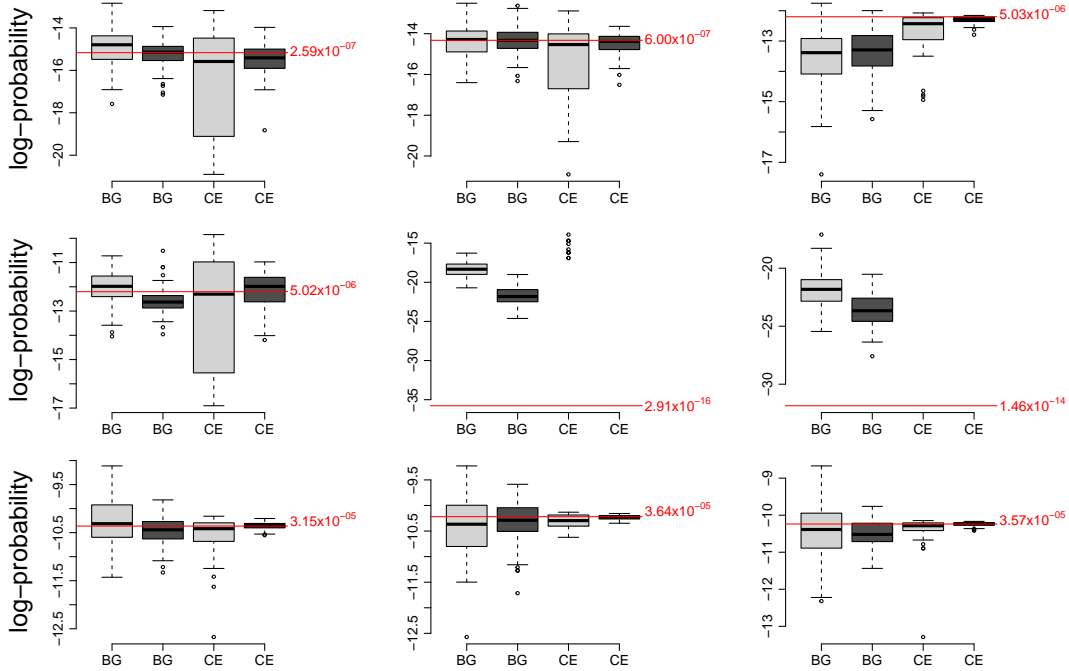


Figure 24: Boxplots of 100 log-means of posterior predictive samples for regions  $B_i$ . Panels from left to right: Output of  $M_3$  fitted on draws from the bivariate Laplace, Gaussian, and max-stable logistic distributions in Laplace margins. Panels from top to bottom:  $\log \mathbb{P}_{B_1|\mathbf{y}}$ ,  $\log \mathbb{P}_{B_2|\mathbf{y}}$ , and  $\log \mathbb{P}_{B_3|\mathbf{y}}$ . Within panels, light grey: sample size  $n_1$ , dark grey: sample size  $n_2$ .

## 6.4 Return sets

We obtain realisations from the posterior distribution of the radial function of the return set  $\mathcal{Q}_{1-1/T}$  using equation (46) on each realisation from the posterior distribution of the radial functions of  $\mathcal{Q}_q$  and  $\mathcal{G}$ . The angle-wise posterior mean of  $r_{\mathcal{Q}_{1-1/T}}$  hence defines a the boundary of a return set with period  $T$  as well as its associated 0.95 simultaneous prediction interval. Figure 25 displays return level-sets return sets of period  $T \in \{100, 1000, 10000\}$  estimated from one sample of  $n_2$  draws from the bivariate Laplace, normal, and max-stable logistic distributions.

## 6.5 Estimation of extremal coefficients

Figure 26 displays boxplots of the means of the samples from the posterior distribution of  $\alpha_{|1}$  obtained from both estimation procedures on each of the 600 samples. Table 3 presents a coverage study of the 0.95 credible intervals for  $\alpha_{|1}$ .

Instances of transformed  $r_{\mathcal{G}_T}$  are displayed in Figure 27. As can be observed, the transformation does not lead to a posterior  $r_{\mathcal{G}_T}$  that respects the limit boundary conditions everywhere, but it is better-behaved in the directional region between the angles  $\mathbf{w}^{(1)}$  and  $\mathbf{w}^{(2)}$ . The improvement in the estimation of  $\eta$  through this transformation procedure is observed in the results of the simulation study. Figure 28 contains boxplots of the posterior means and 0.95 prediction intervals for  $\eta$  resulting from  $\partial\mathcal{G}$  and  $\partial\mathcal{G}_T$ . Table 4 presents a coverage study of the 0.95 credible intervals for  $\eta$ . We argue that our model, especially under the consideration of the transformed  $\partial\mathcal{G}_T$ , can

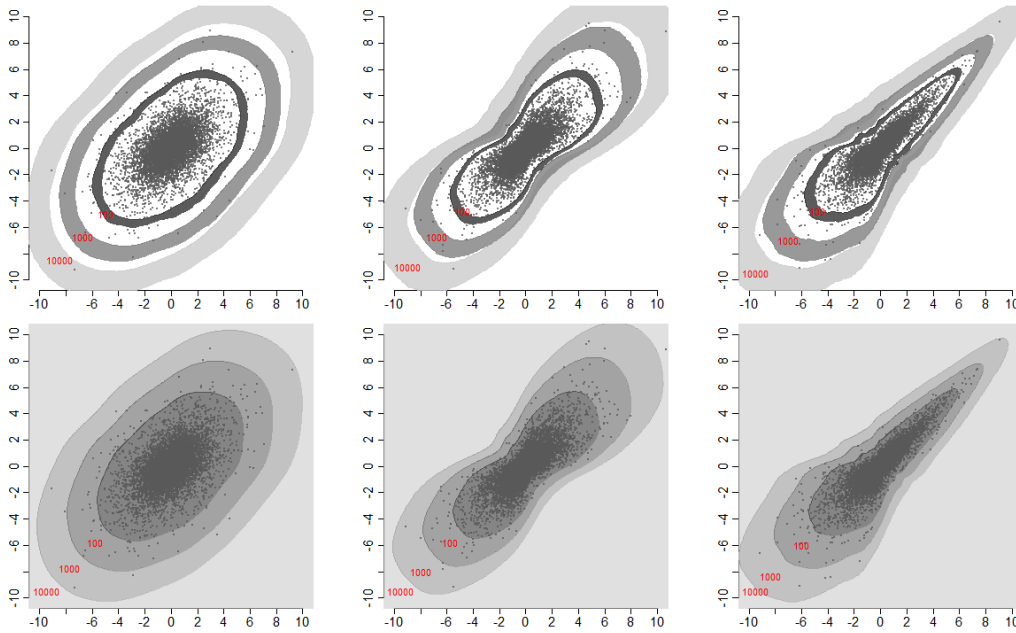


Figure 25: *Top row*: 0.95 prediction intervals for the boundaries  $r_{Q_{1-1/T}}$  of the canonical return sets with associated return period  $T$  displayed in red. *Bottom row*: Posterior mean of the return sets with associated return period (red) defined by the angle-wise posterior mean of  $r_{Q_{1-1/T}}$ . Every return set contains all lighter-grey sets. Columns from left to right: Bivariate Laplace, normal, and max-stable logistic distributions in Laplace margins.

Bivariate distribution	Laplace		Normal		Max-stable	
$n$	1000	10000	1000	10000	1000	10000
Coverage for $\alpha_{ 1}$ , Method 1	1.00	1.00	1.00	1.00	0.80	0.64
Coverage for $\alpha_{ 1}$ , Method 2	1.00	1.00	1.00	1.00	0.73	0.49

Table 3: Coverage study of the 0.95 credible intervals from the posterior distribution of  $\alpha_{|1}$  under both estimation methods for the bivariate Laplace, normal, and max-stable logistic distributions.

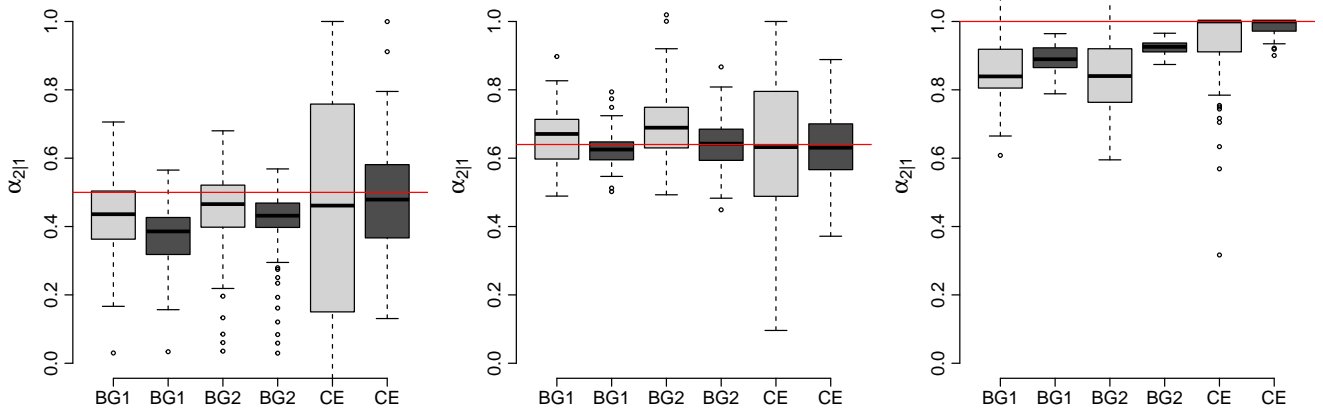


Figure 26: Boxplots of 100 means of realisations from the posterior of  $\alpha_{2|1}$ . Columns from left to right: Output of  $M_3$  fitted on draws from the bivariate Laplace, Gaussian, and logistic distributions in Laplace margins. Within panels, 1: method 1 and  $n_1$ , 2: method 2 and  $n_1$ , 1: method 1 and  $n_2$ , 2: method 2 and  $n_2$ . The true values of  $\alpha_{1|1}$  are given by the red line.

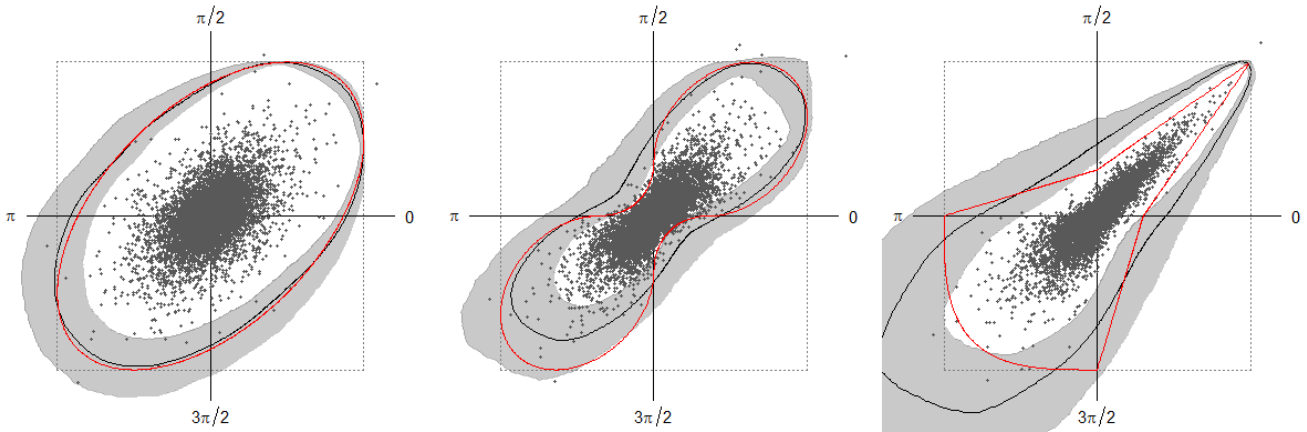


Figure 27: Posterior mean (black line) and associated 0.95 prediction bands (grey) for the transformed posterior distribution  $r_{G_T}$  of the bivariate Laplace (left), normal (centre), and max-stable logistic (right) distributions with true limit set (red line).

provide meaningful estimates of  $\eta$ .

Bivariate distribution	Laplace		Normal		Max-stable logistic	
$n$	1000	10000	1000	10000	1000	10000
Coverage for $\eta$ , Method 1	0.93	0.97	1.00	0.98	0.95	0.85
Coverage for $\eta$ , Method 2	0.95	0.96	1.00	1.00	0.99	0.67

Table 4: Coverage study of the 0.95 credible intervals from the posterior distribution of  $\eta$  under both estimation methods for the bivariate Laplace, normal, and max-stable logistic distributions.

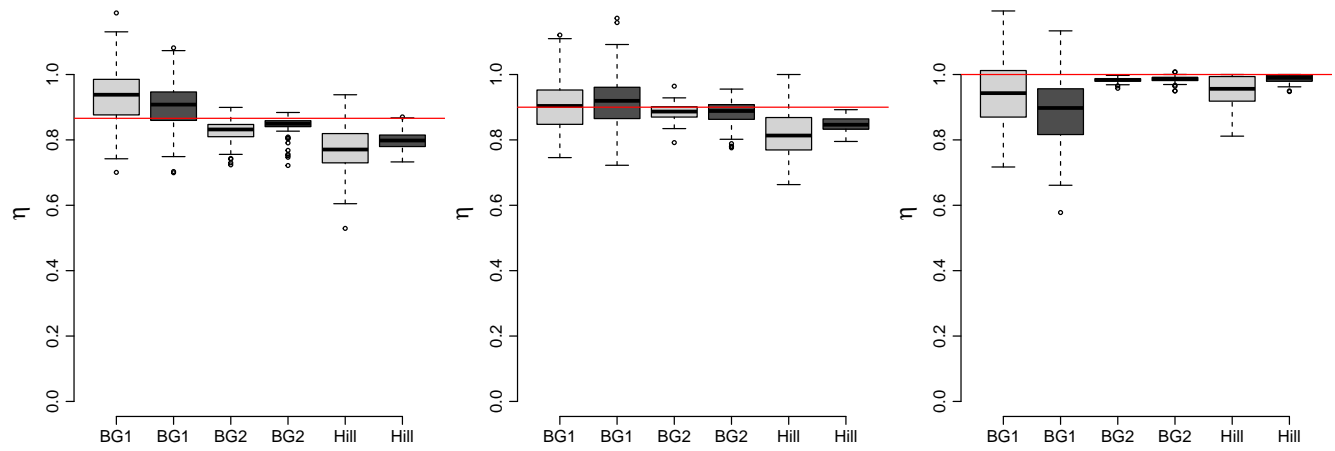
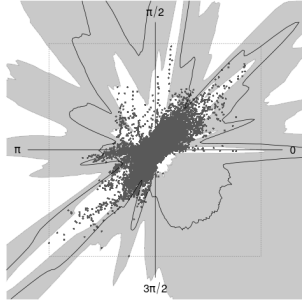


Figure 28: Boxplots of 100 means of posterior predictive samples for  $\eta$ . Panels from left to right: Draws from the bivariate Laplace, Gaussian, and logistic distributions in Laplace margins. Within panels, 1: method 1, 2: method 2. The true values of  $\eta$  are given by the red line.

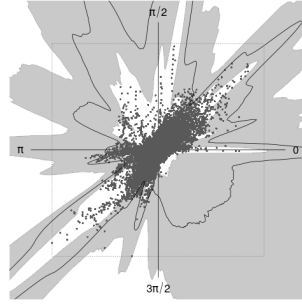
## 7 Case studies

### 7.1 Posterior model fits on river data

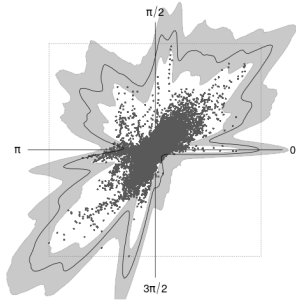
On the bivariate Thames tributary data, we fit models using the three architectures  $M_1$ ,  $M_2$ , and  $M_3$  using data exceeding a high posterior quantile estimate and on all available data. Figures 29 and 30 show posterior mean limit set boundary and posterior directional densities for each of the six fitted models. In these figures, we see that the fitted model associated with the  $M_2$  architecture and fitted on exceedance data only is best. This model's posterior limit set agrees most with log  $n$ -scaled data, while the posterior mean directional density is in good agreement with an empirical sample of angles. The posterior QQ plots in Figure 31 corresponding to this optimal model shows good agreement with the radial exceedance model and the underlying exponential distribution, while the PP plots in 32 show general agreement between the posterior and the underlying directional models.



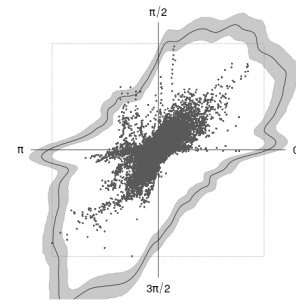
(a)  $M_1$ , exc. only



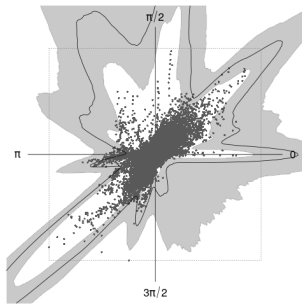
(b)  $M_1$ , all angles



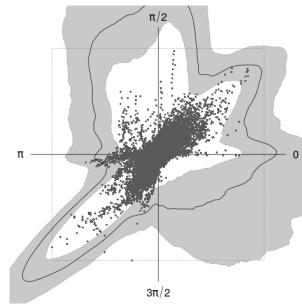
(c)  $M_2$ , exc. only



(d)  $M_2$ , all angles

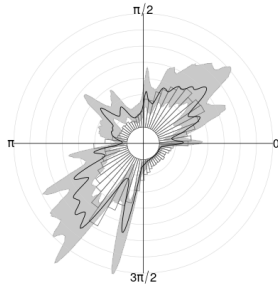


(e)  $M_3$ , exc. only

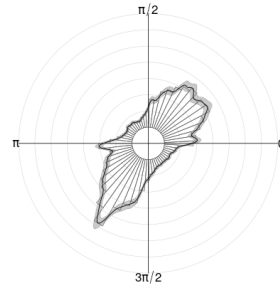


(f)  $M_3$ , all angles

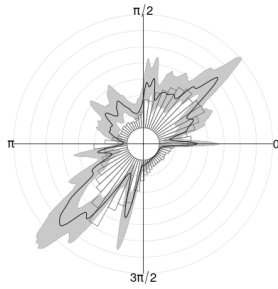
Figure 29: Posterior estimates of the unit level set  $g_G(\mathbf{x}) = 1$  for the river flow dataset. The black line corresponds to the posterior mean, with the 0.95 prediction interval shaded in grey. Black points are the original data in Laplace margins scaled by  $\log(n/2)$ . Dashed border line is the unit box.  $M_1$ ,  $M_2$ , and  $M_3$  define the angle density kernel, as described in section 3.3.



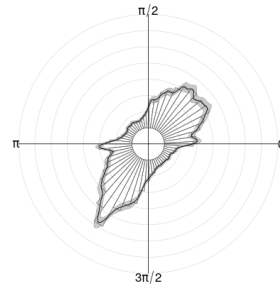
(a)  $M_1$ , exc. only



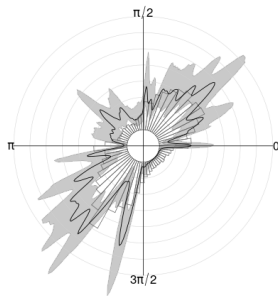
(b)  $M_1$ , all angles



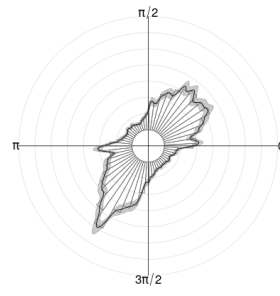
(c)  $M_2$ , exc. only



(d)  $M_2$ , all angles



(e)  $M_3$ , exc. only



(f)  $M_3$ , all angles

Figure 30: Posterior estimates of the mean angle density for the river flow dataset with 0.95 prediction intervals. The empirical density of angles is given by the underlying histogram.  $M_1$ ,  $M_2$ , and  $M_3$  define the angle density kernel, as described in section 3.3.

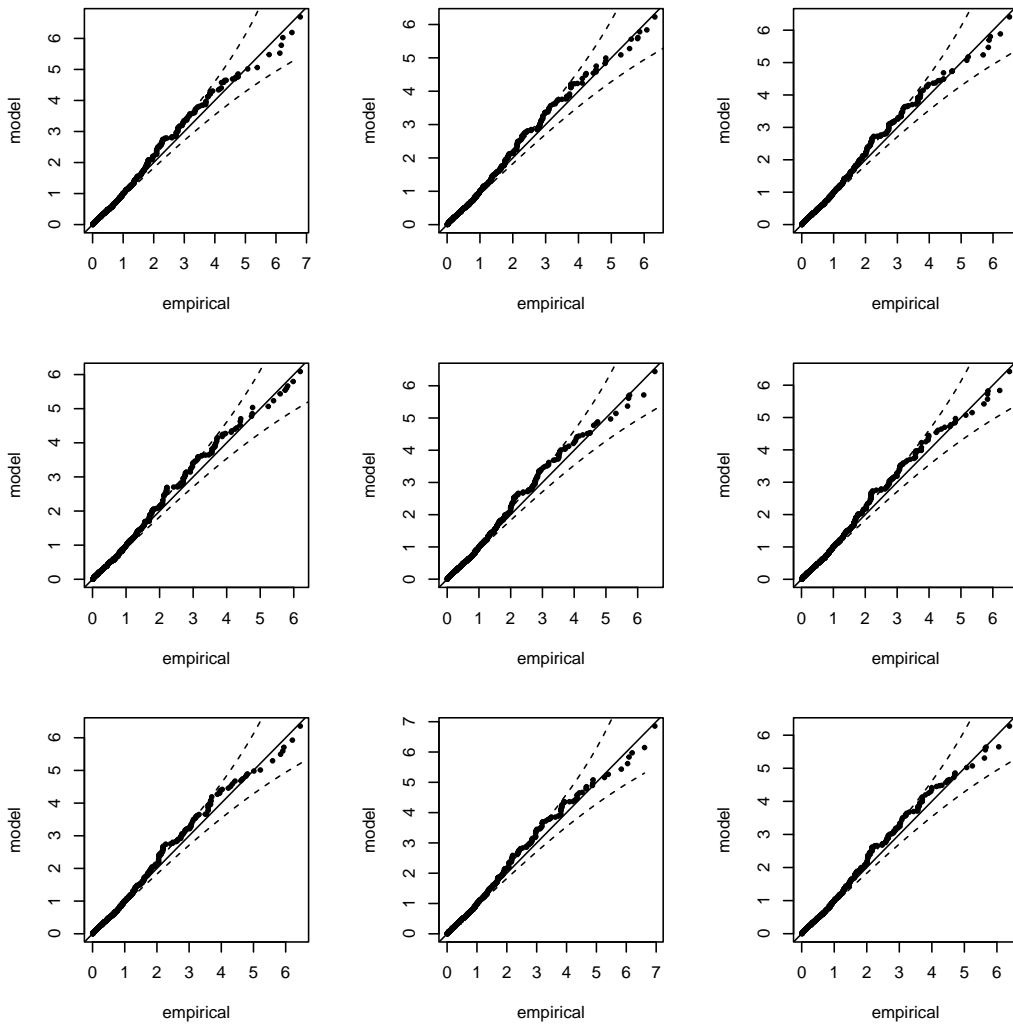


Figure 31: QQ plots for the Thames tributary river flow dataset exceedance model for 9 sampled posterior thresholds  $r_{Q_q}(\mathbf{w})$ , with 95% confidence intervals.

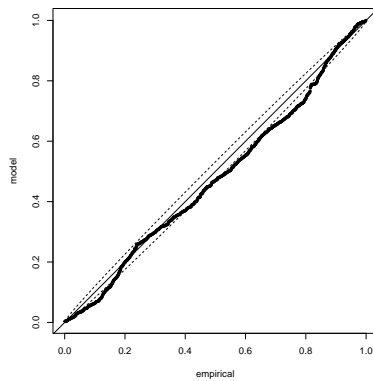


Figure 32: PP plots for the Thames tributary river flow dataset directional model, with 95% confidence intervals.

## 7.2 Additional Newlyn wave height figures

On the three-dimensional Newlyn wave data, we fit models using the three architectures  $M_1$ ,  $M_2$ , and  $M_3$  using data exceeding a high posterior quantile estimate and on all available data. Figure 33 show posterior mean limit set boundaries for each of the six fitted models. In these figures, we see that the fitted model associated with the  $M_2$  architecture and fitted on exceedance data only agrees most with  $\log n$ -scaled data, though all models fit well. The posterior QQ plots in Figure 34 corresponding to this optimal model shows good agreement with the radial exceedance model and the underlying exponential distribution, while the PP plots in 35 show good agreement between the posterior and the underlying directional models. In Section 4 of the main body of this manuscript we see that this model is also very accurate in estimating other diagnostics. One diagnostic not mentioned in Section 4 of the main body is plots of  $\chi_q(A)$ , defined in equation (1) in Section 1 of the main body. Figure 36 shows posterior mean estimates of  $\chi_q(A)$  for  $A \in \{HP, HS, PS, HPS\}$  and for  $q \in (0.9, 1)$  with posterior 95% confidence intervals. [Wadsworth & Campbell \(2024\)](#) establish that the variable groups  $HP$ ,  $PS$ , and  $HPS$  are asymptotically independent, and that  $HS$  is asymptotically dependent. With this in mind, we conclude that our posterior joint model is able to accurately describe the extremal dependence structure presented in this dataset. Figure 36 correctly shows posterior estimates of  $\chi_q(A)$  tending to 0 as  $q$  tends to 1 for the asymptotically independent groups, and tending to a nonzero value close to the empirical estimate for the asymptotically dependent pair  $HS$ .

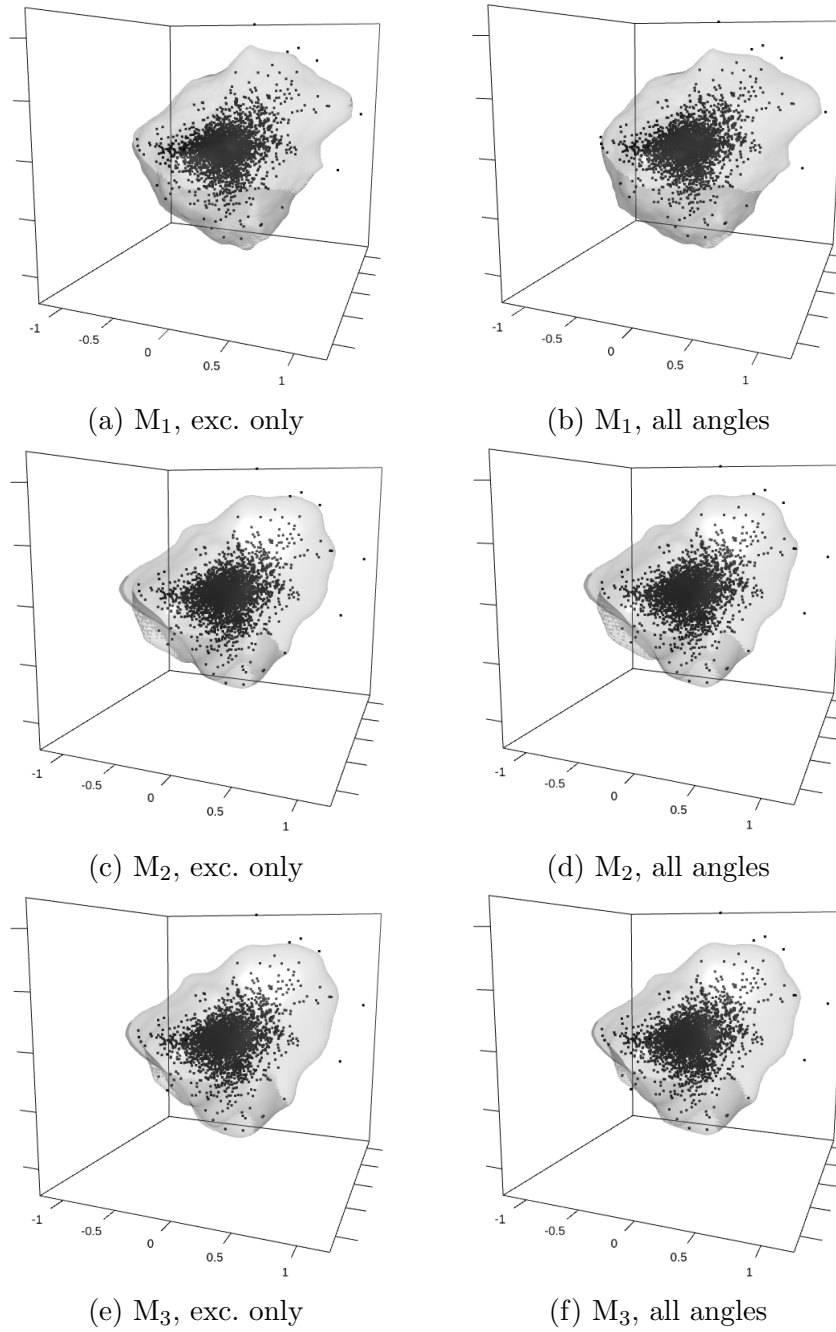


Figure 33: Posterior mean estimates of the unit level set  $g_{\mathcal{G}}(\mathbf{x}) = 1$  for the wave dataset. Black points are the original data in Laplace margins scaled by  $\log(n/2)$ .  $M_1$ ,  $M_2$ , and  $M_3$  define the angle density kernel, as described in section 3.3.

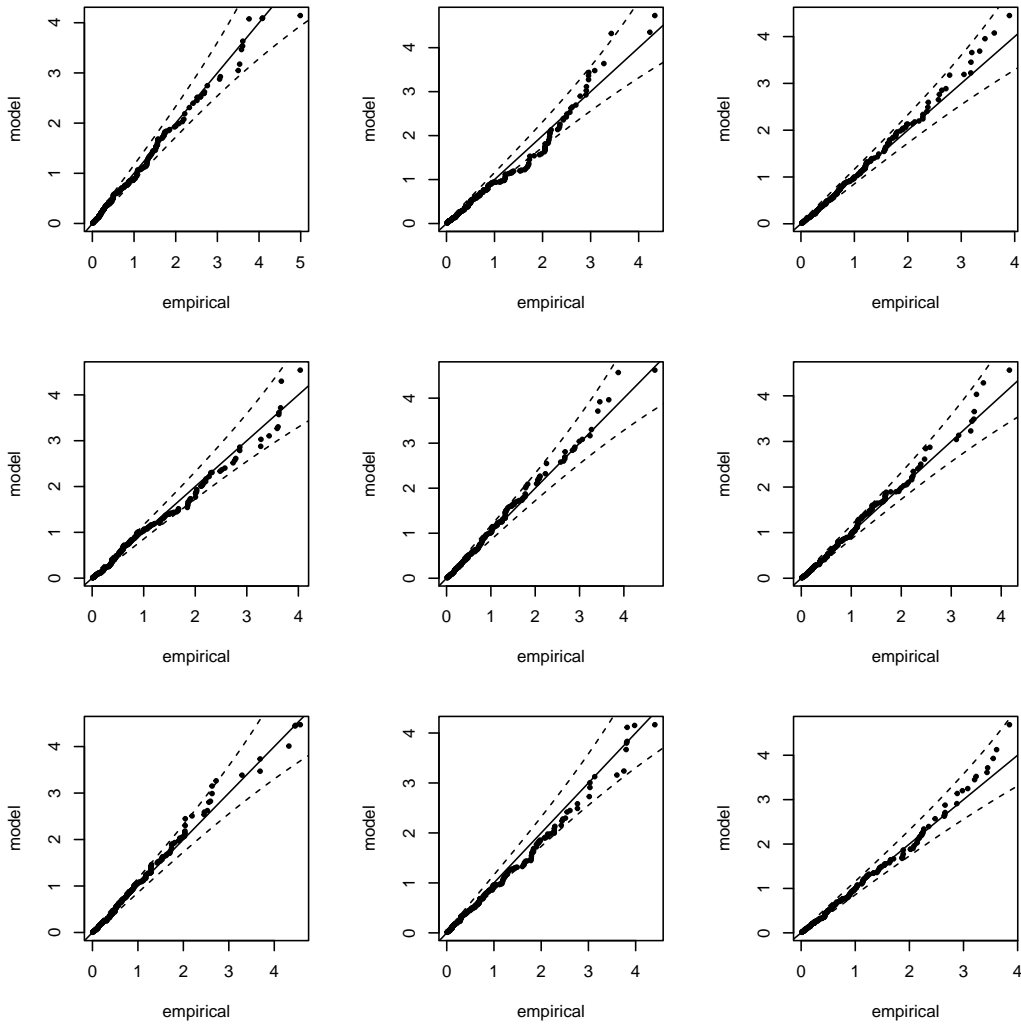


Figure 34: QQ plots for the Newlyn wave dataset exceedance model for 9 sampled posterior thresholds  $r_{Q_q}(\mathbf{w})$ , with 95% confidence intervals.

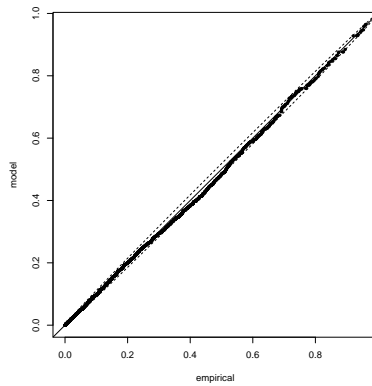


Figure 35: PP plots for the Newlyn wave dataset directional model, with 95% confidence intervals.

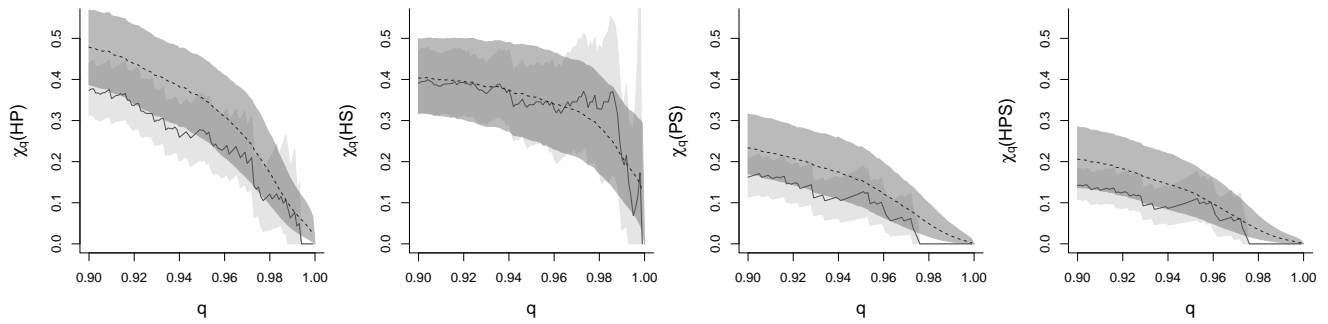


Figure 36:  $\chi_q$  plots for all pairwise combinations of marginal variables and for all three marginal variables. Solid line is an empirical estimate with 95% bootstrap confidence intervals in light grey, and the dashed line is a model-based estimate with 95% posterior confidence intervals in dark grey.

## 8 Bivariate Gaussian mixture model fits

Here, we recreate the task of return level set boundary estimation in the case of bivariate Gaussian mixture data presented in Section 4 of [Hallin et al. \(2021\)](#). Since our approach is non-empirical, we are able to extrapolate to higher levels than observed in the data and introduce uncertainty in our estimates. In Figure 37, the return level curves, along with 0.95 credible intervals, are presented for return periods  $T = 20$  (or  $q = 0.95$ ) and  $T = 10^5$  (or  $q = 1 - 10^{-5}$ ). For this each mixture distribution, we generated  $n = 5,000$  datapoints and fit a quantile regression model with threshold at the  $q = 0.9$  level. For the joint model, we used the  $M_3$  hierarchical structure. For display purposes, 20 posterior observations of  $r_{\mathcal{Q}_q}$  were drawn and a joint radial-directional model was fit at each of these observations. There were 50 draws of posterior return level curves drawn for each of these models for a total of 1,000 return level curves for which to obtain posterior mean and credible intervals for each plot in Figure 37.

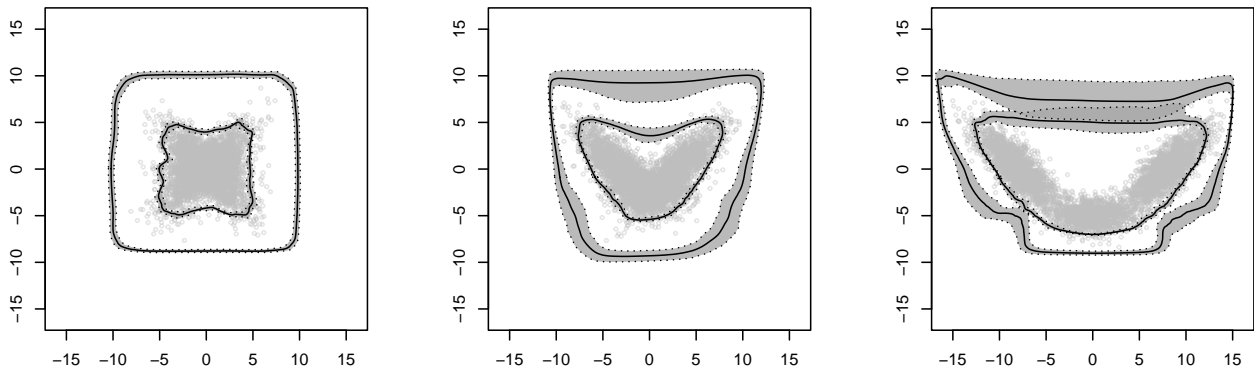


Figure 37: Posterior return level set boundaries for return periods  $T = 20$  (inner) and  $T = 10^5$  (outer) for 3 different bivariate Gaussian mixture distributions. Grey points are the data in original margins, solid black lines indicate the posterior mean return level set boundaries, with dark grey regions indicating the corresponding 0.95 credible bands, bordered by dotted lines.

## References

- Bolin, D. & Lindgren, F. (2015), ‘Excursion and contour uncertainty regions for latent Gaussian models’, *J. Roy. Statist. Soc., B* **77**(1), 85–106.
- Bolin, D. & Lindgren, F. (2017), ‘Quantifying the uncertainty of contour maps’, *Journal of Computational and Graphical Statistics* **26**(3), 513–524.

- Bolin, D. & Lindgren, F. (2018), ‘Calculating probabilistic excursion sets and related quantities using excursions’, *J. Stat. Softw.* **86**(5), 1–20.
- Coles, S. G. & Tawn, J. A. (1991), ‘Modelling extreme multivariate events’, *J. Roy. Statist. Soc., B* **53**, 377–392.
- de Haan, L. & Stadtmüller, U. (1996), ‘Generalized regular variation of second order’, *Journal of the Australian Mathematical Society* **61**(3), 381–395.
- Engelke, S. & Hitz, A. S. (2020), ‘Graphical models for extremes (with discussion)’, *J. Roy. Statist. Soc. Ser. B*.
- Gradshteyn, I. S. & Ryzhik, I. M. (2014), *Table of Integrals, Series, and Products*, Academic Press.
- Hallin, M., del Barrio, E., Cuesta-Albertos, J. & Matrán, C. (2021), ‘Distribution and quantile functions, ranks and signs in dimension  $d$ : A measure transportation approach’, *Ann. Stat.* **49**(2), 1139 – 1165.
- Hansen, G., Herburt, I., Martini, H. & Moszyńska, M. (2020), ‘Starshaped sets’, *Aequationes mathematicae* **94**, 1001–1092.
- Kiriliouk, A., Rootzén, H., Segers, J. & Wadsworth, J. L. (2019), ‘Peaks over thresholds modeling with multivariate generalized Pareto distributions’, *Technometrics* **61**(1), 123–135.
- Klain, D. A. (1997), ‘Invariant valuations on star-shaped sets’, *Advances in Mathematics* **125**(1), 95–113.
- Kotz, S., Kozubowski, T. J. & Podgorski, K. (2001), ‘The laplace distribution and generalizations’, (*No Title*).
- Lindgren, F., Rue, H. & Lindström, J. (2011), ‘An explicit link between Gaussian fields and Gaussian Markov random fields: the stochastic partial differential equation approach (with discussion)’, *J. Roy. Statist. Soc., B* **73**(4), 423–498.
- Lutwak, E. (1988), ‘Intersection bodies and dual mixed volumes’, *Advances in Mathematics* **71**(2), 232–261.
- Papastathopoulos, I. & Paulin, D. (2023), ‘Markov random tail fields and extended multivariate regularly varying functions’. Unpublished research.
- Papastathopoulos, I. & Tawn, J. A. (2013), ‘A generalised Student’s  $t$ -distribution’, *Stat. Probabil. Lett.* **83**, 70–77.
- Pickands, J. (1975), ‘Statistical inference using extreme order statistics’, *Ann. Stat.* **3**(1), 119–131.
- Resnick, S. I. (2007), *Heavy-tail phenomena: probabilistic and statistical modeling*, Springer Science & Business Media, New York.

- Rootzén, H. & Tajvidi (2006), ‘The multivariate generalized Pareto distribution’, *Bernoulli* **12**, 917–930.
- Soms, A. P. (1976), ‘An asymptotic expansion for the tail area of the t-distribution’, *J. Am. Stat. Assoc.* **71**(355), 728–730.
- Wadsworth, J. L. & Campbell, R. (2024), ‘Statistical inference for multivariate extremes via a geometric approach’, *J. Roy. Statist. Soc., B* **86**(5), 1243–1265.